Bolts from the Blue

by

Harald Esdert Edens

Submitted in Partial Fulfillment
of the Requirements for the Degree of

Doctor of Philosophy in Physics
with Dissertation in Atmospheric Physics

New Mexico Institute of Mining and Technology
Socorro, New Mexico

June 10, 2011

This dissertation is accepted on behalf of the faculty
of the Institute by the following committee:

Adviser

Committee member

Committee member

Committee member

Committee member

Date

I release this document to New Mexico Institute of Mining and Technology.

Student's signature Date

I dedicate this work to my parents, Esdert and José. Thank you for your untiring support, motivation and patience.

Harald Edens

Socorro, New Mexico
May 16, 2011

Abstract

A *bolt from the blue* (BFB) is a cloud-to-ground flash that initiates as a classic intracloud (IC) flash between midlevel negative and upper positive charge in a storm. It is of negative polarity, lowering negative charge to ground. BFB flashes can develop from IC flashes when the upper positive charge region of a storm is depleted relative to the midlevel negative charge region, due to the mixing with negative screening charge at the storm top.

The leaders to ground of BFB flashes often exit the cloud at altitudes of 8 km or higher and can be observed visually. Leader characteristics are studied using Lightning Mapping Array (LMA) data, slow and fast electric field change (ΔE) waveforms, broadband VHF recordings, and high-speed video recordings.

Two types of BFB flashes are observed, which are termed Type-I and Type-II. In Type-I BFB flashes the leader to ground develops from the upward negative leader in a continuous manner. In Type-II BFB flashes the leader is initiated by fast negative breakdown along a preexisting channel and either branches off the channel or is an extension of it.

Three stages are defined for BFB flashes: an intracloud stage, a cloud-to-ground stage, and a final stage. The intracloud stage encompasses all intracloud activity up to the initiation of the outward and downward leader, which propagates to ground during the cloud-to-ground stage. The final stage is characterized by continued positive breakdown, which often produces K-leaders into upper positive charge and dart leaders along the channel to ground.

Of the 59 BFB flashes presented in this work, 49% produced more than one stroke to ground; 32% produced three or more strokes to ground. The mean initiation altitude of these flashes was 7.7 ± 0.7 km above MSL. The mean flash duration was 451 ± 173 ms while the time to the first return stroke was 221 ± 87 ms. The average number of strokes was 2.1 ± 1.7; one flash produced nine strokes to ground. The horizontal distance, or offset, of the cloud-to-ground leader from the flash initiation region ranged from 1 to 17 km with a mean distance of 6.5 ± 2.6 km. Also, a correlation was found between wind shear and the preferred cloud exit location of BFB flashes, with a preference for the upwind side of the storm. The wind shear is defined as the vector difference of the mean winds at 4–8 km altitude and at 8–12 km altitude. Some BFB flashes produce positive and negative breakdown in laterally displaced regions, indicating that the two major charge regions in a storm are displaced as a result of the wind shear.

Several interesting observations are made of the cloud-to-ground leader of BFB flashes. *Luminosity recoil waves* are observed during the leader stepping process while the downward developing leader is between 9 and 6 km altitude. These recoil waves appear as bright luminosity events near the tips of the leaders, and appear to travel back up along the channel in a retrograde direction. The velocity of some of these recoil events at 6 km altitude is estimated at 2.5×10^6 m s^{-1}. Another observation is the occurrence of *branch discharges*, which are transient, bright discharges along inactive branches of the main leader channel at altitudes of 6–9 km after the main leader has propagated several kilometers farther downward and is approaching ground. These branch discharges are current surges that transport negative charge from the branch into and down along the main leader channel, heating it and making it more conductive. These cause brief intensifications in the luminosity of the main leader channel.

It is found that fast K-leaders occur during the propagation of the negative leaders, both in the cloud and along the cloud-to-ground leader, which assist the negative breakdown by supplying negative charge to the leader tip(s). For one BFB flash in which these fast K-leaders occurred during the cloud-to-ground stage, a K-leader velocity of 1–2 $\times 10^7$ m s^{-1} was found.

Typical estimates of negative-leader velocities of BFB flashes are on the order of 0.8–2.0 $\times 10^5$ m s^{-1}; dart leaders typically propagate at velocities of 5×10^5 to 1×10^7 m s^{-1}, consistent with leader velocities reported in the literature. BFB flashes typically produce one or more attempted dart leaders that do not succeed in reaching ground. Since BFB flashes have much longer leader channels than those in normal –CG flashes, they are expected to be less successful in producing multiple strokes to ground.

BFB flashes show a characteristic transition in the VHF emissions by the negative cloud-to-ground leader as it propagates from high altitude (above 8 km) to low altitude (below 5 km). At high altitude the leader exhibits impulsive VHF emissions typical of regular IC flashes, while at low altitude the VHF emissions appear more continuous in nature, characteristic of those observed in normal –CG and low-altitude IC flashes. It is found that the rate of emissions increases with decreasing altitude, whereas the emitted source power does not appear to change significantly. The increase in the VHF emission rate by the negative leader appears to be caused by a change in the leader stepping process: The leader step length becomes shorter as the leader reaches lower altitude. From a photograph of a negative leader in clear air at 11 km altitude a step length on the order of 200 m is inferred, while the leader step length inferred from high-speed video at 6 km altitude is on the order of 15–30 m. From two photographs of negative cloud-to-ground leaders of BFB flashes a leader step length on the order of 16 m at 3 km altitude is inferred, which is an order of magnitude shorter than the step length at 11 km altitude. Since the velocity of a negative stepped leader does not appear to change between high and low altitudes,

leader steps must occur at a higher rate at lower altitude, with a correspondingly higher rate of VHF emissions produced during the leader stepping process. This effect is enhanced by an increased number of active leader tips at low altitude from multiple branches; cloud-to-ground leaders of BFB flashes are generally branched profusely at low altitude but not at high altitude.

Acknowledgments

It would be impossible for me to individually thank each and every person who has, over the years, helped me in some way with my dissertation research. I would therefore like to express my gratitude and apologize to those not explicitly acknowledged here.

First, I want to thank my research and academic advisor Paul Krehbiel for his outstanding support over the years, both professionally and on a personal level. Paul, it has been a privilege for me to have been a Ph.D. student under your auspices. I also sincerely thank the other members of my advisory committee: Bill Winn, Ken Eack, Bill Rison and Ron Thomas for their support, for keeping me motivated, and for involving me in several other very interesting projects. I would also like to thank Richard Sonnenfeld, and I am grateful to the many other professors of New Mexico Tech for their excellent teaching skills.

I am indebted to Sandy Kieft, Vida Trujillo and Gina Chavez for their apparent effortless handling of a surely insurmountable pile of paperwork that I suspect must have been in existence as a byproduct of my stay here at New Mexico Tech. Also, thank you for the many interesting, motivating and humorous conversations that we have had over the years.

Steve Hunyady, if it wasn't for your support I would not be writing this today. Also, without your continual and devoted work on the Langmuir Laboratory LMA and networking infrastructure, all that would never be what it is today. Thank you for teaching me to never lay a dead saddle on a horse. I almost get it right nowadays. Thank you for everything.

Graydon Aulich, thanks for everything you have assisted me with and for being an informal mentor to me over the years. I can only hope to one day be half as experienced and knowledgeable as you in designing instrumentation.

Chris Caldwell, thank you for your most efficient help and assistance with my work and stay at Langmuir Laboratory, for making my many long days at the lab so much more enjoyable, and for your friendship.

Victor Pasko, during your brief stay at Langmuir Laboratory in 2006 I learned a great deal from you and I would like to thank you for that and for your company back then. I also thank Mark Stanley, Timothy Hamlin and Jeremiah Harlin for their most helpful discussions on lightning, instrumentation and dissertation writing in general. Sonja Behnke, thank you for being a most friendly and efficient colleague

to work with, both in the office and during field trips. I further thank Jake Trueblood and Elissa Eastvedt for their good company at Langmuir Laboratory.

I thank Kyle Wiens for making sure that I made my first acquaintance with a bolt from the blue from a safe location. Early on during the STEPS program in 2000, I was watching a severe storm roll in from the west from the parking lot of the National Guard Armory in Goodland, Kansas. Moments after Kyle had emerged from the LMA trailer to inform me that it was "probably best to go indoors now" and I got into a parked car, something that can only be described as a bolt out of nowhere, really, struck somewhere near or at the adjacent National Weather Service building, sending a crackling leader upward from a light pole on the parking lot and a massive wave of thunder through my stomach. I have since had the dubious pleasure of experiencing yet closer encounters with bolt-from-the-blue flashes, including one flash at about 30 meters distance while working in the Annex building of Langmuir Laboratory, but that particular day during STEPS is still fresh in my mind.

Terry Pallister, many thanks for your long-term friendship and support over the years. The bolt from the blue in August 2002 that we both photographed over Lake Pontchartrain in New Orleans is one of the finest examples that I have obtained and certainly has helped spawn my interest in this type of lightning. Few things are as joyful as capturing on film, along with a good friend, a spectacular yet elusive (from a photographic point of view) bolt from the blue.

Drew and Heidi Medlin, thank you for your friendship and your patience during my final Ph.D. phase of "writing things down". I look forward to many more lightning photography sessions with you. Also, I will continue to try not to get you and your car stuck in puddles of mud, and to obey the off-road speed limit. Really, I promise.

I thank my sister Saskia and her partner Gert-Jan for the most enjoyable times we spent together both in The Netherlands and New Mexico, and for their motivating help and suggestions over the years. Also, Saskia, thank you for being responsible for triggering my interest in lightning when I was young of age; I still can't bear it that you saw the flower-shaped upward flash of lightning while I didn't.

Last but not least, I am grateful to my parents José and Esdert, for always having supported me. I still remember when I was very young, that during a thunderstorm the antenna cable had to be disconnected from the television set and put on the floor. The sight of that loose antenna cable with its connector on the floor and the thunder outside made a big impression on me—I was terrified of it and I can still vividly remember it. (Incidentally, nowadays I am still terrified to see loose antenna cables on the floor during lightning, but that is because it generally means some piece of instrumentation has been accidentally disconnected and I am losing data.) My insatiable desire to always learn more about Nature and to continue to be amazed by it is largely due to all your support over the years, never limiting my creativity or motivation in any way.

Etymology

"The chaotic Thunder-cloud, with its pitchy black, and its tumult of dazzling jagged fire, in a world all electric: thou wilt not undertake to show how that comported itself—what the secrets of its dark womb were; from what sources, with what specialties, the lightning it held did, in confused brightness of terror, strike forth, destructive and self-destructive, till it ended? Like a Blackness naturally of Erebus, which by will of Providence had for once mounted itself into dominion and the Azure: is not this properly the nature of Sansculottism consummating itself? Of which Erebus Blackness be it enough to discern that this and the other dazzling fire-bolt, dazzling fire-torrent, does by small Volition and great Necessity, verily issue,—in such and such succession; destructive so and so, self-destructive so and so: till it end.

Royalism is extinct; 'sunk,' as they say, 'in the mud of the Loire'; Republicanism dominates without and within: what, therefore, on the 15th day of March 1794, is this? Arrestment, sudden really as a bolt out of the Blue, has hit strange victims: [...]"

Thomas Carlyle, *The French revolution: a history*, Volume 3 (1837)

First known literary use of the idiom 'bolt out of the blue'

Contents

1 Introduction **1**

2 Visual observations **4**

2.1 Introduction 4

2.2 Occurrence 4

2.3 Visual observations 5

2.4 Photographic observations 6

3 General remote-sensing observations **9**

3.1 Introduction 9

3.2 Instrumentation 9

3.2.1 LMA 9

3.2.2 Log-RF radiation 10

3.2.3 Slow and fast antennas 10

3.2.4 Broadband waveforms and spectrograms 11

3.2.5 Sign convention for electric field 11

3.3 Common types of lightning 11

3.3.1 Negative CG flash 13

3.3.2 IC flash 17

3.3.3 BFB flash 20

3.3.4 Low-altitude IC flash 24
3.3.5 Positive CG flash 24
3.4 BFB flash stages 27
3.5 BFB flash types 30
3.6 BFB flash characteristics 31
3.6.1 BFB flash polarity 35
3.6.2 Attempted BFB flashes 35
3.6.3 Flash type 35
3.6.4 Number of strokes to ground 35
3.6.5 Flash duration and time to first stroke 36
3.6.6 Flash initiation altitude 38
3.6.7 Strike distance 38
3.6.8 The effect of wind shear 40
3.7 Summary 44

4 BFB flash of August 2, 2010 at 20:58:11 46

4.1 Introduction 46
4.2 Data correlation 46
4.2.1 Video overlay algorithm 47
4.2.2 LMA data 47
4.2.3 Time reference 47
4.3 Storms on August 2, 2010 48
4.4 Main characteristics 49
4.5 Intracloud stage 54
4.6 Cloud-to-ground stage 60
4.7 Final stage 71

4.7.1 Dart-stepped leader 71
4.7.2 Second dart leader 77
4.7.3 Third dart leader 81
4.7.4 Fourth dart leader 85
4.8 Summary 85

5 BFB storm of August 20, 2010 **88**
5.1 Introduction 88
5.2 Overview of storms 88
5.3 Cloud-to-air leaders 89
5.3.1 Streamer zones on a negative leader 90
5.3.2 Space stem during streamer-to-leader transition 91
5.4 BFB flashes 95
5.5 Overview of BFB flash at 03:25:57 96
5.5.1 Photograph 96
5.5.2 LMA 96
5.5.3 Waveform data 101
5.5.4 High-speed video 101
5.6 Intracloud stage 106
5.6.1 First and second negative breakdown events 106
5.6.2 Third and fourth negative breakdown events 110
5.7 Cloud-to-ground stage 114
5.7.1 Fifth negative breakdown event 114
5.7.2 Cloud-to-ground leader 118
5.7.3 Stepped leader at 8 km altitude 122
5.7.4 Stepped leader at 6 km altitude 128

5.7.5 Step increase in channel luminosity . . . 133
5.8 Final stage . . . 136
5.9 Summary . . . 142
5.9.1 Summary of BFB flash . . . 142
5.9.2 Retrograde luminosity waves at leader tips . . . 143
5.9.3 Branch discharges . . . 143
5.9.4 Streamer-to-leader transition . . . 144
5.9.5 Leader step length . . . 144
5.9.6 Transition from impulsive to continuous breakdown . . . 145

6 Other flashes of interest **146**
6.1 Introduction . . . 146
6.2 BFB flash with multiple strokes to ground . . . 146
6.3 BFB flash with long continuing current . . . 151
6.4 BFB flash with large horizontal extent . . . 155
6.5 BFB flash with impulsive intracloud stage . . . 159
6.6 BFB flash with five attempted dart leaders . . . 164
6.7 BFB flash with low-altitude horizontal branch . . . 169
6.8 Classic Type-I BFB flash . . . 174
6.9 BFB flash with high-altitude upward leader . . . 179
6.10 Summary . . . 184
6.10.1 Number of strokes to ground . . . 184
6.10.2 Unequal extent of positive and negative breakdown . . . 184
6.10.3 Lateral displacement of charge regions . . . 184
6.10.4 Final stage: K-leaders and dart leaders . . . 184
6.10.5 K-leaders during leader development . . . 185
6.10.6 Transition in VHF emissions of cloud-to-ground leader . . . 185

7 Conclusions **186**

7.1 Summary 186

7.2 Main conclusion 188

A Instrumentation **189**

A.1 Lightning mapping array 189

A.1.1 Principle of operation 189

A.1.2 History of the Langmuir Laboratory LMA 190

A.1.3 Operation 191

A.2 Log-RF 192

A.3 Slow and fast antennas 192

A.4 Rohde & Schwarz HE010 broadband antenna 193

A.5 Sirio SD1300N broadband antenna 194

A.6 Computation of spectrograms 195

A.7 Data acquisition system 196

A.7.1 Digitizers 196

A.7.2 Triggering 197

A.7.3 Trigger discrimination 198

A.8 High-speed video 200

A.8.1 Time reference 200

A.8.2 Sensor dimensions 201

A.8.3 Optimal exposure settings 202

A.8.4 Overlaying LMA data on video frames 202

B Calibration **210**

B.1 Waveform timing calibration 210

B.2 Slow antenna 211

B.3 Fast antenna 212

B.4 Broadband antennas 212

B.5 LMA 212

B.6 Log-RF 213

C Other observations **214**

C.1 LMA airplane track masking 214

C.2 Unconnected branches 220

D Photographs **227**

D.1 Introduction 227

D.2 Typical BFB flashes 228

D.3 BFB flashes following cloud boundaries 232

D.4 Forked (multi-channel) BFB flashes 235

D.5 Cloud-enshrouded BFB flashes 237

D.6 Attempted BFB flashes 239

D.7 BFB flashes with upward leader 242

List of Figures

3.1 Common types of flashes 12

3.2 –CG flash example, waveforms 14

3.3 –CG flash example, LMA 15

3.4 IC flash example, waveforms 18

3.5 IC flash example, LMA 19

3.6 BFB flash example, waveforms 21

3.7 BFB flash example, LMA 22

3.8 Low-altitude IC flash example, waveforms 25

3.9 Low-altitude IC flash example, LMA 26

3.10 +CG flash example, waveforms 28

3.11 +CG flash example, LMA 29

3.12 Distribution of number of strokes to ground 36

3.13 Distribution of flash duration 37

3.14 Distribution of time to first stroke 38

3.15 Distribution of flash initiation altitude 39

3.16 Distribution of strike distance 40

3.17 Wind-shear vectors 41

3.18 Wind shear and BFB strike locations 42

4.1 BFB of 8/2/2010, 20:58:11: waveforms 50

4.2 BFB of 8/2/2010, 20:58:11: LMA 51
4.3 BFB of 8/2/2010, 20:58:11: LMA, charge identification 52
4.4 BFB of 8/2/2010, 20:58:11: LMA, source power 53
4.5 BFB of 8/2/2010, 20:58:11: waveforms, intracloud stage 55
4.6 BFB of 8/2/2010, 20:58:11: LMA, intracloud stage 56
4.7 BFB of 8/2/2010, 20:58:11: waveforms, intracloud stage (2) 57
4.8 BFB of 8/2/2010, 20:58:11: LMA, intracloud stage (2) 58
4.9 BFB of 8/2/2010, 20:58:11: waveforms, cloud-to-ground stage 61
4.10 BFB of 8/2/2010, 20:58:11: LMA, cloud-to-ground stage 62
4.11 BFB of 8/2/2010, 20:58:11: video composite 64
4.12 BFB of 8/2/2010, 20:58:11: video–LMA overlay 65
4.13 BFB of 8/2/2010, 20:58:11: waveforms, cloud-to-ground leader (15 ms) 66
4.14 BFB of 8/2/2010, 20:58:11: waveforms, cloud-to-ground leader (15 ms) 68
4.15 BFB of 8/2/2010, 20:58:11: waveforms, luminosity event 70
4.16 BFB of 8/2/2010, 20:58:11: waveforms, final stage 72
4.17 BFB of 8/2/2010, 20:58:11: LMA, final stage 73
4.18 BFB of 8/2/2010, 20:58:11: waveforms, dart-stepped leader 75
4.19 BFB of 8/2/2010, 20:58:11: LMA, dart-stepped leader 76
4.20 BFB of 8/2/2010, 20:58:11: waveforms, second dart leader 78
4.21 BFB of 8/2/2010, 20:58:11: waveforms, second dart leader (detail) . . 79
4.22 BFB of 8/2/2010, 20:58:11: LMA, second dart leader 80
4.23 BFB of 8/2/2010, 20:58:11: waveforms, third dart leader 82
4.24 BFB of 8/2/2010, 20:58:11: waveforms, third dart leader (detail) . . . 83
4.25 BFB of 8/2/2010, 20:58:11: LMA, third dart leader 84

5.1 Upward leader, 8/20/2010 at 03:03:28, detail 92

5.2 Diagram of leader space stem 93
5.3 BFB of 8/20/2010, 03:25:57: LMA 98
5.4 BFB of 8/20/2010, 03:25:57: LMA, charge identification 99
5.5 BFB of 8/20/2010, 03:25:57: LMA, source power 100
5.6 BFB of 8/20/2010, 03:25:57: waveforms 102
5.7 BFB of 8/20/2010, 03:25:57: video composite 103
5.8 BFB of 8/20/2010, 03:25:57: video composite with LMA (time) . . . 104
5.9 BFB of 8/20/2010, 03:25:57: video composite with LMA (charge) . . 105
5.10 BFB of 8/20/2010, 03:25:57: waveforms, intracloud stage 107
5.11 BFB of 8/20/2010, 03:25:57: waveforms, intracloud activity 108
5.12 BFB of 8/20/2010, 03:25:57: LMA, intracloud activity 109
5.13 BFB of 8/20/2010, 03:25:57: waveforms, first and second K-leaders . 111
5.14 BFB of 8/20/2010, 03:25:57: LMA, first K-leader 112
5.15 BFB of 8/20/2010, 03:25:57: LMA, second K-leader 113
5.16 BFB of 8/20/2010, 03:25:57: waveforms, third K-leader 115
5.17 BFB of 8/20/2010, 03:25:57: LMA, third K-leader 116
5.18 BFB of 8/20/2010, 03:25:57: waveforms, cloud-to-ground leader . . . 119
5.19 BFB of 8/20/2010, 03:25:57: LMA, cloud-to-ground leader 120
5.20 BFB of 8/20/2010, 03:25:57: fast ΔE and streak, CG leader 121
5.21 BFB of 8/20/2010, 03:25:57: CG leader, video composite 123
5.22 BFB of 8/20/2010, 03:25:57: waveforms, CG leader at 7–9 km 124
5.23 BFB of 8/20/2010, 03:25:57: LMA, CG leader (30 ms) 125
5.24 BFB of 8/20/2010, 03:25:57: fast ΔE and video, CG leader at 7–9 km 126
5.25 BFB of 8/20/2010, 03:25:57: video composite, CG leader, 6 km altitude 129
5.26 BFB of 8/20/2010, 03:25:57: waveforms, CG leader, 6 km altitude . . 131

5.27 BFB of 8/20/2010, 03:25:57: fast ΔE and video, CG leader, 6 km altitude 132

5.28 BFB of 8/20/2010, 03:25:57: CG leader, luminosity changes 134

5.29 BFB of 8/20/2010, 03:25:57: luminous branches 135

5.30 BFB of 8/20/2010, 03:25:57: video frames, attempted dart leader . . 137

5.31 BFB of 8/20/2010, 03:25:57: waveforms, dart leaders 139

5.32 BFB of 8/20/2010, 03:25:57: LMA, dart leaders 140

5.33 BFB of 8/20/2010, 03:25:57: waveforms, first dart leader 141

6.1 BFB flash of 7/23/2010 at 18:45:30: waveforms 148

6.2 BFB flash of 7/23/2010 at 18:45:30: LMA (time) 149

6.3 BFB flash of 7/23/2010 at 18:45:30: LMA (charge) 150

6.4 BFB flash of 7/30/2010 at 21:28:04: waveforms 152

6.5 BFB flash of 7/30/2010 at 21:28:04: LMA (time) 153

6.6 BFB flash of 7/30/2010 at 21:28:04: LMA (charge) 154

6.7 BFB flash of 8/6/2010 at 21:00:52: waveforms 156

6.8 BFB flash of 8/6/2010 at 21:00:52: LMA (time) 157

6.9 BFB flash of 8/6/2010 at 21:00:52: LMA (charge) 158

6.10 BFB flash of 8/16/2010 at 01:20:49: waveforms 161

6.11 BFB flash of 8/16/2010 at 01:20:49: LMA (time) 162

6.12 BFB flash of 8/16/2010 at 01:20:49: LMA (charge) 163

6.13 BFB flash of 8/16/2010 at 01:54:55: waveform 166

6.14 BFB flash of 8/16/2010 at 01:54:55: LMA (time) 167

6.15 BFB flash of 8/16/2010 at 01:54:55: LMA (charge) 168

6.16 BFB flash of 8/20/2010 at 04:07:09: waveforms 171

6.17 BFB flash of 8/20/2010 at 04:07:09: LMA (time) 172

6.18 BFB flash of 8/20/2010 at 04:07:09: LMA (charge) 173

6.19 BFB flash of 8/22/2010 at 21:50:47: waveforms 176
6.20 BFB flash of 8/22/2010 at 21:50:47: LMA (time) 177
6.21 BFB flash of 8/22/2010 at 21:50:47: LMA (charge) 178
6.22 BFB flash of 8/22/2010 at 22:37:07: waveforms 181
6.23 BFB flash of 8/22/2010 at 22:37:07: LMA (time) 182
6.24 BFB flash of 8/22/2010 at 22:37:07: LMA (charge) 183

A.1 Configuration of the Langmuir Laboratory LMA in 2010 191
A.2 Camera coordinate frame 204
A.3 Imaging of a subject on a camera sensor 207
A.4 Image coordinates on a camera sensor 208

B.1 Calibration of log-RF waveform 211

C.1 Airplane track of 7/23/2010 at 21:45 (LMA, 80 μs) 216
C.2 Airplane track and BFB flash on 7/23/2010 at 21:45 217
C.3 Airplane track on 7/23/2010 at 21:45 (detail) 218
C.4 BFB flash of 7/23/2010 at 21:45:53: LMA (source power) 219
C.5 Unconnected branches, 7/24/2010 at 04:16:01, frame 1 224
C.6 Unconnected branches, 7/24/2010 at 04:16:01, frame 2 224
C.7 Unconnected branches, 7/24/2010 at 04:16:01, frame 3 224
C.8 Unconnected branches, 7/24/2010 at 04:20:50, frame 1 224
C.9 Unconnected branches, 7/24/2010 at 04:20:50, frame 2 224
C.10 Unconnected branches, 7/24/2010 at 04:20:50, frame 3 224
C.11 BFB flash of 7/24/2010 at 04:16:01: LMA 225
C.12 BFB flash of 7/24/2010 at 04:20:50: LMA 226

List of Tables

3.1 BFB flash characteristics 34

3.2 BFB flash parameters: mean values 45

4.1 BFB flash of 8/2/2010, 20:58:11: leader velocities 87

5.1 BFB flashes of 8/20/2010 96

5.2 BFB flash of 8/20/2010, 03:25:57: branch current surges 133

C.1 Leader step length estimates of BFB flashes on 7/24/2010 221

List of Photos

5.1 Upward leader, 8/20/2010 at 02:56:42 UTC 89

5.2 Upward leader, 8/20/2010 at 03:03:28 UTC 90

5.3 BFB flash of 8/20/2010 at 03:25:57 UTC 97

6.1 BFB flash of 8/20/2010 at 04:07:09 UTC 169

C.1 BFB flash of 7/24/2010 at 04:16:01 UTC 222

C.2 BFB flash of 7/24/2010 at 04:20:50 UTC 223

D.1 BFB flash, 8/15/2002 229

D.2 BFB flash, 5/31/2007 229

D.3 BFB flash, 8/8/2007, #1 229

D.4 BFB flash, 8/8/2007, #2 229

D.5 BFB flash, 9/29/2007 at 04:37 UTC 230

D.6 BFB flash, 9/29/2007 at 06:27 UTC 230

D.7 BFB flash, 9/29/2007 at 07:05 UTC 230

D.8 BFB flash, 8/28/2008 230

D.9 BFB flash, 9/9/2009 at 04:43 UTC 231

D.10 BFB flash, 8/25/2009 at 02:38 UTC 231

D.11 BFB flash, 8/3/2010 at 04:02 UTC 231

D.12 BFB flash, 8/7/2010 at 03:35 UTC 231

D.13 BFB flash following cloud boundary 233

D.14 BFB flash following cloud boundary, 9/9/2008 at 04:16 UTC 233
D.15 BFB flash following cloud boundary, 7/23/2009 at 05:34 UTC 233
D.16 BFB flash following cloud boundary, 7/10/2010 at 03:22 UTC 233
D.17 BFB flash following cloud boundary, 8/3/2010 at 03:42 UTC 234
D.18 BFB flash following cloud boundary, 8/13/2010 at 02:52 UTC 234
D.19 BFB flash following cloud boundary, 8/20/2010 at 03:06:15 UTC . . . 234
D.20 BFB flash following cloud boundary, 8/20/2010 at 03:57:19 UTC . . . 234
D.21 Forked BFB flash, 9/29/2007 at 04:41 UTC 236
D.22 Forked BFB flash, 9/29/2007, time unknown 236
D.23 BFB flash within cloud, 7/19/2007 238
D.24 BFB flash within cloud, 8/5/2010 238
D.25 BFB flash within cloud, 8/13/2010 238
D.26 Attempted BFB flash, 9/9/2008 at 04:39 UTC 240
D.27 Attempted BFB flash, 7/23/2009 at 04:58 UTC 240
D.28 Attempted BFB flash, 7/23/2009 at 05:03 UTC 240
D.29 Attempted BFB flash, 7/23/2009 at 05:08 UTC 240
D.30 Attempted BFB flash, 8/3/2010 at 03:10 UTC 241
D.31 Attempted BFB flash, 8/5/2010 at 03:26 UTC 241
D.32 BFB flash with upward branch, 7/20/2007 at 04:28 UTC 243
D.33 BFB flash with upward branch, 7/20/2007 at 04:30:12 UTC 243
D.34 BFB flash with upward branch, 9/9/2008 at 03:52 UTC 243
D.35 BFB flash with upward branch, 8/31/2010 at 05:24:25 UTC 243

Acronyms

A/D	Analog-to-digital
BFB	Bolt from the blue
CG	Cloud-to-ground
–CG	Cloud-to-ground lowering negative charge
+CG	Cloud-to-ground lowering positive charge
DU	Digitizer units
ECEF	Earth-centered, earth-fixed
EFM	Electric field mill
FA	Fast antenna
FFT	Fast Fourier transform
FPS	Frames per second
GPS	Global Positioning System
IC	Intracloud
GJ	Gigantic jet
LDAR	Lightning Detection and Ranging
LL	Langmuir Laboratory
LMA	Lightning Mapping Array
MS	Mega-samples
MSL	(Above) mean sea level
NLDN	National Lightning Detection Network
NMT	New Mexico Tech
RF	Radio frequency
SA	Slow antenna
TLE	Transient luminous event
UTC	Coordinated universal time
VHF	Very high frequency
WGS84	World Geodetic System (1984)
WSMR	White Sands Missile Range

1. Introduction

A large variety of electrical discharges (lightning flashes) are known to occur in and near thunderstorms.

Cloud-to-ground (CG) lightning is a collective name for electrical discharges that interact between the cloud and ground, effectively removing some amount of charge from the cloud [*Uman*, 1984; *Rakov and Uman*, 2002]. Such flashes can either initiate in the cloud and propagate downward to ground, or initiate at ground and propagate upward into the cloud. (More rarely, bidirectional CG flashes may develop from an object such as an aircraft between the cloud and ground.) Cloud-to-ground flashes lowering negative charge from the cloud to ground are most common and are referred to as negative CG or –CG flashes.

Intracloud (IC) lightning refers to a class of electrical discharges that occur within a cloud. These flashes are more difficult to study because the leaders usually cannot be observed visually and positioning instruments at close proximity to intracloud lightning is a challenging task. With the advent of interferometry [e.g. *Rhodes et al.*, 1994; *Shao and Krehbiel*, 1996] and 3D VHF lightning mapping techniques [e.g. *Proctor*, 1981; *Rison et al.*, 1999; *Thomas et al.*, 2004] the nature and general characteristics of these flashes are now better understood.

Normal-polarity thunderstorms generally have a tripolar charge structure with upper positive charge over midlevel negative charge, and a lower positive charge region near the base of the cloud [e.g. *Williams*, 1989; *Marshall and Stolzenburg*, 1998]. The electric field strength within the cloud is largest at the interfaces between these three regions, and according to this simplified model there are therefore two areas where lightning can be expected to initiate within a storm. IC flashes initiate between the midlevel negative and upper positive charge regions, developing upward negative and downward positive leaders in a bidirectional manner [e.g. *Ogawa and Brook*, 1964]. Discharges that occur between the midlevel negative and lower positive charge regions are usually referred to as *low-altitude intracloud flashes*. If the negative leader of a low-altitude IC flash proceeds to ground, a return stroke occurs and the flash becomes a –CG flash.

Transient luminous events (TLE) are a recently discovered class of electrical dis-

charges that occur between thunderstorm tops and the ionosphere [e.g. *Pasko*, 2010]. These include *blue starters* and *blue jets* [e.g. *Wescott et al.*, 1995, 1996] which initiate within a thunderstorm and escape from the cloud top to reach terminal altitudes of up to 40–50 km, as well as *gigantic jets* (GJ), which propagate upward to the ionosphere [e.g. *Pasko et al.*, 2002; *Su et al.*, 2003].

Although IC and –CG flashes are now fairly well understood and studied, *bolt-from-the-blue* (BFB) flashes have received comparatively little attention and have not been understood at all until only recently, when three-dimensional lightning mapping techniques were developed [*Rison et al.*, 1999]. Unlike normal –CG flashes, which initiate between the midlevel negative and lower positive charge regions and exit the cloud through the cloud base, BFB flashes initiate between the midlevel negative and upper positive charge regions and exit the cloud at the side. Both normal –CG flashes and BFB flashes produce leaders to ground that are of negative polarity and their net effect on the storm is the same, namely, the removal of negative charge from the cloud to ground.

Krehbiel et al. [2008] provided a unifying view of how upward electrical discharges (blue jets and gigantic jets) may escape from a thunderstorm by using both modeling and observational studies. In doing so, it became clear that BFB flashes appear to be closely related to GJs. Notably, they showed that GJs and BFB flashes may result from a depletion of upper positive charge, due to the acquisition of screening charge by the storm. It is also suggested that blue starters and blue jets (likely being a single phenomenon, but with different vertical development) initiate between the upper positive charge region and a negative screening charge layer blanketing the storm top, and may in fact be triggered by the occurrence of a –CG flash which enhances the electric field between these two charge layers. *Edens* [2011] has since reported visual and LMA observations of a blue starter that occurred during a –CG flash, confirming that such phenomena are screening-layer discharges between upper positive and screening negative charge and can be triggered by –CG flashes. Blue starters and blue jets are expected to occur when there is a layer of screening charge that does not mix in well with the upper positive charge region. BFB flashes, on the other hand, would be expected to occur when the upper positive charge region is depleted, indicating efficient mixing. The apparent scarcity of blue starters and blue jets in comparison to the relative abundance of BFB flashes indicates that negative screening charge normally tends to mix in with the upper positive charge region, at least to some extent.

The occurrence of BFB flashes thus indicates an imbalance of midlevel negative and upper positive charge, much like the occurrence of a regular –CG flash indicates an imbalance between midlevel negative and lower positive charge.

The phrase *bolt from the blue* (or *bolt out of the blue*) may have originated from the fact that this type of lightning often contacts ground relatively far from a storm's

core downdraft, often at a location that has in fact blue sky overhead. Because of this, it almost always comes as a complete surprise to anyone in the immediate vicinity of the strike location and therefore poses a major danger to those who are outdoors. The phrases *bolt from the blue* and *out of the blue* have in fact entered the English language as idioms, in referring to something that comes as a surprise.

Apart from the safety aspect, BFB flashes are interesting to study because they are the only type of lightning where a high-altitude negative leader can be observed visually or photographically, often against a clear-sky background. Negative leaders from BFB flashes can exit the cloud at 8 km altitude or higher, which is comparable to one scale-height of atmosphere, and the lower air pressure makes these leaders behave differently from those at or near sea level. As will be shown in this work, a negative leader propagating downward responds to the increase in air pressure by transitioning from impulsive breakdown (characteristic of intracloud flashes) to apparently continuous breakdown associated with normal cloud-to-ground flashes at low altitude.

In this work the general morphology and leader characteristics of BFB flashes are studied. This is done by using data from New Mexico Tech's Lightning Mapping Array (LMA), broadband electric field recordings, high-speed video and photographic observations.

Chapter 2 introduces BFB flashes from a purely observational standpoint to give an overview of their basic characteristics. Chapter 3 introduces BFB-flash data from remote-sensing instruments (LMA and broadband electric field waveforms) and places them in context with other common flashes in normal-polarity thunderstorms. It also discusses general characteristics of BFB flashes, including flash duration, initiation altitude, number of strokes to ground, cloud-to-ground leader "reach", and the effect of wind shear on the cloud exit region of BFB flashes. Chapters 4 and 5 are detailed case studies of two BFB flashes using LMA, waveform and high-speed video data; Chapter 4 studying the various components of a BFB flash and Chapter 5 focusing on characteristics of high-altitude negative leaders. Chapter 6 discusses eight other BFB flashes in less detail, to illustrate the similarities and differences between various BFB flashes.

In this work, *high altitude* refers to altitudes of 8–12 km above MSL, which generally correspond to the upper positive charge region in New Mexico thunderstorms. *Mid-level* altitudes indicate altitudes of 5–8 km, typically including the midlevel negative charge region, while *low level* or *low altitude* refers to altitudes below 5 km MSL. All times and dates are in coordinated universal time (UTC) unless indicated otherwise.

2. Visual observations

2.1 Introduction

BFB flashes are often spectacular and readily observed visually once one knows what to look for. Numerous BFB flashes were observed and photographed by the author over the course of several summers at Langmuir Laboratory (from 2006 to 2010). These observations are important because the electric field waveforms and LMA data discussed later in this work generally do not give a complete picture of the characteristics of the storm and the state of the atmosphere in which BFB flashes occur. It is therefore helpful in interpreting these data to have a general background of the visual characteristics of BFB flashes, which will be discussed here.

2.2 Occurrence

BFB flashes appear to be quite common in the state of New Mexico as well as elsewhere. Most thunderstorms (both single-cell airmass storms and larger storm complexes) will often produce one or more BFB flashes during their lifetime.

Visual observations of BFB flashes are often impaired due to the fact that leaders of BFB flashes usually do not exit the cloud completely when at mid–high altitudes but remain near or within the cloud boundaries until they appear below the cloud base. One (uncertain) way to visually tell a BFB from a regular CG flash in this case is to observe the leader below the cloud base off to the side of the area around the main precipitation shaft, to which regular cloud-to-ground lightning is usually confined. During the evening and nighttime hours, BFB flashes can also be identified visually by observing the initial intracloud stage of the flash, which is usually detectable just before the bright return stroke from the cloud-to-ground leader occurs.

In addition to the cloud obscuring the high-altitude part of a BFB flash, BFB flashes may exit the cloud away from the observer, or—more often than not—midlevel and low-level ancillary clouds prevent an unobstructed view of the storm. These factors

make the observation of a BFB leader along its full path to ground a fairly uncommon occurrence.

2.3 Visual observations

Several years of visual observations of BFB flashes and their parent storms have yielded the following observations, which appear to be somewhat consistent. It is emphasized that these observations are purely visual and therefore anecdotal in nature, and not deduced from the electric field and LMA data discussed in the following chapters.

Weak convection: BFB flashes are likely to occur in slow-growing, single-cell localized thunderstorms when these are relatively young. Already the second (or even the first) discharge in a new maturing storm can be a BFB flash, usually following an initial intracloud discharge.

Stronger convection: BFB flashes are also likely in more vigorous thunderstorms in a high-wind-shear environment. They do occur in strong convection as well, but appear to be less common.

Atmospheric conditions: On some days, BFB flashes appear to be the main carrier of negative charge to ground, while regular –CG flashes seem to be rare; on other days, BFB flashes appear not to occur at all. In other words, storms can be almost exclusively IC/CG producers, exclusively IC producers, or IC/BFB producers, indicating that the state of the atmosphere has some effect on conditions that are favorable for BFB flashes.

Attempted BFB flashes: Storms that become predominantly IC/BFB producers often change to "BFB mode" with the production of one or more cloud-to-air discharges that are the result of a negative intracloud leader leaving the cloud. They can range from a few hundred meters to several kilometers in length outside the cloud. They tend to occur near the same region (flank) of the storm as later BFB flashes and are therefore a convenient indicator of impending BFB activity in a storm. An estimated 5–10% of BFB flashes are such cloud-to-air flashes and will be referred to as *attempted BFB flashes* or *cloud-to-air discharges*.

Multiplicity: Small, single-cell thunderstorms generally do not produce more than three to five BFB flashes over their lifetime of 30 minutes to one hour, after which the storm generally either dies or organizes itself into a larger multicell system that changes to predominantly IC and normal –CG lightning.

Succession: BFB and IC flashes tend to alternate; while several IC flashes may occur in succession, BFB flashes generally do not succeed each other.

Wind shear: When wind shear causes a thunderstorm to be asymmetric, with the anvil shearing off the main body of the storm, BFB flashes tend to occur on the upwind side or flanks of the storm. They are not observed downwind, under the main anvil region. Often, a sheared storm has a shelf-like cloud on the upwind side at the height of the cloud base, through which BFB flashes tend to propagate.

Dart leaders: A small fraction of BFB flashes are visually observed to have multiple return strokes (i.e. dart leaders), and an even smaller fraction appear as forked lightning (i.e. a dart-stepped leader occurs, where a dart leader diverts from a preexisting channel and becomes a new stepped leader).

Brightness and thunder: BFB flashes produce relatively bright return strokes and loud thunder.

2.4 Photographic observations

From the study of photographs a few additional observations can be made of BFB flashes. Thirty-five photographs are reproduced in Appendix D to illustrate the general morphology of BFB flashes. Some of these photographs will be referred to in the following list of observations. Since these observations are deduced from still photographs, some may duplicate the visual observations from the previous section.

Branching: Almost invariably, BFB leaders lack branches at higher altitudes (above 6 km), becoming profusely branched with more tortuous channels while they propagate to lower altitudes. Photos D.4, D.10, and D.14 show this phenomenon of branching clearly, and Photo D.7 shows the change in tortuosity as the leader propagates downward to ground.

Upward leaders: It is not uncommon for BFB flashes to produce an upward leader that emerges from the top (or near the top) of the storm. This leader may propagate upward for several hundred meters to several kilometers. Photographs that show upward leaders are Photos D.32, D.33, D.34 and D.35.

Multi-channel: As mentioned in Section 2.3, some BFB flashes appear *forked* in photographs, meaning that they exhibit multiple channels to ground that share a common high-altitude leader channel (see Photos D.21 and D.22). Since it is unlikely that two branches of the stepped leader contact ground simultaneously over such long distances of propagation, this indicates that—like regular –CG

flashes—BFB flashes can produce multiple strokes to ground. This will be confirmed in the following chapters.

Low-level horizontal development: BFB flashes sometimes produce a low-level horizontal branch that proceeds to propagate near the cloud base or through precipitation. Photo 6.1 in Section 6.7 shows such a BFB flash.

Following cloud boundary: Cloud-to-ground leaders of BFB flashes often follow the cloud boundary for some distance as they propagate down to ground (Photos D.9, D.13, D.14, D.19 and D.20). This indicates that there may be positive screening charge at the cloud boundary in response to the midlevel negative charge region.

Following cloud shelf: In addition to following cloud boundaries, BFB flashes may also propagate along a "cloud shelf": Low-level convection which often develops at the upwind side of a storm. Photos D.8, D.15, D.23 and D.24 show this effect.

Cloud-enshrouded: Some BFB flashes remain mostly in the cloud along their path to ground, only emerging from underneath the cloud base like a regular –CG flash. When storms are photographed from a distance, the flash can usually be identified as a BFB flash by small sections of branches at high altitude which are seen to "bridge" cloud turrets, as well as the general in-cloud illumination at high altitude, indicative of intracloud activity in upper positive charge. Photos D.24, D.33 and D.34 are examples of such cloud-enshrouded BFB flashes.

Preference to upwind side of storm: When the anvil of a storm is laterally displaced from the storm by wind shear, BFB flashes tend to occur at the upwind side of the storm, or at either flank, but not under the downwind anvil. Photos D.8, D.11, D.13 and D.19 illustrate this apparent dependence on wind shear.

Attempted BFB flashes: Attempted BFB flashes—at least those with the negative leader terminating in clear air outside the storm cloud—tend to be erratic in their direction of propagation shortly before terminating (Photos D.26–5.2). Some attempted BFB leaders also propagate upward for several kilometers before stopping (Photos D.27, D.29, D.31 and 5.2).

Visible streamers at leader tip: Attempted BFB flashes that terminate in clear air have visible streamers, blue to purple in color, at the tips of the main leader and its branches. These streamers can be imaged with a still-camera set at high sensitivity. Photos D.27 and 5.2 show such cloud-to-air leaders with streamers attached to the leader tips; Section 5.3 discusses a close-up image of these streamers.

These general observations will be augmented by a statistical analysis of BFB flash characteristics in the next chapter. Using data from the LMA and broadband electric

field waveforms, 59 flashes are studied in more detail. The apparent preference of BFB flashes for the upwind side of storms is also discussed, as well as the multiplicity of strokes to ground in BFB flashes. High-altitude leader characteristics will be studied in Chapters 4 and 5; Chapter 5 also discusses leader stepping, branching and channel tortuosity, and streamers at leader tips of attempted BFB flashes.

3. General remote-sensing observations

3.1 Introduction

Waveform and LMA data of a total of 59 BFB flashes were recorded during the summer monsoon of 2010 in New Mexico. (The LMA recorded many more.) The main characteristics of these 59 flashes will be discussed in this chapter. This chapter also serves as a general introduction to the waveform and LMA data of the BFB flashes that will be studied in detail in the following chapters. An overview of the instrumentation used in these studies is given first.

3.2 Instrumentation

A full description of the instrumentation is given in Appendix A. Here, the various instruments that are pertinent to this chapter will be briefly outlined.

3.2.1 LMA

The data from the Langmuir Laboratory Lightning Mapping Array (LMA) are of key importance in these studies. In 2010 the Langmuir LMA was composed of 17 stations, two of which were co-located at the Annex of Langmuir Laboratory together with the other instruments. The stations were operated in 10 μs mode, with each individual station time-tagging peak-power events in successive 10 μs-long windows with 40 ns resolution [*Rison et al.*, 1999; *Thomas et al.*, 2004]. All stations in 2010 (except one of the two co-located stations) operated at a center frequency of 63 MHz with a bandwidth of 6 MHz.

All LMA data used in this work was processed at the full data rate (10 μs mode), unless noted otherwise.

3.2.2 Log-RF radiation

One of the most useful waveforms to study radio-frequency (RF) emissions of lightning is that of received power. This is a waveform of logarithmically-detected VHF radiation at some bandwidth and center frequency. Here the center frequency is chosen to be 63 MHz with a bandwidth of 6 MHz, identical to that of the LMA stations. Because the waveform is logarithmic in amplitude, weak VHF emissions from lightning can be seen as well as strong emissions. The log-RF waveform in the following studies was derived from the LMA station situated at the Langmuir Laboratory Annex building, which was also taking data (performing peak-detection on the log-RF waveform) normally.

The Annex LMA station suffered from large-amplitude background noise generated by various electrical equipment in the laboratory. This reduced its sensitivity to (typically) -65 to -70 dBm of received power. VHF emissions were therefore not recorded by this station when their received power was much lower than this threshold. That said, the station was still quite useful, since most of the BFB flashes studied here occurred at close range to the laboratory.

The log-RF waveforms presented here are generally plotted as a two-dimensional colored histogram, indicating the density of samples in a particular area of the plot. The areal density of samples is itself color-coded logarithmically, with red indicating the highest density and purple the lowest density. Plotting the log-RF waveform as a histogram is preferred because it conveys more information about the waveform than plotting it as a simple curve, which would only show the waveform envelope in larger time intervals. When a short time interval of the log-RF waveform is plotted in the following chapters, it is generally plotted as a scatter plot of individual samples.

3.2.3 Slow and fast antennas

A set of slow and fast ΔE antennas were operated at the Annex observation deck of the laboratory. The slow antenna is sensitive to all electric field changes that occur faster than the relaxation time constant of the instrument (10 seconds) and up to 1 MHz. The fast antenna has a relaxation time constant of 0.1 ms and detects the faster, smaller-amplitude electric field changes well. It, too, is sensitive to field changes up to 1 MHz.

The waveforms of the slow and fast antennas were sampled along with the log-RF waveform with a single four-channel digitizer, which was normally operating at 25 MS/s.

3.2.4 Broadband waveforms and spectrograms

The spectrograms used in this work are derived from the waveform data of two broadband antennas that were also installed on the observation deck of the Annex building. One antenna, a Rohde & Schwarz HE010 monopole antenna, is sensitive to RF electric field changes from 10 kHz up to 80 MHz (Section A.4). The other antenna is of a biconical design, having a single downward-pointing cone, a horizontal disc and a top vertical element, and is sensitive to frequencies between 25 and 1300 MHz (Section A.5). Both antennas were low-pass filtered at 100 MHz and digitized at 200 MS/s with a single two-channel digitizer.

Spectrograms, which indicate the spectral density (power) of RF emissions as a function of frequency and time, can be calculated from the broadband waveforms and provide much more information than the waveform plotted in the amplitude–time domain. The calculation and image processing of the spectrograms is discussed in more detail in Section A.6.

3.2.5 Sign convention for electric field

Throughout this work the physics sign convention is used, which is opposite to the atmospheric electricity (potential gradient) convention. In the physics sign convention, a negative change in electric field corresponds to the removal of negative charge overhead (i.e. from a location nearby the instrument), or equivalently, the addition of positive charge. Since all instruments used in these studies are ground-based and the electric field is practically perpendicular to the surface, all electric field measurements represent the vertical component E_z of the vector electric field $\mathbf{E}$. Whenever the term "electric field" is used in the text in regard to the waveform data, it refers to the vector component E_z, and if a field change is referred to as ΔE in the text, a change in E_z is indicated; the other two Cartesian components E_x and E_y are not measured at the ground. The field changes detected by the slow antenna are referred to as ΔE, while the changes detected by the fast antenna are generally referred to as *fast* ΔE.

3.3 Common types of lightning

In a normal-polarity thunderstorm four types of flashes commonly occur (Figure 3.1). These are the negative cloud-to-ground (–CG), the classic bilevel intracloud (IC), the low-altitude intracloud, and the bolt from the blue (BFB) flash. Sometimes—either in inverted-polarity storms, or during the dissipative stage of larger normal-polarity

thunderstorms—positive cloud-to-ground (+CG) flashes may also occur, but these are not commonly observed in the small, localized thunderstorms in New Mexico.

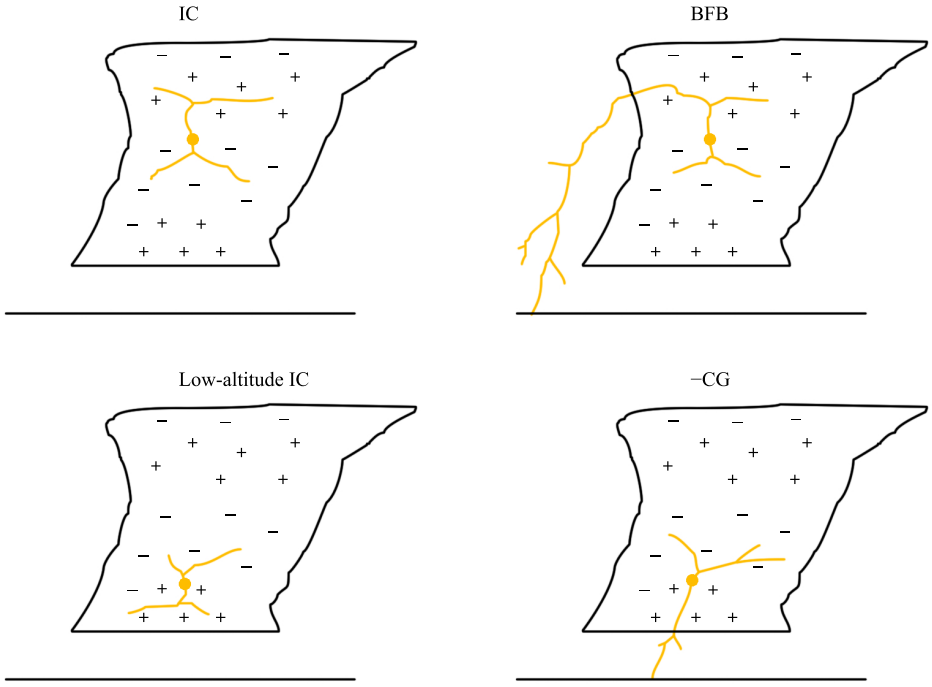

Figure 3.1: Four types of lightning commonly observed in New Mexico thunderstorms, with inferred charge structure. Top left, a classic bilevel IC flash; top right, BFB flash; bottom left, low-altitude IC flash; bottom right, –CG flash. Approximate initiation points of all flashes are indicated by a dot. A negative screening charge near the cloud top is also indicated, sometimes capable of producing blue jets or blue starters (not shown). The initiation regions, general appearance and extent of all flashes is based on interpretation of LMA data.

All four types of flashes occur between two adjacent charge regions within the cloud. Low-altitude IC and –CG flashes initiate between the midlevel negative charge and lower positive charge regions. When this lower positive charge is relatively small in magnitude the negative leader may leave the cloud and propagate to ground, resulting in a –CG flash.

A classic bilevel IC flash initiates between midlevel negative and upper positive charge [e.g. *Shao and Krehbiel*, 1996; *Rison et al.*, 1999]. In analogy to the –CG flash developing from a low-altitude IC flash, an IC flash can evolve into a BFB flash if the upper positive charge is small in magnitude (depleted) with respect to the midlevel negative charge [*Krehbiel et al.*, 2008]. The negative leader may then exit the cloud, typically at an altitude of 8–10 km in localized monsoonal thunderstorms,

and propagate to ground either outside or partially within the cloud boundary. In a normal-polarity thunderstorm a BFB flash therefore lowers negative charge to ground, contrary to what one might expect based on the fact that it emerges from the cloud near the positively charged anvil. Therefore, BFB and –CG flashes have the same effect of discharging the midlevel negative charge region to ground, leaving the storm at a more positive electric potential.

These four types of flashes each produce characteristic ΔE waveforms and similarly characteristic VHF signatures, in particular BFB flashes. The following sections show example data for each flash type to illustrate this.

3.3.1 Negative CG flash

This example of a –CG flash is shown to illustrate the characteristic waveforms associated with a low-altitude negative stepped leader and associated return strokes.

Figures 3.2 and 3.3 show waveform and LMA data for the –CG flash. Figure 3.2 shows the first 350 ms of waveform data of the flash, which lasted about 1.7 seconds (Figure 3.3). Like most –CG flashes, this flash initiated at 5–6 km altitude between the midlevel negative and lower positive charge regions.

The first panel in Figure 3.2 shows a log-RF waveform of 63 MHz VHF emissions at a bandwidth of 6 MHz. The waveform is reproduced as a two-dimensional histogram of the areal density of samples in the plot panel, scaled logarithmically. Red indicates a high density of samples while purple indicates a low density. For large time intervals, plotting the log-RF waveform as a density-histogram is preferred to plotting the waveform by individual samples, which would only show the waveform envelope. The second panel in the figure shows VHF sources located by the LMA, colored by charge. Red VHF sources are from negative breakdown propagating in positive charge, while blue VHF sources are associated with positive breakdown in negative charge. Green VHF sources indicate negative breakdown in undetermined charge, which may or may not occur outside the cloud. The third and fourth panels show slow and fast ΔE waveforms and the fifth and sixth panels are two spectrograms of the broadband waveform data. The spectrograms show the intensity or power of VHF emissions as a function of frequency and time, with black indicating low-power, and white, high-power VHF emissions.

The slow and fast ΔE waveforms indicate that the flash produced 10 or 11 strokes to ground during the first 350 ms. Each return stroke is associated with a large-amplitude fast ΔE pulse. Some of these pulses are of negative polarity (from return strokes after a stepped leader), or bipolar (from return strokes following a dart leader). Two stepped leaders occurred: one at 0.646–0.658 seconds past 23:47:57,

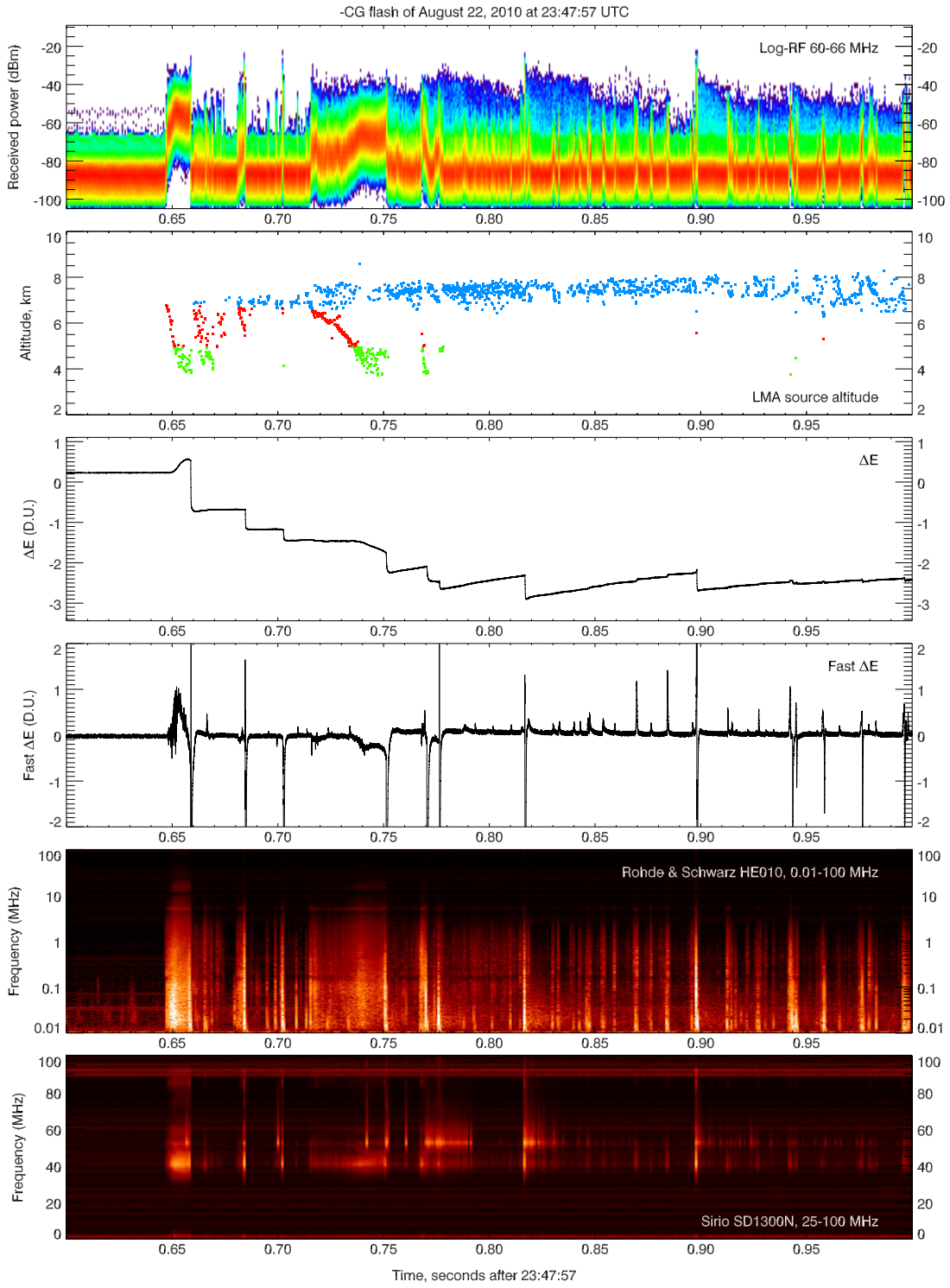

Figure 3.2: Waveforms for the –CG flash of August 22, 2010 at 23:47:57 UTC. The plotted time interval is 400 ms. From top to bottom: Log-RF, VHF source altitude (colored by charge), ΔE, fast ΔE, spectrogram of Rohde & Schwarz HE010 antenna (0.01–80 MHz), and spectrogram of Sirio SD1300N biconical antenna (25–100 MHz).

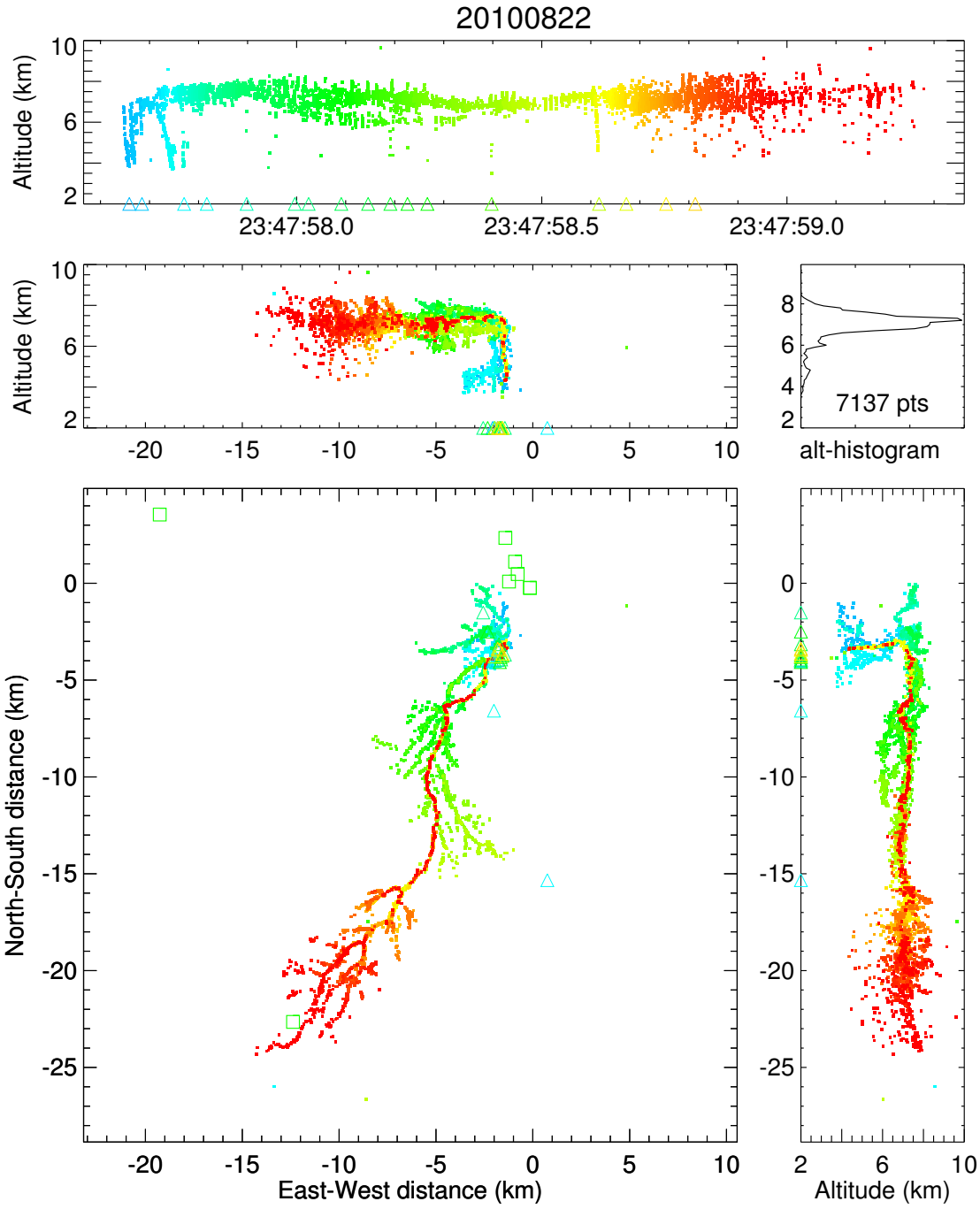

Figure 3.3: VHF sources located by the LMA for the –CG flash of August 22, 2010 at 23:47:57 UTC. The sources are colored in time from blue (earlier) to red (later). Strokes to ground located by the NLDN are indicated by triangles. The coordinate origin is at the Annex of Langmuir Laboratory.

which was approaching the instrument, and a second leader at 0.715–0.750 seconds past 23:47:57, away from the instrument.

The log-RF waveform shows *apparently continuous* VHF emissions during the two time intervals during which the negative leaders were developing to ground. Later on in time, a number of short-duration pulses are observed, which are associated with strong VHF emissions by dart leaders to ground. The apparently continuous VHF emissions from the negative breakdown as well as those from the various dart leaders are also clearly seen in both spectrograms.

In this work, these apparently continuous VHF emissions will also be referred to as "near-continuous" or "more continuous" (as opposed to more impulsive). The emissions are not continuous at all, but negative breakdown from the stepped leaders of –CG flashes produces strong VHF emissions at such a high rate that the log-RF waveform is lifted off the background and gives the appearance of continuous VHF emissions.

The continued breakdown that is located by the LMA in the midlevel negative charge region is associated with fast negative breakdown along paths of previous, undetected, weak positive leaders. This type of retrograde negative breakdown is called *K-breakdown* or *K-events* [*Kitagawa and Brook*, 1960], which carry negative charge back along the positive leader channels toward the base (starting point) of the negative leader channel to ground. These K-events can initiate new negative breakdown along those leader channels as *K-leaders*, which are identical to dart leaders [*Shao et al.*, 1995].

A number of K-events can be seen in the ΔE and fast ΔE waveforms during the interstroke time intervals in Figure 3.2, for example at 0.82–0.90 seconds past 23:47:57. A number of fast ΔE pulses of positive polarity occur at this time, indicating K-events that do not result in a dart leader to ground.

The flash developed in a SSW direction with extensive breakdown in the midlevel negative charge region, transporting negative charge back toward the source region by K-leaders that went to ground as dart leaders (Figure 3.3). Some of these leaders are well-mapped by the LMA and are visible as VHF sources that retrace the established channels to ground.

In this example, positive breakdown is occurring at higher altitudes than negative breakdown, further distant from the instruments. VHF emissions from positive breakdown are also intrinsically weaker than those of negative breakdown [*Shao et al.*, 1999]; *Thomas et al.* [2001] found that VHF emissions associated with positive breakdown, which are located by the LMA, are weaker by at least an order of magnitude. Therefore, the strong VHF emissions observed during the stepped leader stage in this –CG flash are usually associated with negative breakdown from the stepped leader.

3.3.2 IC flash

The classic bilevel intracloud flash is by far the most common type of flash in most New Mexico monsoonal storms. In typical normal-polarity storms it initiates near 7–8 km altitude between the upper positive and midlevel negative charge regions as an upward negative leader [*Liu and Krehbiel*, 1985], producing VHF sources that tend to be mapped quite well by the LMA. This negative leader may propagate upward several kilometers into upper positive charge, where it typically changes direction to more horizontal. Concurrent with this negative breakdown, positive breakdown occurs in the midlevel negative charge region, which usually only becomes apparent in LMA data after a short delay in activity.

Figure 3.5 is an example of a normal-polarity intracloud flash as mapped by the LMA that illustrates this delay. It is a good example of the bilevel structure of an intracloud flash, with (in this case) an upward connective channel $\sim$ 3 km in length.

Figure 3.4 shows the accompanying waveform data for this flash, with the ΔE waveform being typical for an intracloud flash at close range (within the reversal distance for the electric field). The electric field changes to more negative, indicative of negative charge receding (i.e. increasing in altitude) from the instrument. More notably, the VHF emissions during the leader development are very different from those shown earlier for the –CG flash. The emissions and fast ΔE changes are more impulsive and intermitted in nature, as is evident from the log-RF and fast ΔE waveforms as well as both spectrograms.

The exact cause of the delay between the onset of negative breakdown and detected positive breakdown is as yet unknown. A generally accepted idea is that lightning leader development occurs in a bidirectional, bipolar manner [e.g. *Kasemir*, 1960; *Mazur*, 1989]. However, interferometric studies of an IC flash by *Shao and Krehbiel* [1996] show no hints of positive breakdown for the first $\sim$ 100 ms of the flash. After a short delay from the onset of negative breakdown, K-events begin to occur along the channels of undetected positive breakdown, which tend to be located quite well by the LMA [*Rison et al.*, 1999].

In some IC flashes, K-events during the later stage of the flash can produce *K-leaders* that propagate upward along the previous channel [e.g. *Ogawa and Brook*, 1964; *Rhodes et al.*, 1994], in full analogy to dart leaders in –CG flashes which propagate down to ground [*Shao and Krehbiel*, 1996]. These K-leaders carry negative charge upward and are usually mapped by the LMA as several (or even a large number of) VHF sources, depending on the residual conductivity of the channel. They are also detected as fast step changes in the electric field, termed *K-changes*. The flash in this example shows a single K-change toward the end of the flash, associated with a K-leader that is observed in all waveforms.

Although this example treats a single intracloud flash, all intracloud flashes at similar

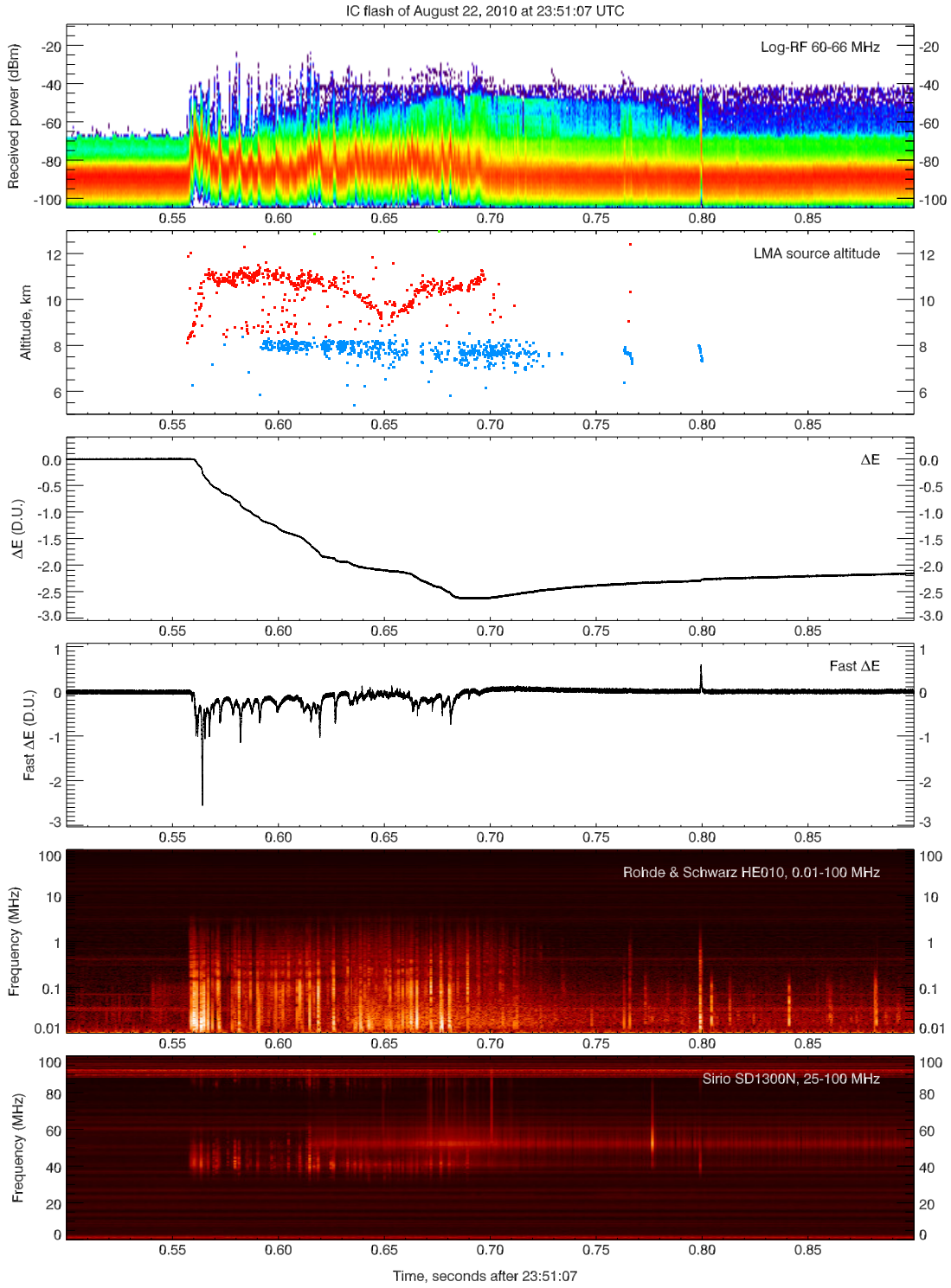

Figure 3.4: Waveforms for the IC flash of August 22, 2010 at 23:51:07 UTC. The plotted time interval is 400 ms.

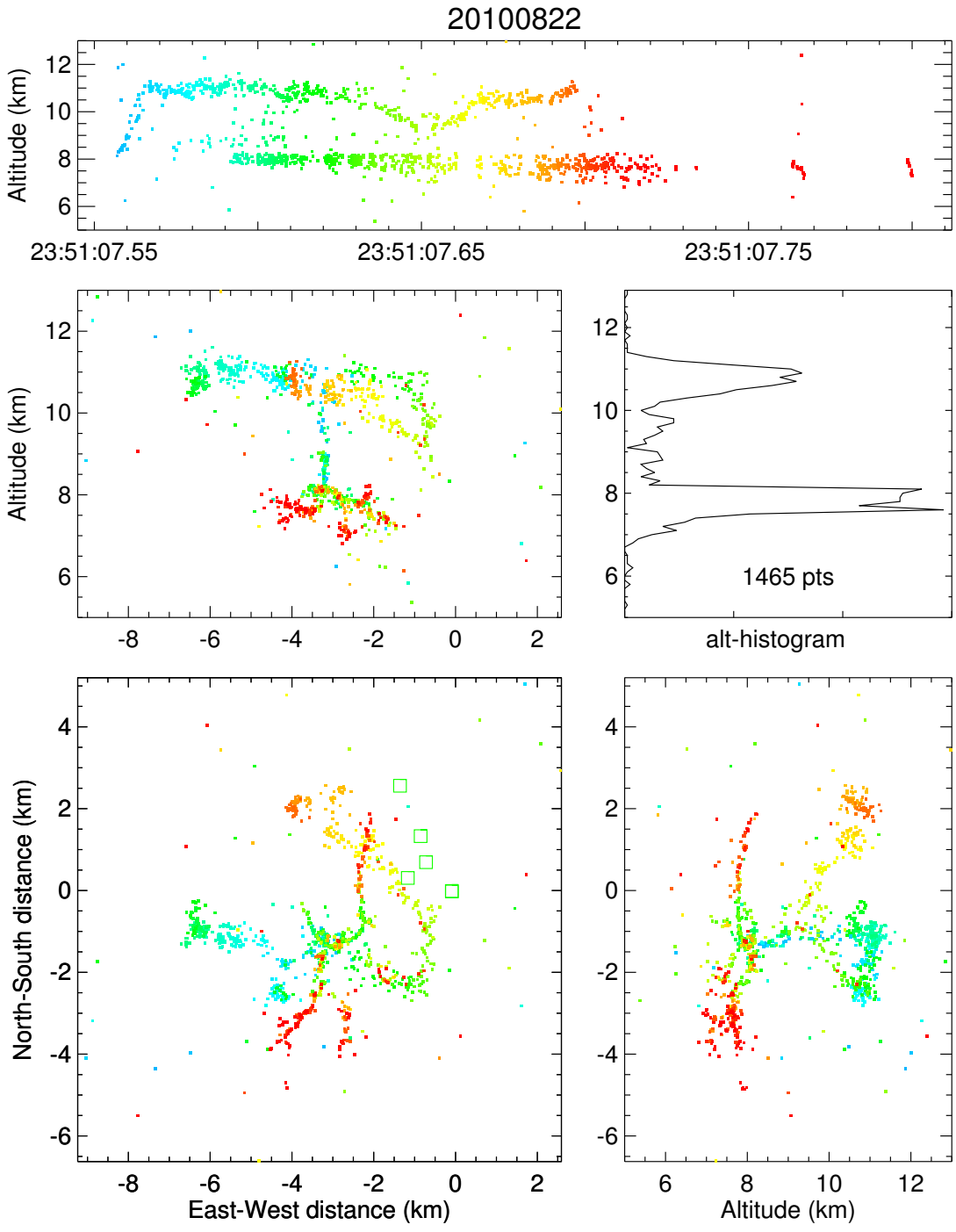

Figure 3.5: VHF sources located by the LMA for a classic bilevel intracloud flash on August 22, 2010 at 23:51:07 UTC.

altitudes that the author has studied exhibit this impulsiveness in VHF emissions. More than a thousand of these common flashes have been observed (with LMA and waveform data) at Langmuir Laboratory during 2006–2010, and all tend to show this impulsive VHF signature to some degree, which is clearly different from that produced by low-altitude leaders.

3.3.3 BFB flash

The effect of altitude (and therefore pressure) on leader behavior can be studied quite well with BFB flashes, since these initiate as an IC flash where the negative leader evolves into a cloud-to-ground leader. This leader typically covers (in typical New Mexico storms) an altitude range up to or over one scale height of atmospheric pressure (roughly 7.5–8.5 km depending on air temperature). Therefore, the leader propagating to ground might be expected to show some kind of transition if leader propagation is affected by air pressure. Such an effect is indeed observed in BFB flashes, and manifests itself as a transition from more impulsive to more continuous VHF emissions from the negative stepped leader as it propagates to lower altitude. This transition is one of the key topics of study in this work.

The LMA data of the flash in Figure 3.7 show a typical BFB flash which occurred on August 22, 2010, 36 km to the northeast of the laboratory. In comparing this figure to Figure 3.5 of the IC flash example, it is clear that the leader that evolves into a cloud-to-ground leader is of negative polarity. In this figure the VHF sources are color-coded by charge, not by time, to indicate the sign of the space charge through which the various leaders propagated. Blue indicates negative charge, red indicates positive charge, and green indicates undetermined charge, which could be outside the cloud. (This flash is also discussed in Section 6.8, and Figure 6.20 shows the flash with VHF sources colored in time.)

The transition from impulsive to apparently continuous VHF emissions associated with negative breakdown is documented well in the log-RF waveform during the initial 75 ms of the flash (Figure 3.6, first panel, between 0.960 and 1.035 seconds past 21:50:47). Two observations regarding this transition are pointed out here. First, the transition in VHF emissions by the leader appears to occur gradually, with a steady increase in *average* received power. This is visualized as the "lifting" of the highest sample-density band (colored red) off the background level in the log-RF waveform. Second, although the average received power increases, the maximum received power does not increase to any significant degree, staying at or below -40 dBm of received power for this particular station. Since the flash is far from the instruments relative to its extent, the received power is not affected to any significant degree by the leader propagating toward or away from the LMA station, since a change in distance gives a negligible change in received power for successive VHF sources of equal power at

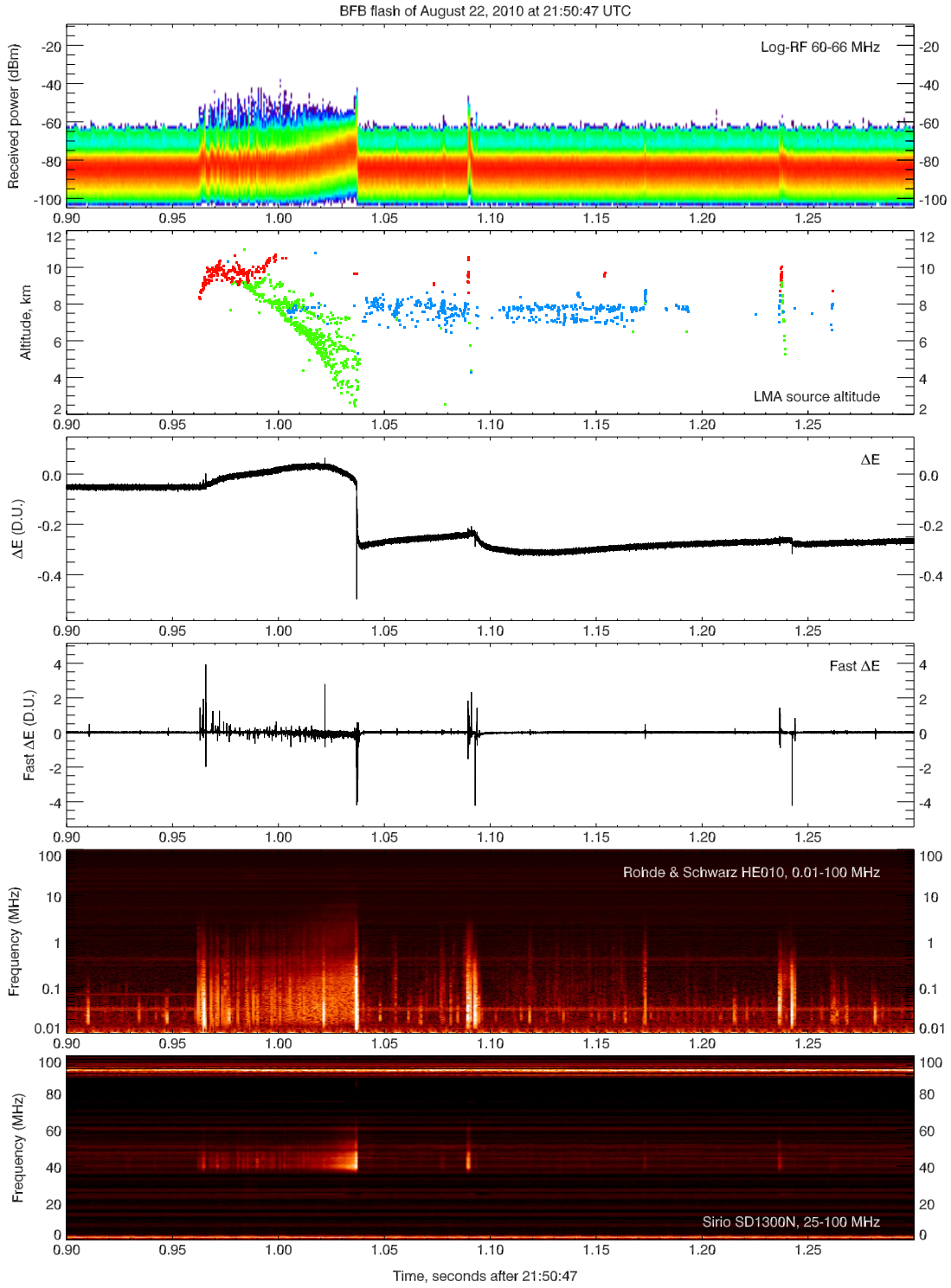

Figure 3.6: Waveforms for the BFB flash of August 22, 2010 at 21:50:47 UTC. The plotted time interval is 400 ms.

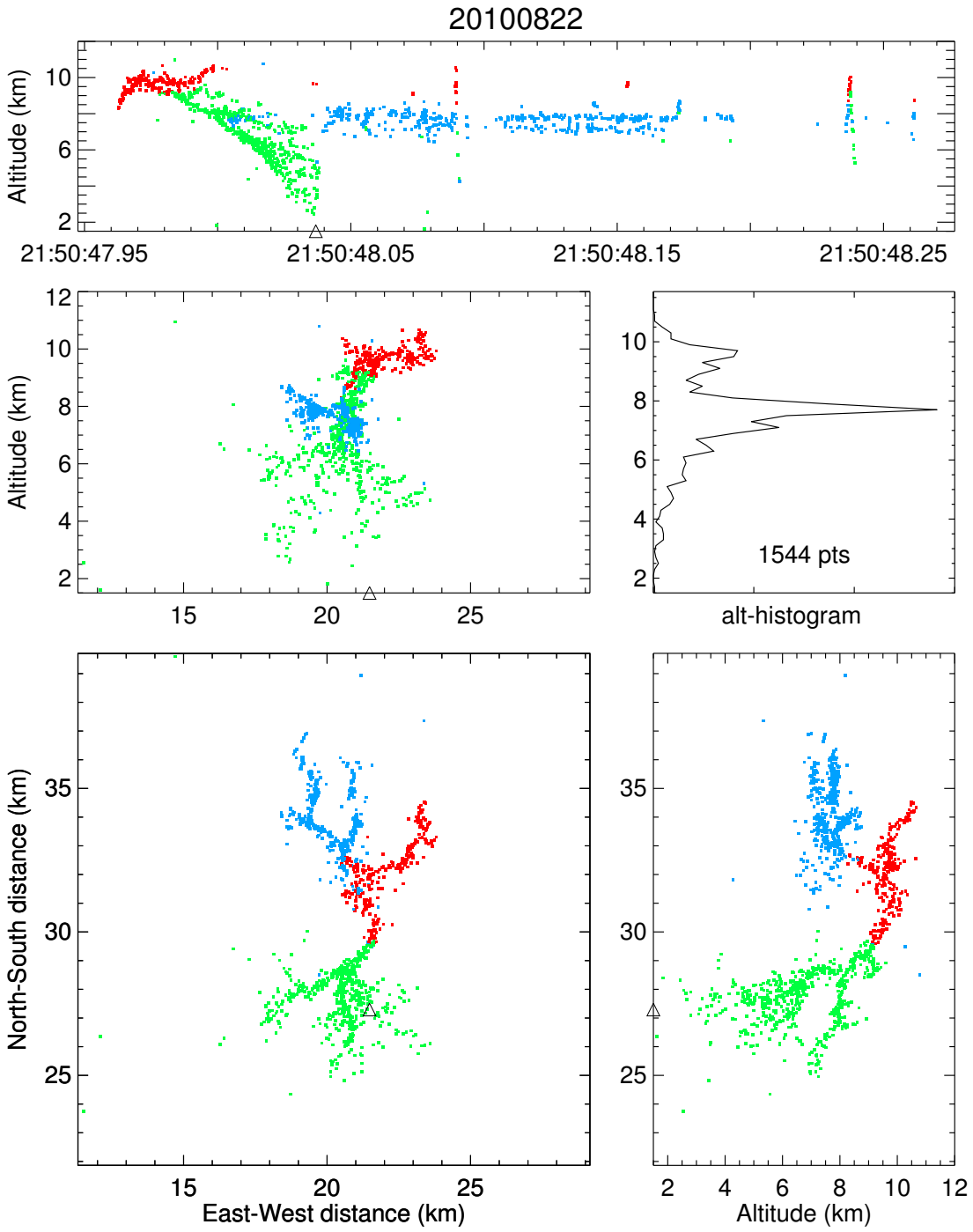

Figure 3.7: VHF sources located by the LMA for a BFB flash on August 22, 2010 at 21:50:47 UTC. Sources are colored by charge, with red indicating negative breakdown in positive charge, blue indicating positive breakdown in negative charge, and green indicating negative breakdown in undetermined or neutral charge.

the range of the flash. Also, the antenna pattern of the LMA receiver antenna will not have much of an effect on the received power since, again, the flash is distant and therefore occupies a limited range in elevation angle. Thus, the received power by this particular LMA station is by approximation proportional to the emitted source power, if one assumes an isotropically radiating source.

Both spectrograms in Figure 3.6 also show the transition from impulsive to more continuous VHF emissions during the cloud-to-ground leader stage. Initially, the VHF emissions appear as impulsive, short bursts of radiation in the spectrograms, gradually changing to a more continuous nature (reminiscent of the VHF emissions from the –CG leader in Figure 3.2) toward the later stage of the leader to ground.

As the leader propagated to lower altitude the rate of pulses in the fast ΔE waveform is also seen to increase (Figure 3.6, fourth panel).

The high-rate VHF emissions from the negative leader at low altitude tend to "mask" VHF emissions associated with positive breakdown in the midlevel negative charge region. This effect is apparent during the later stages of the cloud-to-ground leader, as it propagates below 5–6 km altitude; very few sources corresponding to positive breakdown in the midlevel negative charge region are located by the LMA (Figure 3.6, second panel). As the leader approaches ground, the negative charge region appears quiet, until shortly after the time of the return stroke, when activity again picks up. This effect can be explained by the *masking effect* of the LMA discussed in Section C.1. Although the LMA may not have located any VHF events from positive breakdown, that does not mean that positive breakdown was not occurring at that time.

In conclusion, for this particular BFB flash the transition from impulsive to apparently continuous VHF emissions by the cloud-to-ground leader, as it traveled from an altitude of 9 km altitude down to 2 km, is gradual in time, appearing as an increase in average received power, while the maximum received power does not appear to change by any significant amount. This same effect is observed in all BFB flashes to some degree and will be studied in the following two chapters.

The flash discussed here is also a good example of a BFB flash with multiple strokes to ground, where the second stroke was followed by a continuing current. The third stroke to ground shows the characteristic (for BFB flashes) *inverted-V* shape of VHF source altitudes in time, as a dart leader initiated in the negative charge region, propagated upward to the positive charge region and then down to ground (Figures 3.7 and 3.6, LMA altitude–time panels at 21:50:48.24 UTC.). The second stroke at 21:50:48.09 shows the effect too, but less clearly so because the dart leader propagated faster.

3.3.4 Low-altitude IC flash

Similar to a classic –CG flash, a low-altitude IC flash initiates between the main midlevel negative charge region and the lower positive charge region. *Marshall and Winn* [1982] found that (in a New Mexico thunderstorm) the lower positive charge is mainly carried by precipitation, which supports the general observation that low-altitude IC and –CG activity tend to be delayed relative to IC flash activity in a developing storm. Also, if the lower positive charge region is comparable in magnitude to the negative charge region, a negative stepped leader may not propagate through the lower positive charge to ground but remains within the cloud or near its base. At Langmuir Laboratory, low-altitude IC flashes are occasionally seen to propagate partway down to ground but not reaching it.

Figures 3.8 and 3.9 show waveform and LMA data for a low-altitude IC flash. This is not a very good example, since the flash is extensive and complex, but is the only example for which waveform data were recorded in 2010 and illustrates the characteristic VHF emissions of a low-altitude negative leader well.

By comparison of the log-RF waveforms and spectrograms of Figure 3.8 with those of the –CG flash in Figure 3.2, there is a similarity in the nature of VHF emissions. Both examples show VHF emissions that are of an apparently continuous nature during negative leader development.

The ΔE waveform recorded by the slow antenna shows only a gradual positive excursion of the electric field, due to the approaching negative leader. The flash initiated with a downward negative leader and the first 50 ms of the flash are characteristic of a low-altitude IC flash. After that time, a negative leader propagated upward at a shallow angle (from 5 km altitude to 8 km altitude) and evolved into a complex intracloud discharge. A typical low-altitude IC flash in New Mexico thunderstorms is of a shorter duration.

3.3.5 Positive CG flash

Figures 3.10 and 3.11 show waveform and LMA data of a +CG flash that occurred in the evening of August 15, 2010 and was visually observed to strike the mountainous terrain about 2 km to the north of the laboratory. This example is included for the sake of completeness, even though it does not relate to the main topic of this work. It does demonstrate the relative ineffectiveness of the LMA in locating VHF sources associated with positive leaders. From the various waveforms and spectrograms it is clear that VHF radiation was quite strong and the electric field made a large excursion, initiating corona discharges that were picked up by both the LMA and the Sirio broadband antenna situated at the Annex. The VHF emission has a signature similar to that of a low-altitude IC flash, being apparently continuous in nature; it

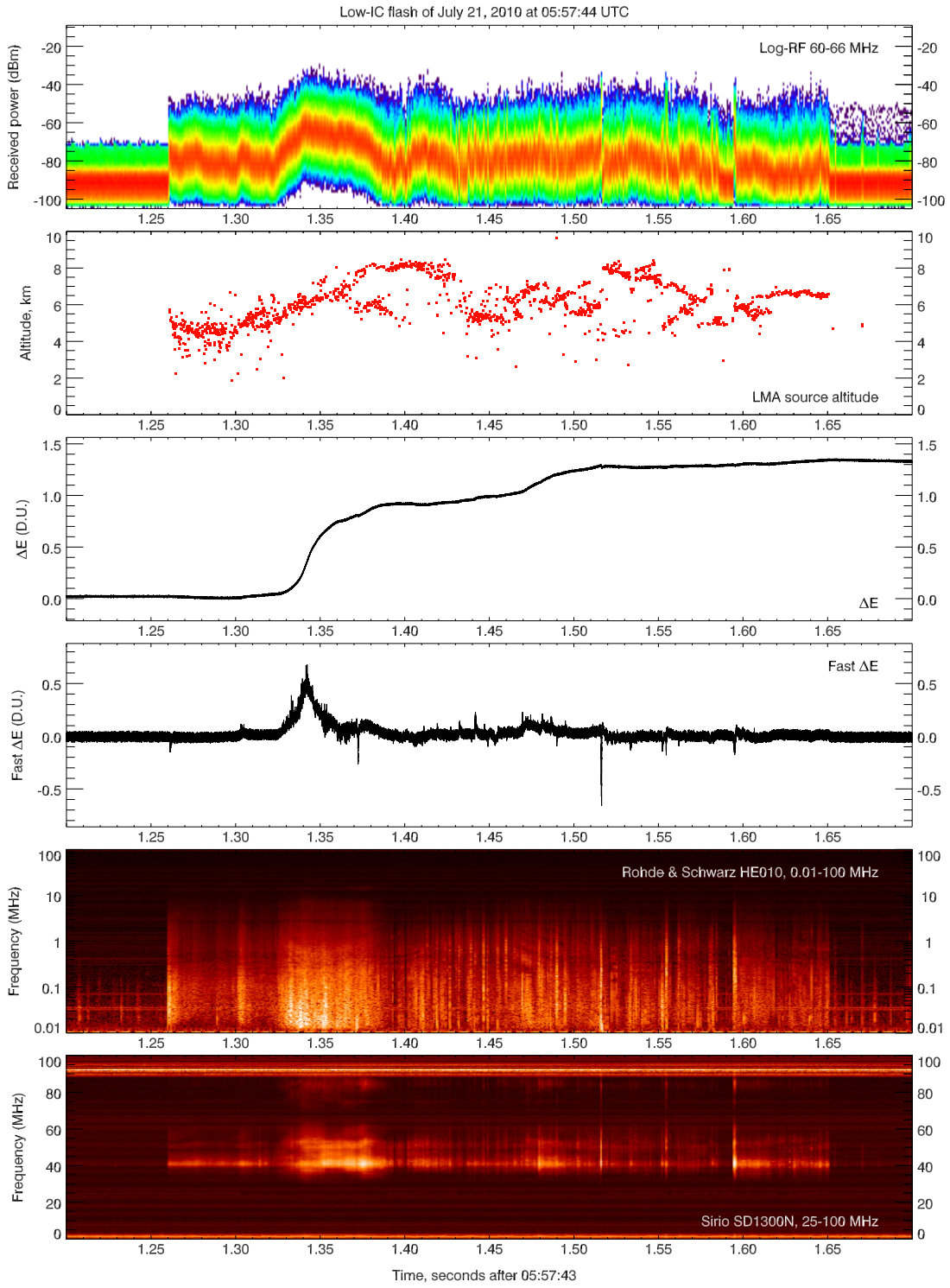

Figure 3.8: Waveforms for the low-altitude IC flash of July 21, 2010 at 05:57:44 UTC. The plotted time interval is 500 ms. Note the gradual transition from apparently continuous to more impulsive VHF emissions as the negative leader propagates up in altitude at a shallow angle.

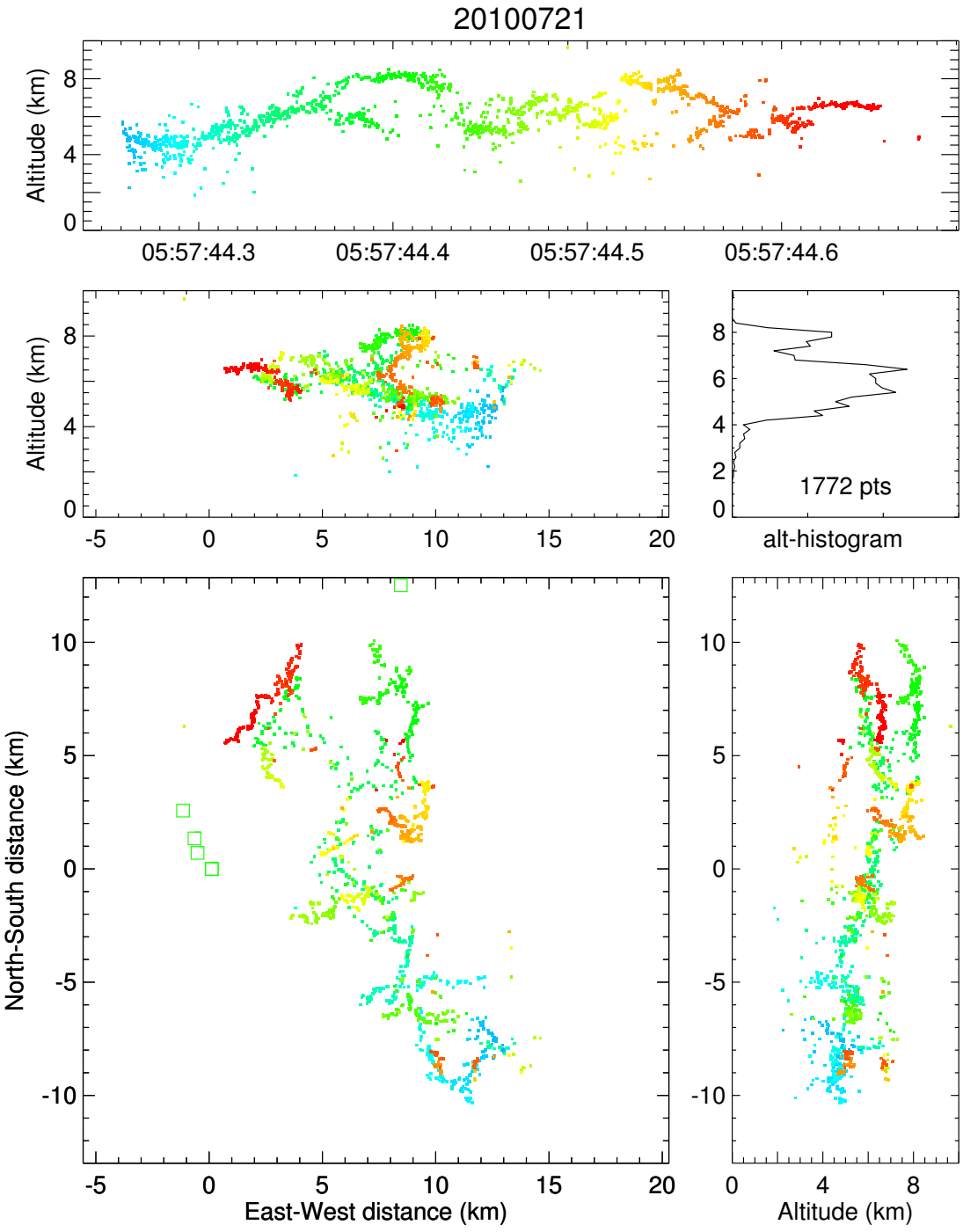

Figure 3.9: VHF sources located by the LMA for a low-altitude IC flash on July 21, 2010 at 05:57:44 UTC.

is not certain if the VHF emissions observed in the broadband spectrograms and the log-RF waveform are predominantly associated with positive or with negative breakdown. Those emissions associated with negative breakdown have higher power, but occurred farther away from the instrument. The negative breakdown is mapped well by the LMA, occurring at 6 km altitude. The positive leader, on the other hand, went completely undetected by the LMA.

3.4 BFB flash stages

With this discussion of different types of flashes in the context of LMA and waveform data, a general overview has been given of what sets a BFB flash apart from IC and regular –CG flashes. In preparation for the in-depth studies done in the following two chapters it is useful to think of a BFB flash as composed of three successive stages during the lifetime of the flash. This is reminiscent of the definition of three stages for a classic IC flash as proposed by *Kitagawa and Brook* [1960], albeit a bit differently. *Kitagawa and Brook* defined an IC flash to consist of an initial stage, a very active stage, and a junction stage, which has later caused some controversy [*Villanueva et al.*, 1994] regarding the initial and active stages. A similar classification can be made for BFB flashes which is proposed to be:

Intracloud stage: This is the initial stage during which negative and positive breakdown initiate and the leaders propagate into their respective charge regions. This stage encompasses roughly (and conveniently) the initial and active stages of an IC flash as proposed by *Kitagawa and Brook* [1960];

Cloud-to-ground stage: This is the time interval during which the cloud-to-ground leader initiates and propagates to ground. This stage ends at the time of the (first) return stroke;

Final stage: This stage encompasses the time interval starting immediately after the first return stroke and lasting until the end of the flash. During this stage continued positive breakdown occurs in the midlevel negative charge region, which often produces K-leaders, dart leaders with associated return strokes, or attempted dart leaders that do not succeed in contacting ground. This final stage corresponds to the "junction stage" of classic IC flashes as proposed by *Kitagawa and Brook* [1960].

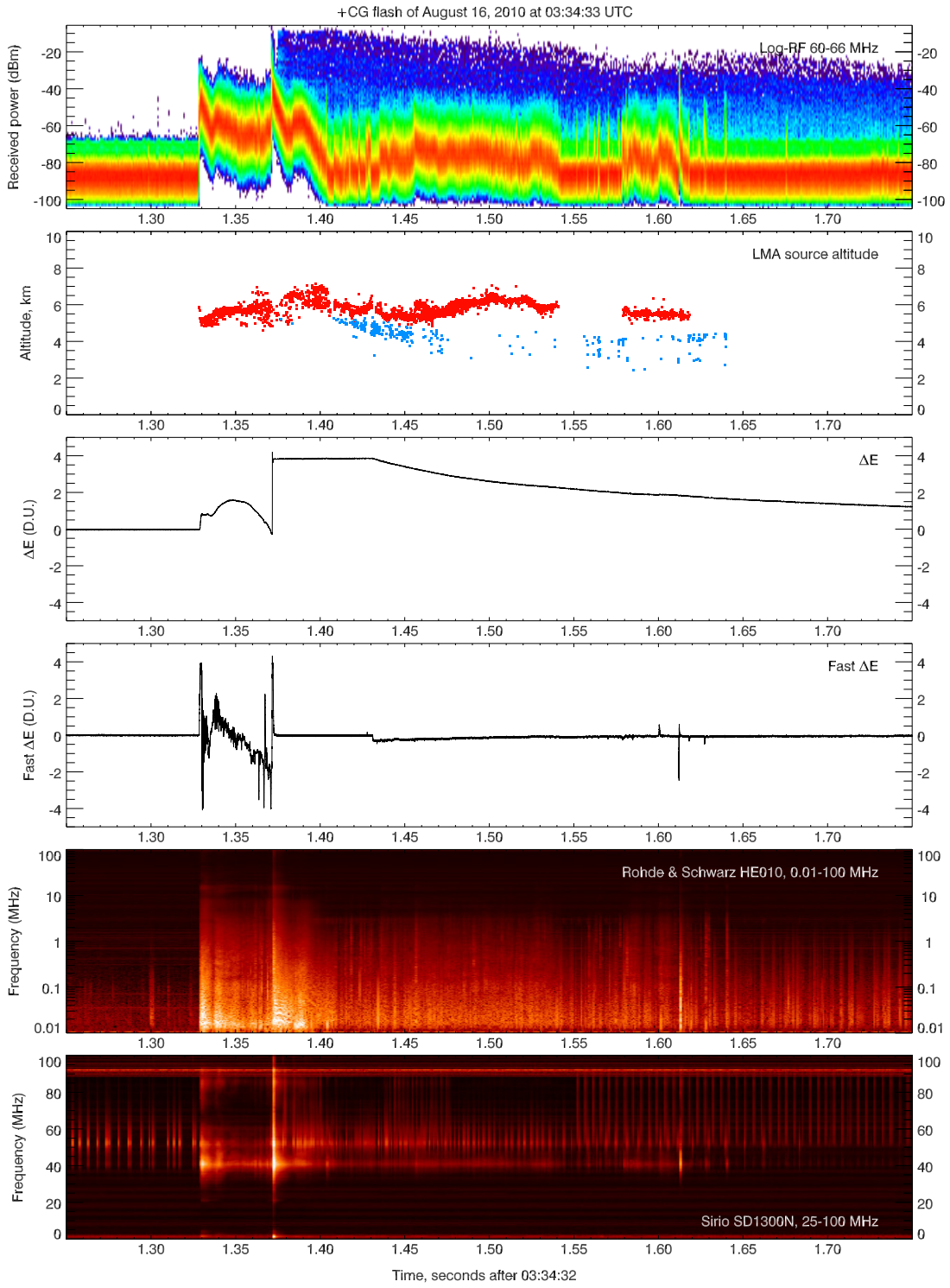

Figure 3.10: Waveforms for the +CG flash of August 16, 2010 at 03:34:33 UTC. The plotted time interval is 400 ms. The electric field excursion during and after the return stroke saturated the output of the slow antenna, which also inhibited any fast-ΔE pulses during this time.

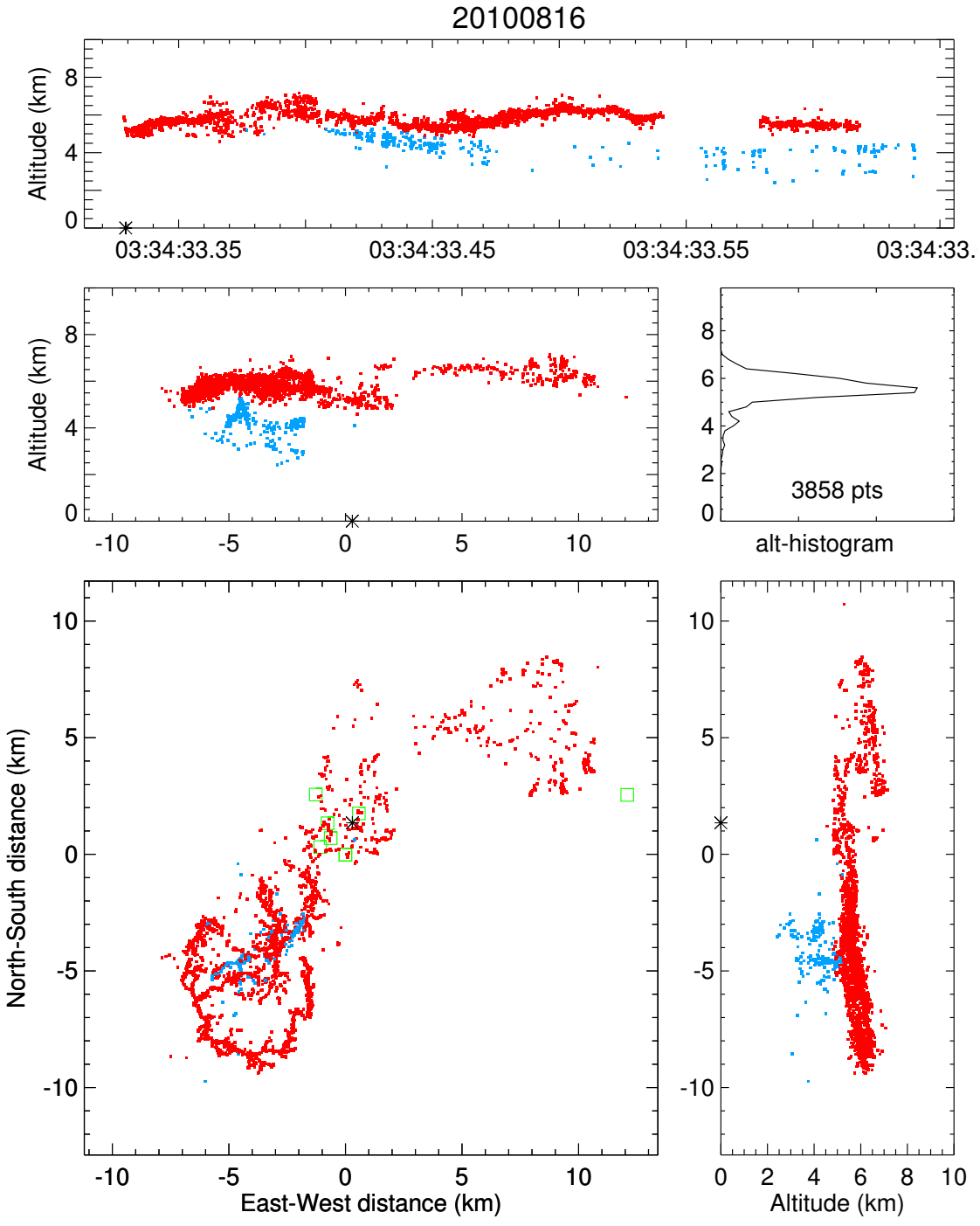

Figure 3.11: VHF sources located by the LMA for a +CG flash on August 16, 2010 at 03:34:33 UTC, colored by charge. The positive leader to ground (located by the NLDN at $(x = 0.3, y = 1.3)$ in the plan view) was not mapped by the LMA.

3.5 BFB flash types

The transition from the intracloud to the cloud-to-ground stage in a BFB flash is not always well-defined. The BFB flash of Section 3.3.3 is an example of a BFB flash where these two stages appear to be merged into one (IC–CG) stage. This flash had a single negative upward leader which—although branching multiple times—continued to ground in a continuous fashion without interruption. Such BFB flashes, where the initial negative leader evolves into the cloud-to-ground leader in a continuous manner, appear to be uncommon. They will be referred to in this work as *Type-I* BFB flashes.

Unlike Type-I BFB flashes, most BFB flashes have a well-defined initial intracloud stage during which one or more negative leaders propagate concurrently or successively within the positive charge region. The successive leaders branch off older leader channels, all sharing the same original upward channel that connects positive breakdown and negative breakdown. The successive leaders appear to be initiated by fast K-leaders that originate in the midlevel negative charge region and travel upward into the upper positive charge region along previous channels. The resulting new negative leader may then branch off, or continue negative breakdown at the tip of an older leader channel. (This process will be discussed in Chapter 4.) The leader that becomes the cloud-to-ground leader also appears to initiate as a fast K-leader (heralding the cloud-to-ground stage of the flash), either branching off or extending a previous channel and propagating to ground. These BFB flashes, in which the cloud-to-ground leader appears to initiate with a K-leader, will be referred to as *Type-II* BFB flashes.

In summary, two types of BFB flashes are identified:

Type-I BFB flashes produce a cloud-to-ground leader that is a continuation (extension) of the original upward negative leader from the intracloud stage, and that develops in a continuous fashion without pause;

Type-II BFB flashes produce a cloud-to-ground leader that may be initiated from the initial, main negative leader in upper positive charge, or as a new branch; the cloud-to-ground leader appears to be initiated by a K-leader propagating through a previous channel. If the leader extends a former channel, this is evident from a brief pause (typically 1–10 ms) during leader propagation.

The distinction between both types of flashes in this work was always made by looking at animations of LMA data to determine where and when the cloud-to-ground leader initiated. If no noticeable pause could be detected in the propagation of the initial negative leader and it therefore evolved into the cloud-to-ground leader (while either branching or not branching) without interruption, a flash was categorized as Type-I;

otherwise, as Type-II. However, this does not necessarily mean that Type-I BFB flashes produce cloud-to-ground leaders without the help of a K-leader; perhaps all BFB flashes continually produce K-leaders (i.e. ionization waves) that carry relatively small currents, but are fast and frequent, and carry a supply of negative charge to help the negative breakdown along. Such K-leaders, if they occur, might be too small in magnitude to be detectable by LMA or in ground-based ΔE waveform data. If that is the case, no clear difference of physical importance can be made between the two types.

If the two types are physically distinct, the occurrence of Type-I BFB flashes could be an indication of how depleted upper positive charge is in comparison to midlevel negative charge. This is because Type-II BFB flashes (before the cloud-to-ground leader occurs) appear to discharge various regions of upper positive charge in successive stages while spawning renewed leaders, until at one point the leader decides to leave the charge region altogether and go to ground. A Type-I BFB flash, on the other hand, may indicate that the negative leader finds very little upper positive charge at all and decides to leave the charge region immediately, with negative charge in the midlevel charge region made available at a fast enough rate to keep negative breakdown going.

In this work, the two types will be regarded as distinct.

3.6 BFB flash characteristics

Table 3.1 is a compilation of statistics of 59 BFB flashes observed during the 2010 summer season in New Mexico. Listed are the date and UTC time of each flash; flash type (I or II); total flash duration t_{f}; time from flash initiation to first return stroke t_{s}; number of strokes n_{s}; number of attempted strokes (attempted dart leaders) n_{a}; flash initiation altitude z_0 (above MSL); plan-view distance d_{f} of the cloud-to-ground leader from flash initiation point; the bearing (relative to true north) a_{f} of the cloud-to-ground leader relative to the flash initiation point; and the strength u_{s} and (inverse) direction α_{s} of the wind-shear vector, defined in Section 3.6.8.

The effect of wind shear and how the wind shear parameters are calculated in Table 3.1 will be discussed in Section 3.6.8.

Nr.	Date and time, UTC		Type	t_f (ms)	t_s (ms)	n_s	n_a	z_0 (km)	d_f (km)	α_f (°)	u_s (kt)	α_s (°)
1	7/22/2010	23:24:32	II	437	294	2	0	8.3	8.8	313	4.1	18
2	7/22/2010	23:32:49	II	473	247	3	1	8.6	6.8	324		
3	7/23/2010	18:23:45	II	555	214	4	0	7.6	5.9	340	5.7	149
4	7/23/2010	18:45:30	II	504	161	3	0	8.6	4.6	229		
5	7/23/2010	20:45:32	II	285	237	1	0	8.0	4.6	311		
6	7/23/2010	21:11:23	II	251	219	1	0	7.2	5.3	199		
7	7/23/2010	21:34:07	II	547	215	3	0	7.7	4.2	135		
8	7/23/2010	21:45:53	II	635	194	3	0	8.8	5.9	160		
9	7/25/2010	04:02:31	I	173	148	1	4	6.2	3.3	90	10.0	165
10	7/28/2010	17:31:39	II	201	173	1	0	7.2	4.9	352	9.0	37
11	7/28/2010	17:37:59	II	315	131	3	0	7.4	5.4	22		
12	7/28/2010	17:44:42	I	251	115	5	0	8.0	1.7	353		
13	7/28/2010	17:48:37	II	249	171	1	0	7.9	5.0	56		
14	7/28/2010	17:53:22	I	192	113	1	0	7.5	3.5	129		
15	7/28/2010	17:56:27	II	321	175	1	0	7.0	4.1	106		
16*	7/28/2010	18:07:58	II	508	268	3	0	5.9	2.9	252		
17	7/30/2010	21:28:04	II	454	116	3	0	7.4	4.7	153	4.6	0
18†	8/02/2010	20:58:11	II	738	287	4	2	8.2	3.9	146	9.7	218
19	8/03/2010	19:25:06	II	438	239	1	0	7.5	5.7	171	8.4	188
20	8/06/2010	21:00:52	II	872	250	6	0	8.0	10.6	167	12.1	203
21	8/06/2010	21:03:52	II	770	160	6	0	8.0	6.7	90		
22	8/06/2010	21:07:16	II	507	187	4	0	7.7	3.6	111		
23	8/08/2010	19:15:08	II	381	196	1	0	8.0	10.9	171	14.1	166
24	8/08/2010	19:18:54	II	614	155	6	0	6.8	4.9	192		
25	8/08/2010	19:49:38	II	349	119	2	0	6.5	3.4	67		

Continued on next page

Table 3.1 – Continued

Nr.	Date and time, UTC		Type	t_f (ms)	t_s (ms)	n_s	n_a	z_0 (km)	d_f (km)	α_f (°)	u_s (kt)	α_s (°)
26	8/16/2010	01:20:49	II	564	456	1	0	8.4	10.8	317	5.8	308
27	8/16/2010	01:31:50	II	508	252	1	2	8.3	5.8	337		
28	8/16/2010	01:54:55	I	545	191	1	2	8.4	7.3	142		
29	8/16/2010	02:03:21	II	680	254	2	0	8.7	8.0	94		
30	8/20/2010	03:06:15	II	271	235	1	0	8.0	7.5	260	13.3	230
31	8/20/2010	03:10:22	II	250	160	1	1	6.3	7.0	172		
32‡	8/20/2010	03:25:57	II	382	274	1	1	7.3	7.3	353		
33	8/20/2010	03:57:19	II	318	236	1	3	8.2	5.2	314		
34	8/20/2010	04:07:09	II	456	240	2	0	8.4	7.1	195		
35	8/22/2010	21:22:08	II	195	163	1	0	7.2	7.0	109	10.8	28
36	8/22/2010	21:50:47	I	298	74	3	0	8.3	5.7	186		
37	8/22/2010	22:29:52	II	761	409	1	0	8.4	6.3	257		
38	8/22/2010	22:31:07	II	522	285	2	0	8.2	3.7	273		
39	8/22/2010	22:37:07	II	644	285	1	1	8.5	11.1	150		
40	8/22/2010	23:09:13	II	281	145	2	0	7.0	5.8	143		
41	8/22/2010	23:58:54	I	330	134	2	0	7.5	6.2	63		
42	8/29/2010	00:07:05	II	314	238	1	0	7.6	6.1	235	18.9	232
43	9/08/2010	19:09:53	II	445	278	1	0	7.8	10.3	235	9.8	276
44	9/08/2010	19:20:09	II	847	137	9	0	6.6	5.1	261		
45	9/08/2010	19:28:32	I	314	190	1	3	8.2	8.5	223		
46	9/08/2010	19:57:17	II	493	347	1	0	7.9	16.8	114		
47	9/08/2010	20:21:34	II	460	243	3	0	7.4	9.9	157		
48	9/13/2010	20:36:20	II	660	569	1	0	6.3	7.8	188	26.3	205
49	9/13/2010	20:37:32	II	549	327	3	0	7.0	5.6	240		

Continued on next page

Table 3.1 – Continued

Nr.	Date and time, UTC		Type	t_f (ms)	t_s (ms)	n_s	n_a	z_0 (km)	d_f (km)	α_f (°)	u_s (kt)	α_s (°)
50	9/13/2010	20:44:54	II	417	192	1	1	7.5	4.6	264		
51	9/13/2010	20:56:20	II	284	220	1	0	7.2	9.0	308		
52	9/13/2010	21:49:33	II	360	216	1	3	9.6	7.8	196		
53	9/13/2010	21:52:11	II	408	196	1	3	8.5	7.4	135		
54	9/13/2010	22:22:57	I	592	118	2	0	6.8	6.3	176		
55	9/13/2010	22:24:18	II	494	293	1	0	7.5	10.3	263		
56	9/13/2010	22:25:27	II	654	261	3	0	6.7	6.3	162		
57	9/13/2010	22:28:49	II	651	311	2	0	7.6	9.4	164		
58	9/14/2010	19:38:38	II	243	109	2	0	7.7	3.6	167	13.7	234
59	9/14/2010	20:29:00	II	426	238	1	0	7.1	8.1	312		

Table 3.1: Characteristics of 59 BFB flashes observed in 2010. See text for the explanation of symbols. The flashes are grouped per storm; wind-shear data are only listed for the first BFB flash, but apply to all related BFB flashes.

*Possibly not a BFB flash, but hybrid IC–CG

†Studied in Chapter 4

‡Studied in Chapter 5

3.6.1 BFB flash polarity

All BFB flashes observed thus far, both the set of 59 flashes discussed in this chapter as well as all other BFB flashes observed in LMA data by the author, were of negative polarity (i.e. lowering negative charge to ground). These could therefore be referred to as –BFB flashes. It is not known whether or not +BFB flashes (lowering positive charge to ground) occur in inverted-polarity storms, but there is no reason to assume they do not. +BFB flashes, if they do occur, would be hard to distinguish from regular inverted-polarity IC flashes by LMA data alone since the positive leader to ground would remain mostly undetected by the LMA. Inverted-polarity storms are also uncommon in New Mexico. Since at the present time no observations of +BFB flashes are known to exist, –BFB flashes will be referred to as BFB flashes (without explicit sign).

3.6.2 Attempted BFB flashes

All of the 59 BFB flashes listed in Table 3.1 were *successful* (as opposed to *attempted*) in developing a cloud-to-ground leader that reached ground. This is not statistically significant, however, since there is a bias in the manual triggering of the instruments. This bias is toward successful BFB flashes because attempted BFB flashes are hard to distinguish from IC flashes in waveform and LMA data, and recording waveform data of IC flashes was of a lower priority than of BFB flashes during 2010.

3.6.3 Flash type

Of all days on which BFB flashes were recorded, July 23 and 28 were particularly productive, as were August 22 and September 13. Eight of the 59 flashes could be classified as Type I; the rest as Type II. The Type-I flashes did not seem to be concentrated in particular storms but occurred randomly throughout the time period from July 22 to September 14.

3.6.4 Number of strokes to ground

A surprisingly large fraction of BFB flashes produced more than one stroke to ground: 29 of the 59 flashes (49%) were multi-stroke, while 19 flashes (32% of the total) had three or more strokes to ground. Some of the single-stroke BFB flashes produced attempted dart leaders, which propagated along the established cloud-to-ground channel, but did not succeed in reaching ground. (Many more BFB flashes produced K-leaders, but only those producing K-leaders along the cloud-to-ground channel

were classified as having attempted dart leaders.) The distribution of the number of strokes to ground for all 59 BFB flashes is shown in Figure 3.12. Type-I flashes do not appear to have a different distribution than Type-II flashes. The mean number of strokes is 2.12 ± 1.65. The BFB flash with the most strokes to ground occurred on September 8, 2010 at 19:20:09 UTC; it was a Type-II flash that produced nine return strokes to ground and lasted 847 ms.

The number of return strokes was determined from the electric field-change waveform recorded by the slow antenna.

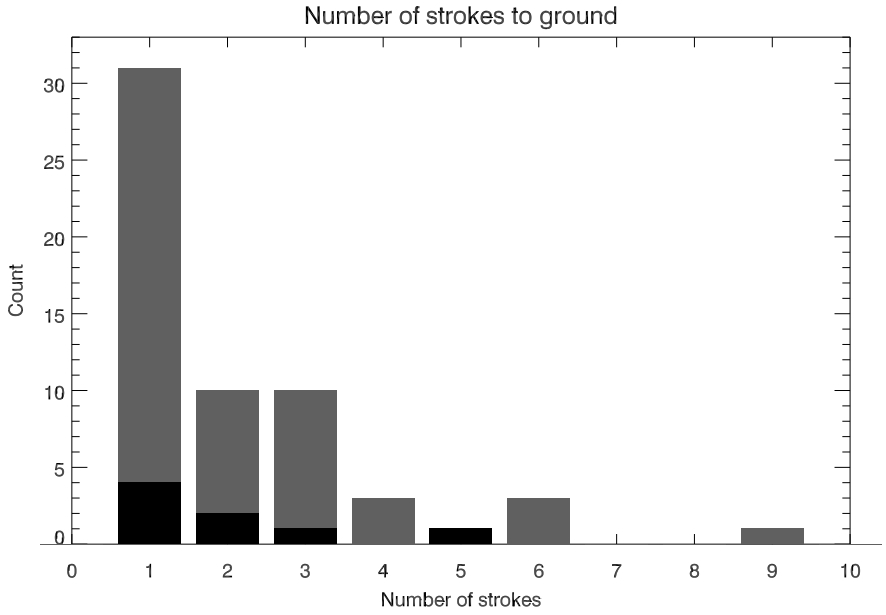

Figure 3.12: Distribution of the number of strokes to ground in all 59 BFB flashes (grey) and Type-I flashes (black).

3.6.5 Flash duration and time to first stroke

The BFB flash duration was determined from LMA data, by looking at the time difference between the first and last VHF source that was located by the LMA. There is an estimated error of 1 ms in these numbers from the way they were measured; the actual error may be larger, since the first and last VHF sources located by the LMA do not necessarily indicate the start and end times of electrical activity associated with the flash. The time to the first return stroke was determined by correlating VHF source altitude and ΔE waveform data and has, in most cases, also an estimated error of 1 ms. For distant BFB flashes with a poorly resolved onset of electric field

change (e.g. the August 20 BFB flashes), slow and fast ΔE waveforms were jointly considered in combination with LMA VHF source altitude.

The mean flash duration t_{f} for all 59 BFB flashes is 451 ± 173 ms. The mean time to the first return stroke t_{s} was 221 ± 87 ms, about half of the mean flash duration.

Distributions of flash duration and time to first stroke are shown in Figures 3.13 and 3.14. The figures indicate that Type-I flashes tend to last shorter than Type-II flashes, and also need short times to produce the first stroke to ground.

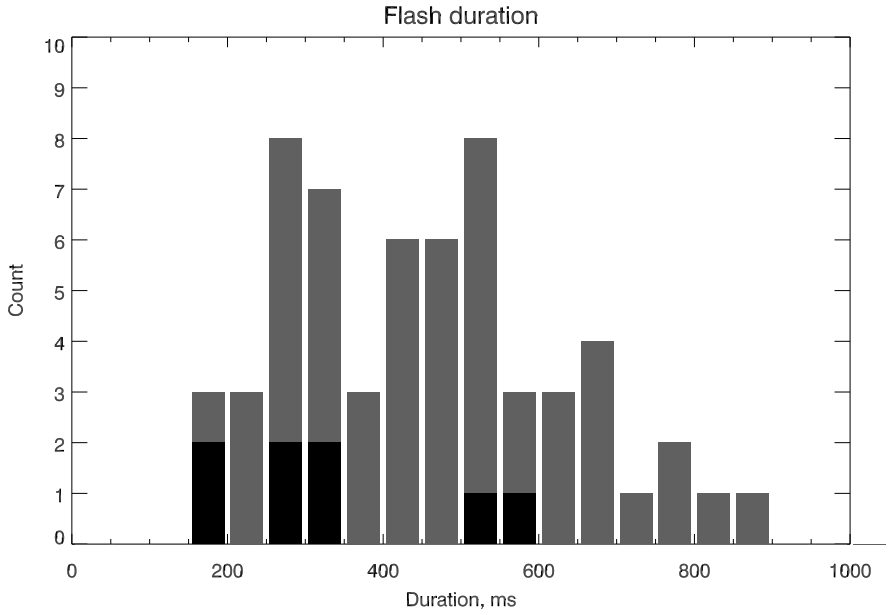

Figure 3.13: Distribution of total duration of all 59 BFB flashes (grey) and Type-I flashes (black).

The shortest-duration BFB flash occurred on July 25, 2010 at 04:02:31 UTC, lasting only 173 ms; this was a Type-I flash with the return stroke occurring 148 ms after initiation of the flash. The BFB flash with the longest duration lasted 872 ms and occurred in the afternoon of August 6, 2010 at 21:00:52 UTC. It produced six strokes to ground, with the first stroke occurring 250 ms after initiation of the flash. It is discussed in Section 6.4.

The BFB flash that most promptly produced the first stroke occurred on August 22, 2010 at 21:50:47 UTC, with 74 ms between initiation and first return stroke. The flash itself lasted 298 ms and produced three strokes to ground. It was categorized as a Type-I flash and is discussed in Section 3.3.3 and Section 6.8.

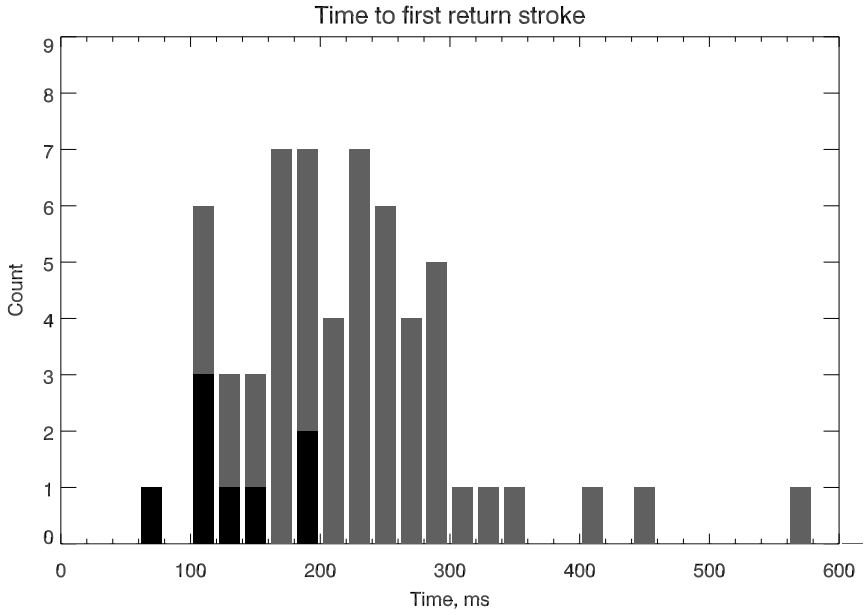

Figure 3.14: Distribution of the time to first stroke for all 59 BFB flashes (grey) and Type-I flashes (black).

3.6.6 Flash initiation altitude

The initiation altitude was determined from the first VHF source located by the LMA, or, if it was grossly different in location from several successive VHF sources associated with the upward leader, the altitude of a successive VHF source was chosen. The estimated error in determining the initiation altitude using this method is $\lesssim$ 100 m (for sources over the network, the location accuracy of source altitude for a typical LMA is 20–30 m depending on the array configuration [*Thomas et al.*, 2004]).

The mean initiation altitude for the 59 BFB flashes was 7.66 ± 0.74 km, which is typical for intracloud flashes in New Mexico thunderstorms (from observations by the author). A distribution of the flash initiation altitude is shown in Figure 3.15. Type-I flashes do not differ significantly from Type-II flashes in their initiation altitude.

3.6.7 Strike distance

BFB strike distance in this work is defined to be the plan-view distance (lateral displacement) of the cloud-to-ground leader from the flash initiation point. This distance was determined from LMA data, using the coordinates (x_0, y_0) of the first

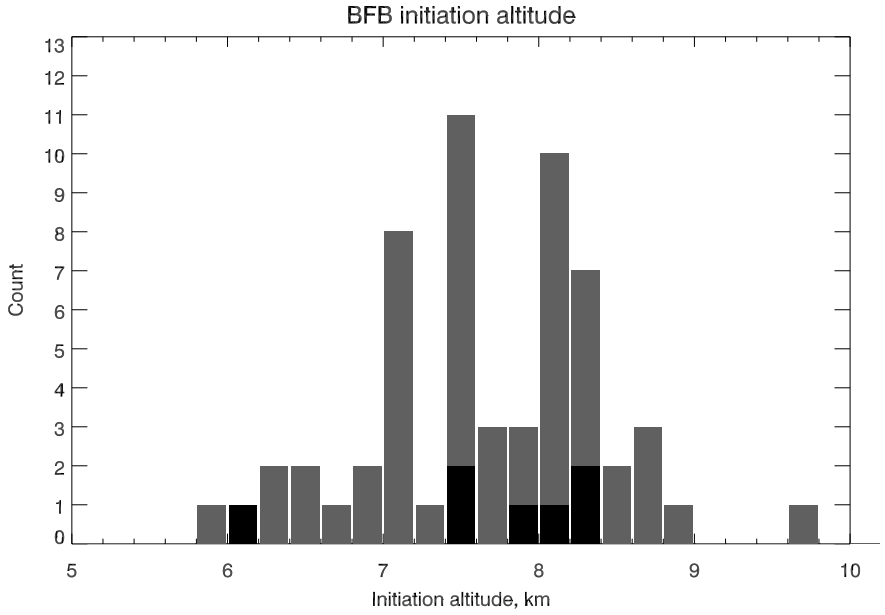

Figure 3.15: Distribution of initiation altitudes for all 59 BFB flashes (grey) and Type-I flashes (black).

located VHF source and estimating the position (x, y) of the main cloud-to-ground leader channel at 4.0 km altitude. The altitude of 4.0 km was chosen for the representative position of the leader because it is believed to be the most meaningful as a measure of strike distance. At this altitude the leader has cleared the altitude range of the midlevel negative charge region (which might have an effect on the direction of the leader) but it is not yet too low for the LMA to produce accurate source locations.

For several flashes the position of the leader channel at 4.0 km altitude could not be determined very well; the estimated error in plan location is typically ~ 1 km, due to multiple branches. The error in plan location by the LMA is typically 15–20 m for sources within the array [*Thomas et al.*, 2004].

Figure 3.16 shows the distribution of the flash strike distance d_{f} for all 59 BFB flashes. Most flashes produced cloud-to-ground leaders 3–11 km away from the initiation point. The flash with the largest strike distance occurred on September 8, 2010 at 19:57:17 UTC with a strike distance of 16.8 km (this is equal to the distance between Langmuir Laboratory and the city of Magdalena). This was a Type-II flash that lasted 493 ms and produced one stroke to ground.

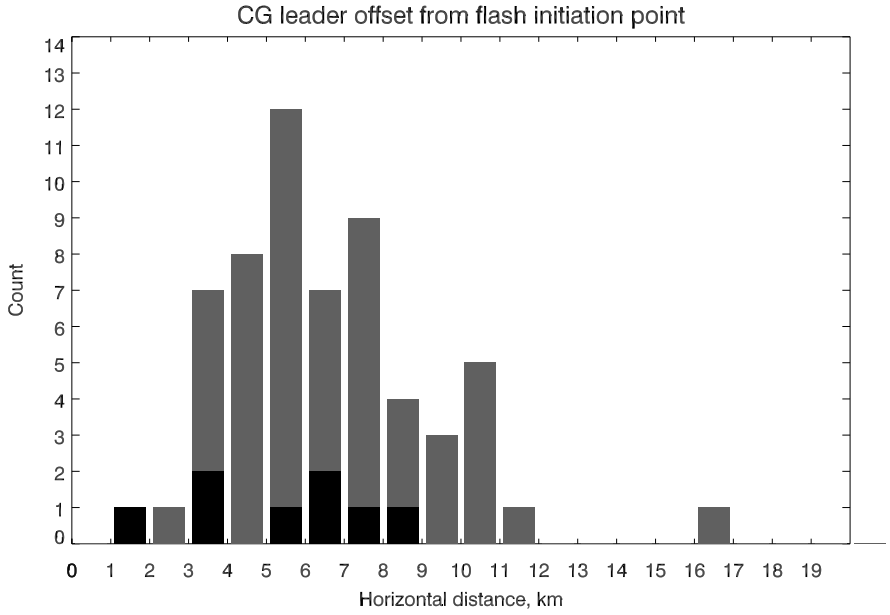

Figure 3.16: Distribution of strike distances (horizontal offset of cloud-to-ground leader at 4.0 km altitude from initiation region) for all 59 BFB flashes (grey) and Type-I flashes (black).

3.6.8 The effect of wind shear

As discussed in Chapter 2, photographic and visual observations indicate that BFB flashes tend to prefer the upwind side of the cloud in the presence of wind shear. In other words, BFB flashes tend to occur away from the sheared-off anvil. In this section an attempt is made to quantify this behavior and see if there is a strong correlation between BFB flash direction and wind shear.

In severe storm forecasting, *bulk shear* is a number defined to be the vector difference between the mean 0–6 km wind and surface winds. It is used as an indication of storm severity, in combination with convective available potential energy (CAPE) to form the Bulk Richardson Number (BRN). The altitudes over which the bulk shear is determined are, however, different from the approximate charge region boundaries of a typical New Mexico thunderstorm and therefore a different measure of wind shear will be used here. The shear vector $\mathbf{u}_\mathrm{s}$ will be defined as

$$\mathbf{u}_\mathrm{s} = \langle \mathbf{u}_+ \rangle - \langle \mathbf{u}_- \rangle \tag{3.1}$$

where, for a normal-polarity storm with upper positive charge and midlevel negative charge regions, $\langle \mathbf{u}_- \rangle$ represents the vector mean wind speed at 4–8 km altitude, and $\langle \mathbf{u}_+ \rangle$ that at 8–12 km altitude, as an approximation for the locations of the midlevel negative and upper positive charge regions, respectively.

The vector mean values $\langle \mathbf{u}_- \rangle$ and $\langle \mathbf{u}_+ \rangle$ were calculated from atmospheric soundings of Albuquerque (ABQ), using either the 0000 UTC or 1200 UTC sounding. BFB flashes occurring between 0600 and 1800 UTC were compared with the 1200 UTC sounding and those occurring outside this time interval with the 0000 UTC sounding. However, if a storm produced several BFB flashes and went on across a time boundary (such as the July 28 storm, which passed the 1800 UTC boundary) data from only one sounding was used.

Figure 3.17 illustrates the shear vector for a simple one-dimensional case where both $\langle \mathbf{u}_- \rangle$ and $\langle \mathbf{u}_+ \rangle$ have the same direction. Table 3.1 lists the magnitude u_s and direction or azimuth α_s of $-\mathbf{u}_\mathrm{s}$ (i.e. the opposite direction of the shear vector, which points to the upwind side of a storm) because this makes it easier to numerically compare BFB leader bearing with wind-shear bearing in the table. Graphically, the definition in Equation 3.1 is more intuitive.

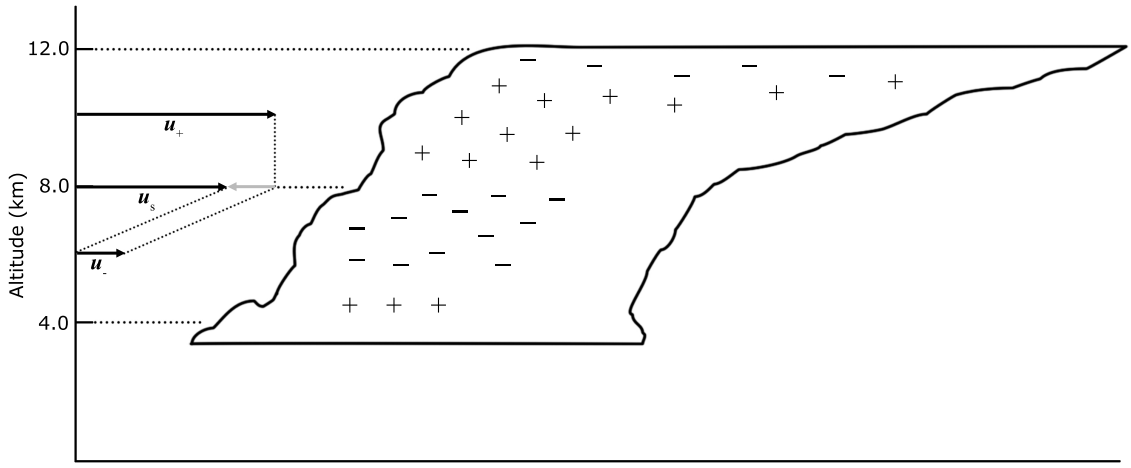

Figure 3.17: Schematic one-dimensional representation of wind shear affecting a storm cloud (with inferred charge structure) and calculation of the shear vector $\mathbf{u}_\mathrm{s}$. The vectors $\mathbf{u}_-$ and $\mathbf{u}_+$ represent the 4–8 km and 8–12 km mean winds, respectively (corresponding to $\langle \mathbf{u}_- \rangle$ and $\langle \mathbf{u}_+ \rangle$ in the text).

Figure 3.18 shows six cases to visualize the effect of wind shear (as defined above) and the plan location at 4 km altitude of the cloud-to-ground leader relative to the flash initiation point (which is always located at $(x = 0, y = 0)$ in the various panels). In each case the wind-shear vector, which has units of km/h, is drawn at a length that represents the expected shear distance between the midlevel negative and upper positive charge layers during one hour, had these been static during that time. The locations of the cloud-to-ground leaders at 4 km altitude, relative to the initiation location for each flash at $(0, 0)$, are indicated by blue crosses.

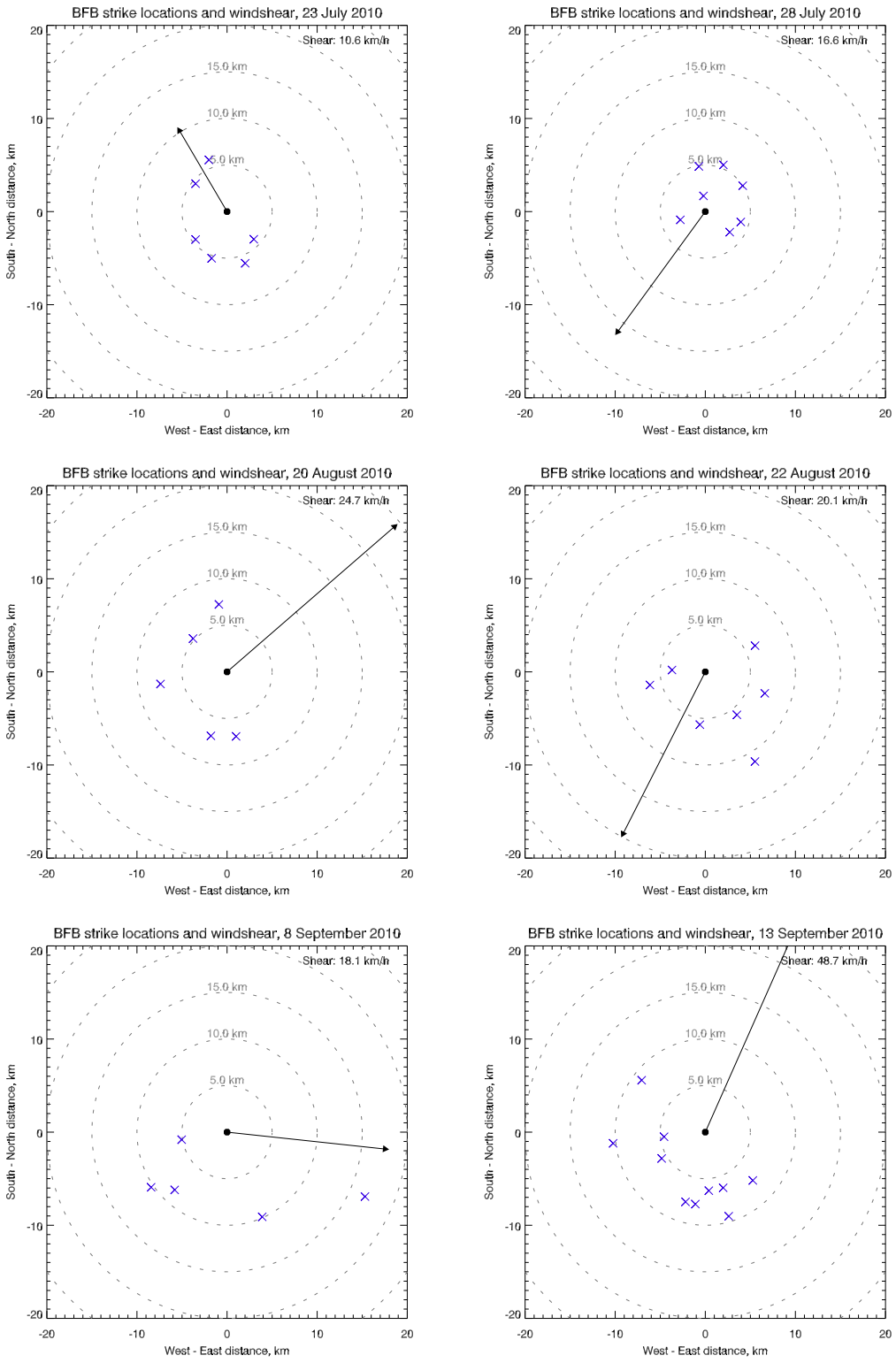

Figure 3.18: Approximate strike locations of BFB flashes (blue crosses) relative to the initiation location of each flash at $(0, 0)$ and wind shear over the period of one hour (indicated by vector arrows) for six days during 2010 (see text).

From the figure, there does indeed appear to be a correlation between BFB strike locations and wind shear, most notably in the cases of July 28, 2010 and September 13, 2010, where almost all (of the relatively large number of) BFB flashes appear at the upwind (or "upshear") side of the storm, in the opposite direction to the shear vector. On other days a possible correlation is not so clear, but there are no cases in which the BFB flashes seem to *prefer* the downshear side of the storm. The case of July 23, 2010 shows two BFB flashes occurring in the downshear direction, but it should be pointed out that the wind shear on this day was apparently quite weak at only 10 km/h, thus displacing the midlevel negative and upper positive charge layers by about 10 km in one hour. Such low shear is not expected to have a significant effect on a typical New Mexico storm that usually grows, matures and dissipates within one hour (the BFB flashes recorded on July 23 occurred over several hours in successive storms).

It should be noted that the soundings that were used to estimate shear were up to six hours earlier or later than the occurrence of the storms and made about 120 km away from Langmuir Laboratory. In photographic observations (Section 2.4) BFB flashes are also commonly seen to exit the storm at the flank and not exclusively at the upwind side.

In conclusion, wind shear causing a lateral shift of the two major charge layers in a normal-polarity storm does appear to have an effect on where BFB flashes tend to occur, with the upwind side and flanks preferred over the downwind flank.

A possible explanation for the dependence on wind shear is that the down-sheared anvil is older than the upwind anvil region of a storm and may therefore have upper positive charge that is more depleted due to the continued acquisition of negative screening charge. This negative screening charge would be expected to either eliminate the upper positive charge in older, inactive anvil regions, or at the very least, form a relatively thick negative screening charge at all boundaries. In the first case, an intracloud leader would not necessarily go downstream into the older anvil, and in the second case, it could be prevented from leaving it due to the screening charge at the boundaries. The upwind side, which usually has young, cumuliform convection, will better mix in any accrued screening charge and may provide an easier escape out of the cloud for leaders.

Visual observations by the author over the past years of typical, localized New Mexico storms, indicate that the older down-sheared anvils in storms in high-wind-shear environments do not seem to exhibit much, if any, intracloud electrical activity at all. In many cases, these older regions of anvils are electrically dead. The BFB storm of August 20, 2010 (see Chapter 5) is a good example of this. Residual charge in inactive anvils of localized storms may perhaps be neutralized fairly quickly by screening charge.

The extent of BFB flashes within the midlevel and upper-level charge regions some-

times appears shifted contrary to what one would expect based on wind shear: The upper-level intracloud activity may be displaced upstream relative to the positive breakdown in the midlevel negative charge region. Figure 6.9 in Chapter 6 demonstrates this with the BFB flash that occurred on August 6, 2010 at 21:00:52 UTC. (This was also the longest-duration flash studied, as discussed in Section 3.6.5.)

The argument that screening charge neutralizes older, down-sheared anvils of storms would not only explain the preference of BFB flashes for the upwind side of the storm, but also supports the visual observation that BFB flashes are likely to occur in the first place in storms in high-wind-shear environments (discussed in Section 2.3): The upper positive charge region may be depleted faster when wind shear is stronger, as the anvil is blown downwind and extended.

3.7 Summary

An overview has been given of several types of lightning commonly observed in New Mexico thunderstorms. This was done using data from two sets of instruments: LMA, and various broadband waveforms (63 MHz log-RF, slow and fast ΔE, and broadband RF up to 100 MHz). The log-RF and broadband waveforms can be used to study VHF emissions from positive and negative breakdown, while the slow and fast ΔE waveforms indicate motion of charge. Along with LMA data, this is a comprehensive set of instruments to study BFB flashes.

VHF sources associated with negative breakdown tend to be of intrinsically higher power than those associated with positive breakdown. This is evident from the LMA, which locates predominantly negative breakdown.

A cloud-to-ground leader of a BFB flash produces VHF emissions that transition from more impulsive to more continuous in nature as the leader propagates to lower altitude into denser air. The impulsive VHF emissions at high altitude (8–12 km) are characteristic of those of regular IC flashes, while the VHF emissions at low altitude (2–5 km) assimilate those of –CG and low-altitude IC flashes.

LMA and broadband waveform data of 59 BFB flashes were recorded in 2010 and basic characteristics are presented in this chapter. It was concluded that all 59 BFB flashes were of negative polarity (lowering negative charge to ground). A large fraction (about half) of the BFB flashes produced more than one stroke to ground. Flash initiation altitudes (7–8 km) are comparable to regular IC flashes. BFB flashes on average lasted about 450 ms and produced a stroke to ground after about 220 ms. These strokes to ground can occur anywhere from 1 km up to 17 km distance from the flash initiation region.

The various parameters that were discussed in the preceding sections are summarized in Table 3.2.

Parameter	Symbol	Mean value	Unit
Initiation altitude	z_0	7.66 ± 0.74	km
Flash duration	t_f	451 ± 173	ms
Time to first stroke	t_s	221 ± 87	ms
Number of strokes	n_s	2.12 ± 1.65	—
Strike distance	d_f	6.5 ± 2.6	km

Table 3.2: Mean values for the various flash parameters discussed in the text.

Three stages are defined for a BFB flash. During the *intracloud stage*, an upward negative leader propagates into the upper positive charge region, while associated positive breakdown occurs in the midlevel negative charge region. During the *cloud-to-ground stage*, a negative leader develops outward from the negative breakdown, which can occur at the altitude of upper positive charge, and propagates down to ground. The *final stage* is characterized by continued positive breakdown in the midlevel negative charge region, which may or may not initiate K-leaders into upper positive charge, and dart leaders to ground.

Two types of BFB flashes are observed. *Type-I* BFB flashes produce a cloud-to-ground leader from an intracloud leader as a continuation of original negative breakdown, which proceeds without interruption. *Type-II* BFB flashes, on the other hand, produce a cloud-to-ground leader that is initiated by an inferred K-leader, which may either branch off an earlier channel or be a continuation of an earlier negative leader tip.

There is a correlation between wind shear and the cloud exit region of BFB flashes, with the upwind side or both flanks being preferred over the downwind region of the storm. The proposed explanation for this behavior is that the positive upper charge region at the upwind side of a storm is younger and has had less time to collect (and mix in) screening charge. The screening charge that it does collect would mix in well by active convection in that area, allowing negative leaders in the positive charge region to escape the cloud on the upwind side without much impediment.

4. BFB flash of August 2, 2010 at 20:58:11

4.1 Introduction

In this chapter one BFB flash is studied in detail, using correlated data from the LMA, broadband electric field waveforms and high-speed video recordings. The BFB flash occurred on August 2, 2010 at 20:58:11 UTC to the southwest of Langmuir Laboratory. Although the BFB flash was cloud-enshrouded and the leader to ground was only visible below the cloud base, it occurred close to the laboratory and yielded high-quality waveform and LMA data. This chapter focuses on the various components of a BFB flash: the intracloud leader, cloud-to-ground leader, K-events, dart leaders, attempted dart leaders, and M-components during continuing-current return strokes. Chapter 5 discusses another BFB flash, which produced a leader to ground that was visible outside the cloud, and focuses on high-altitude leader characteristics.

4.2 Data correlation

LMA data are most easily compared with waveform data by plotting VHF source altitude against time along with the various waveforms. Video data can be correlated to LMA data by overplotting LMA data on video frames as a point-projection with the camera as the origin (Section A.8.4). This can be done either on a time-integrated video image that is a composite of successive video frames, or by studying individual video frames with LMA data overplotted for the specific time interval of the exposure.

The video data and waveform data can be correlated in two ways. First, a particular pixel in the video frame can be selected (e.g. at the location of a leader in the frame) and a brightness (luminosity) curve can be extracted from the video data, which is plotted against time and incorporated into the various waveform plots. The second way is to produce a time-shifted overlay of successive video frames, where

each successive video frame is offset horizontally by some pixel distance relative to the previous frame. This produces a composite image reminiscent of a streak image [e.g. *Ogawa and Brook*, 1964; *Berger and Vogelsanger*, 1966] and helps in identifying leader channel luminosity changes that occur during propagation.

4.2.1 Video overlay algorithm

To overlay video images, either with the time-shifted or regular (static) overlay method, an algorithm in the IDL language was used. This algorithm first subtracts a background frame off each frame, the background frame being any suitable frame of the video recording that does not show any leader activity. This leads to dark or black frames with only the lightning leaders visible. The algorithm then takes, for each individual pixel of the composite frame, the lighter value of that pixel for two successive frames and keeps that pixel value. When stepped leaders are studied, only those frames showing leader activity are processed in this way; frames in which a return stroke occurs are left out, to prevent overexposure of the composite image. If no time shifting is applied, the composite image looks very much like what would have been obtained with a still camera making a time exposure, except that the contrast with the background is higher because the background has been subtracted out. For the time-shifted video overlay the algorithm shifts the composite image to the left by a specified number of pixels as an extra step after doing the overlay of two frames.

4.2.2 LMA data

All LMA data in this chapter were processed at the 10 μs rate and filtered using a constraint of $\chi^2_\nu \leq 1.0$ (assuming a 70 ns timing accuracy) and a minimum of eight participating stations in solutions. Because relatively many stations (typically 12–14) were active in the array during most of 2010 this constraint produces clean, high-quality data without filtering out too many located VHF sources.

4.2.3 Time reference

There are different time bases for the various instruments. The time base most often used in LMA-related studies is simply the LMA (VHF) source time (UTC) which is taken to be the inferred VHF event time. However, there is an absolute time delay inherent in the LMA which has not yet been accurately determined at the time of this writing. Circumstantial evidence for this delay (by a comparison between an LMA station co-located with an LDAR station) indicates that it is on the order of

1.3 μs, but this relies on the timing accuracy of an LDAR station being accurately known, which has not been independently verified. Therefore, the LMA data in this study does not take this time delay into account.

Another time base is that of the digitizers for the waveform data, which are free-running in time on a computer that is poorly synchronized to UTC. These can be calibrated to match the time base of the Annex LMA station as described in Appendix B.

For the sake of comparison with waveform data and video data, LMA VHF source time (as determined by the LMA data processing algorithm) is converted to signal arrival time at the location of the instruments by adding the signal propagation time $\Delta t_i = d_i/c$ to the calculated event time of the i^{th} source, where d_i is the line-of-sight distance between the i^{th} source and the Annex. The speed of light c is taken to be that at 600 mb pressure, i.e. 299,792,458.0 / 1.0002 m s^{-1}, which is equal to the value for c used by the LMA processing software [*Thomas et al.*, 2004].

The high-speed video camera is synchronized to UTC by the IRIG-B standard; its manufacturer specifies a timing accuracy of 1 μs. This has not been independently verified either, but appears to be a correct upper-bound estimate from earlier LMA–video correlations by the author. Since this accuracy is on the order of the inferred LMA absolute time delay, and for these studies much smaller than the frame exposure time of 150 μs, the LMA time delay can be neglected when comparing LMA data with video data. It would need to be considered only when looking at VHF sources occurring very close to the start or end time of a frame exposure.

Since all pertinent instruments are co-located at the Annex observation deck of Langmuir Laboratory, all instruments essentially share this same time base, the *LMA time of arrival*. Thus, the time base used in correlating the various waveform plots with LMA and high-speed video imagery is not *actual event time*, but *perceived* or *retarded event time* at the location of the Langmuir Laboratory Annex. The time base used in the various LMA plots is still the actual VHF source time, however.

4.3 Storms on August 2, 2010

The BFB flash studied in this chapter occurred in the afternoon of August 2, 2010 at a distance of 22.5 km to the southwest of Langmuir Laboratory. The parent storm started producing lightning at 20:20 UTC, and was to the southeast of a larger storm that was already producing lightning prolifically. Most of the lightning activity in both storms was intracloud. The storm started producing BFB flashes at 20:48 with a flash toward the ESE, followed by four more BFB flashes in the 20:50–21:00 ten-minute time interval, of which the subject BFB flash was the last. All of these BFB flashes occurred at the ESE flank of the storm (according to LMA data).

During the 40 minutes leading up to the BFB flash the storms drifted in a general northerly direction and by 21:10 the BFB-producing storm had merged with its larger companion to form a NNW–SSE oriented line. Extensive leaders in the upper positive charge region were seen in LMA data to propagate to the west, with one leader reaching 25 km in length. According to the Albuquerque sounding from 8/3/2010 at 00 UTC, the upper-level winds (at 8–12 km altitude) were from the SSW at 30 knots; midlevel winds (at 4–8 km altitude) were also from the SSW but with speeds of only about 10 knots. The BFB flashes thus occurred to the eastern flank of the storm.

By 21:50 lightning activity had mostly ceased in the line of storms. A new storm, with supercell-like characteristics, had started to the north of the lab and was electrically very active with (almost exclusively) intracloud lightning at up to one flash per second and flashes reaching up to 15 km altitude. This storm, too, produced several BFB flashes at a later stage.

4.4 Main characteristics

Figure 4.1 shows waveform data of the BFB flash for a 900 ms time interval. The flash was beyond the reversal distance for intracloud electric field changes and the electric field in the ΔE waveform is thus seen to become more positive during the intracloud stage of the flash. The BFB flash produced four strokes to ground, each with an increasingly longer continuing-current component. The flash was a Type-II BFB flash of 738 ms duration, with the intracloud stage lasting 205 ms, the cloud-to-ground leader lasting 82 ms and the final stage lasting 451 ms.

Figure 4.2 shows LMA data (colored by time) for the full BFB flash, and Figure 4.3 indicates the cloud charge configuration inferred from the flash. The storm that produced the BFB flash was a normal-polarity storm with midlevel negative charge and upper positive charge, with the boundary situated near 8 km altitude above MSL at the time of the BFB flash.

Like all observed BFB flashes, the flash began as a normal-polarity bilevel IC flash. It initiated at 8 km altitude with a negative leader propagating up to 12 km altitude. The cloud-to-ground leader initiated at or very near to the initiation point of the intracloud flash while a K-leader started propagating upward along the original upward channel. During the final stage several dart leaders and K-changes occurred, typical of BFB flashes. Overall, the flash occupied a region of approximately 12×10 km in horizontal area and 10 km in altitude (above ground level).

Figure 4.4 shows VHF source power of the BFB flash, illustrating the generally higher-power VHF radiation associated with negative breakdown.

The three stages of this BFB flash will be studied in detail in the following sections.

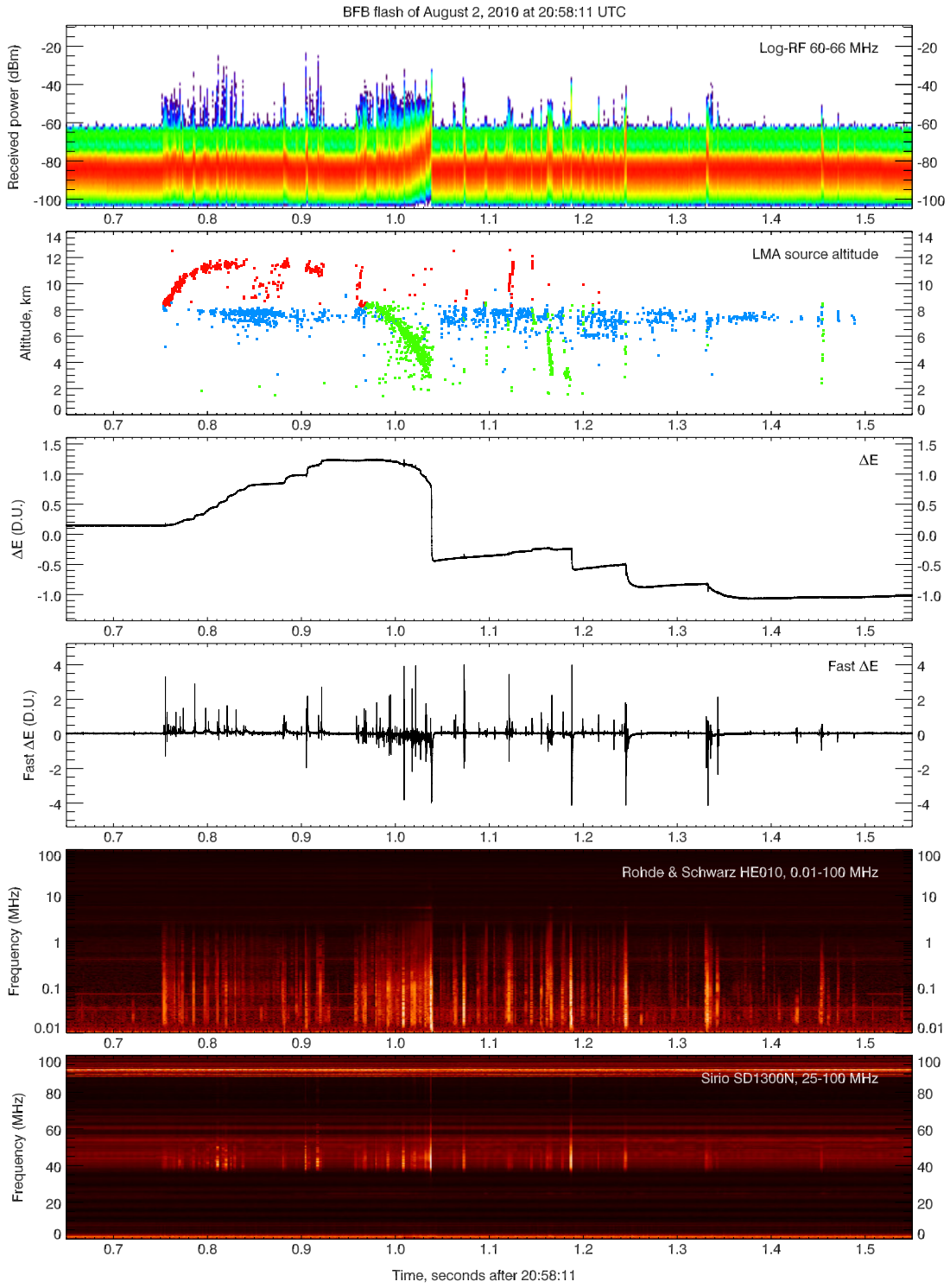

Figure 4.1: Full waveform data for the BFB flash of August 2, 2010 at 20:58:11 UTC. Top panel shows 63 MHz log-RF waveform as a two-dimensional sample-density histogram. Second panel shows an altitude–time plot of located VHF events, colored by charge (see Figure 4.3). Third through sixth panels show slow and fast ΔE, 0.01–100 MHz and 25–100 MHz broadband waveforms, respectively.

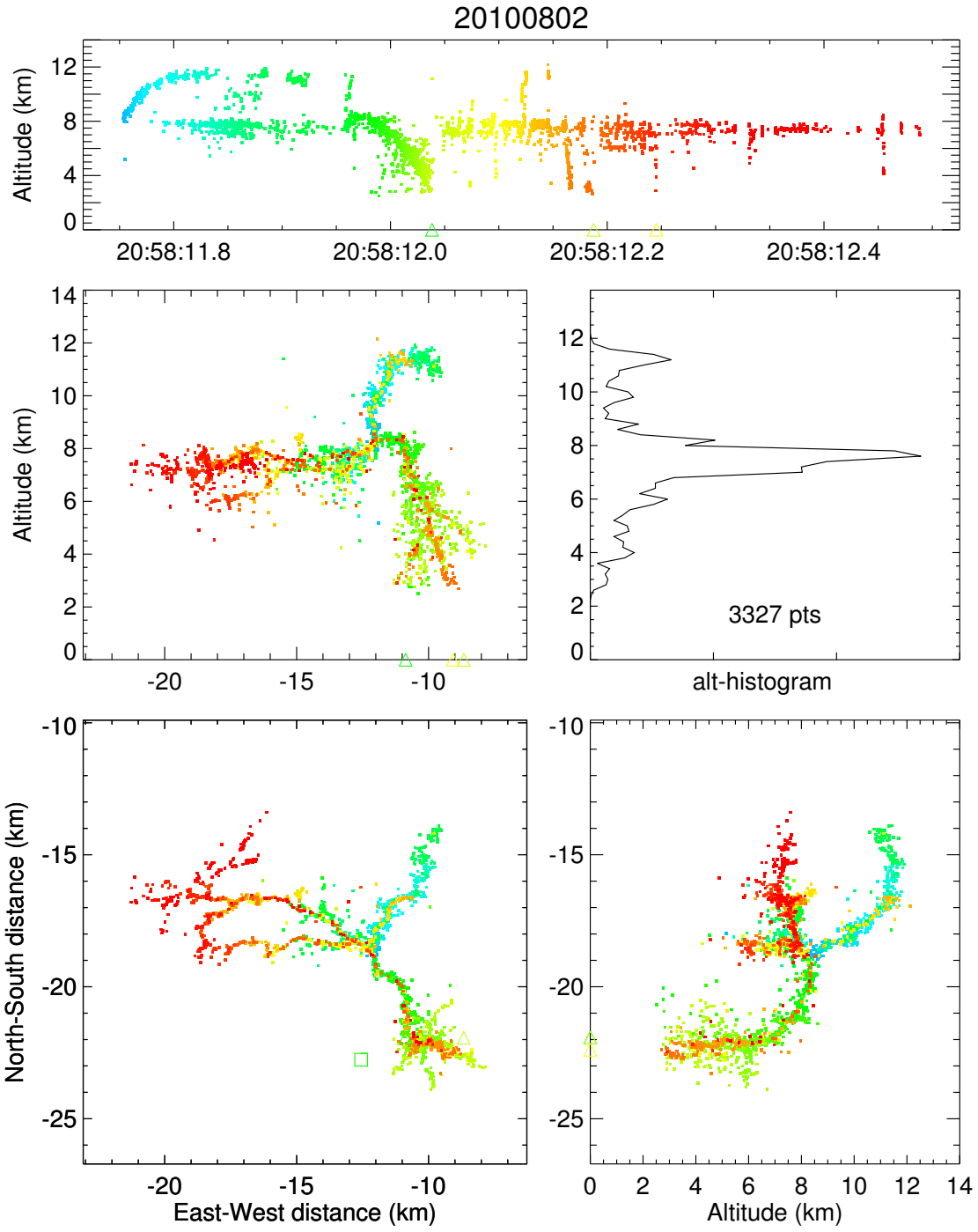

Figure 4.2: LMA data for the BFB flash of August 2, 2010 at 20:58:11 UTC, colored by time. Strokes to ground located by the NLDN are indicated by triangles. The leader to ground occurred close to the Tigner LMA station (green square).

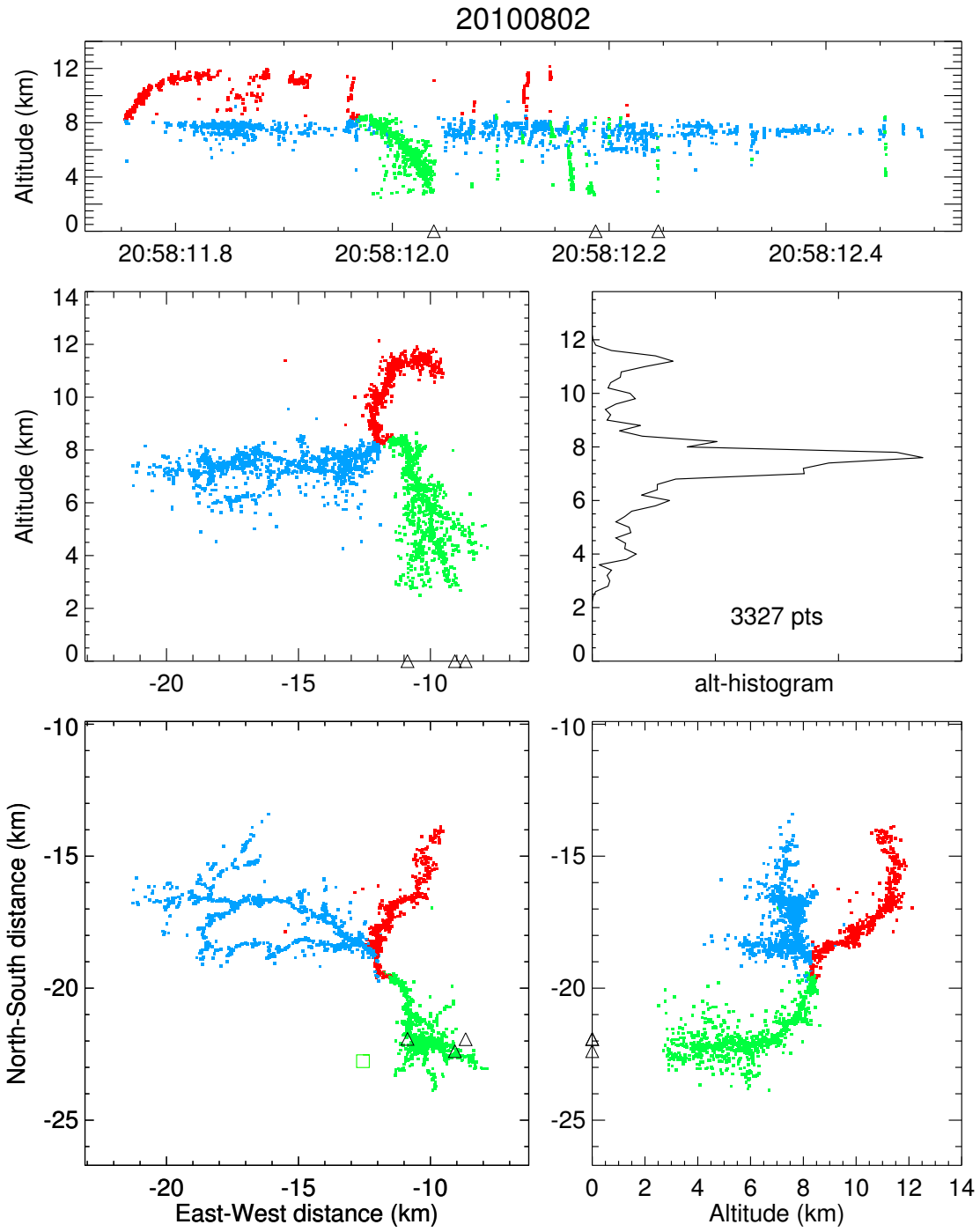

Figure 4.3: LMA charge identification for the BFB flash of August 2, 2010 at 20:58:11 UTC. Blue indicates positive breakdown propagating through negative charge while red indicates negative breakdown propagating through positive charge. Green sources indicate negative breakdown propagating through undetermined space charge.

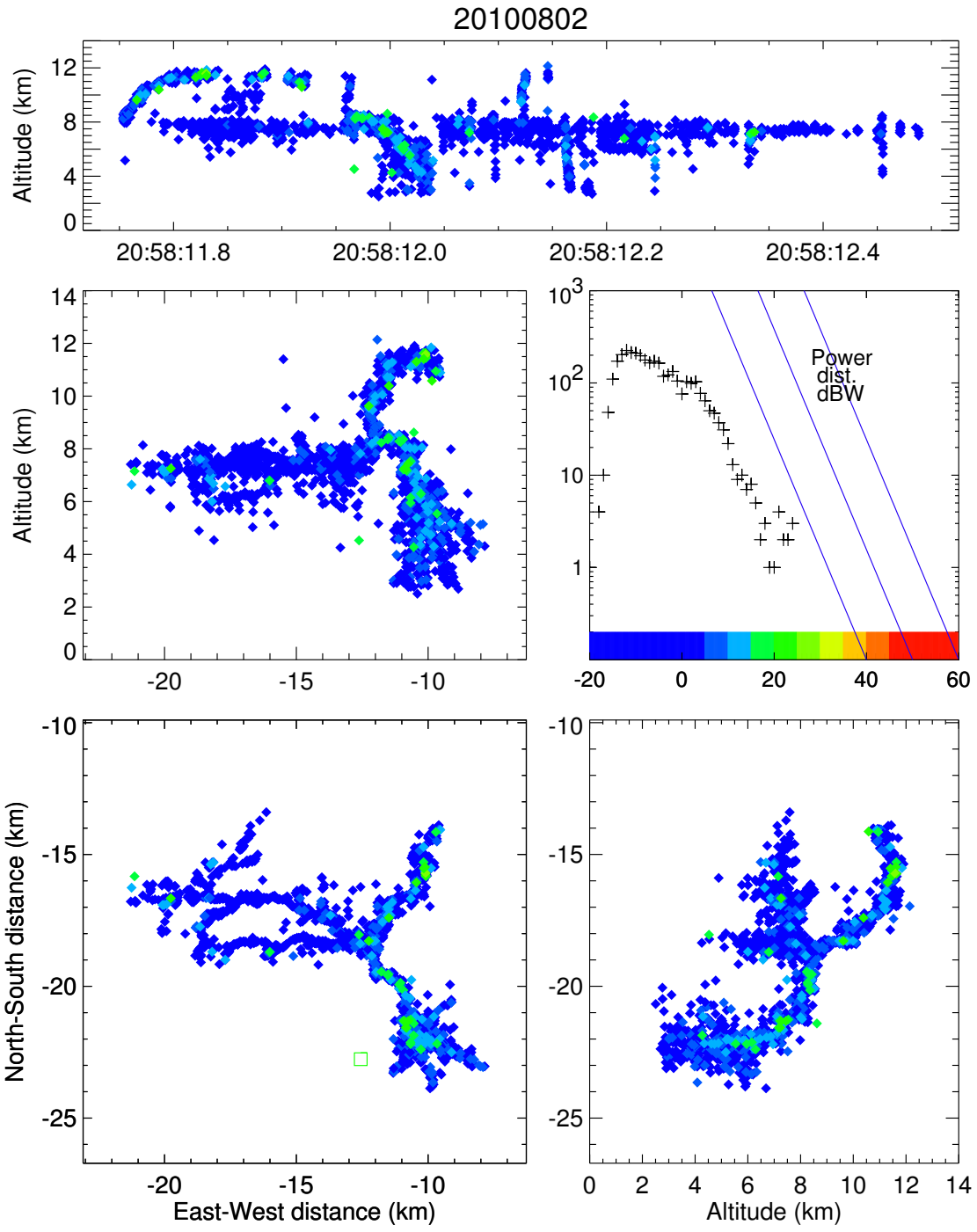

Figure 4.4: VHF source power for the BFB flash of August 2, 2010 at 20:58:11 UTC. The VHF sources associated with negative breakdown tend to have higher source power.

4.5 Intracloud stage

The intracloud stage started at 20:58:11.7525 UTC and lasted for 205 ms, until the initiation of the cloud-to-ground leader. The flash initiated with a negative leader at 8.2 km altitude, which proceeded to propagate upward into the upper positive charge region following a slanted trajectory toward the northeast. It traveled about 2.5 to 3.0 km during the first 20 ms, at an average velocity of 1.3–1.5$\times 10^5$ m s^{-1}, which is typical of intracloud negative leaders [e.g. *Proctor*, 1981; *Liu and Krehbiel*, 1985; *Shao and Krehbiel*, 1996; *Behnke et al.*, 2005]. Interestingly, VHF sources that appear to be associated with positive breakdown started almost simultaneously with those of negative breakdown. Several VHF sources are located at the base of the negative upward leader (Figure 4.5, second panel), which are delayed by about 500 μs from those associated with the negative leader.

After 25 ms and for a duration of 63 ms the negative leader started exhibiting intermittent growth with brief ($\sim$ 5 ms long) pauses, during which VHF sources associated with positive breakdown in the midlevel negative charge region were located by the LMA (Figures 4.5 and 4.6). The VHF activity of the negative leader in the upper positive charge region and the inferred positive leader in the midlevel negative charge region thus seemed to alternate. The path of the negative leader shows no spatial gaps, so the upward leader temporarily stopped propagating during the pauses before being rejuvenated.

It is unclear if positive breakdown halted during the time when the negative leader was propagating, or whether positive breakdown was occurring concurrently with negative breakdown but not being located by the LMA.

During each burst of VHF emissions from negative breakdown an enhanced current flow was observed, with generally one single narrow, high-amplitude fast ΔE pulse superimposed (Figure 4.5, fourth panel). This intermittent enhanced current flow with superimposed pulses gives rise to the staircase appearance of the ΔE waveform (third panel). The fast pulses are on the order of 3–4 μs width. The polarity of the pulses and the enhanced current flow indicate negative charge being carried up to higher altitude, or equivalently, positive charge being lowered. These pulses also appear bright in VHF against a background of weaker impulsive VHF events (spectrogram in fifth panel), which can be observed in the spectrogram at times when the negative leader has temporarily stopped propagating and may therefore be associated with K-events in the positive breakdown region.

The large-amplitude pulses are most likely associated with K-leaders that carry negative charge upward into the upper positive charge region and help the negative breakdown there along. Because the K-leaders occur *during* a brief burst of negative breakdown and not *before*, it appears as if the negative breakdown is inducing the K-leaders, rather than the K-leaders being initiated solely due to the positive

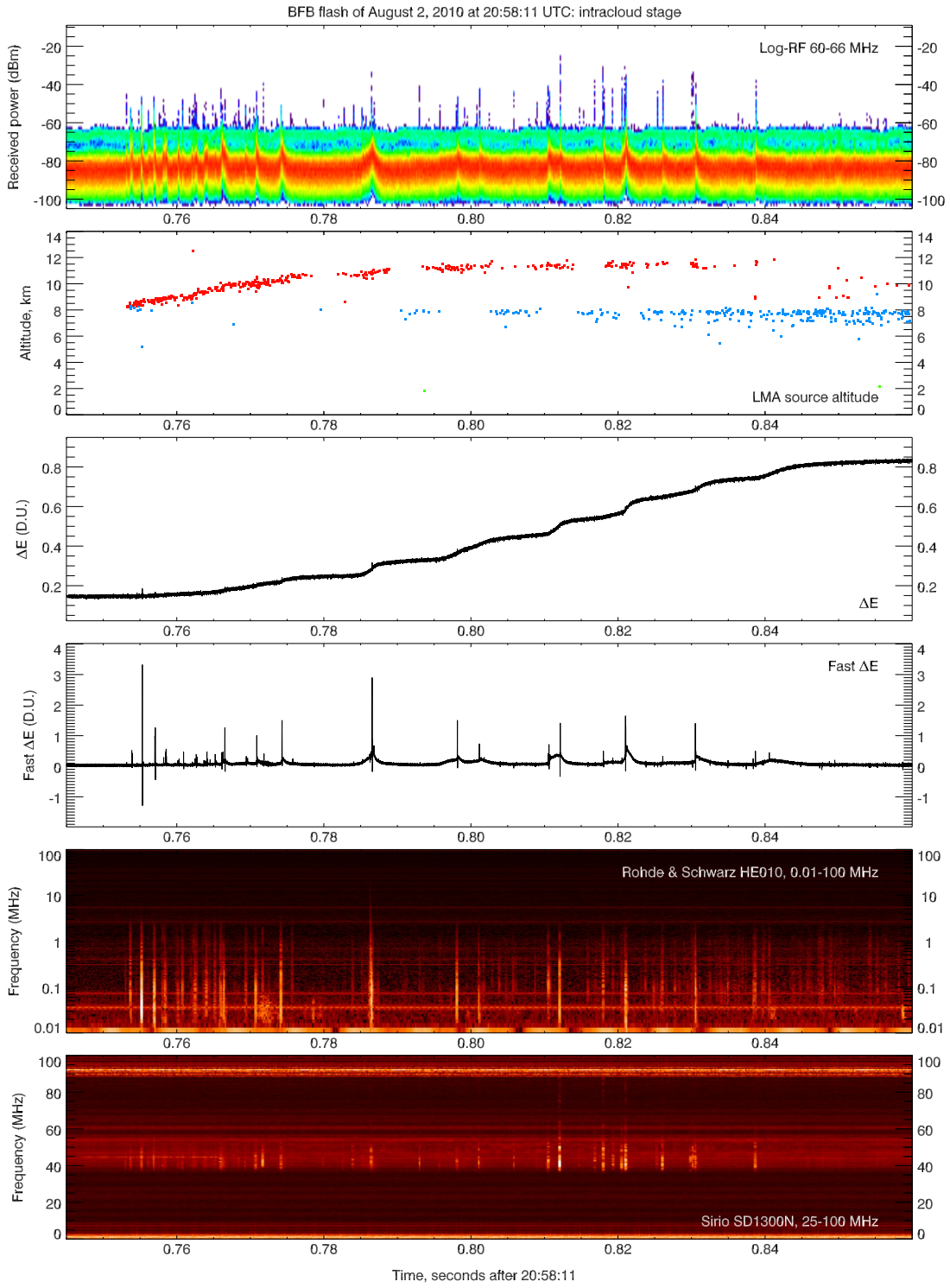

Figure 4.5: Waveforms for a time interval of 115 ms during the initial intracloud activity. Note the bright RF emissions during current pulses, causing stepwise positive changes in the ΔE waveform (third panel). These current pulses occur during the 5–10 ms long bursts of VHF sources associated with negative breakdown (second panel). Also note positive breakdown apparently starting nearly simultaneously with negative breakdown (see text).

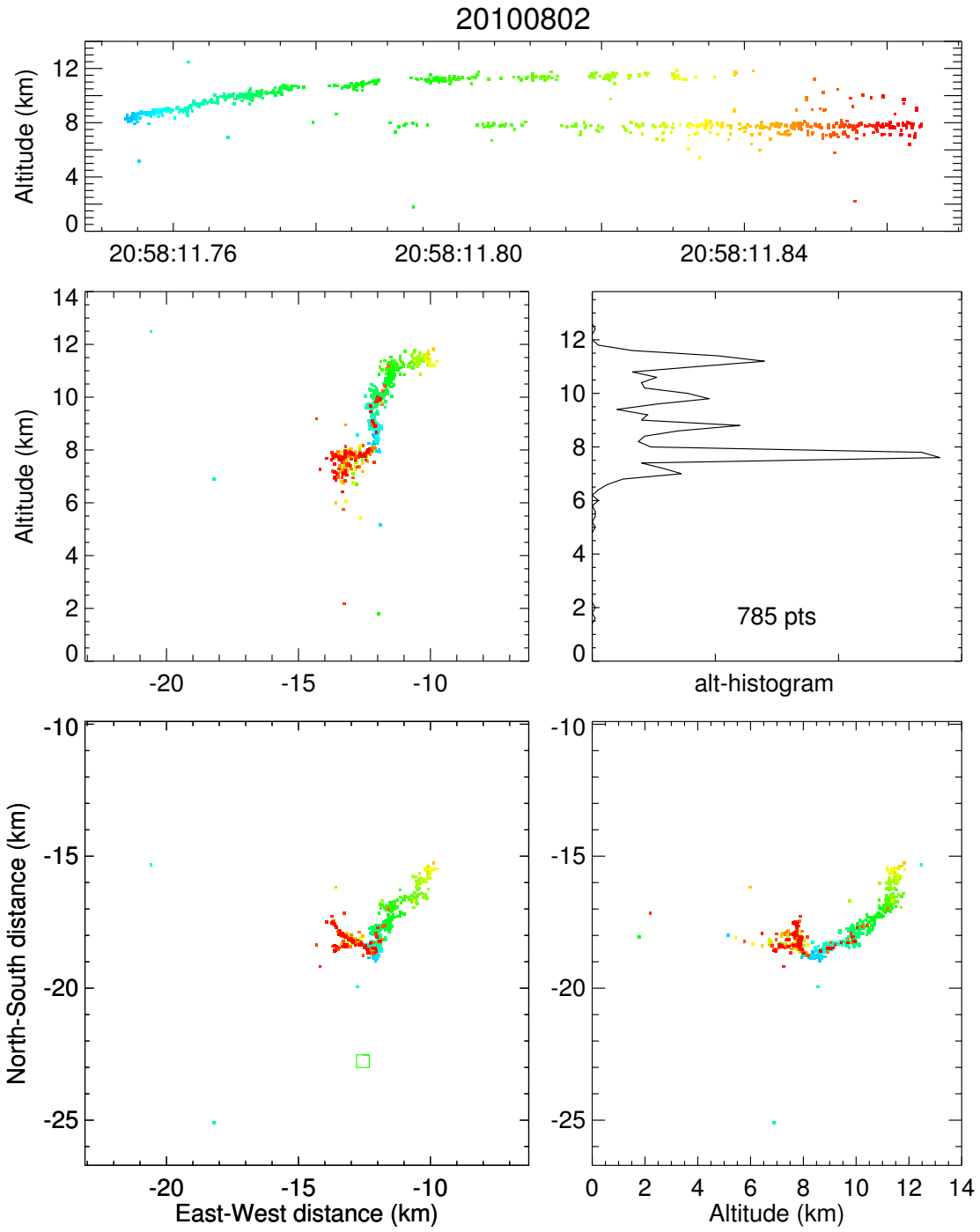

Figure 4.6: VHF sources located by the LMA during the initial intracloud activity. VHF emissions from the upward negative leader and those associated with positive breakdown below 8 km altitude are seen to alternate. Note the VHF sources located along the original upward channel later in the time interval.

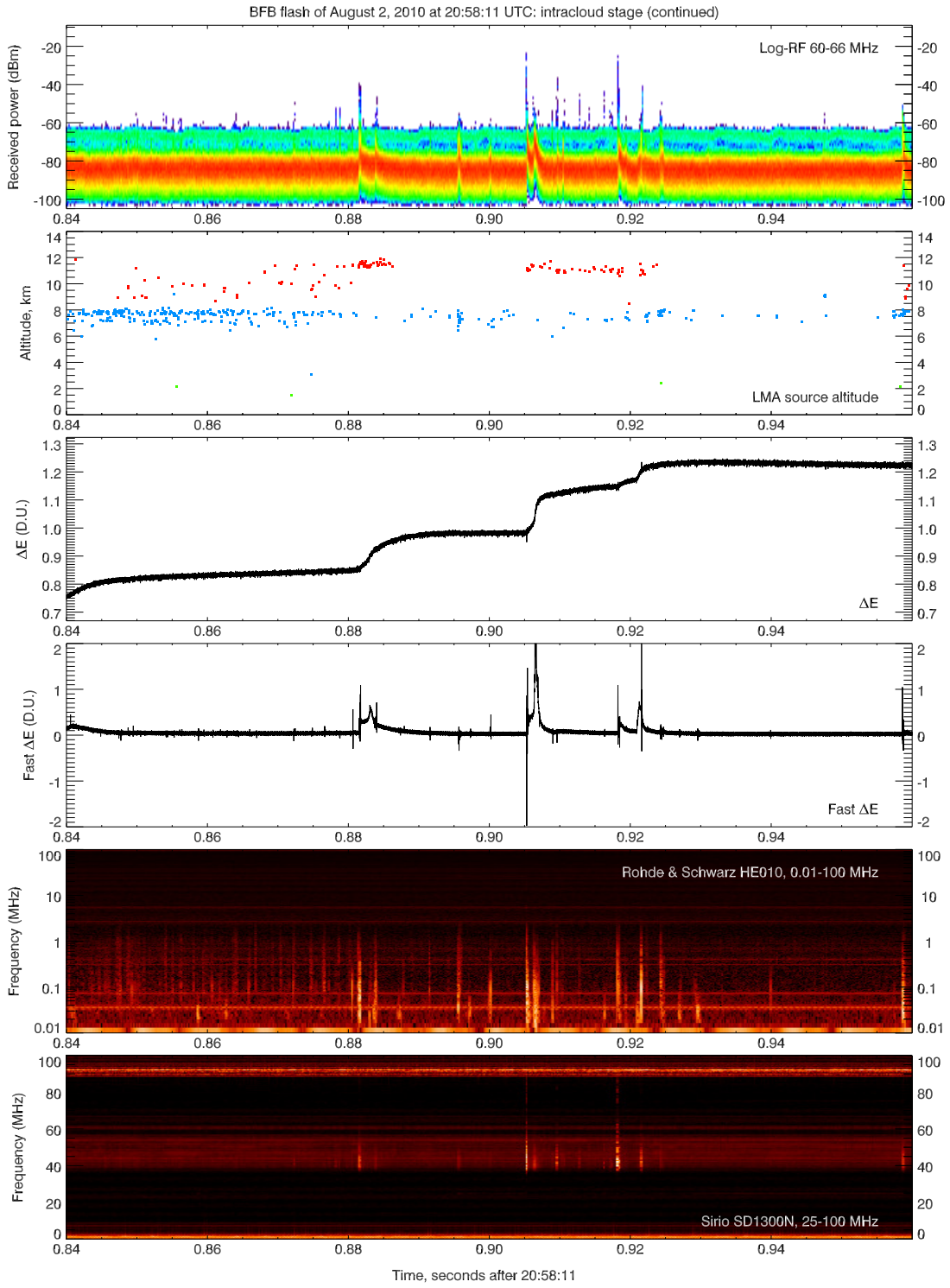

Figure 4.7: Waveforms for the later phase of the intracloud activity, leading up to the cloud-to-ground leader. The time interval is 120 ms. Note the three major ΔE changes (K-changes), each leading to renewed negative breakdown in the upper positive charge region.

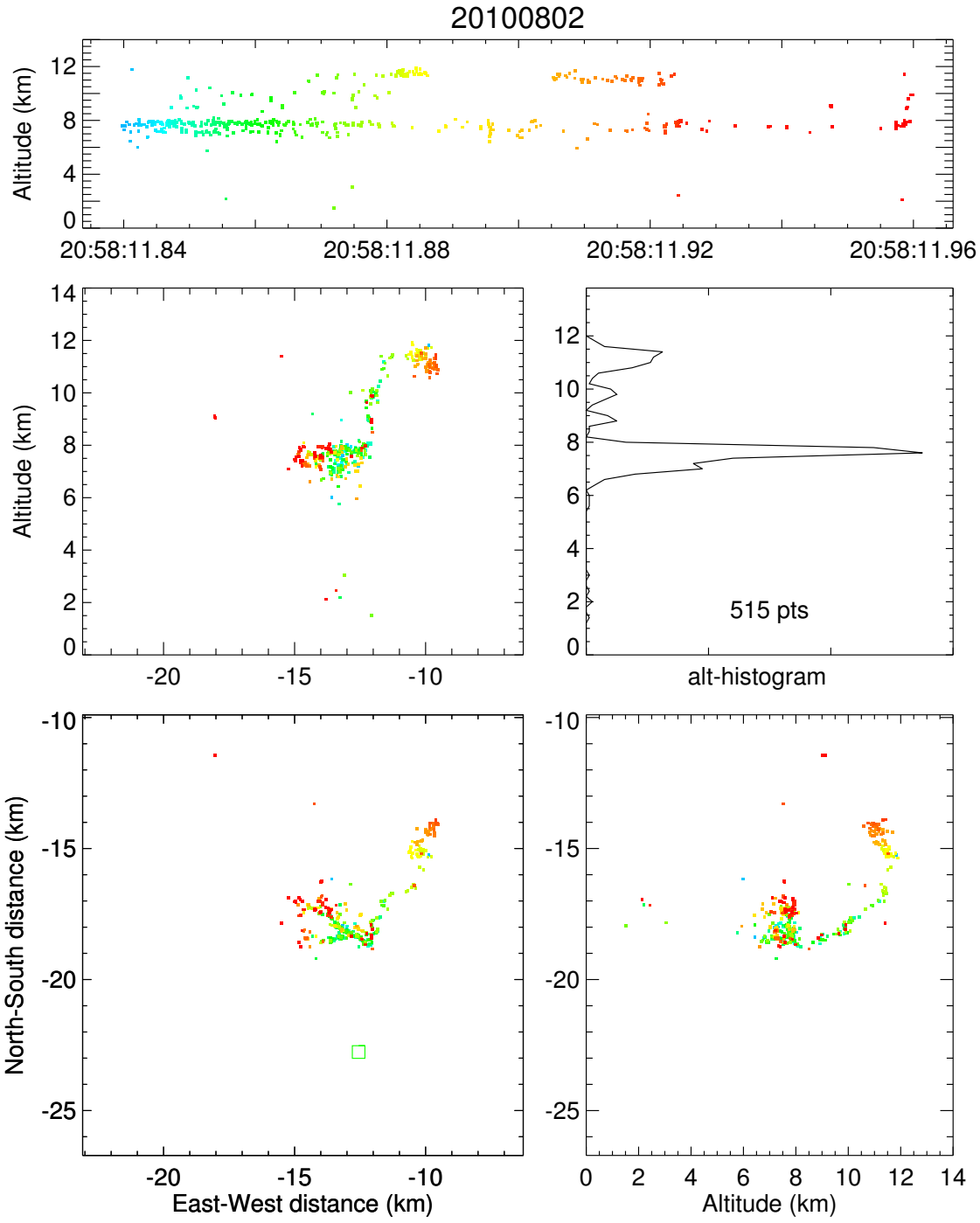

Figure 4.8: VHF sources located by the LMA during the later phase of intracloud activity, leading up to the leader to ground. Both the negative and positive breakdown were extended by about 2 km during the time interval of 120 ms.

breakdown process. It is possible that the negative breakdown, while it is ongoing, is changing the potential of the channel up to the point that a K-leader is initiated. However, it is unusual that the negative leader propagates so intermittently; it could be the result of weak positive breakdown.

Very similar K-leader pulses were observed by *Shao and Krehbiel* [1996] in an IC flash (e.g. event I1 in their Figure 4). These pulses occurred during some fast negative breakdown events propagating upward (i.e. K-leaders) and were associated with a burst of positive breakdown occurring at the base (starting point) of the upward negative breakdown channel. The bursts of positive breakdown propagated a short distance in the opposite direction, away from the starting point. The bursts are quite strong in VHF and can be located by interferometric or lightning mapping techniques. The burst of positive breakdown can produce a "forward stroke" (in the same direction as the K-leader) that causes a sudden current increase along the negative breakdown channel and a step change in the electric field [*Shao et al.*, 1995].

During the 40 ms time interval following the series of K-leader pulses (starting at 20:58:11.843, 90 ms into the flash), upper-level negative breakdown temporarily ceased while VHF sources associated with positive breakdown were being located by the LMA in the midlevel negative charge region. These sources extended along channels of positive breakdown in a general WNW direction. This positive breakdown was mapped quite well by the LMA by virtue of the numerous K-events. During the extension of the positive breakdown a number of discrete and scattered (in both time and altitude) VHF sources were detected along the existing channel from the upward negative leader, at 8–12 km altitude (Figure 4.6). It appears that charge was still being supplied to this upward channel, but not sufficiently so to re-initiate leader growth until the end of the 40 ms interval at 20:58:11.880. At that time a relatively large K-change occurred (Figure 4.7) and new negative breakdown initiated for 5 ms, extended the negative channel in the upper positive charge region by about 1 km (Figure 4.8).

The negative breakdown was reinitiated two more times, at 0.906 and 0.922 seconds after 20:58:11. Each event was started by a fairly strong K-change. These two events extended the negative breakdown again by about 1 km. All three K-changes appear bright in the log-RF and fast ΔE waveform, as well as in both spectrograms of Figure 4.7.

After the third K-change at 20:58:11.922 in Figure 4.7, the negative charge region became more quiet for about 33 ms, until the cloud-to-ground leader initiated at 20:58:11.957.

4.6 Cloud-to-ground stage

Figures 4.9 and 4.10 show waveform and LMA data during the 100 ms long time interval of the cloud-to-ground leader. The leader took about 80 ms to propagate from 8 km altitude to ground (1.8 km altitude above MSL) at an apparent (vertical) velocity of 8×10^4 m s^{-1}. During the leader propagation to ground no in-cloud VHF sources other than those belonging to the negative leader were located by the LMA; in other words, no signs of positive breakdown in the negative charge region were detected. It is likely that positive breakdown was ongoing at that time but was not detected by the LMA.

In the LMA data of Figure 4.10 various branches of the cloud-to-ground leader are resolved. These can be discerned clearly in the plan view. The altitude of VHF sources in these branches is much more poorly determined, partly because the elevation of these sources was low relative to the plane within which most LMA stations were situated; small timing errors translate to large altitude variations for VHF sources near this plane. This effect is exacerbated by the mountainous terrain, which blocks line-of-sight view of several LMA stations to low-altitude VHF sources.

The negative leader to ground initiated close to the original initiation point of the flash, as a new branch that started simultaneously with a K-leader that propagated upward along the original upward channel. VHF sources from this K-leader were located by the LMA at up to 11 km altitude, slightly lower than the maximum altitude of the channel.

The log-RF waveform in Figure 4.9 shows the characteristic VHF emissions of the cloud-to-ground leader of a BFB flash quite well, as a transition from more impulsive to more continuous breakdown. At 8 km altitude, VHF emissions from the leader consist of intermittent pulses with quieter periods of 1–5 ms in between pulses. As the leader propagates to ground the time between peak events becomes shorter to the point when peak-power events succeed one another so frequently that VHF emissions appear to be continuous in nature. This is seen in the log-RF waveform as the "lifting" of the waveform off background levels. It is important to note that VHF emissions by the leader are not increasing in peak power, but rather increasing in rate, causing an increase in the *time-averaged* VHF source power. As shown in Section 3.3.1, regular –CG flashes, which initiate between midlevel negative and lower positive charge at 5–6 km altitude, also exhibit these apparently continuous emissions, as do low-IC flashes (Section 3.3.4). Classic IC flashes, which typically initiate at about 8 km altitude, exhibit more impulsive breakdown (Section 3.3.2).

A series of relatively high-power VHF and current pulses occur during the cloud-to-ground leader stage (Figure 4.9). After each pulse, VHF emission rates are temporarily enhanced. The cause of these pulses will be studied below, by correlating high-speed video recordings to the waveform and LMA data.

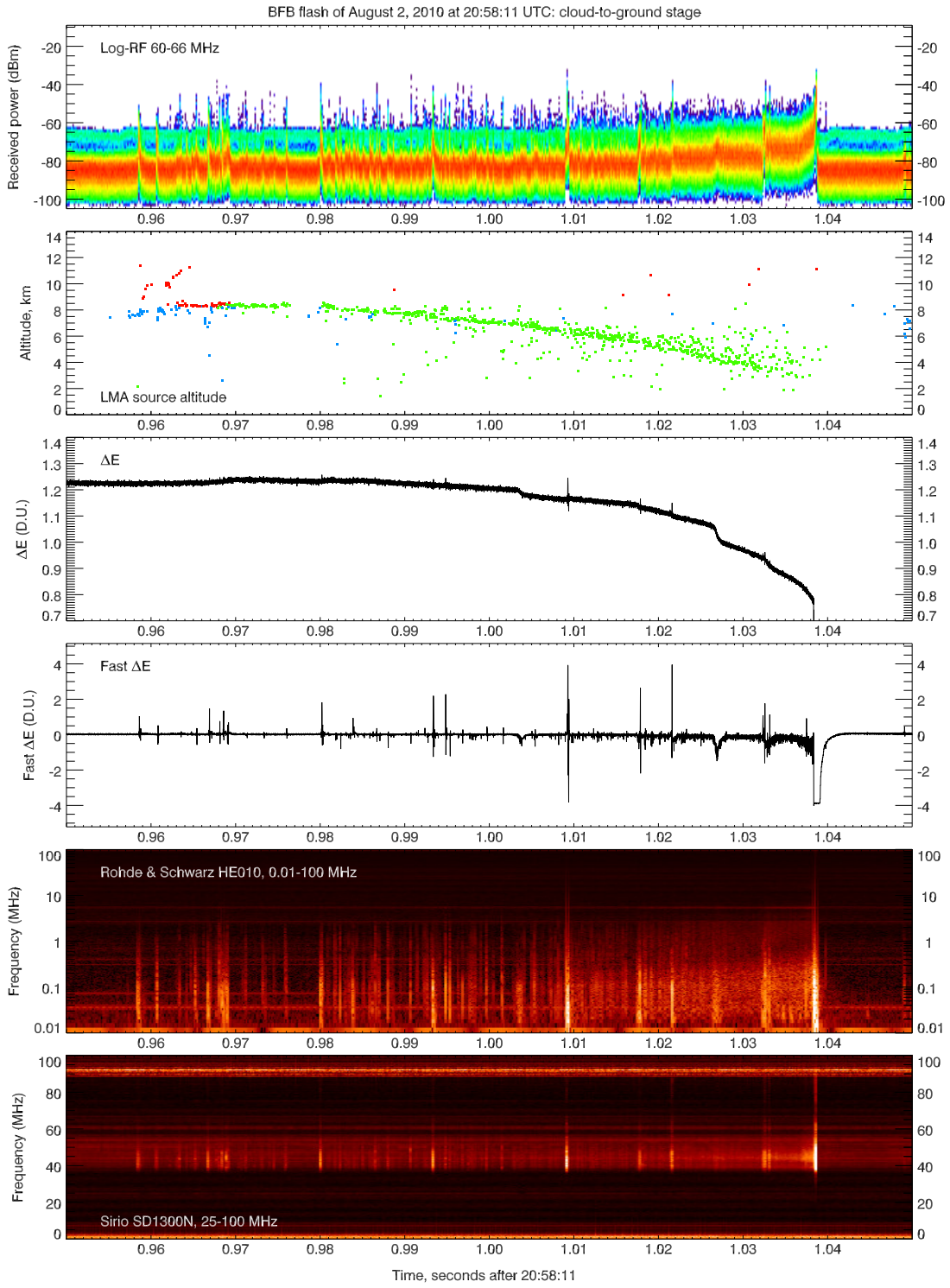

Figure 4.9: 100 ms of waveform data during the cloud-to-ground negative leader. The leader starts at 8 km altitude with impulsive, intermittent breakdown, gradually transitioning to more continuous breakdown. The peak amplitude of the various pulses does not change much (see log-RF waveform); rather, the VHF pulse rate increases as the leader propagates to ground.

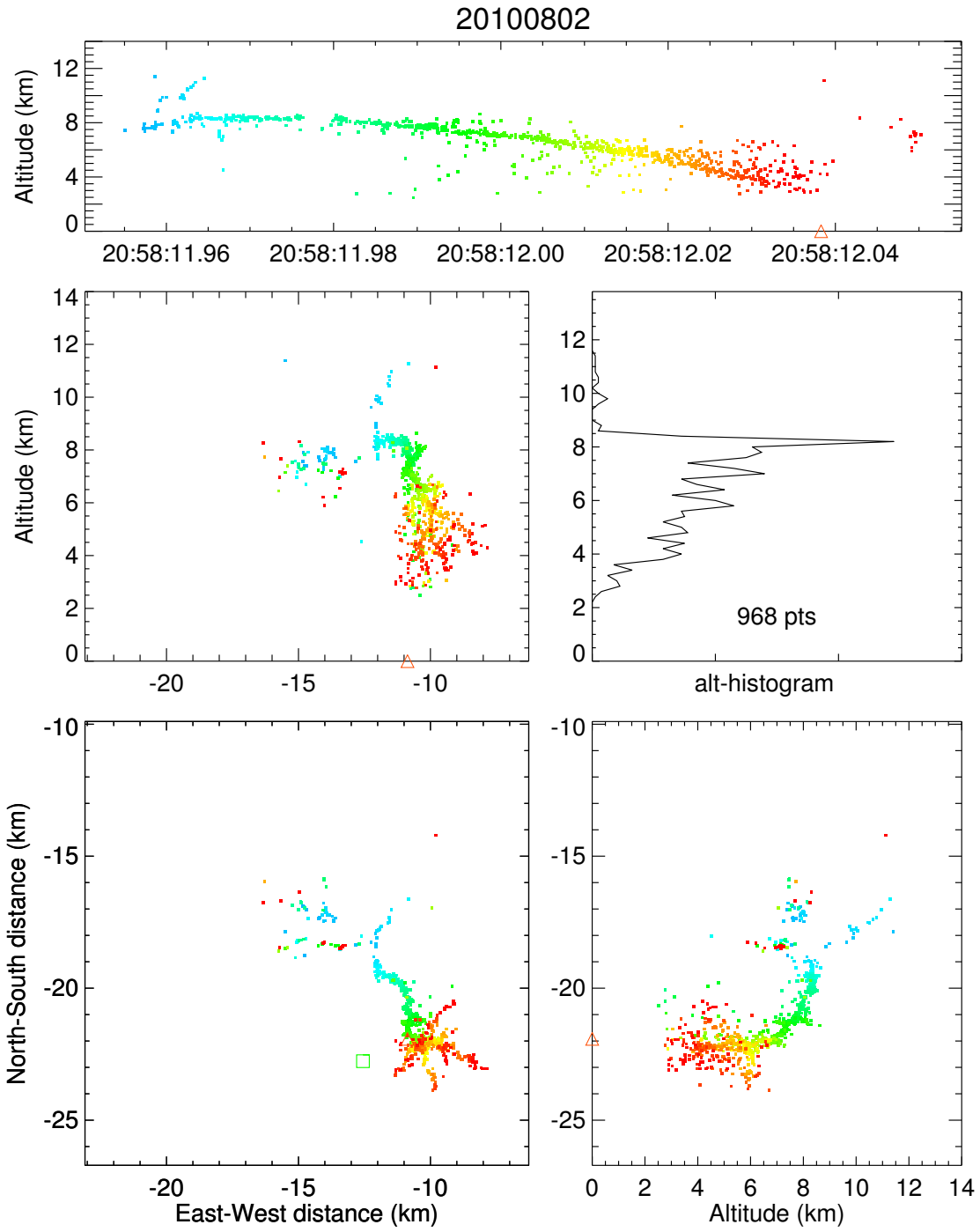

Figure 4.10: LMA data of the cloud-to-ground leader of the BFB flash. The exiLMA sting upward channel is retraced by a K-leader while a new negative leader initiates and becomes the cloud-to-ground leader. Note how the LMA resolved the individual low-altitude branches of the main cloud-to-ground leader well in plan location, but less so in altitude.

The high-speed video camera was operated at 6400 FPS at a frame size of 800×600 pixels. Figure 4.11 shows a composite of all high-speed video frames leading up to the first return stroke. The composite was made by overlaying successive frames, keeping the lighter value of each individual pixel. Because a BFB flash was expected during the recording, but at a much closer range, a relatively wide-angle lens was fitted to the camera, making the leader appear relatively small in the full video frame.

Four distinct branches can be identified in the video images, which show the leaders below the cloud base (which was at about 4.2 km altitude). Branch 1, itself split into two major branches (Branches 1a and 1b), was the first leader to contact ground, producing the first return stroke of the flash. Interestingly, Branch 2 and not Branch 1 became the main leader to ground for all successive dart leaders (which will be discussed in Section 4.7).

Each leader became profusely branched as they propagated to ground, an effect commonly seen in BFB flashes (e.g. Photos D.4, D.10, and D.14). Branch 4 emerged below the cloud base at a late stage, when Branches 1, 2 and 3 had already propagated farther down to ground.

Figure 4.12 shows the first return stroke frame (as the full uncropped frame) with VHF sources overlaid by a point-projection (Section A.8.4). The VHF sources are color-coded by time. The figure illustrates how much both the upward negative leader and cloud-to-ground leader were offset from the main midlevel negative charge region farther to the right (west) in the image. The associated main downdraft can be seen to the far right in the video frame. Several K-leaders along the upward branch and dart-leaders along the cloud-to-ground branch can be seen in the overlay. The upward negative leader propagated in the general direction of the camera; the cloud-to-ground leader and the positive breakdown in midlevel negative charge occurred in generally transverse directions relative to the camera.

Figure 4.13 shows waveform data for the last 15 ms of the cloud-to-ground leader. Two bursts of enhanced current flow through the leader channel can be discerned in the ΔE waveform. The first ΔE excursion (at 20:58:12.027) shows up well at lower frequencies (below $\sim$ 300 kHz) but not at VHF, unlike the second event (at 20:58:12.032), which had several fast ΔE pulses that are clearly visible in VHF. The polarity of the fast ΔE excursions indicates that negative charge is receding from the instruments. In this case, negative charge originating from the positive breakdown can flow either to the upper positive charge region along the preexisting upward branch or downward along the (partially completed) path of the leader to ground. No other negative breakdown is being detected by the LMA. Since the upward branch lies in the general direction of the instrument, the polarity of the fast ΔE pulses indicates that negative charge was carried down along the partially completed cloud-to-ground leader channel.

The second current pulse (at 20:58:12.033) shares similar characteristics with the first

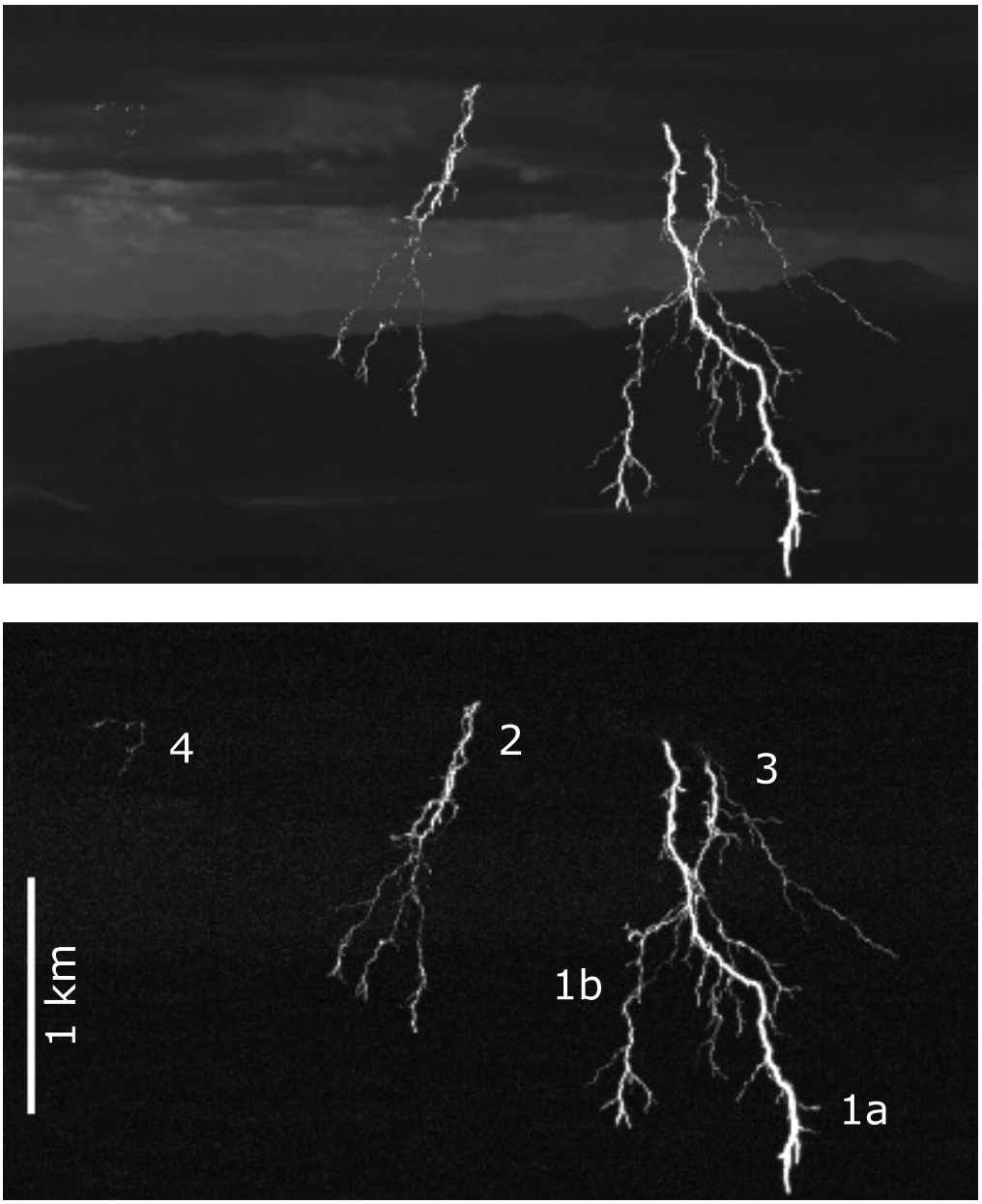

Figure 4.11: A composite of all video frames of the cloud-to-ground leader leading up to the first return stroke. The frame represents about 2.5 km altitude at the location of the leader, which is at a distance of 22.5 km from the camera. In the bottom figure the background has been subtracted. Four individual branches are visible below the cloud base, all of which were connected to the main channel higher up in the cloud. Branch 1a became the main (first) cloud-to-ground channel, while Branch 2 was later connected to ground by a dart-stepped leader. Branch 4 emerged from the cloud base at a late stage when Branch 1 was approaching ground. The prominent peak in the background to the right is Vicks Peak; its coordinates were used to determine the azimuth and elevation angle of the camera. The video camera was fitted with a lens of 50 mm focal length set at an aperture of $f/16$.

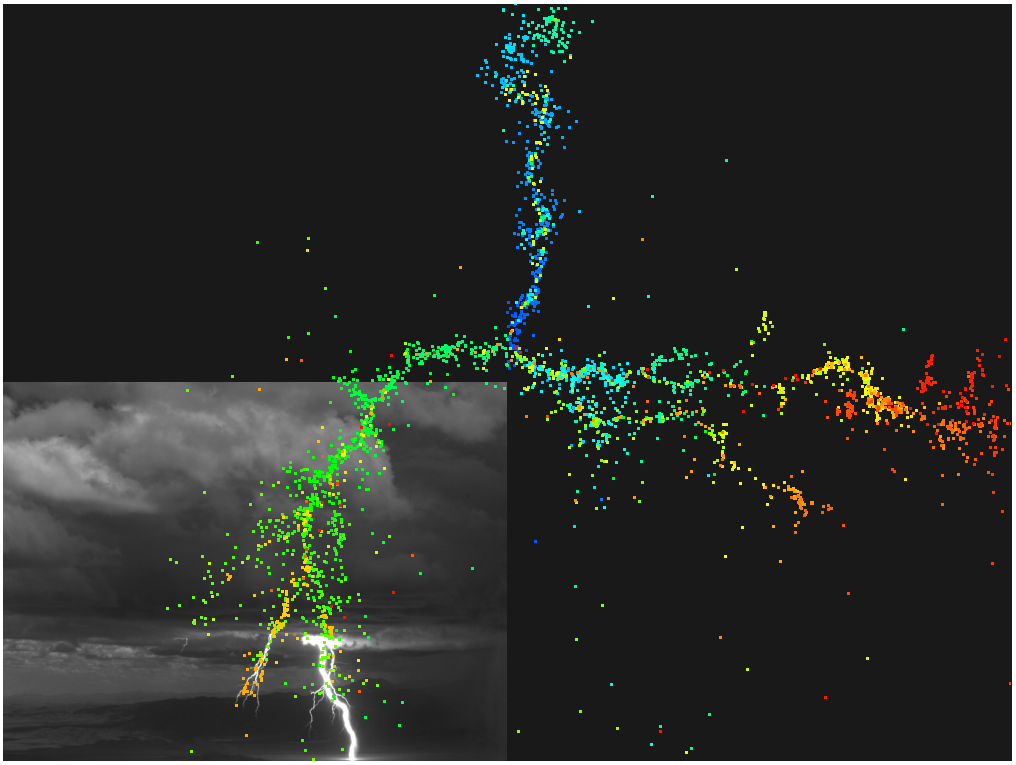

Figure 4.12: An overlay of VHF sources located by the LMA on the first return-stroke video frame by a point-projection (i.e. in the way the camera would have imaged the full extent of the flash had the cloud not been in the way). Note how little of the full extent of the flash is actually observed below the cloud base. The upward negative leader approaches the camera; the positive breakdown occurs to the right (west). Branch 2 (Figure 4.11) has several well-located VHF sources superimposed on it, which occurred during a later dart-stepped leader. The main channel (Branch 1) has very few located VHF sources superimposed on it below the cloud base.

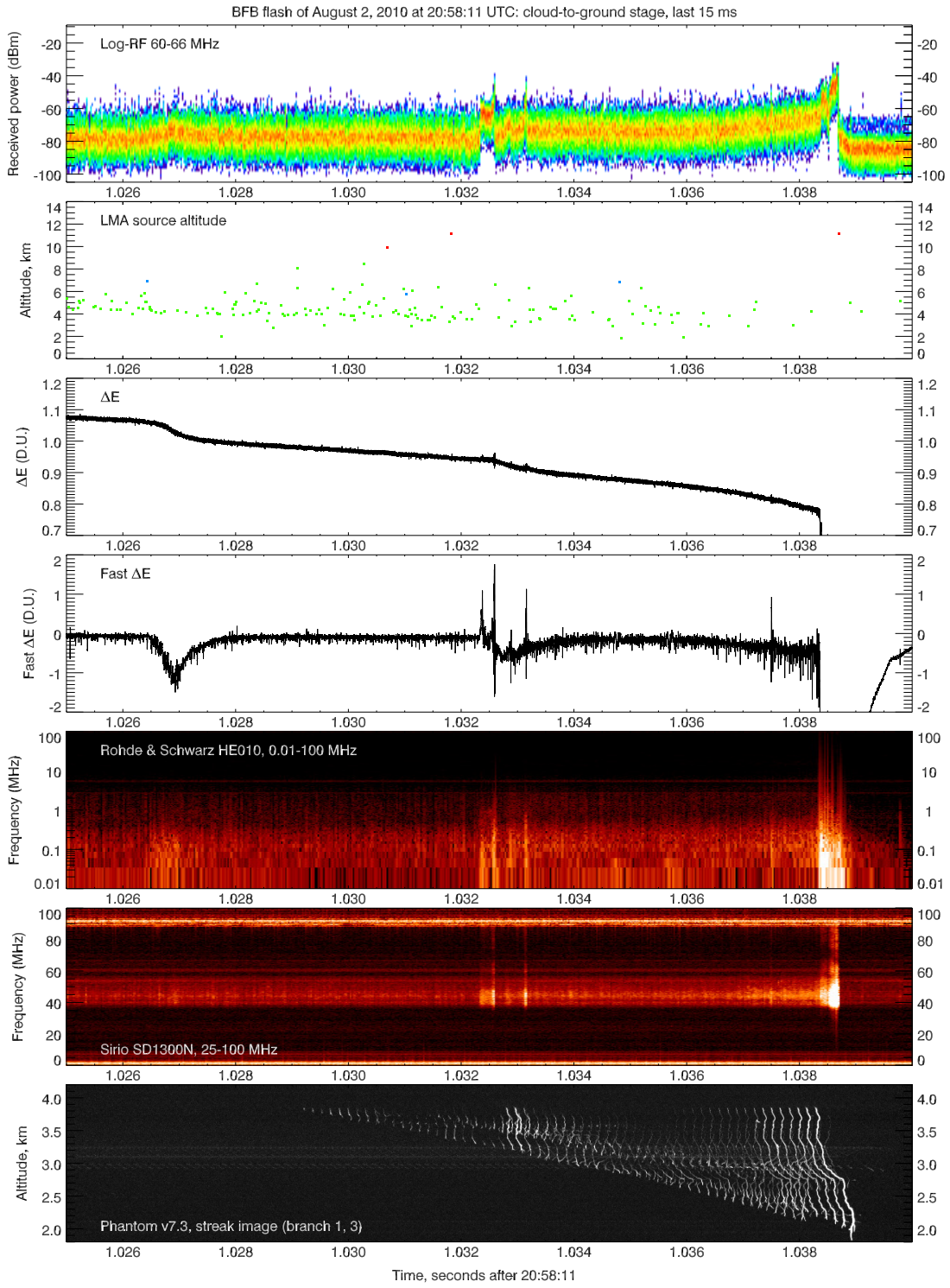

Figure 4.13: Waveforms and video streak image (of Branches 1 and 3) during the final 15 ms of the cloud-to-ground leader. The enhancement in luminosity of both leader channels at 1.033 seconds past 20:58:11 is associated with a series of fast ΔE and VHF pulses. These pulses are seen clearly in the spectrograms. (See also Figure 4.14.)

pulse, but it has several VHF pulses superimposed on it and the current flow is not as large as that during the first pulse. However, at this time three of the four branches had emerged below the cloud base and were recorded on high-speed video. Shortly after the onset of the series of pulses (about three video frames or 450–470 μs later in time) all three branches were brightly illuminated along their entire visible length. This illumination event lasted for two video frames (each 156.25 μs in duration), after which the channel luminosity slowly decreased as the leader continued to propagate to ground. No significant change in leader velocity is seen after the second current pulse but the leader was more luminous along a longer section of its visible channel, and the VHF pulse rate is slightly higher in the log-RF waveform.

The location of the leader tip of Branch 1 was very near to or at the location where it produced a major branch (Branch 1b) at the time of the luminosity event. It is possible that the branching was in fact caused by the event.

Some mechanism caused a sudden increase in the flow of charge along the length of the leader channel, which in turn enhanced the conductivity of the channel and "rejuvenated" the negative stepped leader (with VHF emissions occurring at a higher rate). The occurrence of K-leaders was inferred during the intracloud leader stage (Section 4.5) and there is no reason to assume K-leaders do not occur during the cloud-to-ground leader stage as well. K-leaders initiate by K-events that are associated with positive breakdown in the midlevel negative charge region [e.g. *Kitagawa*, 1957; *Ogawa and Brook*, 1964; *Shao and Krehbiel*, 1996]. *Shao et al.* [1995] have shown that K-events are responsible for both K-leaders propagating upward in IC flashes and for dart leaders propagating downward in –CG flashes, and they found that K-leaders and dart leaders are the same phenomenon: fast negative breakdown along a previous leader channel that propagates at speeds between 10^6 and 10^7 m s^{-1}. The luminosity event observed here was thus a K-leader (dart leader) that occurred before the return stroke.

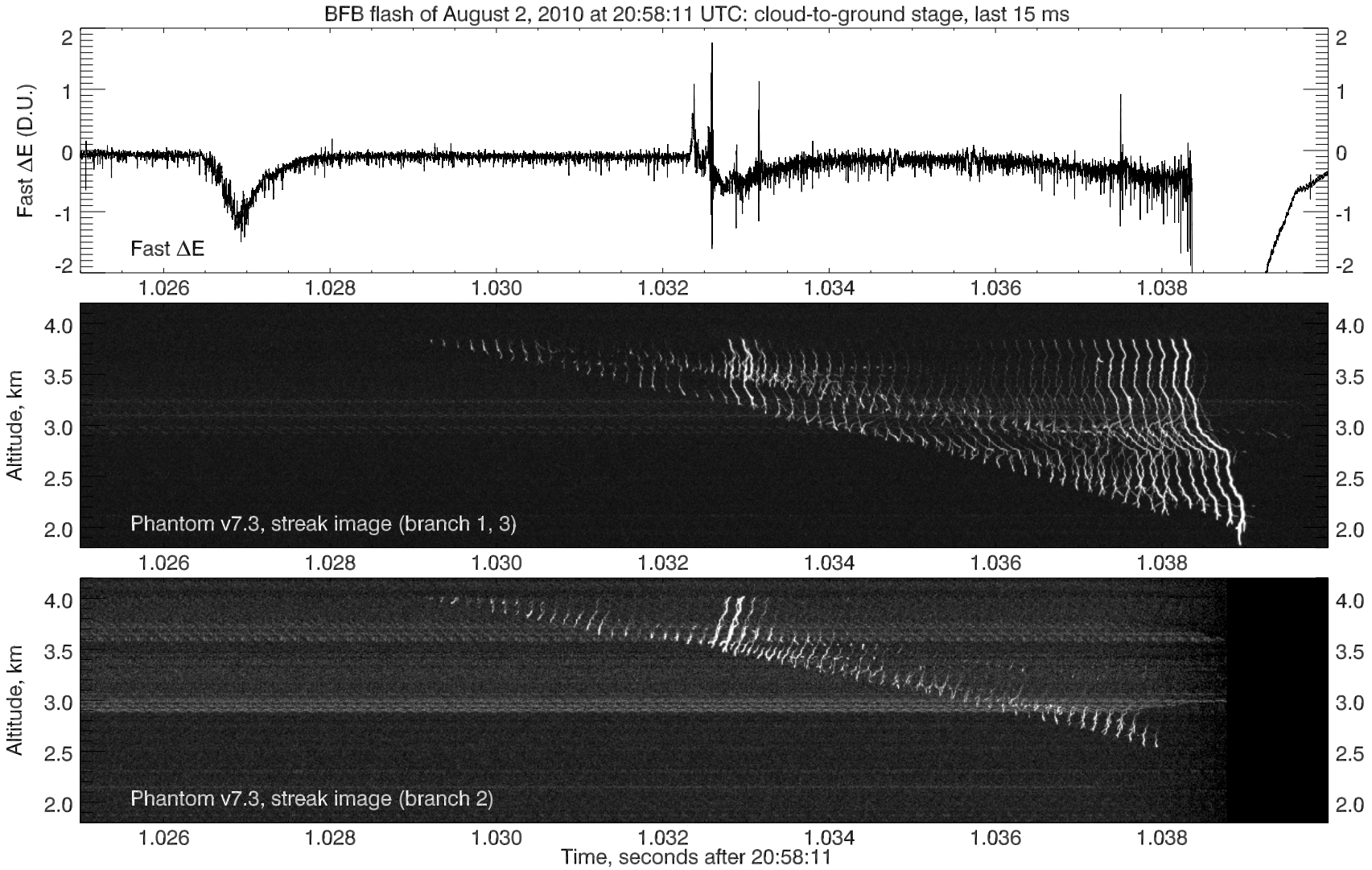

Figure 4.14: Fast ΔE waveform (top panel) and video streak images of Branches 1 and 3 (middle panel) and Branch 2 (bottom panel), during the last 15 ms of the cloud-to-ground leader. Both streak images have as their time reference the cloud exit location of the respective leaders near 4 km altitude.

It is likely that the K-leaders travel along the entire channel from (near to, or at) the tip of the positive leader all the way back to the tips of negative leaders, and in doing so, increase the channel conductivity by heating it. This would reduce the potential drop along the leader channel and thereby increase the local electric field at both ends of the leader.

K-leaders are not the only possible cause of sudden luminosity enhancements of the leader channel. The high-speed video recordings of the BFB flash of August 20, 2010 (Section 5.7.5) demonstrate that there can be a second source for such luminosity events, at least for leaders with relatively long channels such as those of BFB flashes. However, since a similar observation cannot be made for this flash, the fast ΔE pulses discussed here will still be referred to as K-changes from associated K-leaders.

In the BFB flash studied here, K-leaders occur at intervals of ~ 5 ms during the final stage of the cloud-to-ground leader, and about six or seven of these events can be seen in the waveform data during the entire cloud-to-ground leader stage. Only one of these K-events occurs during the time the leader is visible below the cloud base.

As determined from the high-speed video streak image in Figure 4.14 the negative leader of Branch 1 took 10 ms to cover the distance from the cloud base to ground (about 2 km) at an apparent velocity of 2.0×10^5 m s^{-1}; the leader of Branch 2 propagated slightly slower on average (1.5×10^5 m s^{-1}). This may only be an apparent effect due to the orientation of both branches relative to the camera.

Figure 4.15 shows 2.0 ms of waveform data around the time of the final fast ΔE pulse before the return stroke. The onset of the inferred K-leader occurs at 20:58:12.03235 as a positive excursion of the electric field. The pulse polarity indicates negative charge initially approaching the instrument, which likely occurs along one of the two branches of the positive breakdown in the midlevel negative charge region (Figure 4.3). Both of these branches exist at the time of the leader propagation to ground but are not yet fully developed at this time. Both are on the order of 5 km in length. The negative cloud-to-ground leader is also about 5 km in length at this time (ignoring channel tortuosity).

Near-continuous VHF emissions are seen in the log-RF waveform and the Sirio broadband antenna spectrogram during a time interval of 250 μs starting at 20:58:12.03235. The first sign of enhanced luminosity at the tip of the negative leader occurs in the video frames between 20:58:12.03265 and 20:58:12.03280. Assuming that the event was a K-leader initiating near the tip of a positive leader channel and propagating to the tip of the negative leader, this leader would have traveled a distance of about 10 km in 485 μs or less, with an upper bound for its velocity of 2.1×10^7 m s^{-1}, which is comparable to the velocity of $\sim 10^7$ m s^{-1} for fast K-leaders [*Shao et al.*, 1995]. After the K-leader reaches the tips of the negative cloud-to-ground leaders an enhanced negative current occurs along the leader channel for about 500 μs (viz. the steeper slope in the ΔE waveform, and an associated dip in the fast ΔE waveform

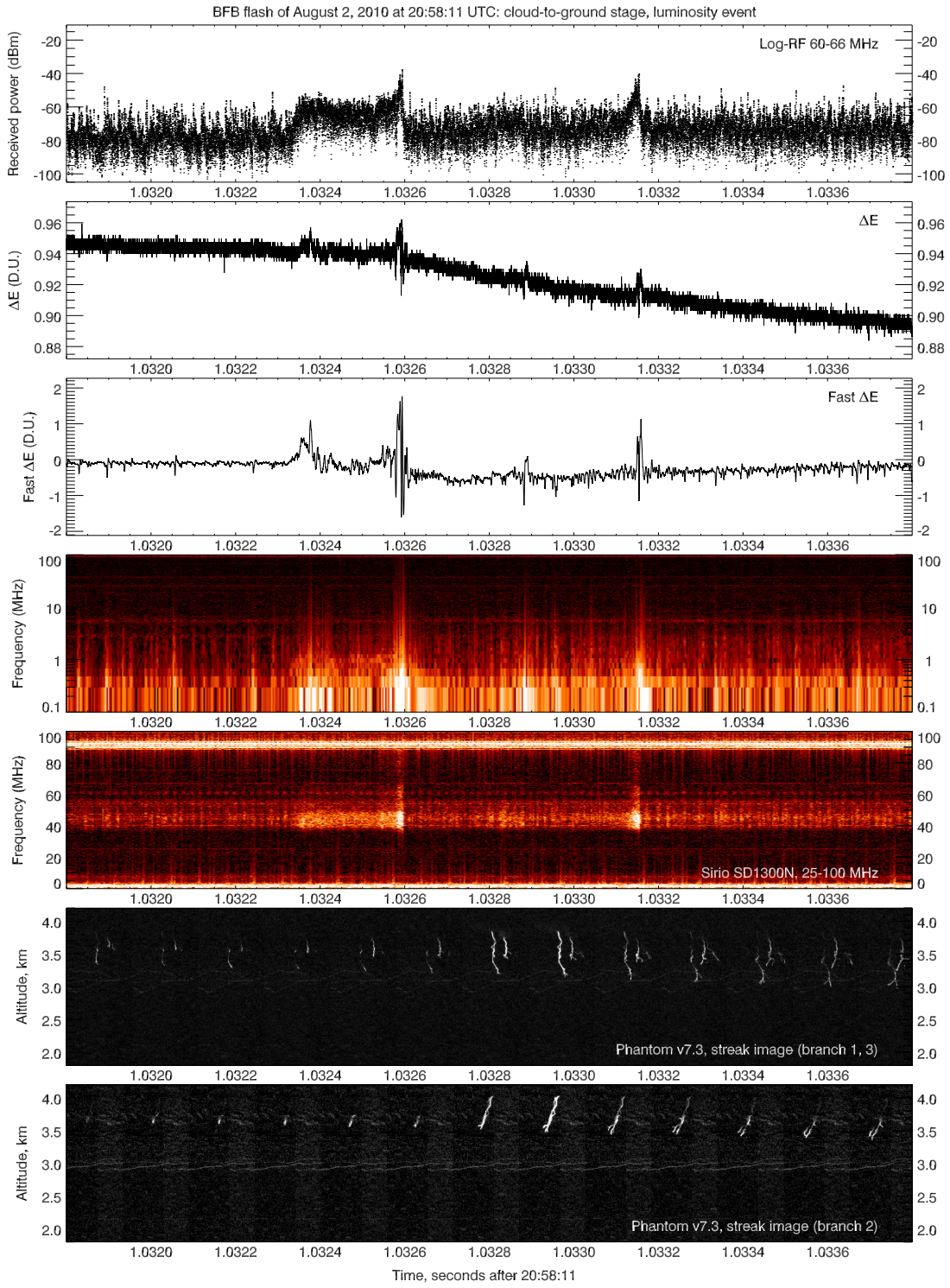

Figure 4.15: Time interval of 2 ms during the leader luminosity event. The log-RF waveform is plotted by samples in the first panel. Fourth panel contains spectrogram of Rhode & Schwarz HE010 broadband antenna. Note the delayed increase in leader luminosity after the onset of VHF emissions.

in Figure 4.15). Such an increase in current might be expected, because a K-leader would have heated the channel and made it more conductive. (A similar current surge associated with fast K-leaders is seen during the intracloud stage of the flash, as discussed in Section 4.5.) The current surge is followed by a second (smaller) fast ΔE pulse, which is bright in VHF, and may or may not be directly associated with the K-leader or current surge.

No VHF sources were located by the LMA during the luminosity event, probably due to the near-continuous nature of the VHF emissions and the K-leader not being a point source.

The cloud-to-ground leader channel showed a general, gradual increase in luminosity as the leader approached ground.

4.7 Final stage

The final stage of the BFB flash was relatively active compared to other BFB flashes. Figures 4.16 and 4.17 show waveform and LMA data for the entire time interval spanning the final stage, which commenced after the first return stroke at 20:58:12.0387 UTC. From LMA data, VHF activity in the midlevel negative charge region was mostly continuous during the 450 ms long time interval.

Most of the prior extent of the flash was "retraced" by the K-leader activity during the final stage (Figure 4.17). The K-leaders initiated in the midlevel negative charge region and traveled outward and down to ground as dart leaders, as well as upward along the branch into upper positive charge. However, the upward branch was not extended in length.

A total of six dart leaders along the channel to ground were attempted, three of which succeeded in contacting ground and produced return strokes. All three successful dart leaders that were observed on high-speed video followed Branch 2 to ground rather than the main channel (Branch 1a). The first dart-leader return stroke was brightest, both optically and in VHF. The second dart-leader return stroke had a short-duration continuing current; the last dart-leader return stroke was optically less bright but had a longer continuing current with several M-components.

4.7.1 Dart-stepped leader

No dart leader activity was seen below the cloud base in the video imagery until 20:58:12.1653, when a slow dart leader emerged, traveling along Branch 2 (Figure 4.18). This leader took about 10 video frames (1.5 ms) to travel a transverse

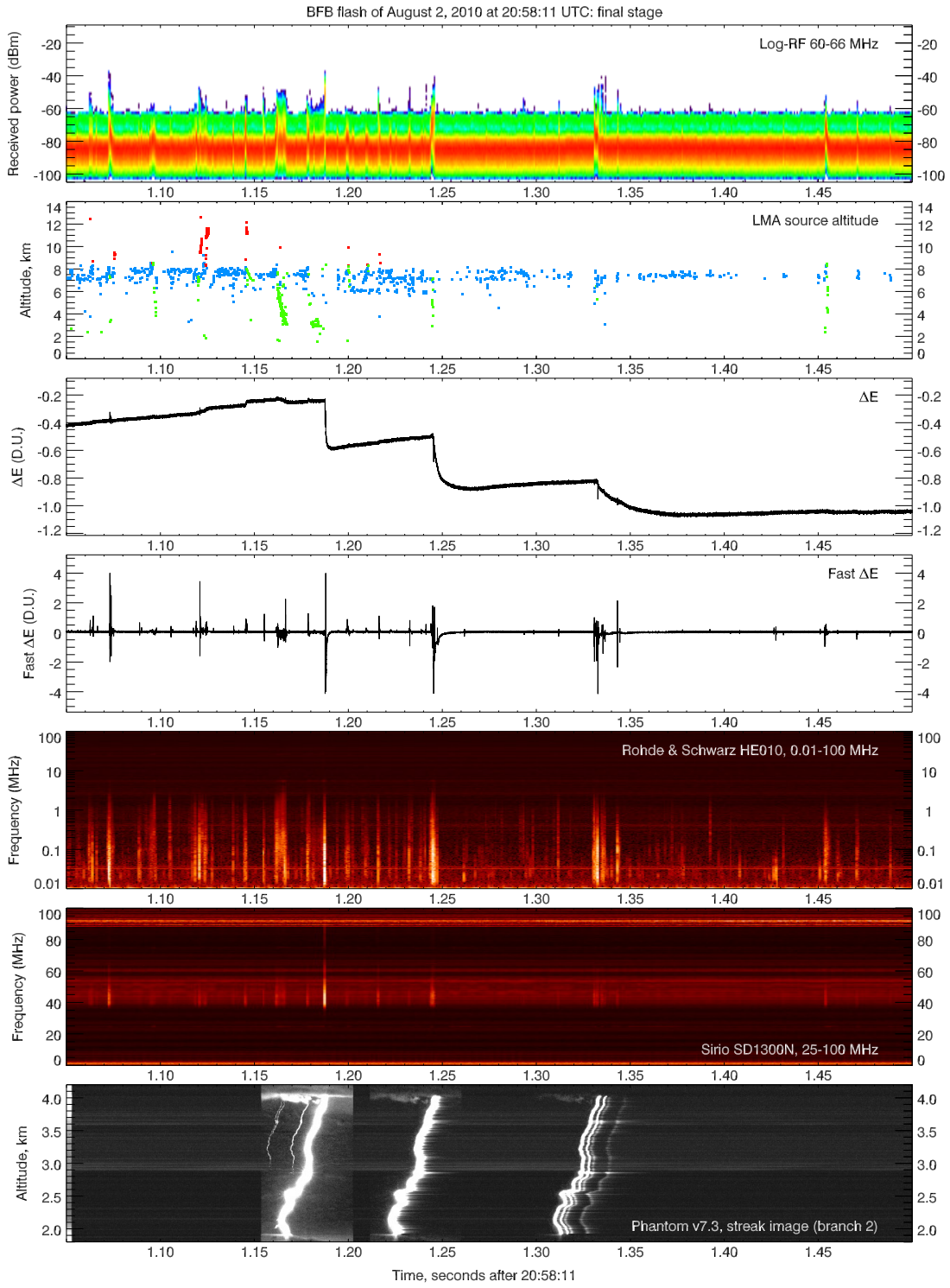

Figure 4.16: Waveform data during the final stage of the BFB flash. The plotted time interval is 450 ms. Branch 2 was extended to ground by the dart-stepped leader between 1.16 and 1.19 seconds after 20:58:11, which was followed by two more dart leaders and associated return strokes through the same channel. Note the unsuccessful dart leader at 1.45 seconds after 20:58:11 (second panel).

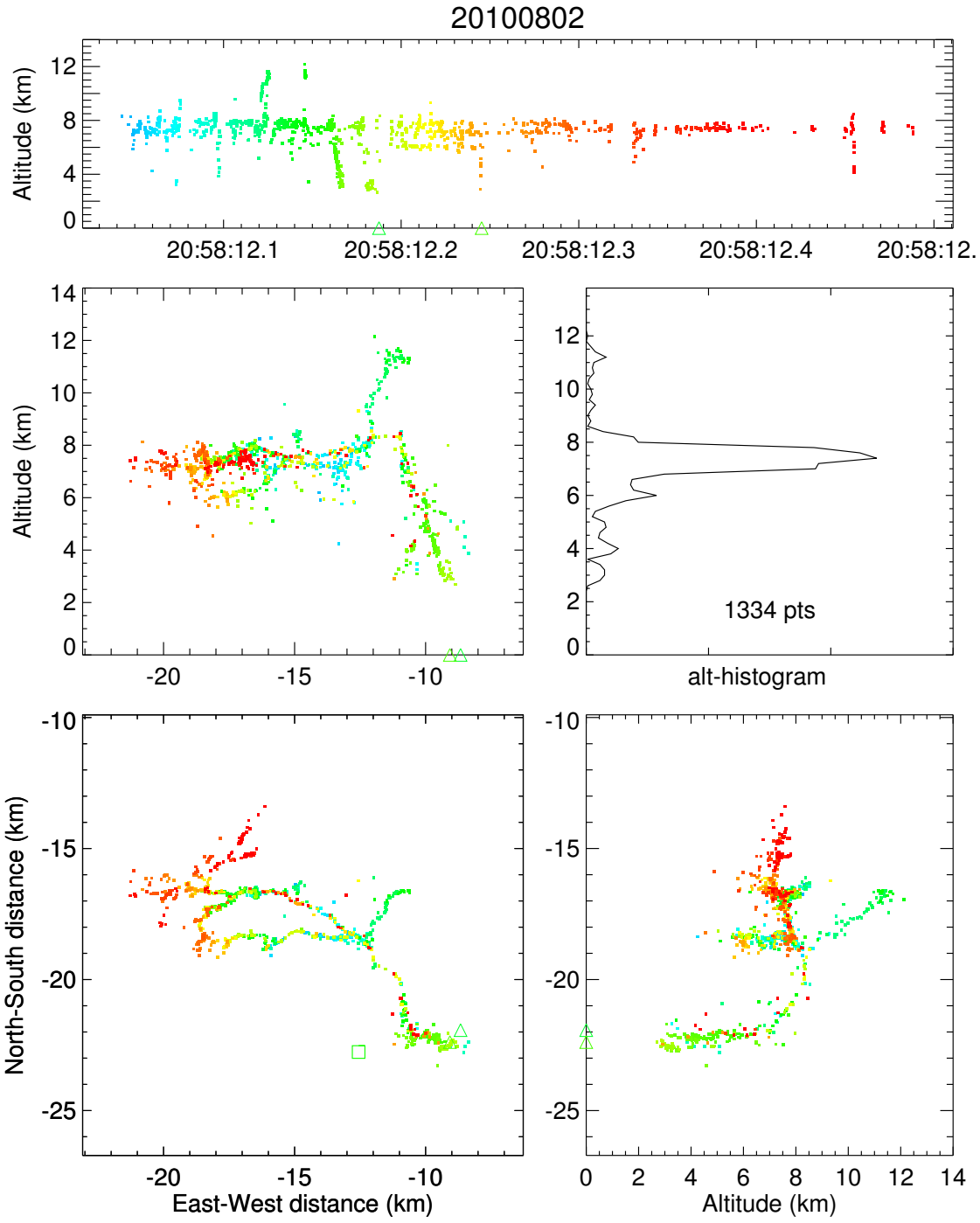

Figure 4.17: VHF sources located by the LMA during the final stage. The various K-leaders retraced most if not all of the original extent of the flash, including the upward channel.

distance of 1 km, at an apparent velocity of 6.7×10^5 m s^{-1}. About 600 μs after the dart leader of Branch 2 emerged from the cloud base another dart leader along Branch 1 also emerged, which propagated at a faster pace of 1.7×10^6 m s^{-1}. (Again, this difference could simply be a geometric effect of different channel orientations relative to the camera.) The latter dart leader stopped halfway between the cloud base and ground. At this point in time a channel illumination event occurred along both branches, similar to that during the first stepped leader to ground. From the spectrogram data it was determined that this ionization wave or current pulse lasted for about 250 μs while LMA data (Figure 4.19) indicate a channel length of 12 km between the extremities of positive breakdown and the tips of the dart leaders, which indicates an estimated velocity of 4.8×10^7 m s^{-1} (as an upper bound).

The channel luminosity event did little or nothing to sustain the dart leaders along both branches; the dart leader along Branch 1 stopped immediately after the luminosity event and the dart leader along Branch 2 stopped about 1 ms later.

Another dart leader propagated down 22 ms later in time (at 20:58:12.1785), and only along Branch 2. The fact that it did not also seem to propagate along Branch 1 is remarkable and may indicate that this branch had residual negative charge distributed along it that prevented further dart leader activity from occurring. (However, Branch 2 must also have had residual charge on it from the first attempted dart leader.) According to the LMA, this dart leader initiated at 20:58:12.178031 with a series of seven VHF sources that occurred during a time interval of 320 μs, which were all concentrated in a 200 $\times$ 200 m area at 8 km altitude along the major northwestern branch of the positive breakdown (Figure 4.19, near the branching point in the northwestern branch at $x = -17$ km, $y = -17$ km). After these VHF sources two more sources were located by the LMA further east along the positive leader channel. During the next 500 μs a positive excursion is seen in the ΔE and fast ΔE waveforms, indicating motion of negative charge back along the positive leader channel toward the channel to ground. The current pulse was also bright in VHF, yet no VHF sources were located during this time. After the initial series of VHF sources, it took the dart leader 960 μs (traveling an estimated distance of 12 km at a velocity of 1.3×10^7 m s^{-1}) until it emerged from the cloud base.

At 3 km altitude the dart leader reached the tip of the previous channel and became a stepped leader, extending the original channel to ground. After the transition from dart leader to stepped leader, VHF emissions were relatively weak (Figure 4.18, spectrograms and log-RF waveform). On high-speed video the stepped leader had low luminosity and took 8.1 ms to bridge the last 1 km to ground at an apparent velocity of 1.2×10^5 m s^{-1}.

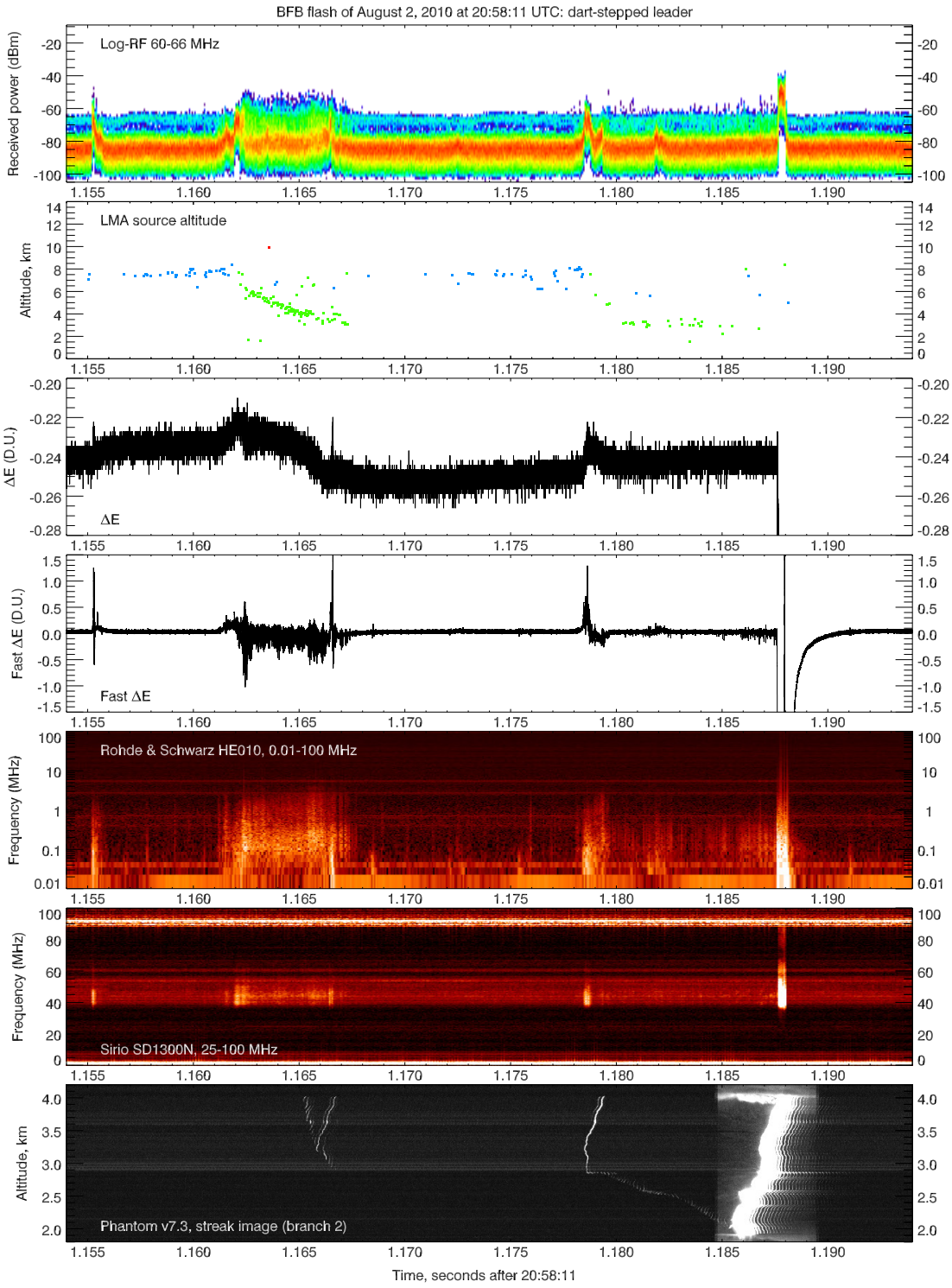

Figure 4.18: Waveforms for a time interval of 40 ms during the first dart-stepped leader. The first attempt of the dart leader to contact ground (at 20:58:12.165) was unsuccessful, as it did not extend the original branch (Branch 2). The second dart leader (starting at 20:58:12.178) converted to a stepped leader at 3 km altitude and was successful.

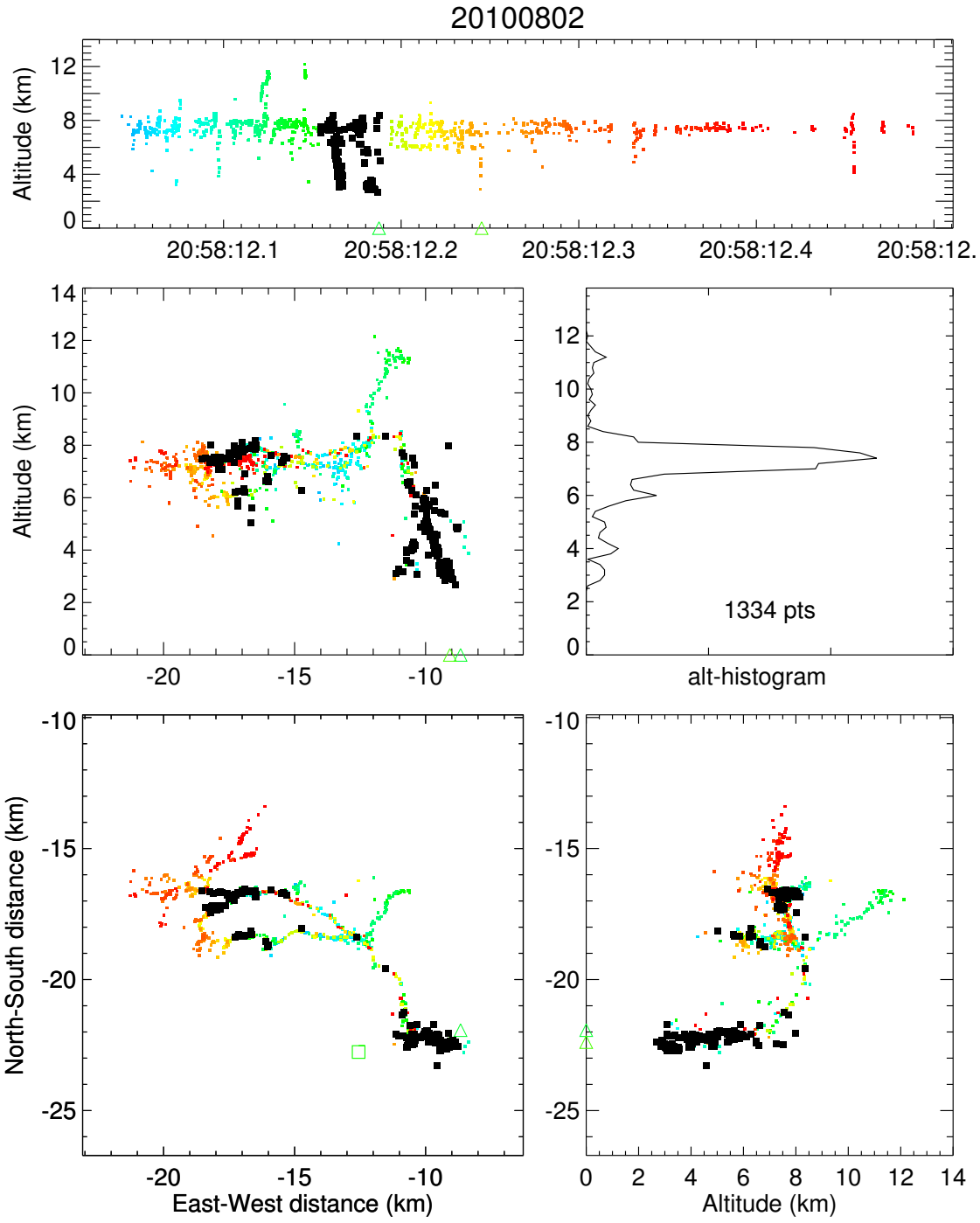

Figure 4.19: VHF sources located by the LMA during the final stage, with those occurring during the 40 ms time interval of the dart-stepped leader in Figure 4.18 highlighted in black.

4.7.2 Second dart leader

The second successful dart leader initiated at 20:58:12.2436, 55 ms after the start of the return stroke of the first dart-stepped leader. During this preceding time interval there was ongoing activity in the midlevel negative charge region as the positive leader channels were being extended in a general WNW direction (Figure 4.17). A relatively high-power VHF event occurred 2.3 ms before the first sign of the second dart leader (Figure 4.20, pulse in log-RF waveform at 20:58:12.2413). This event was accompanied by three VHF sources that occurred at or near the tip of the southern branch of the positive leader (i.e. the branch going in a westward direction and positioned to the south of the major WNW branch in Figure 4.22). This branch was at a lower altitude (6 km) at that location. It is unclear whether or not the bright VHF event had a direct effect on the initiation of the second dart leader, but it is unlikely because the dart leader itself initiated during activity in the WNW branch.

The dart leader initiated with three VHF sources located by the LMA, which were within 200 m from each other at 7.5 km altitude in the WNW branch of the positive breakdown. (The positive breakdown was still progressing in a westward direction and the branch to the northeast, near $x = -17$ km, $y = -15$ km in Figure 4.22, had not yet developed at this time.) After a delay of 200 μs a small positive ΔE excursion occurred (Figure 4.21), indicative of negative charge moving to the east toward the channel to ground. The dart leader emerged from the cloud base 1.5 ms later. It propagated at an average velocity of 8.0×10^6 m s^{-1}, assuming that the dart leader started immediately after the last of the three VHF sources and that the channel was 12 km in length. The dart leader appears to slow down in the video streak image in Figure 4.21, likely due to a change in conductivity of the upper and lower segments of the channel below the cloud base.

The return stroke had a short continuing current with a decay time constant of 2.5 ms (Figure 4.20, ΔE waveform). During this continuing current slight variations in luminosity of the channel can be seen in the high-speed video imagery (Figure 4.20). An M-component started at 20:58:12.2475 with a bright VHF pulse and associated fast ΔE pulse, leading to a small luminosity increase on the channel below the cloud base about 500 μs later. Assuming that the M-component initiated in the region of ongoing positive breakdown, it would have traveled at a velocity of 2.8×10^7 m s^{-1}. The M-component increased the negative current through the channel to ground (Figure 4.20, fast ΔE waveform). The LMA located one VHF source in the midlevel negative charge region during the M-component.

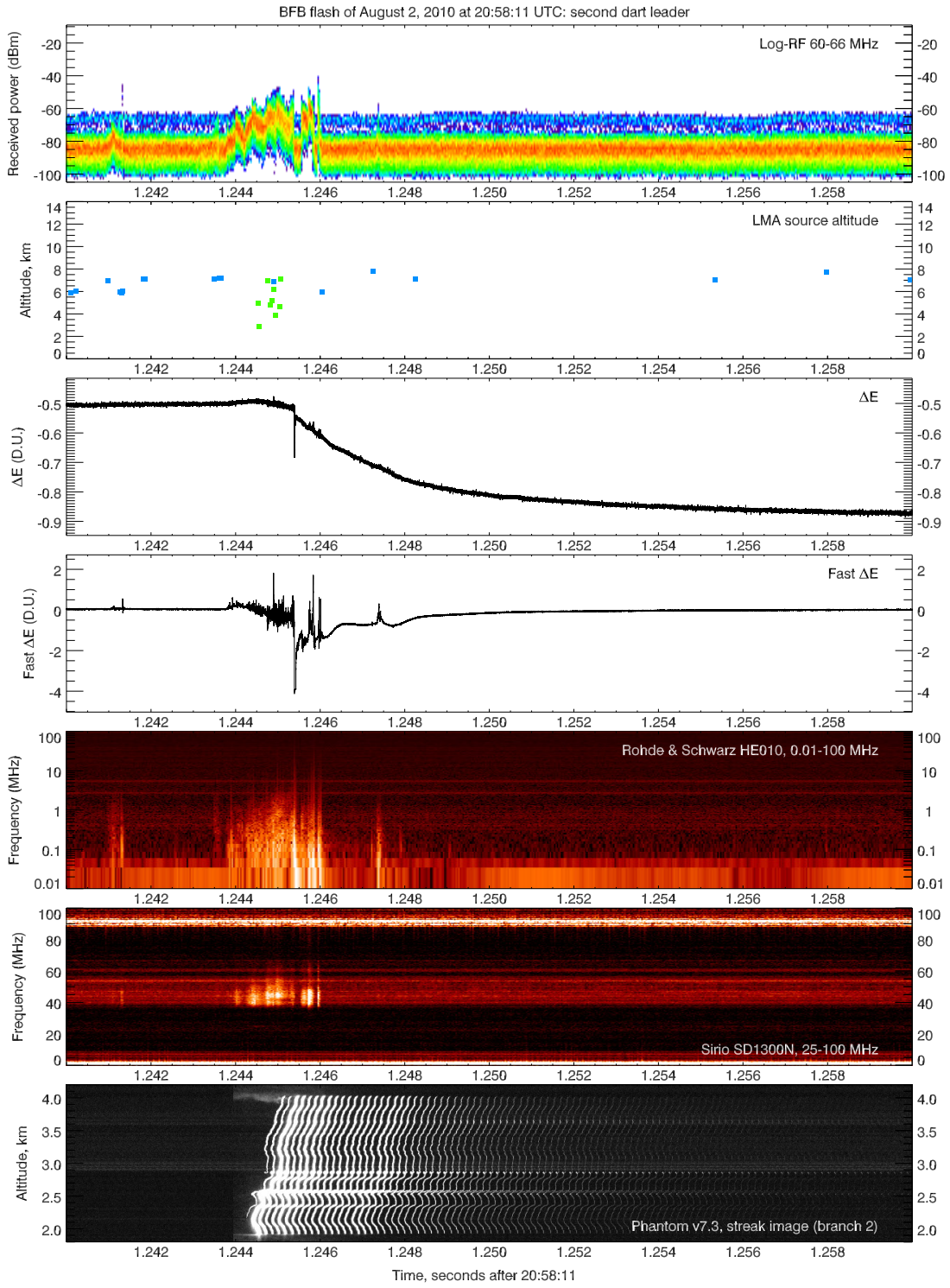

Figure 4.20: Waveform data for a 20 ms time interval during the second dart leader to ground. The dart leader and ensuing return stroke appear bright in both spectrograms. During the continuing-current stage very few VHF sources were located in the midlevel negative charge region. Two M-components can be discerned in the video streak image.

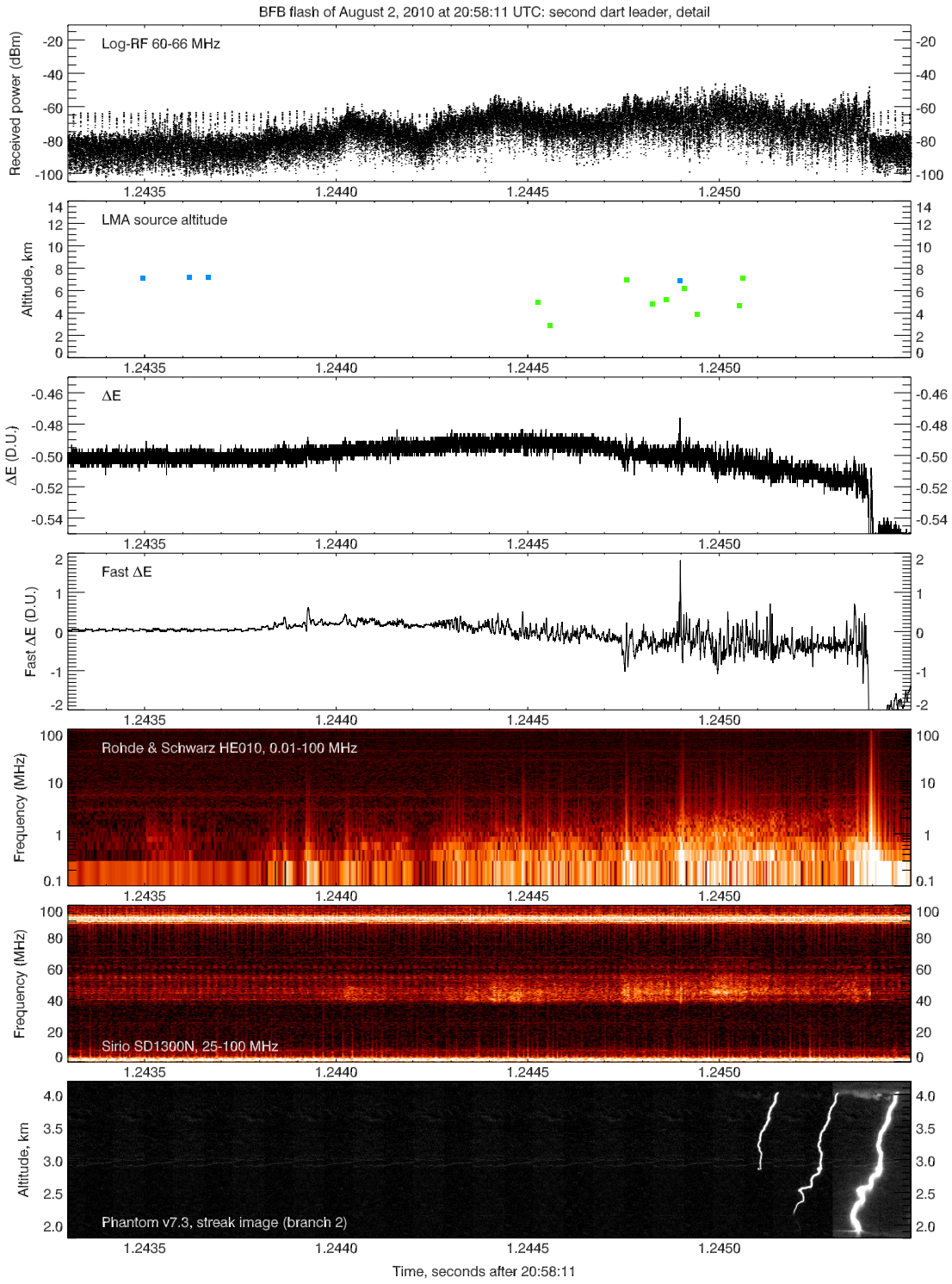

Figure 4.21: Waveform data for the second dart leader to ground during a time interval of 2.2 ms. The log-RF waveform is plotted by samples. Note the different frequency scale (0.1–100 MHz) of the Rohde & Schwarz spectrogram, due to the frequency resolution being larger than 100 kHz.

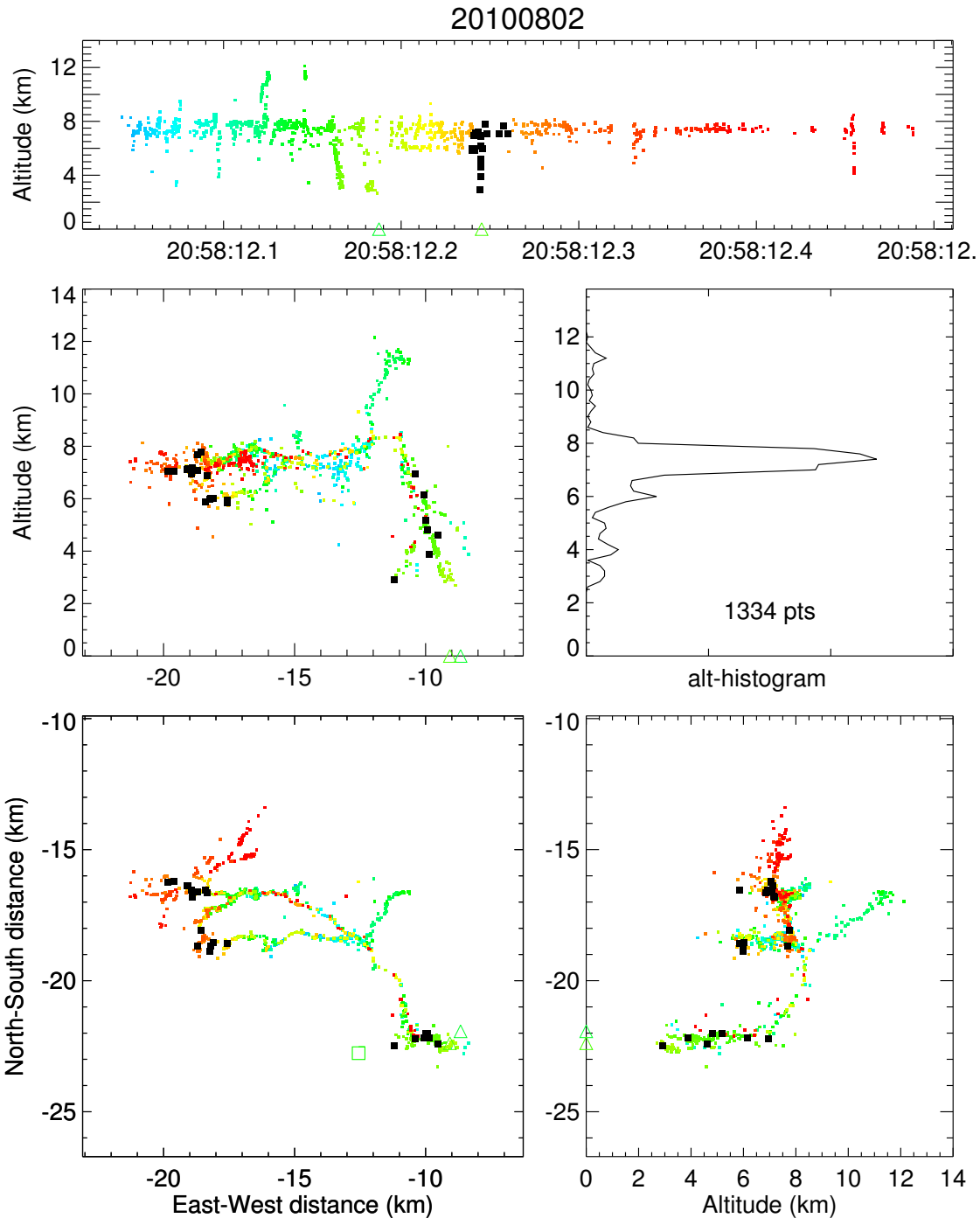

Figure 4.22: Located VHF sources during the final stage, with those occurring during the time interval of Figure 4.20 (second dart leader) highlighted in black.

4.7.3 Third dart leader

The third and last dart leader that reached ground initiated at 20:58:12.3308 (Figures 4.23 and 4.24). The electric field perturbation associated with this dart leader occurred about 300 μs before associated VHF sources were located by the LMA. These VHF sources started along a near-vertical segment of channel associated with positive breakdown between 5 and 7 km altitude, which was connected to the main WNW branch of the positive breakdown (Figure 4.25; it is possible that the two VHF sources below 5 km altitude were mislocated). Few VHF sources were located along the cloud-to-ground segment of the leader channel.

The entire dart-leader stage from onset of electric field excursion to the return stroke lasted 2.0 ms along a channel that now had a length of at least 14 km, with the dart leader traveling at a velocity of 7.0×10^6 m s^{-1}. During the propagation of the dart leader one large-amplitude pulse was seen both in the fast ΔE waveform and in VHF. No VHF sources were located close in time to this pulse, however. The two VHF sources immediately before and after the pulse occurred at an altitude of 6 km along the cloud-to-ground channel, which may therefore have been where the tip of the dart leader was at the time of the fast ΔE pulse. It is possible that the fast ΔE pulse was in fact associated with continued breakdown back in the negative charge region and led to the first M-component (discussed below).

The return stroke had the longest continuing current of the four return strokes, with a decay time constant of 4.8 ms (Figure 4.23, ΔE waveform). Four M-components are observed in the high-speed video imagery during the continuing-current stage; the first two M-components were the brightest of the four.

Due to the M-components being very closely spaced in time it is hard to tell which ΔE or VHF event is responsible for each M-component. What is clear from Figures 4.23 and 4.25, however, is that the M-components in this flash were associated with short bursts of located VHF sources which occurred near the extremities of the positive breakdown, while the northeasterly branch of the positive breakdown was being initiated. With each M-component new positive breakdown was initiated in the negative charge region to extend the positive leaders there, and the negative charge made available by this breakdown could then move along the conductive channel to ground as a current wave.

Because of the ambiguity in fast ΔE pulses and M-components, no reliable estimate for the velocities of the various M-components can be made in this case.

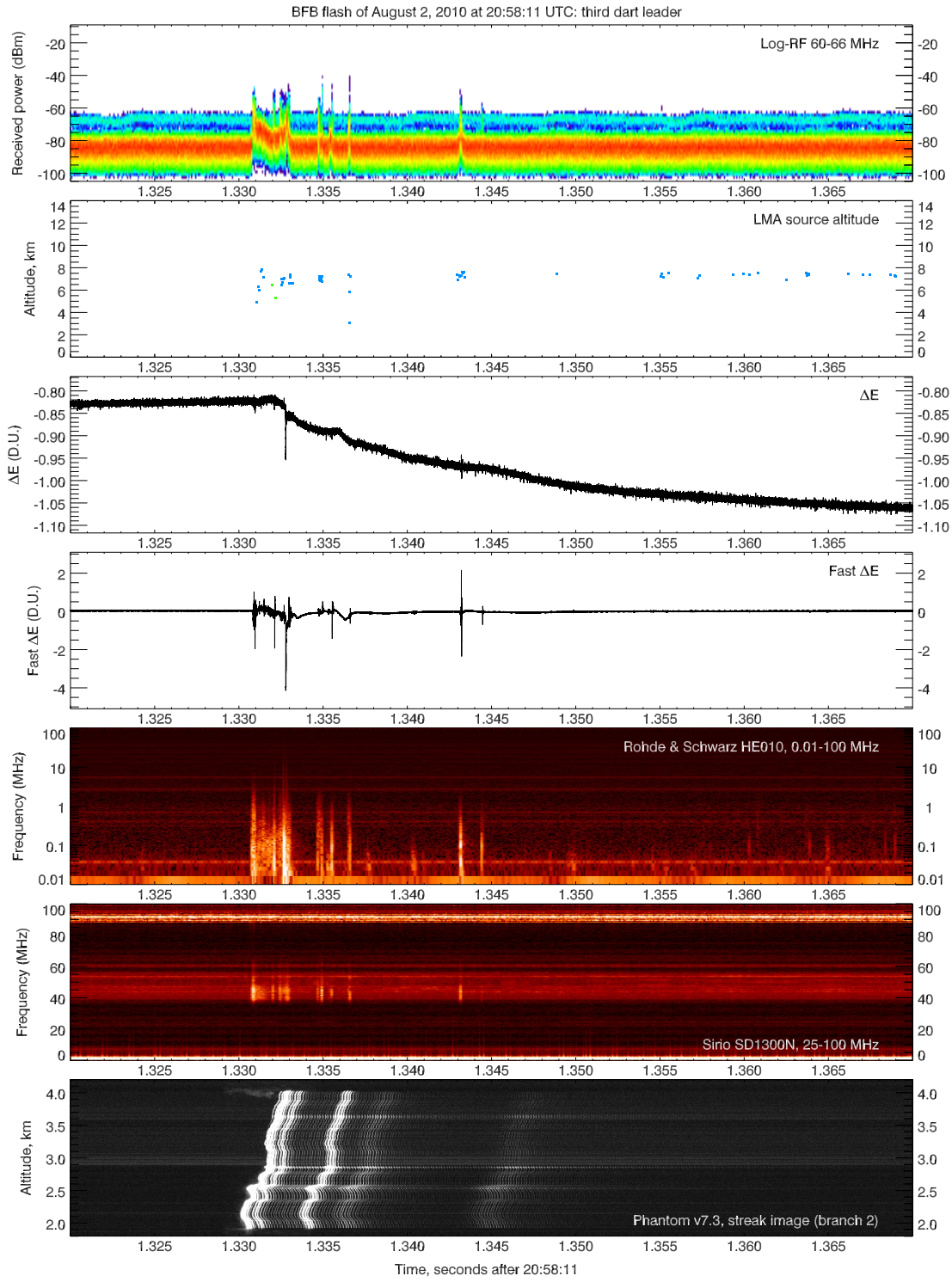

Figure 4.23: 50 ms of waveform data around the time of the third dart leader to ground. Four distinct M-components can be resolved in the high-speed video streak image. Note the located VHF sources during the second M-component at 1.3365 seconds past 20:58:11. Each M-component is associated with one or more narrow VHF pulses and several located VHF sources in the midlevel negative charge region.

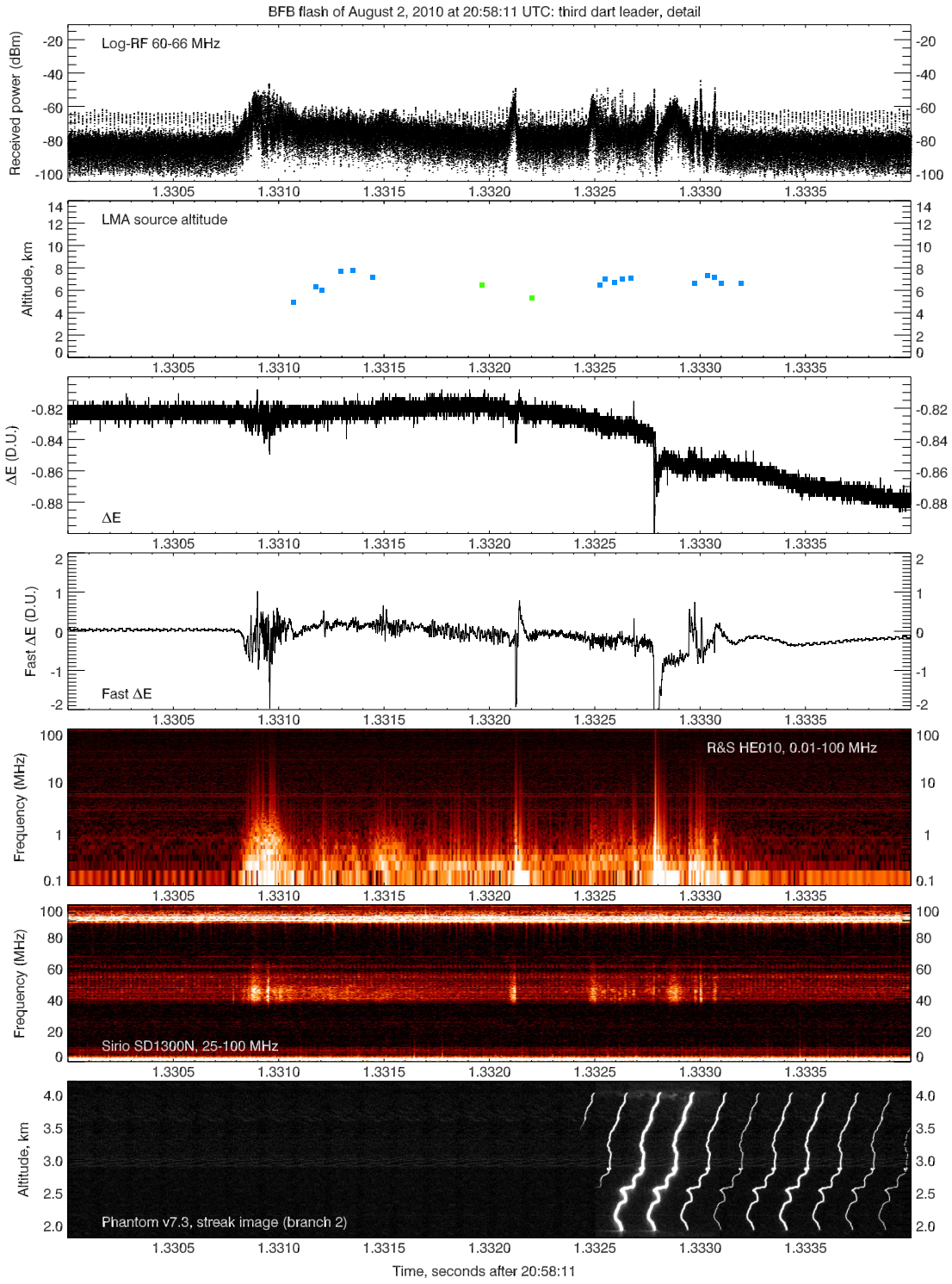

Figure 4.24: Waveform data for the third dart leader to ground during a time interval of 4 ms. The dart leader can be seen well in VHF (in log-RF waveform and both spectrograms), lasting about 2 ms.

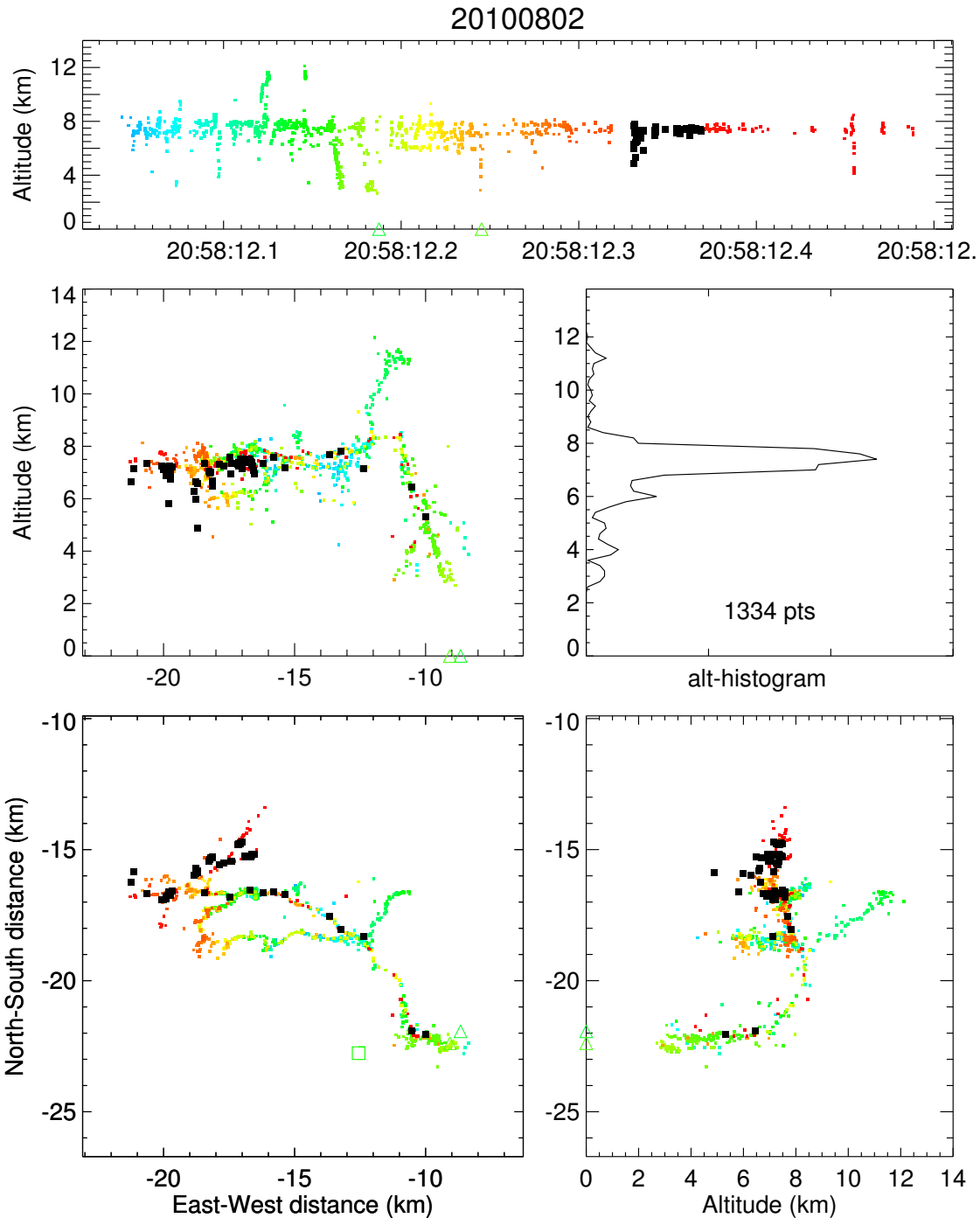

Figure 4.25: Located VHF sources during the final stage, with those occurring during the 50 ms time interval of Figure 4.23 (third dart leader) highlighted in black.

4.7.4 Fourth dart leader

A fourth dart leader was attemped, which can be seen in LMA data (Figures 4.16 and 4.17, at 20:58:12.454), but no leader is seen below the cloud base in the high-speed video imagery and no electric field change associated with a return stroke was observed. This dart leader was initiated during continuing positive breakdown along the northeasterly branch that initiated near the very westernmost end of the positive breakdown. The elapsed time since the third dart leader and onset of this fourth dart leader—on the order of 100 ms—was comparable to the time between the first return stroke and the dart-stepped leader, and since that leader had some difficulty in reaching ground, it is not surprising that the fourth dart leader did not complete the path to ground. The lowest VHF sources located by the LMA occurred near 4 km altitude, near the cloud base at 4.2 km altitude. The dart leader propagated at 5.5×10^6 m s^{-1} (determined from LMA).

4.8 Summary

The BFB flash studied in this chapter was a four-stroke flash lowering negative charge to ground.

The flash had a number of characteristics commonly observed in regular –CG flashes: It produced multiple strokes to ground, with some continuing current during the later strokes along with M-components.

The flash initiated at 8.2 km altitude with an upward leader into upper positive charge. This leader propagated in an intermittent fashion, producing short 5–10 ms long bursts of located VHF sources. During each burst a K-leader propagated upward, which initiated at positive breakdown in the midlevel negative charge region but appeared to be induced by the negative breakdown. Six or seven of these K-leaders were detected during the initial upward leader stage.

K-leaders also occurred during the cloud-to-ground leader stage, initiated by K-events in the positive breakdown region. One of these events occurred while the leader was visible below the cloud base and was observed to be a luminosity enhancement in all three branches. The inferred velocity of the K-leader was 2.1×10^7 m s^{-1}. The main branch (Branch 1) branched into two major branches (1a and 1b) at this time.

With each K-leader during the cloud-to-ground stage, the rate of VHF emissions from the negative leader(s) increased abruptly and an associated increase in negative current was observed, indicative of an increase in channel conductivity.

After the first return stroke a dart leader was attempted, but it did not succeed in contacting ground. A second dart leader was attempted, which did not follow

the original branch to ground (Branch 1a) but created a new path to ground using another branch (Branch 2). It became a stepped leader for the last 1 km of distance to ground. Two more dart leaders occurred along this later path to ground. With its two channels to ground, this BFB flash was therefore an example of "forked lightning" (compare Photos D.21 and D.22).

The dart-stepped leader is intriguing, in particular because no persuasive argument can be made for the dart leader not continuing to follow the original path to ground (i.e. along Branch 1a). It is possible that some amount of negative charge was still flowing to ground when the channel cooled enough to cut the current off, leaving the decaying channel with a net negative charge along its length. This could then have prevented the first dart leader from propagating all the way down, but instead continuing along Branch 2, which would have been mostly discharged at an early stage during the first return stroke.

Dart-stepped leaders and attempted dart leaders are expected to be more common in BFB flashes than in regular –CG flashes, because the cloud-to-ground leader of BFB flashes—which initiates at the upper boundary of the midlevel negative charge region rather than near the lower boundary—is generally much longer, with a correspondingly larger potential drop. All other things being equal, it would take more negative charge for a dart leader to reionize a longer length of channel, and this larger quantity of negative charge may not always be made available quickly enough for a dart leader to succeed in contacting ground.

The various leader velocities estimated from this BFB flash are summarized in Table 4.1. The velocities of stepped leaders, dart leaders and K-leaders are in general agreement with those reported in the literature. Also, there appears to be no physical difference between dart leaders, K-leaders and M-components except for their velocities, as found by *Shao et al.* [1995].

Time	Event	Branch	Velocity (m s^{-1})	Instrument
0.7525	SL (upward)	—	1.5×10^5	LMA
0.9575	SL (CG)	1	2.0×10^5	Video
0.9575	SL (CG)	2	1.5×10^5	Video
1.0323	KL	1, 2	2.1×10^7	Video, ΔE
1.1550	ADL	1	1.7×10^6	Video
1.1665	KL	1, 2	4.8×10^7	LMA, VHF
1.1780	ADL	2	6.7×10^5	Video
1.1780	DSL 1 (dart)	2	1.3×10^7	Video
1.1780	DSL 1 (step)	2	1.2×10^5	Video
1.2436	DL 2	2	8.0×10^6	LMA, video
1.2475	MC	2	2.8×10^7	LMA, video
1.3308	DL 3	2	7.0×10^6	LMA
1.4498	DL 4	—	5.5×10^6	LMA

Table 4.1: Initiation times (seconds after 20:58:11 UTC) and estimated leader velocities for various types of leaders during the BFB flash. The instrument(s) that were used to calculate the velocities in each case are also listed, along with the relevant cloud-to-ground branch (where applicable). The error in the velocity estimates is on the order of 10% (relying on the validity of assumptions made in the text); leader velocities that were estimated solely from video may have larger errors because only the transverse component of the leader velocity could be estimated. SL = stepped leader; KL = K-leader; ADL = attempted dart leader; DSL = dart-stepped leader; DL = dart leader; MC = M-component.

5. BFB storm of August 20, 2010

5.1 Introduction

The second BFB flash from 2010 that was recorded on high-speed video occurred on August 20, 2010 (UTC day). Correlated LMA, waveform and video data will be studied in this chapter in a similar way as for the flash studied in Chapter 4. Although this flash was farther away from the laboratory and the quality of the LMA and waveform data is considerably lower, the negative leader exited the cloud at high altitude and could be imaged on high-speed video.

This chapter also discusses a photographic observation of a cloud-to-air leader with visible streamers at the leader tip, which occurred shortly before the BFB flash of interest.

5.2 Overview of storms

In the evening of August 19, 2010 a small convective cell started to develop over the northern end of WSMR, just south of highway US 380. Visual and photographic observations began just after sunset when the first small, localized IC flash occurred at 02:14:35 UTC. The second IC flash occurred 4 minutes later, after which activity increased somewhat to about one flash every 2 minutes. All of these were IC flashes with initiation altitudes of 6 km.

There was relatively strong wind shear relative to the weak updraft in the storm, resulting in a sheared-off anvil cloud that drifted to the northeast.

Between 02:20 and 02:30 electrical activity increased to 1.3 flashes per minute. Both IC and CG activity was observed at this point and IC flashes were reaching up to 11 km altitude in the cloud.

Activity further increased to about 2 flashes per minute between 02:30 and 02:40, with IC flashes reaching up to 12 km altitude. Their initiation altitude was now

around 7 km and the flashes occurred at a distance of $\sim$ 100 km from the laboratory. IC, –CG and low-IC flashes were all observed, but no BFB flashes occurred at this time. The top of the active part of the storm had a cumuliform appearance, being at lower altitude (10 km) than the sheared-off anvil to the east (about 12 km).

5.3 Cloud-to-air leaders

At 02:52:05 a second storm started that was 53 km distant from the laboratory and partially in front of the original storm. This storm became active with lightning at 4 flashes per minute, with about 10% being –CG flashes and the rest IC flashes.

At 02:56:42 a short segment of a leader emerged from the new storm cloud, which was photographed. Because the digital still camera was adjusted for short but high-sensitivity exposures, blue filaments at the leader tip were imaged. (These streamers had been observed earlier by the author in photos of other cloud-to-air flashes; e.g. Photo D.27.) From LMA data (not shown) this was a regular IC flash that occupied an approximate volume of $2 \times 2 \times 2$ km, with an initiation altitude of 10 km and reaching up to 11.5 km altitude.

Photo 5.1: A branch of an IC flash emerging from the cloud top at 02:56:42 UTC, with several blue filaments visible ahead of the leader tip.

At this time a conflict of interest ensued between capturing events at very low luminosity near the cloud top, requiring sensitive camera settings, and capturing a possible BFB flash out of the side of the storm. An attempt was made to do both, with limited success.

At 03:03:28 the upward leader in Photo 5.2 was imaged, while the camera was making 1.3 second-long exposures at the maximum zoom possible (200 mm focal length) and at the highest usable sensitivity, toward the top of the active region of the storm. The visible length of this leader is on the order of 1.5 km, but probably longer by several hundred meters because the leader was not only going upward but was also slanted to the west, toward the camera.

Photo 5.2: A cloud-to-air leader emerging from the side or top of the storm. The tip of the leader was at an altitude of 11 km and was going almost straight up at a slight angle toward the west. The visible part of the leader is 1.5–2.0 km in length.

5.3.1 Streamer zones on a negative leader

The attempted upward or BFB leader in Photo 5.2 is shown at high resolution in Figure 5.1 and several interesting phenomena can be resolved in the image. At each bend or kink of the main leader channel a network of blue streamer filaments can be seen that are about 100 m in length, some of which appear to be branched. There are as many as six or more filaments connected to the main leader in some locations and

they fan out at a rather large angle of as much as 90 degrees. Some of the streamer filaments are connected to the main leader channel by a brighter stem of 10–20 m in length.

The streamer filaments are not randomly distributed along the entire length of the channel but concentrated at specific locations along the leader, separated by more or less equal distances of about 200 m along the leader channel.

Some sections of the main leader channel appear to show a magenta or purple fringe. This is chromatic aberration of the camera lens, unrelated to the leader itself.

The proposed explanation for the discrete concentrations of streamer filaments along the leader channel is that these streamer filaments only occur at intermittent times during leader propagation and only at the current tip of the developing leader. *Berger and Vogelsanger* [1969] reported very similar observations of streamer zones (corona) at leader tips of upward negative lightning, which initiated from towers on Monte San Salvatore in Switzerland at an altitude of about 700 m above MSL. From moving-film recordings it was determined that the corona developed almost instantaneously, in less than 5 μs, and developed at the tip of the leader during each step. The visible part of the corona was estimated to be at least 6 m in extent and developed at the time a new leader step was produced. Since the photograph reproduced above is a time exposure, several of these steps with associated streamer filaments were imaged as the leader propagated. The visible part of the streamer zones in the photograph are estimated to be about 100 m in extent at 11 km altitude.

By the spacing of the various streamer zones in the photograph, the length of the leader steps can be estimated. These steps are on the order of 200 m in length. Some steps appear to be shorter in length due to the channel propagating toward or away from the camera.

5.3.2 Space stem during streamer-to-leader transition

Also of interest is a short stem of about 20 m length (indicated by the arrow in Figure 5.1) that appears to be unconnected to the main leader channel and appears orange–red in color. The short stem transitions to a narrowly collimated blue filament of smooth appearance that connects with the main leader; at the other end, away from the leader, the stem branches into at least two other streamers. The entire phenomenon appears to be about 150–200 m in length.

It should be noted that the upward leader was about 56 km distant from the camera and Rayleigh scattering in the atmosphere causes a color shift toward the red for distant light sources. Although Langmuir Laboratory is at an altitude of 3.2 km above MSL and the upward leader itself reached up to 11 km in altitude, with

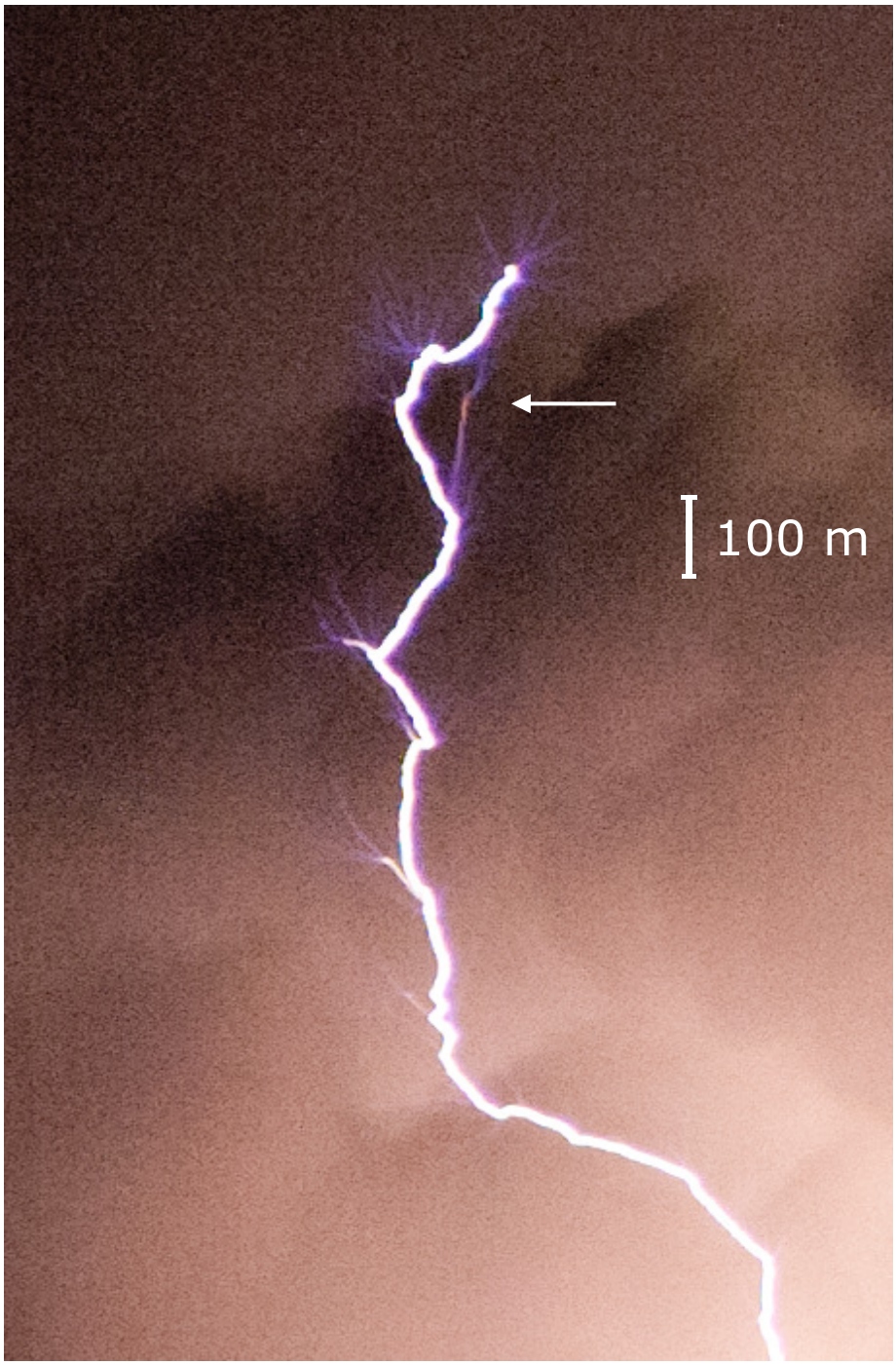

Figure 5.1: A close-up view of the cloud-to-air leader in Photo 5.2. Note the multitude of blue streamer filaments that tend to occur where the channel is kinked, and at the tip of the leader. Also note the weak glow of a short segment (indicated by the arrow) that appears to be unconnected to the main leader channel, apart from the glow of a streamer with smooth appearance and narrow collimation toward the main leader. The resolution of the photograph is 2.4 m per pixel; the leader is 56 km distant.

comparatively low-density air in between, there was still a substantial length of atmosphere in between and it is assumed that at least part of the red glow of the stem is caused by Rayleigh scattering. The same scattering probably causes the blue streamer filaments to appear slightly violet in color. However, the effect of Rayleigh scattering at this distance is still relatively small. This is evident from the photographic observation of a blue starter on August 4, 2010 [*Edens*, 2011], which occurred at twice the distance yet does not suffer from much reddening by atmospheric scattering.

The short stem indicated by the arrow in Figure 5.1 shows a streamer-to-leader transition in progress, which apparently did not succeed in completing the transition process before the main leader completed another step (along another newly formed branch) and preempted the process by bypassing it. The short luminous section of channel ahead of a negative leader tip (which must have been at that location at the time of the event) has been observed by streak cameras in laboratory air-gap spark studies and has been called a "space stem" [*Gorin et al.*, 1976] or "secondary volume leader channel" [*Bazelyan and Raizer*, 2000, pp. 83–88]. This space stem forms ahead of the leader tip in a bidirectional, bipolar manner, and transitions into a new leader step when the positive end of the channel makes contact with the leader tip (Figure 5.2). The positive streamer is resolved in the photograph as the diffuse, narrowly collimated blue filament toward the main channel; the negative streamers at the far end have a different, more defined appearance.

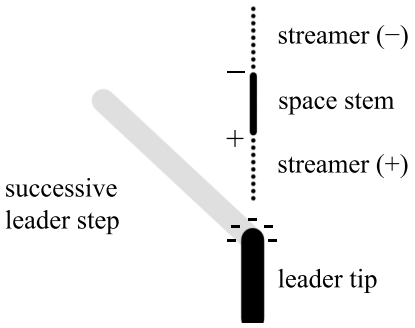

Figure 5.2: Schematic diagram of the space stem imaged in Figure 5.1. A bipolar leader channel (space stem) forms ahead of the negative leader tip, with positive streamers toward the leader tip and negative streamers away from it. The stem grows in length until it contacts the leader tip, forming a new leader step. In the case of Figure 5.1, the step formation process is interrupted by the completion of another leader step (indicated in gray to the left).

The short branches that are connected to the main channel at almost every leader step in Figure 5.1 may be extensions of the leader tip along a newly forming branch

during the formation of a new step. When looking closely at the space stem in Figure 5.1, there appear to be two negative streamers connected to the space stem at its far end, away from the main leader channel. If the space stem had been successful, both streamers could have become part of the new leader step, with the leader extending along only one of them. This could have resulted in a short luminous branch similar to those observed farther down along the main leader channel. It is remarkable that so many leader steps produce short "attempted branches".

The unattached space stem during the streamer-to-leader transition also explains the phenomenon of "unconnected branches" photographed at two close BFB flashes on July 24, 2010, which are reproduced in Section C.2.

In summary, several observations can be made regarding Figure 5.1:

1. Clusters of streamers are only observed at discrete times during leader propagation;
2. The leader steps at 11 km altitude are on the order of 200 m in length;
3. In most instances there are more than one and sometimes as many as 6–8 streamers attached to the leader tip;
4. The streamers connected to the leader tip are on the order of 50–100 m in length, forming a streamer zone of about 100–200 m in extent at 11 km altitude;
5. Sharp bends or kinks in the leader channel appear to be caused by a step in the direction of a dominant streamer that did not lie along the axis of the leader but made an angle, as evident from the large angle some streamers make with the leader in Figure 5.1;
6. Branches may develop when two or more dominant streamer-to-leader transitions ahead of the leader tip occur simultaneously;
7. Similar to laboratory sparks in air gaps, the streamer-to-leader transition (step formation) in natural lightning also appears to occur in a detached, bidirectional manner ahead of the leader tip, as a luminous channel (space stem) with streamers at both ends, which initially is not attached to the main leader. The space stem along with its streamers appears to be about 200 m in length in the photograph, consistent with the nominal 200 m step length inferred from the spacing of streamer zones along the leader.

Berger and Vogelsanger [1966] reported negative leader step lengths of 3–50 m length, which are typical values reported in the literature for low-altitude negative leaders, while *Schonland* [1956] reported a larger range of 10–200 m. *Winn et al.* [2011]

inferred step lengths for a negative leader at 9.1 km altitude of 50–600 m using balloon-borne vector electric field measurements.

Schonland further suggested that channel tortuosity is caused by successive leader steps being formed in non-uniform directions (an observation that is illustrated well in Figure 5.1). If leader steps have longer lengths at high altitude than at low altitude, the cloud-to-ground channel of a BFB flash would be expected to show less small-scale tortuosity at high altitude than at low altitude. Visual and photographic observations suggest that this is indeed the case (Section 2.4 and Photo D.7).

The observations made from Figure 5.1 are important for the studies of the subject BFB flash presented later in this chapter (Sections 5.5–5.8), since that BFB flash occurred in close vicinity to this upward leader, and only 22 minutes later in time. Also, the subject BFB flash had an upward branch like the upward leader.

5.4 BFB flashes

The close storm changed to "BFB mode" starting at 03:00 and continued in that mode for the next 30 minutes. In addition to BFB flashes, regular –CG and IC flashes also occurred frequently (with several flashes per minute on average). In 30 minutes six BFBs were detected by the LMA, five of which were photographed. Two additional BFB flashes occurred later during the storm's lifetime. Most of the BFB flashes exited the storm at the northwest flank but some exited toward the south or southwest, through a cloud shelf that was part of the updraft at the southwest flank of the storm. –CG flashes occurred under and near this updraft, while IC flashes extended more to the northeast in the sheared anvil.

Between 03:30 and 04:10 the storm gradually became more active. At 03:50 it was producing lightning at a rate of 3–4 flashes per minute. Two more BFB flashes occurred (Table 5.1). After that, the storm produced only IC, low-IC and –CG flashes and continued doing so until 05:50, when it died. At this time it was at a distance of 130 km from the laboratory and intervening clouds prevented a view of the storm. Also, the moonlight interfered with low-light observations. This was unfortunate, because the LMA detected three possible screening-layer flashes at high altitude (between 13 and 15 km) in the 04:30–05:00 time interval. At that time the storm system was producing intracloud lightning at up to 15 km altitude. Observations were commenced of a distant storm to the WNW of the laboratory, but no upward lightning was observed.

Time (UTC)	Exit flank	Remarks
03:01:19	SW	
03:04:55	NW	
03:06:15	W	Photo D.19; through cloud
03:08:04	N	Attempted BFB flash or extensive intracloud branch
03:10:22	S	
03:16:20	ESE	
03:25:57	NW	Photo 5.3; studied in this chapter
03:57:19	NW	Photo D.20
04:07:09	W	Photo 6.1; BFB flash with low-altitude branch

Table 5.1: Observed BFB flashes in the August 20, 2010 storm.

5.5 Overview of BFB flash at 03:25:57

The BFB flash of 03:25:57 UTC will now be studied in detail. This flash was chosen for a case study because the leader was not obscured by clouds very much while it propagated to ground, and high-speed video as well as broadband waveforms were recorded in conjunction with LMA data.

The BFB flash exited the cloud at the northwest flank. Upon emerging from the cloud at 9 km altitude it produced a branch, and then appeared to follow the cloud boundary for several kilometers downward, after which it propagated into clear air, through a cloud bank of ancillary cumulus, and on to ground. An overview of the various data sets will be given first, followed by detailed analysis of the intracloud, cloud-to-ground, and final stage of the flash.

5.5.1 Photograph

A still photograph of the flash is reproduced in Photo 5.3, in which the segment of the leader where it follows the cloud boundary appears overexposed due to scattered light. The photo shows that the storm was sheared toward the east or northeast by wind shear and also demonstrates how far from the main downdraft a BFB flash can strike ground—at least 7–8 km in this case.

5.5.2 LMA

Figures 5.3, 5.4 and 5.5 show VHF sources located by the LMA for the flash, colored by time, charge, and source power respectively. The flash was a Type-II BFB flash

Photo 5.3: The BFB flash of August 20, 2010 at 03:25:57 UTC, imaged with a Nikon D700 digital still camera. The view is to the ESE, with Stallion Range and the distant Oscura Mountains to the lower left of the frame. The main precipitation shaft is to the right at the SW part of the storm. The upper part of the storm is sheared off to the NE, to the left and away from the camera. The BFB flash originated near the precipitation region and went to ground 7–8 km to the NW.

with a total duration of 382 ms. The intracloud stage lasted 154 ms, the cloud-to-ground stage 120 ms and the final stage 108 ms.

Compared to the BFB flash from August 2, 2010, studied in Chapter 4, this is a less complicated flash of shorter duration but with more intracloud activity leading up to the cloud-to-ground stage.

As inferred from LMA charge identification for this flash (Figure 5.4), the storm was a normal-polarity thunderstorm with upper positive charge and midlevel negative charge, with some lower positive charge present as well (evident from –CG activity).

The BFB flash initiated at 7.3 km altitude with an upward negative leader that traveled in a northwesterly direction, with a total length of 4–5 km and reaching up to 10 km altitude. This leader stopped and another negative leader branch started at or near the initiation point, traveling in a southerly direction at relatively low altitude, not going upward. After this, several successive negative breakdown events

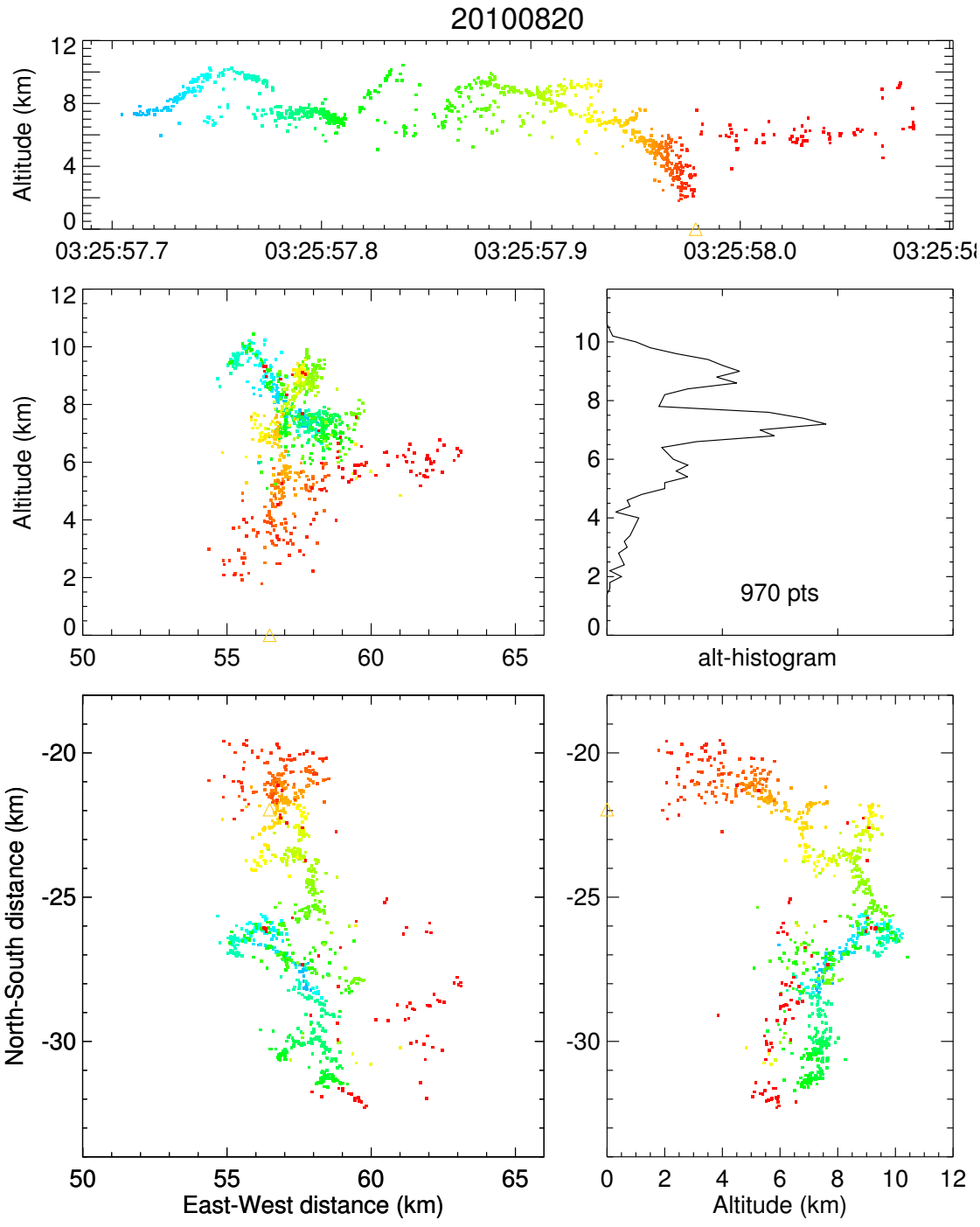

Figure 5.3: LMA data for the BFB flash of August 20, 2010 at 03:25:57 UTC, colored by time. The stroke to ground located by the NLDN is indicated by a triangle.

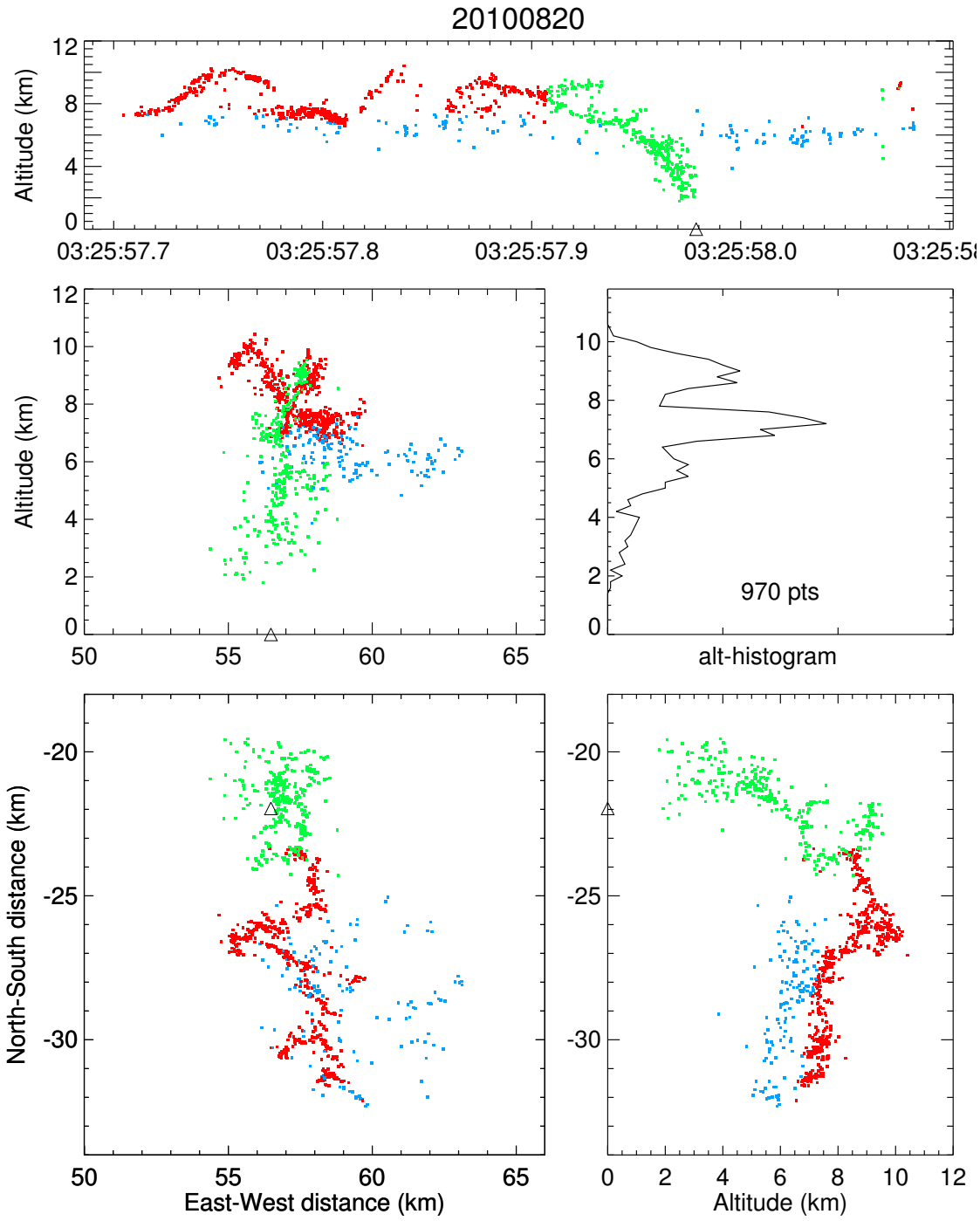

Figure 5.4: LMA data for the BFB flash of August 20, 2010 at 03:25:57 UTC, colored by charge. Blue indicates positive breakdown propagating through negative charge while red indicates negative breakdown propagating through positive charge. Green sources indicate negative breakdown propagating through undetermined charge. In this case, the green sources correspond to the leader being outside the cloud.

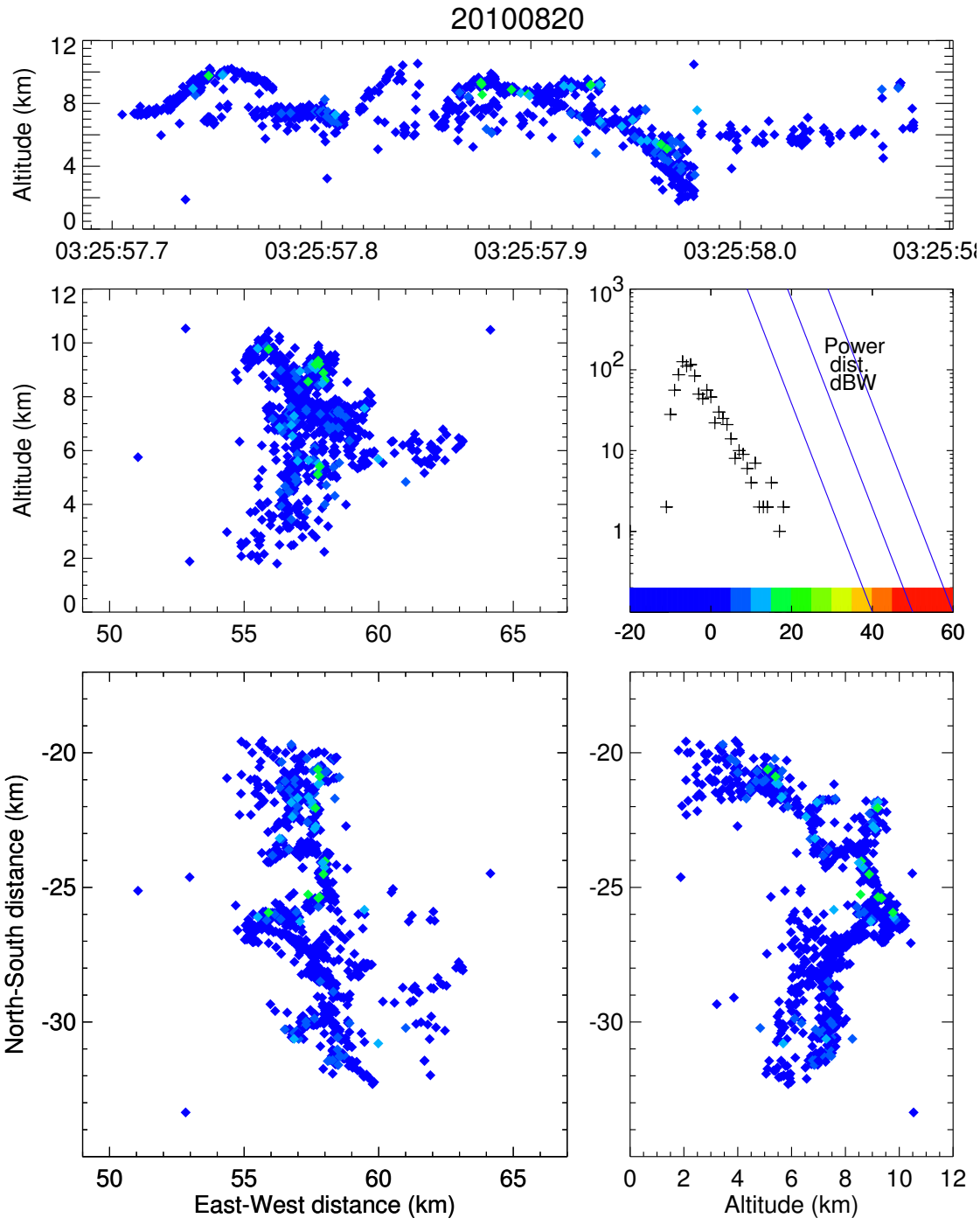

Figure 5.5: LMA data for the BFB flash of August 20, 2010 at 03:25:57 UTC, colored by source power. The higher-power sources are associated with negative breakdown.

occurred along the original upward channel. Finally, yet another negative leader traveled upward and branched off the main upward channel to become the cloud-to-ground leader, contacting ground 7.3 km north of the intracloud initiation point. Two dart leaders were attempted along the channel to ground during the final stage, neither of which succeeded in contacting ground.

5.5.3 Waveform data

The waveform data of 63 MHz log-RF, ΔE, fast ΔE and a 0.01–100 MHz broadband spectrogram are reproduced in Figure 5.6, along with VHF source altitude colored by charge. Unfortunately, due to the distance to the flash and the noisy RF environment at the Annex of Langmuir Laboratory, the waveforms are of limited use. A 53.2 kHz pulse train adds 10–15 dB to the noise background of the log-RF, hiding most of the weaker intracloud activity leading up to the cloud-to-ground leader.

The slow and fast antennas were operated on a sensitive gain setting and the waveforms are dominated by sferics of the return stroke. Sferics from remote flashes were also detected by the fast antenna, which can be seen in the fast ΔE waveform in Figure 5.6 before the initiation of the BFB flash.

5.5.4 High-speed video

The high-speed video camera was operated at 6400 FPS at a frame size of 800×600 pixels. It was fitted with a 50 mm lens set at an aperture of $f/2.8$. At the distance of the BFB flash, the resolution of the video imagery is 26.7 m/pixel. A composite overlay of all video frames leading up to the return stroke is shown in Figure 5.7, and the same composite with projected VHF sources located by the LMA is shown in Figures 5.8 (with VHF sources colored by time) and 5.9 (colored by charge).

The video composite overlay algorithm used here (both the fixed overlay and time-shift algorithm), is outlined in Section 4.2.1. Section A.8.4 discusses the point-projection algorithm used for overlaying VHF sources on the video frames.

In this chapter video data is also correlated with the waveform data by extracting *light curves* from the video data. The light curves were made by selecting a single pixel coordinate and plotting the pixel brightness as a function of time. The light curves in this chapter are normalized relative to the full pixel brightness and have a sampling resolution of 156.25 μs; the frame exposure time was 150 μs. Since the camera sensor integrates light during the exposure, each pixel value in a light curve represents the integrated light value *over the previous* 156.25 μs (refer to Section A.8.1 for more details on the video time reference).

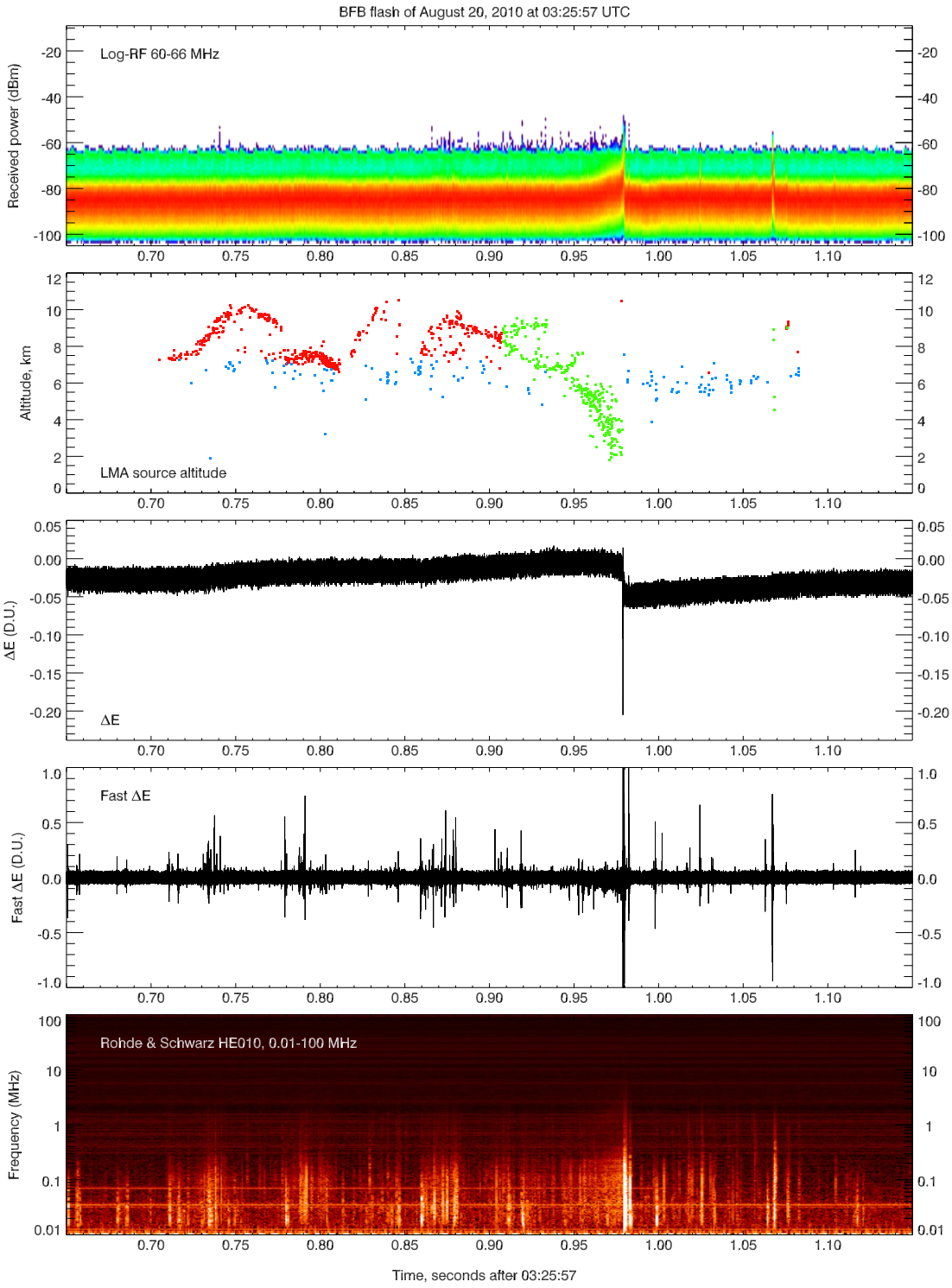

Figure 5.6: Waveform data of the BFB flash of August 20, 2010 at 03:25:57 UTC. The plotted time interval is 500 ms. From top to bottom: 63 MHz log-RF, VHF source altitude colored by charge (as in Figure 5.4), ΔE waveform, fast ΔE waveform, and 0.01–100 MHz spectrogram of the Rohde & Schwarz broadband antenna.

Figure 5.7: A composite of all video frames leading up to the first return stroke. A lens with a focal length of 50 mm and an aperture of $f/2.8$ was used on the high-speed camera.

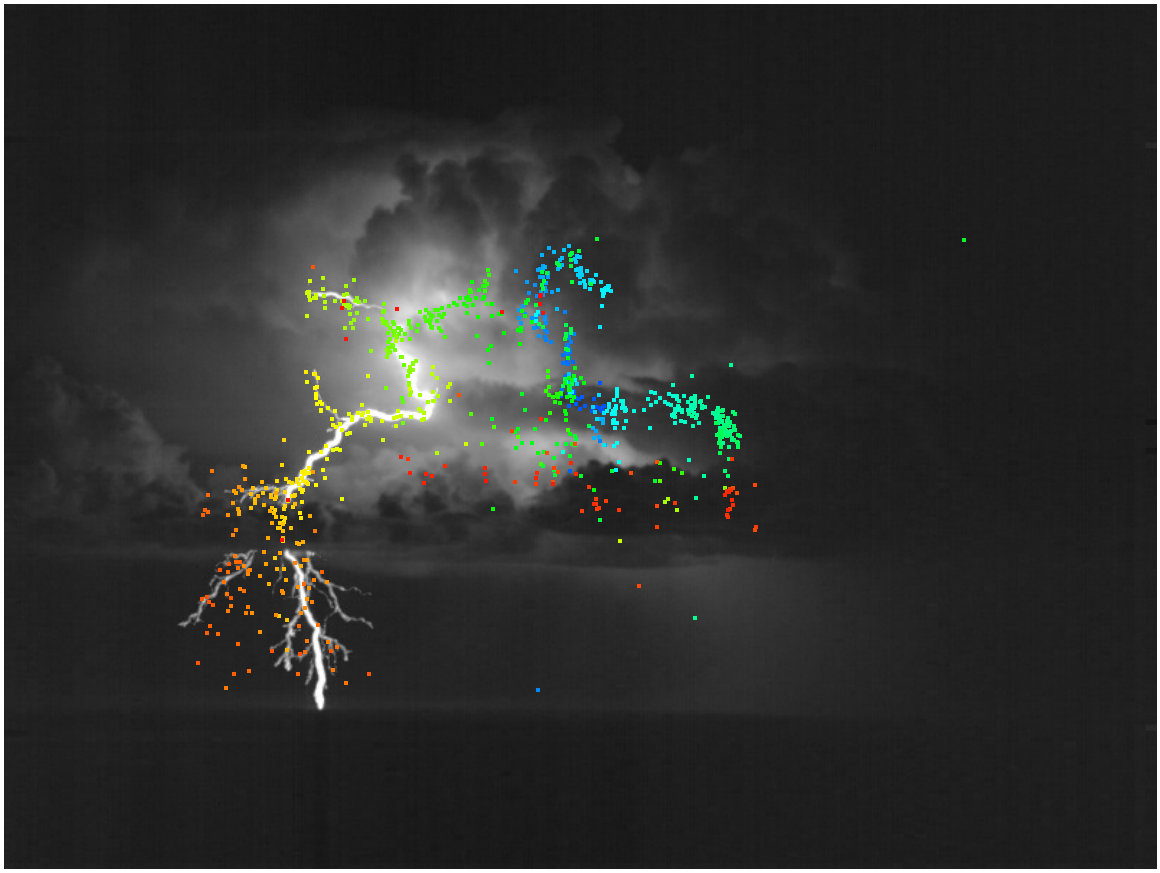

Figure 5.8: The video composite frame of Figure 5.7 with VHF sources detected by the LMA overlaid by a point-projection. The sources are colored by time, where blue is earlier and red is later in time.

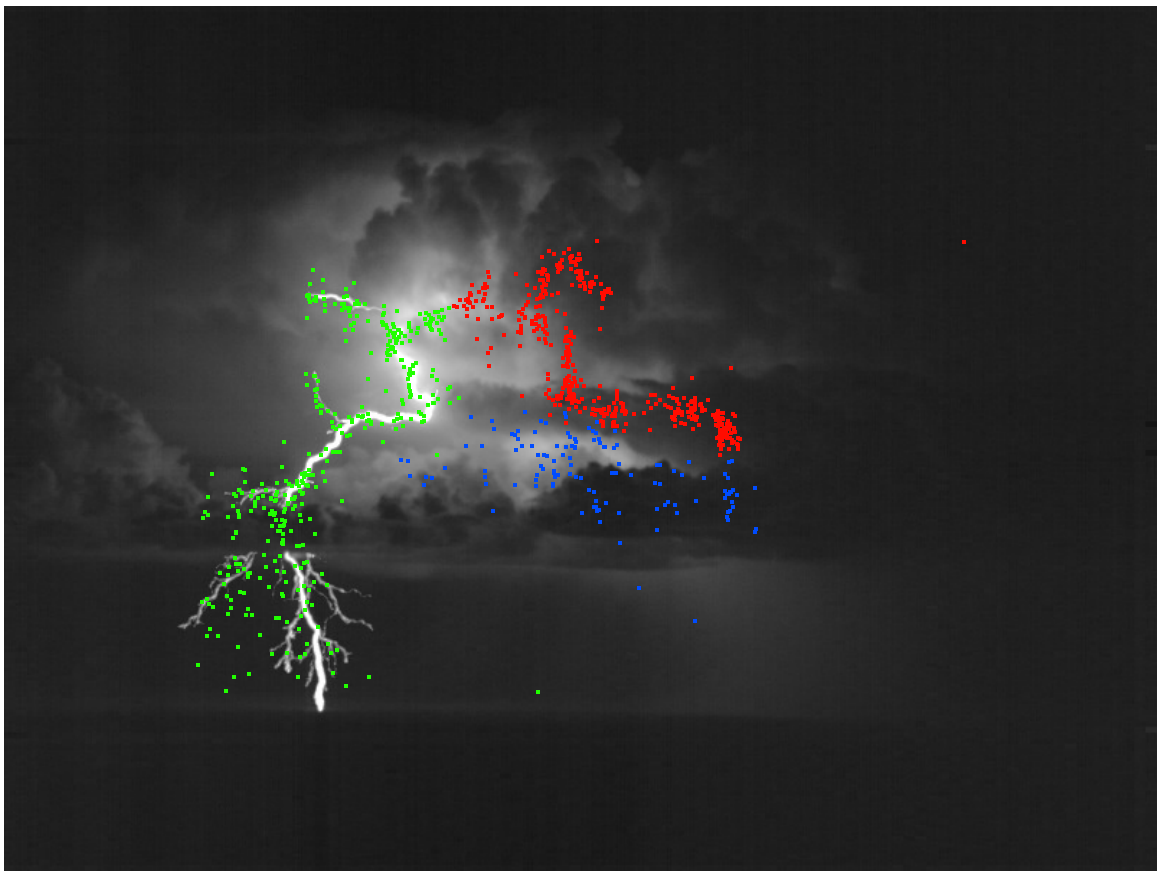

Figure 5.9: The video composite frame of Figure 5.7 with VHF sources overlaid by a point-projection. The VHF sources are colored by charge in correspondence with Figure 5.4. The second leader branch (counting from the cloud exit point down) was mapped quite well by the LMA, like the main cloud-to-ground channel in general. VHF sources associated with the high-altitude branch exiting the cloud were also located fairly well by the LMA but these sources suffer from altitude (elevation) inaccuracies, as do the low-altitude VHF sources. Many of the low-altitude sources appear to lie on different "shells" of hyperboloid surfaces, corresponding to different sets of contributing stations. Note that the upward intracloud leader changes direction to the right in the frame, possibly propagating through charge within the cloud turret.

5.6 Intracloud stage

Five individual negative breakdown events occurred in the flash, leading up to the leader to ground. The first two of these events will be discussed in Section 5.6.1 and the third and fourth events in Section 5.6.2. The fifth event was the negative breakdown that developed into the cloud-to-ground leader, which will be treated separately in Section 5.7.

5.6.1 First and second negative breakdown events

Figure 5.10 shows 80 ms of waveform data for the first upward negative leader and the accompanying Figure 5.12 shows LMA data, highlighted in black, during the corresponding time interval. Figure 5.11 shows an expanded time interval of the same waveforms.

The flash started at 03:25:57.705 UTC with a single mapped VHF source at 7.3 km altitude, followed by a pause of 5.5 ms after which a negative leader developed to the NNW. This leader traveled more or less horizontally for about 500 m before heading upward. The leader took 25 ms to propagate an initial distance of 2 km at a velocity of 8.0×10^4 m s^{-1}. Two bursts of fast ΔE pulses (also seen in VHF) were produced by the leader at an early stage, about 5 ms after each other (Figure 5.10, at 0.711 and 0.716 seconds past 03:25:57).

When the negative leader had changed its direction from mostly horizontal to more vertical, a series of large-amplitude fast ΔE pulses occurred (Figures 5.10 and 5.11, between 0.730 and 0.745 seconds past 03:25:57). These pulses correlate in time with scattered-light pulses seen by the high-speed video camera on two points on the cloud (Figure 5.10, fourth and fifth panels). These light pulses, which succeeded each other at fairly regular intervals of about 2.2 ms, occurred at increasingly higher altitudes while the negative breakdown propagated upward. Initially, the brightest pulses occurred in the midlevel negative charge region, followed by brighter pulses toward the upper positive charge region. The pulses are also observed in VHF (Figure 5.10, spectrogram) and are most likely associated with fast K-leaders that carried negative charge upward. VHF sources from negative breakdown occurred at a higher rate around the time of the series of light pulses than before and after the series.

At 03:25:57.748 there was a brief lull of about 4 ms in negative breakdown during which some activity in the midlevel negative charge region was located by the LMA (Figure 5.12). After the short pause, negative breakdown resumed but the leader made a sharp turn toward the southwest (Figure 5.12, plan view). The high-speed video imagery with overlaid VHF sources (Figure 5.7) indicates that this turn may

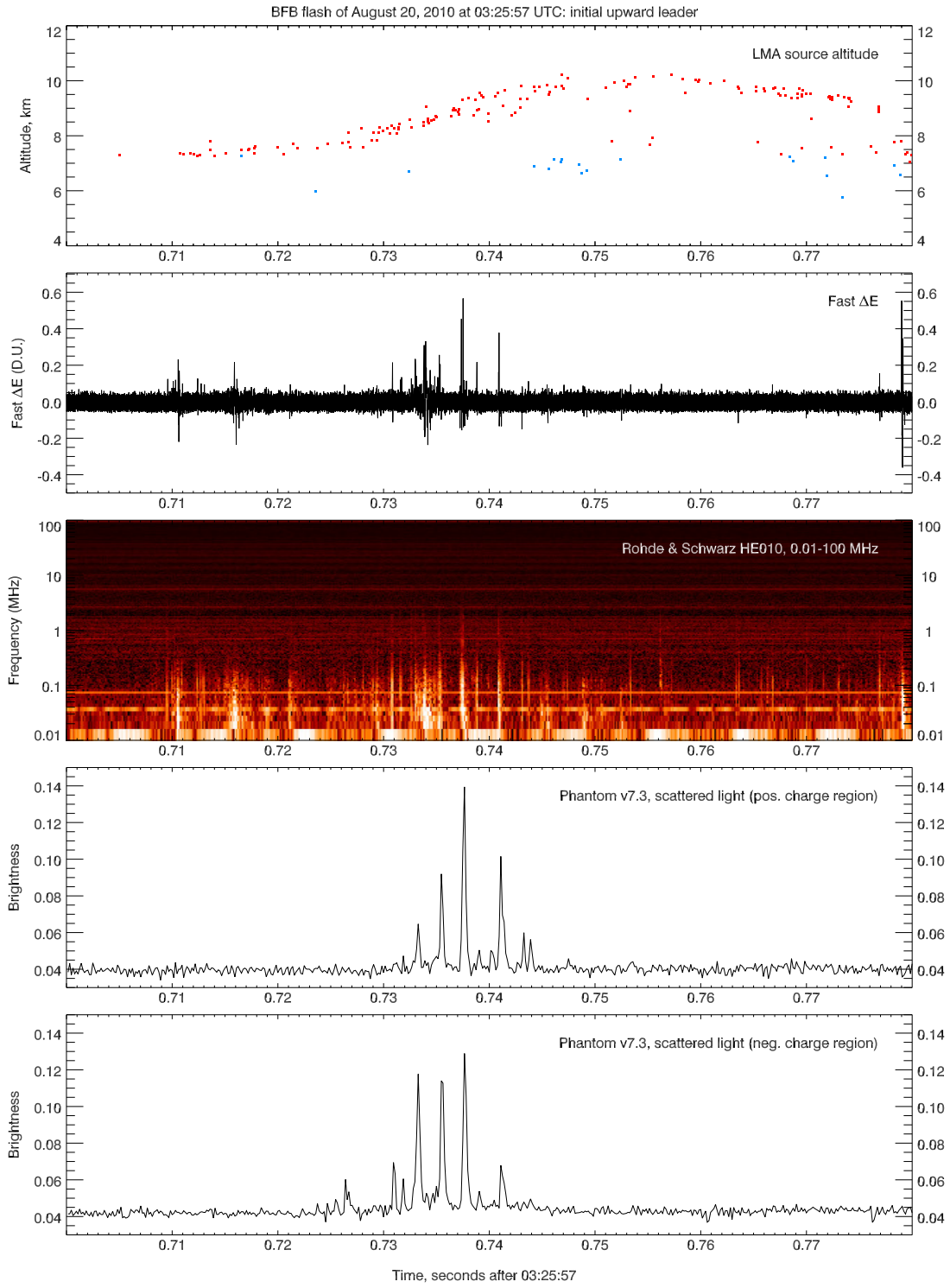

Figure 5.10: Waveforms for a time interval of 80 ms during the initial upward leader. The two bottom panels show curves of light scattered by the cloud. The pixel coordinate of the light curve in the fourth panel represents an altitude of 8.8 km; that of the bottom panel, an altitude of 6.4 km.

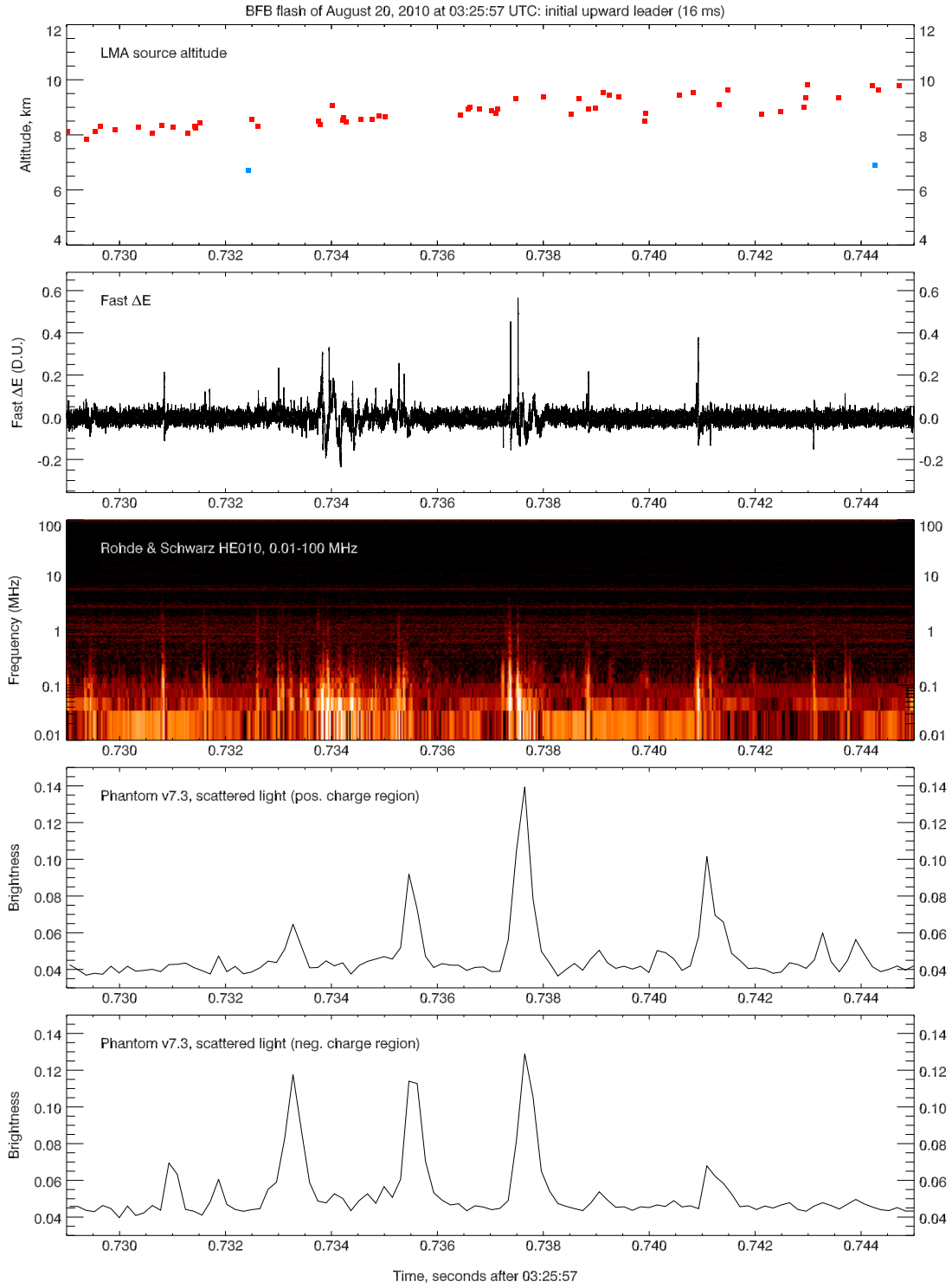

Figure 5.11: The waveform data of Figure 5.10, expanded to a time interval of 16 ms around the light pulses.

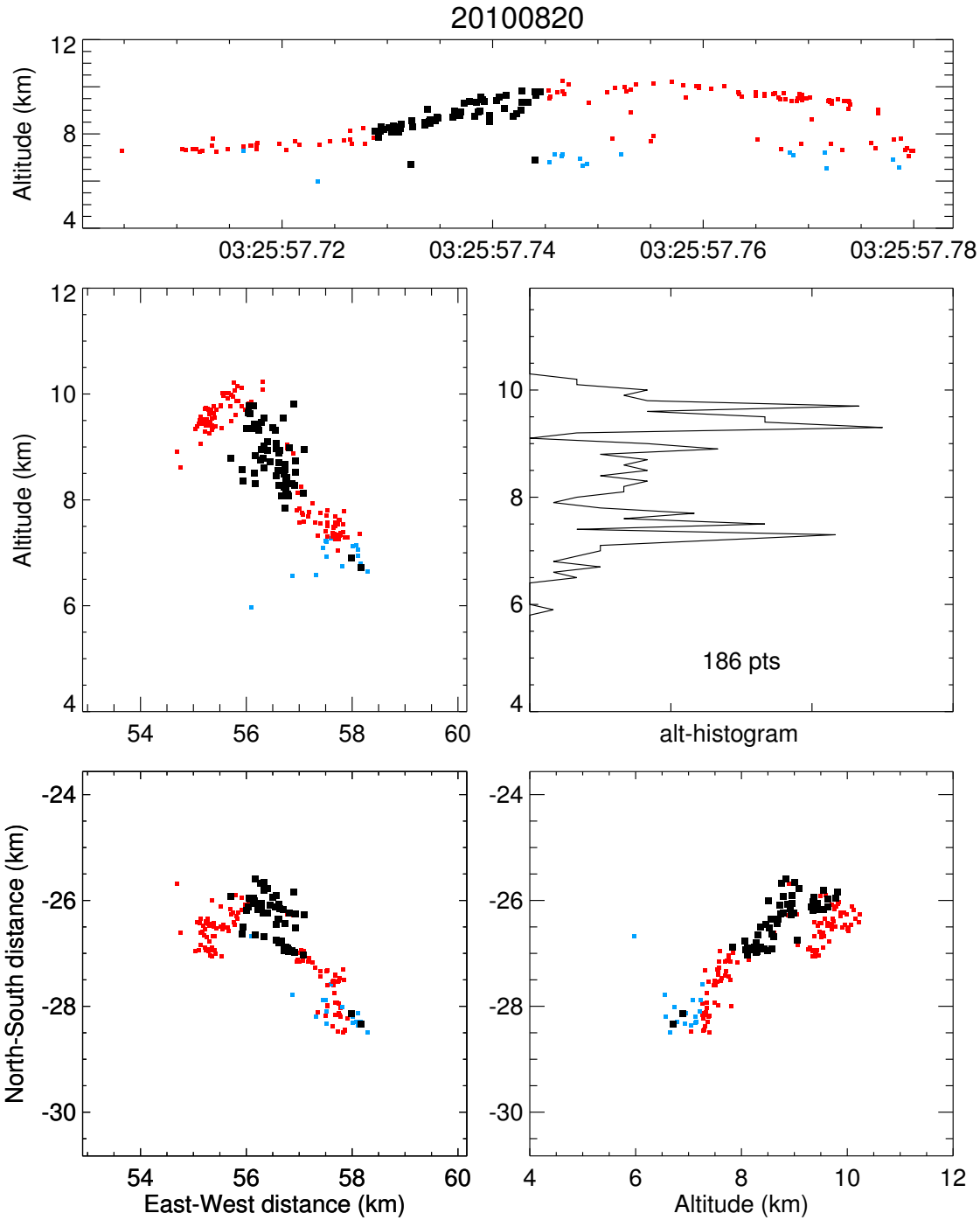

Figure 5.12: VHF sources located by the LMA within the time interval of 80 ms from Figure 5.10, with those located during the time interval of 16 ms from Figure 5.11 highlighted in black. The sources are colored by charge.

have been made by the leader to stay within the cloud. The leader channel extended by about 1 km until the leader stopped, making it 5 km in total length.

The second negative breakdown event started at 03:25:57.78 as the upward negative leader came near the end of its development. The new negative breakdown initiated near the flash initiation region and propagated horizontally at 7 km altitude in a SSE direction, toward the main downdraft of the storm (Figures 5.3, 5.4 and 5.6, between 0.780 and 0.815 seconds past 03:25:57). It propagated over a distance of 4.5 km and made multiple branches. The general extent of the various leaders may be explained by the strong wind shear, which could have made the charge regions asymmetric in extent.

5.6.2 Third and fourth negative breakdown events

The third negative breakdown event initiated at 03:25:57.818, 113 ms after the initiation of the flash, with the negative leader traveling upward along the channel established by the initial upward leader. It propagated at a velocity of 2×10^5 m s^{-1} as determined from LMA data (Figure 5.14), slightly faster than the first negative leader. Several VHF sources appear clustered in groups along the leader channel in the figure. One such group occurred at 8.6 km altitude along (but adjacent to) the main channel and was apparently caused by new breakdown at the tip of an earlier branch. This indicates that the original channel had lost most of its conductivity since the first breakdown event and the new negative leader was about to choose a new path. The new leader did not extend the original channel by much or at all, with only two VHF sources located near the end of the original channel.

Figure 5.13 shows 35 ms of waveform data around the time of the third negative breakdown event. Some weak scattered-light pulses occurred within the negative charge region (bottom panel in figure) but no associated light pulses were observed in the positive charge region. Some of the light pulses are correlated with fast ΔE pulses, indicative of K-leader activity. The largest-amplitude fast ΔE pulse (at 03:25:57.8284) occurred 1.22 ms after a weak light pulse and associated VHF source in the midlevel negative charge region; this could be a (poorly-resolved) K-event that initiated a K-leader.

As the negative leader propagated upward, some VHF sources from K-events were located in the midlevel negative charge region near 6 km altitude.

The clustered VHF sources from negative breakdown during the third negative breakdown event indicate that the negative breakdown was helped along by fast K-leaders that each carried negative charge upward along the original channel to increasingly higher altitudes. The various light pulses in the midlevel negative charge region during this stage (Figure 5.13, between 0.819 and 0.840 seconds past 03:25:57) suggest

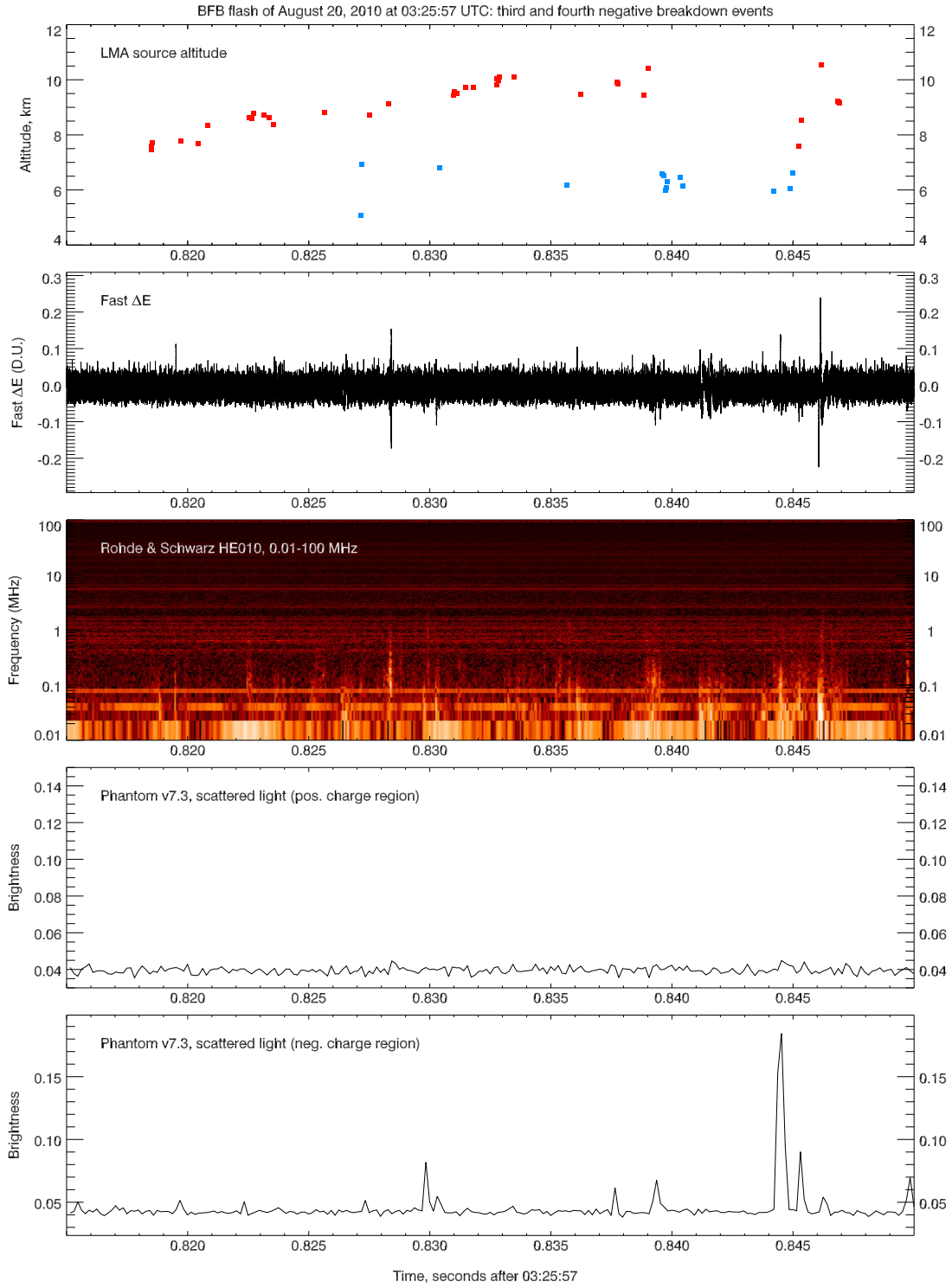

Figure 5.13: Waveforms for a time interval of 35 ms during which a number of K-leaders propagated upward along the original channel.

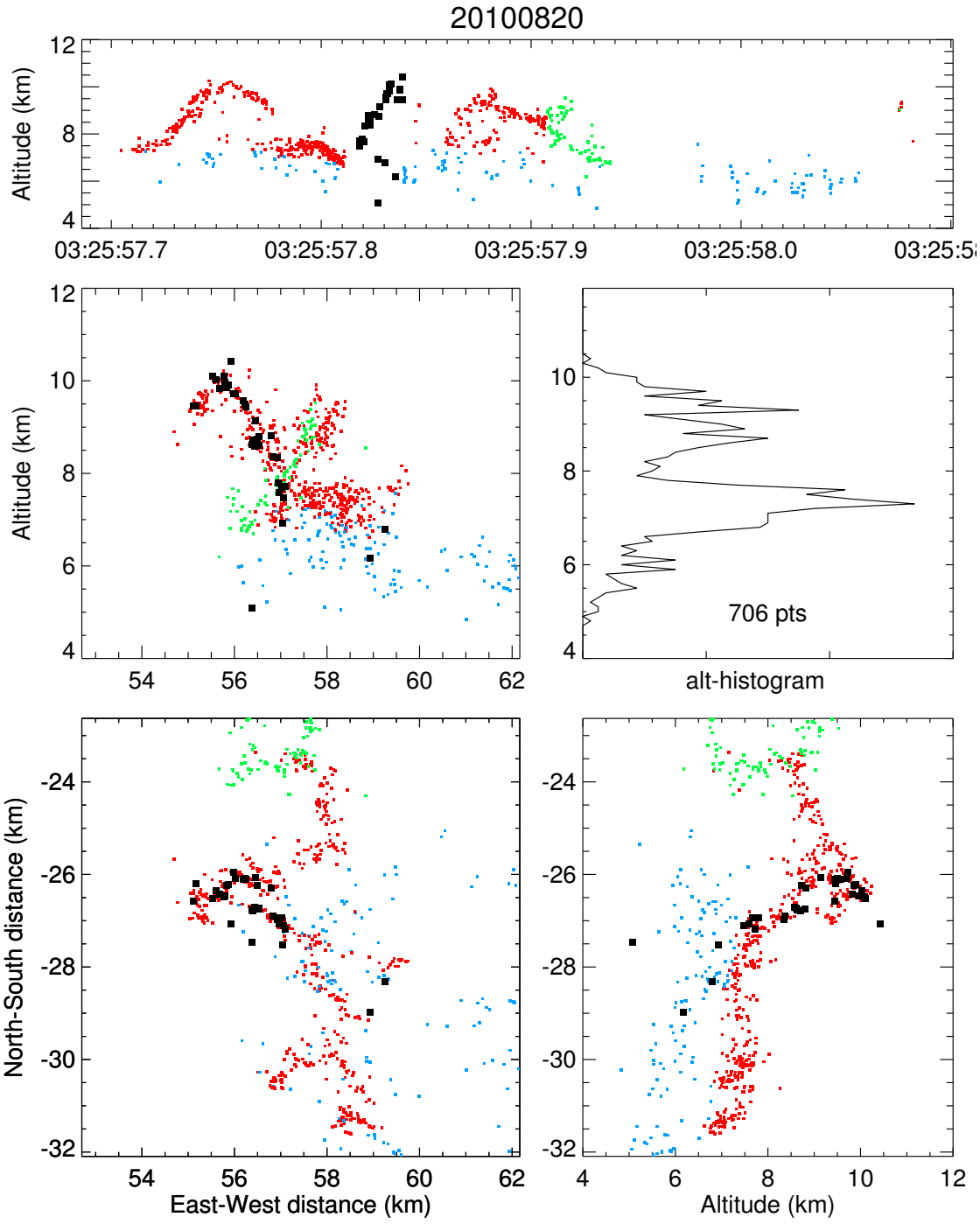

Figure 5.14: VHF sources located by the LMA and colored by charge, with those during the time interval of the third negative breakdown event (0.815–0.839 seconds past 03:25:57) in Figure 5.13 highlighted in black.

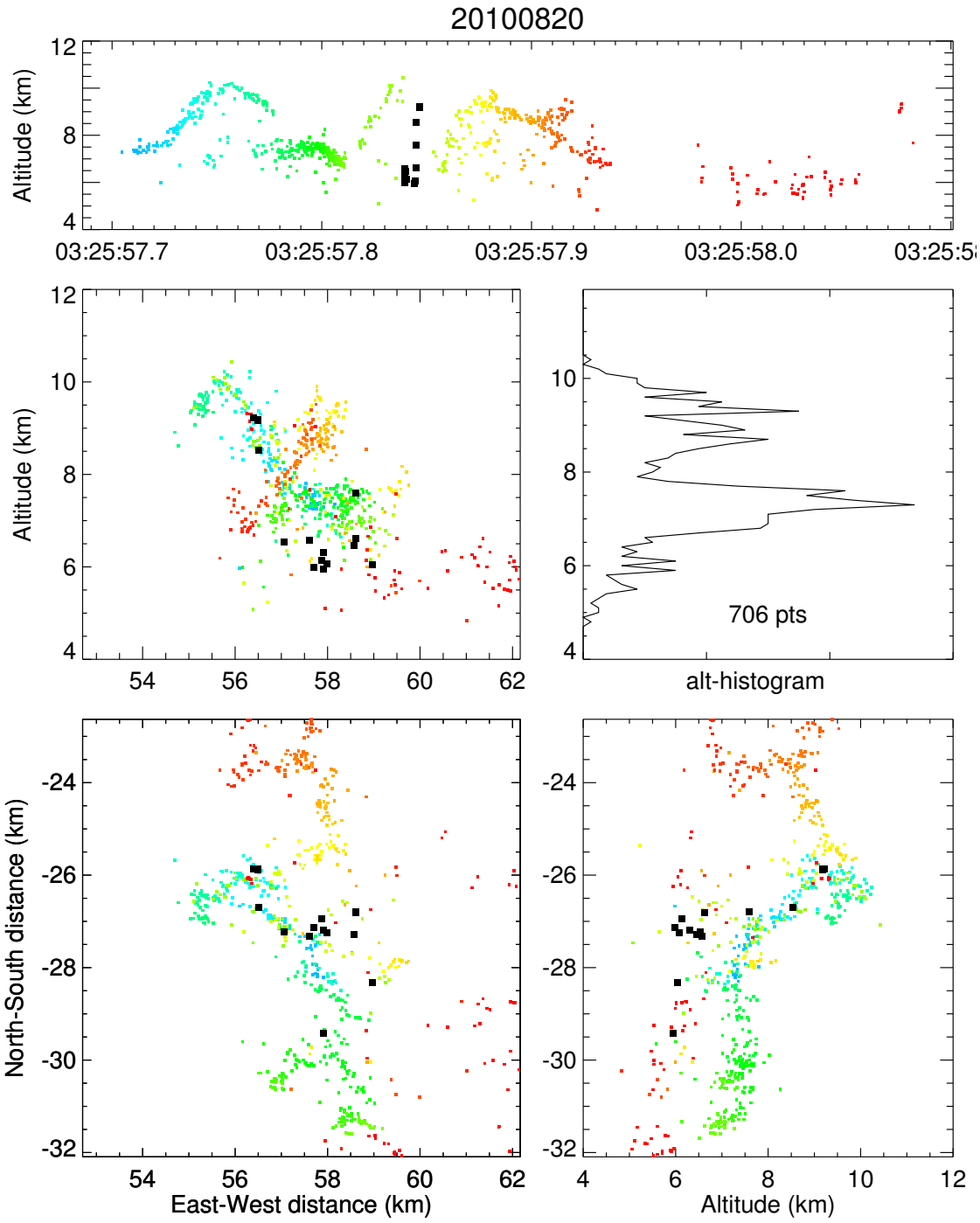

Figure 5.15: VHF sources colored by time, with the sources from the fourth negative breakdown event highlighted in black. The last three sources (not individually resolved in this figure but appearing as a single, large point) occurred close to the subsequent branching point of the cloud-to-ground leader.

that at least six K-leaders occurred during the negative leader development.

The fourth negative breakdown event initiated at 03:25:57.8445 with a bright light pulse in the midlevel negative charge region, three associated VHF sources and a relatively small fast ΔE pulse of positive polarity. A much larger-amplitude fast ΔE pulse occurred 1.69 ms later in time, after several VHF sources were located by the LMA along the original upward leader channel (Figure 5.15). This leader had a velocity of 2.5×10^6 m s^{-1} (from LMA data). It did not reach all the way to the end of the original channel but stopped partway along it at 9.2 km altitude. The stopping point is close to where the succeeding negative breakdown branched off the upward channel and developed into the cloud-to-ground leader, suggesting that the latter may have branched off because of residual negative charge along the original channel.

5.7 Cloud-to-ground stage

The cloud-to-ground stage started with the initiation of the fifth negative breakdown event at 03:25:57.859 UTC and lasted for 120 ms, when the stepped leader contacted ground. The fifth negative breakdown event that occurred in the cloud will be discussed first, followed by a detailed analysis of the stepped leader as it exited the cloud and went to ground.

5.7.1 Fifth negative breakdown event

The negative leader that became the cloud-to-ground leader initiated at 03:25:57.859 and traveled upward along the established channel for about 3 km (Figure 5.17). At 8.5 km altitude, close to the point where the original channel made a turn from NW to SW, the leader branched off and started a new channel. It continued upward at a slant angle to the NE for 3–4 km, produced an upward branch that reached an altitude of 10.0 km, turned north, and exited the cloud.

Figure 5.16 shows 60 ms of waveform data during the initial stage of the leader. In this figure, the scattered-light curve associated with the upper positive charge region was derived from a different pixel coordinate, close to the leader exit location near 9 km altitude. The scattered-light curve associated with the midlevel negative charge region is the same pixel coordinate as before, which represents an altitude of 6.4 km.

In comparing the fast ΔE waveform and spectrogram of Figure 5.16 it is remarkable how active the initial stage of the negative breakdown was relative to the later stage, when it became relatively quiescent at VHF. This transition occurs at the time when the leader has produced the upward branch and heads north, still within the cloud.

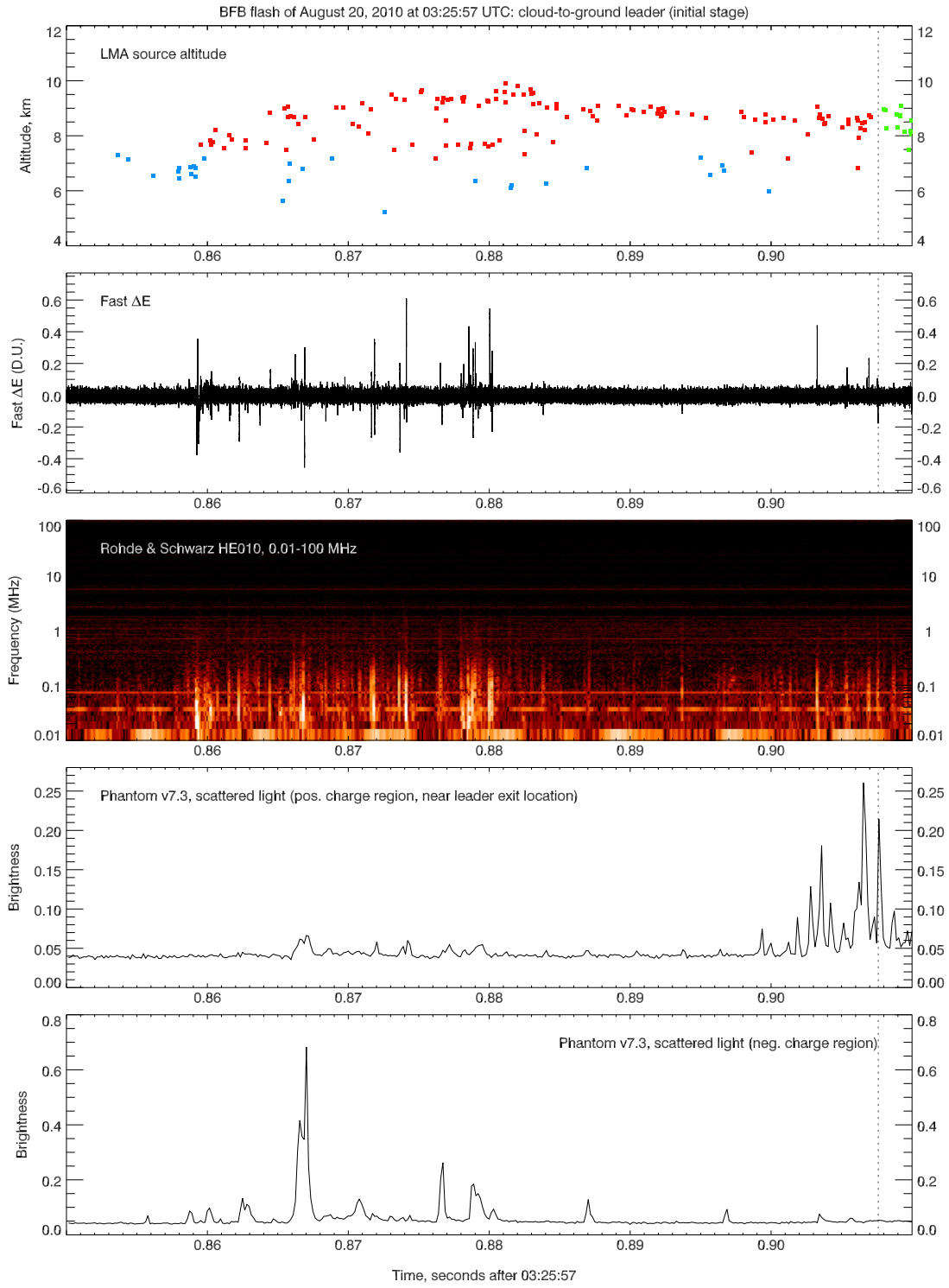

Figure 5.16: Waveform data for a time interval of 60 ms while the fifth negative breakdown event (initiating the cloud-to-ground leader) traveled upward along the established intracloud channel. The green-colored VHF sources toward the end of the time interval correspond to those of the negative leader after it exits the cloud (determined from high-speed video).

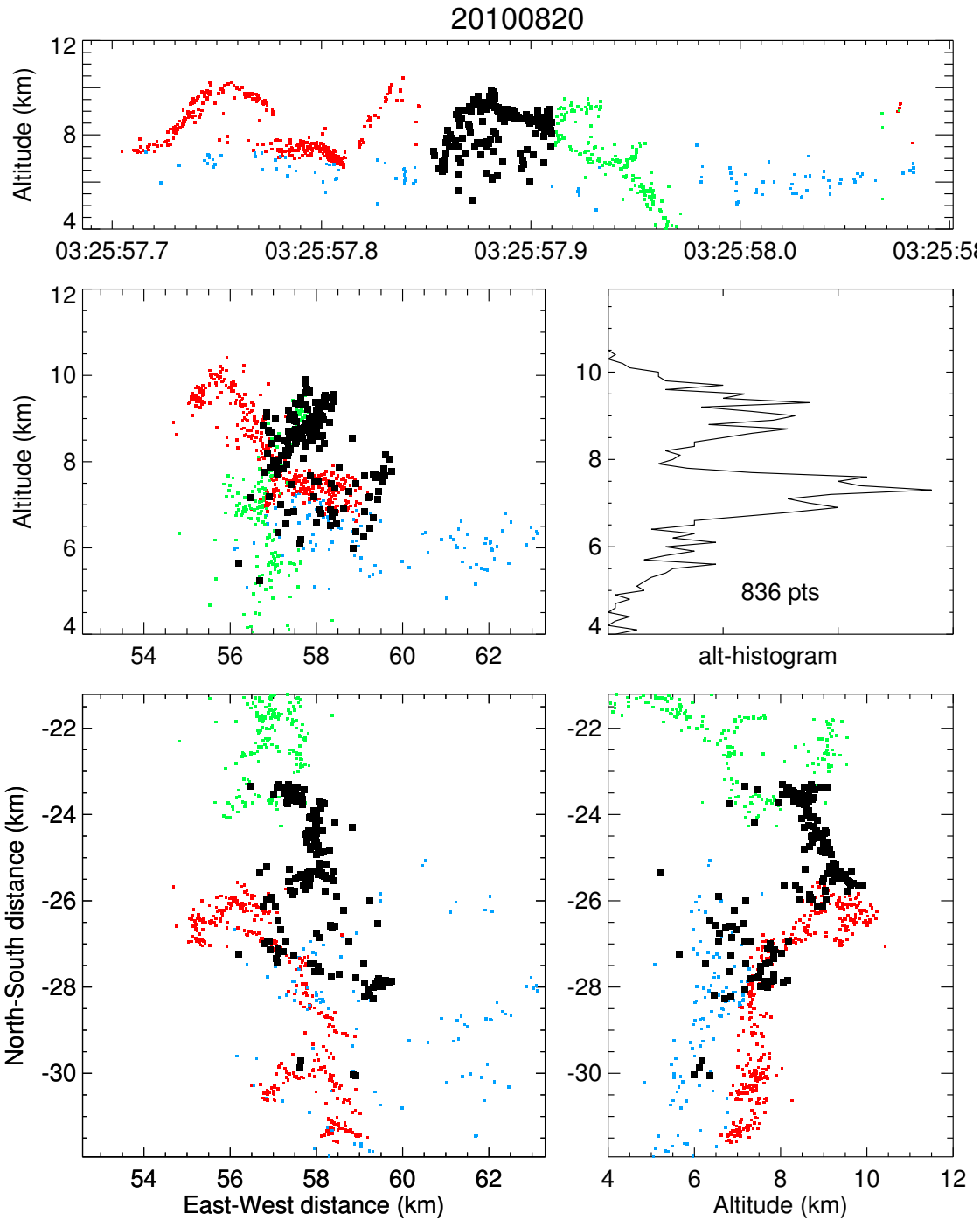

Figure 5.17: VHF sources located by the LMA, colored by charge, with those during the time interval of the cloud-to-ground K-leader (Figure 5.16) highlighted in black.

The large-amplitude fast ΔE pulses correlate with VHF and optical activity in the negative charge region. The bright light pulse at 03:25:57.867 in the negative charge region is correlated with a light pulse in the positive charge region, but this could simply be scattered light from the negative charge region as the latter is relatively bright. The four light pulses in the negative charge region at 03:25:57.870–881 each happen shortly before corresponding pulses in the positive charge region (by 500–1000 μs), and they correlate with fast ΔE pulses. These indicate current surges of negative charge upward along the leader channel, which travel at velocities of 1–2 $\times 10^7$ m s^{-1}, assuming a channel length of 10 km between the tip of the negative leader and the initiation region.

The more quiescent stage of the upward negative leader commences at 03:25:57.881. It is possible that by now the upward channel, including the new breakdown path, has become conductive enough to allow a lower but more continuous current to flow. (Channels carrying current can be quiescent in VHF, as found by *Shao et al.* [1995] who observed a continuing-current component of a return stroke without VHF emissions; e.g. their Figure 21a.) During this quiescent period six faint light pulses occurred in the high-speed video imagery that were emitted by the negative leader in the cloud while it was approaching the cloud boundary (Figure 5.16, fourth panel, at 03:25:57.881–898). These light pulses are likely caused by the leader stepping process and occur at a fairly constant rate of 3.03 ms between pulses on average; the negative leader travels a distance of 700 m during this time at 8.9 km altitude, heading north. If the light pulses do represent leader steps, the steps are a minimum of 140 m in length on average, neglecting the effect of channel tortuosity. A value of $\sim$ 200 m for the step length for a negative leader at 11 km altitude was found from analysis of Figure 5.1. That leader was rather tortuous, however, exhibiting channel bends of up to 90 degrees. This may account for the factor of 1.4 difference in step length estimated here; also, it was at a higher altitude, with a correspondingly longer step length.

The VHF sources associated with the negative leader tip occur at a more or less continuous rate and do not seem to be clustered around the time of each light pulse. In fact, at 03:25:57.892 seven VHF sources occur as a short burst during a 400 μs interval *in between* two light pulses. VHF emission therefore does not appear to occur simultaneously with emission of visible light during each leader step. The VHF emission detected by the LMA during leader stepping may produce visible light as well, but of a much lower intensity that is not resolved on high-speed video.

Toward the end of the time interval in Figure 5.16 the negative leader approached the cloud boundary (from the inside), resulting in brighter light pulses being observed. Around this time the leader split into an upward branch and a main branch, which both continued on. This, and possibly a third branch unresolved by the LMA, are probably responsible for the increased rate of light pulses (from 3.03 ms down to 0.78 ms per pulse) toward the end of the plotted time interval. As the leader exited

the cloud the individual branches could be resolved, from which the actual step duration and length can be determined. This will be done in the following section, which discusses the cloud-to-ground leader.

5.7.2 Cloud-to-ground leader

The negative leader became visible on high-speed video at 03:25:57.9076 as it exited the cloud at 8.5 km altitude. As seen in the composite video images of Figures 5.7–5.9, the leader immediately branched, with one branch going horizontally outward to the north and slightly upward, leveling off at 9.2 km altitude, and the main branch following the cloud boundary downward. The main branch continued to descend until it reached 7.0 km altitude, when it abruptly changed direction to more horizontal in a northerly direction, farther away from the cloud. It continued on this trajectory for about 1.2 km and then again turned downward to ground. It produced a second upward branch at 6.5 km altitude that propagated upward for about 1.5 km.

At 5.5 km altitude the downward leader started branching profusely, with as many as 10–15 individual branches visible in high-speed video imagery as the leader approached ground. It propagated through a bank of shallow cumulus clouds near 5 km altitude and contacted ground at 1.47 km altitude.

After the return stroke two dart leaders were attempted, and several light flashes occurred in the midlevel negative charge region. These events will be discussed in the next section.

Figures 5.18 through 5.20 provide an overview of the observations after the leader had exited the cloud and was imaged by the high-speed video. Figure 5.18 shows 103 ms of waveform data during the cloud-to-ground leader stage. Two high-speed video light curves are included with these waveforms: One curve of the scattered light in the cloud near the midlevel negative charge region (representing an altitude of 6.4 km as before), and another curve from a pixel of the video frame which the stepped leader crossed shortly after it emerged from the cloud. This pixel represents an altitude of 8.1 km. A video streak image, of all video frames leading up to the return stroke, is also reproduced. Figure 5.20 shows only the fast ΔE waveform and streak image at a larger scale, and Figure 5.19 shows VHF sources located by the LMA during the same time interval.

The scattered-light curve representing the midlevel negative charge region is seen to gradually increase toward the later stage of the cloud-to-ground leader in Figure 5.18. This is probably not caused by light emissions from within the cloud, but scattered light emitted by the cloud-to-ground leader.

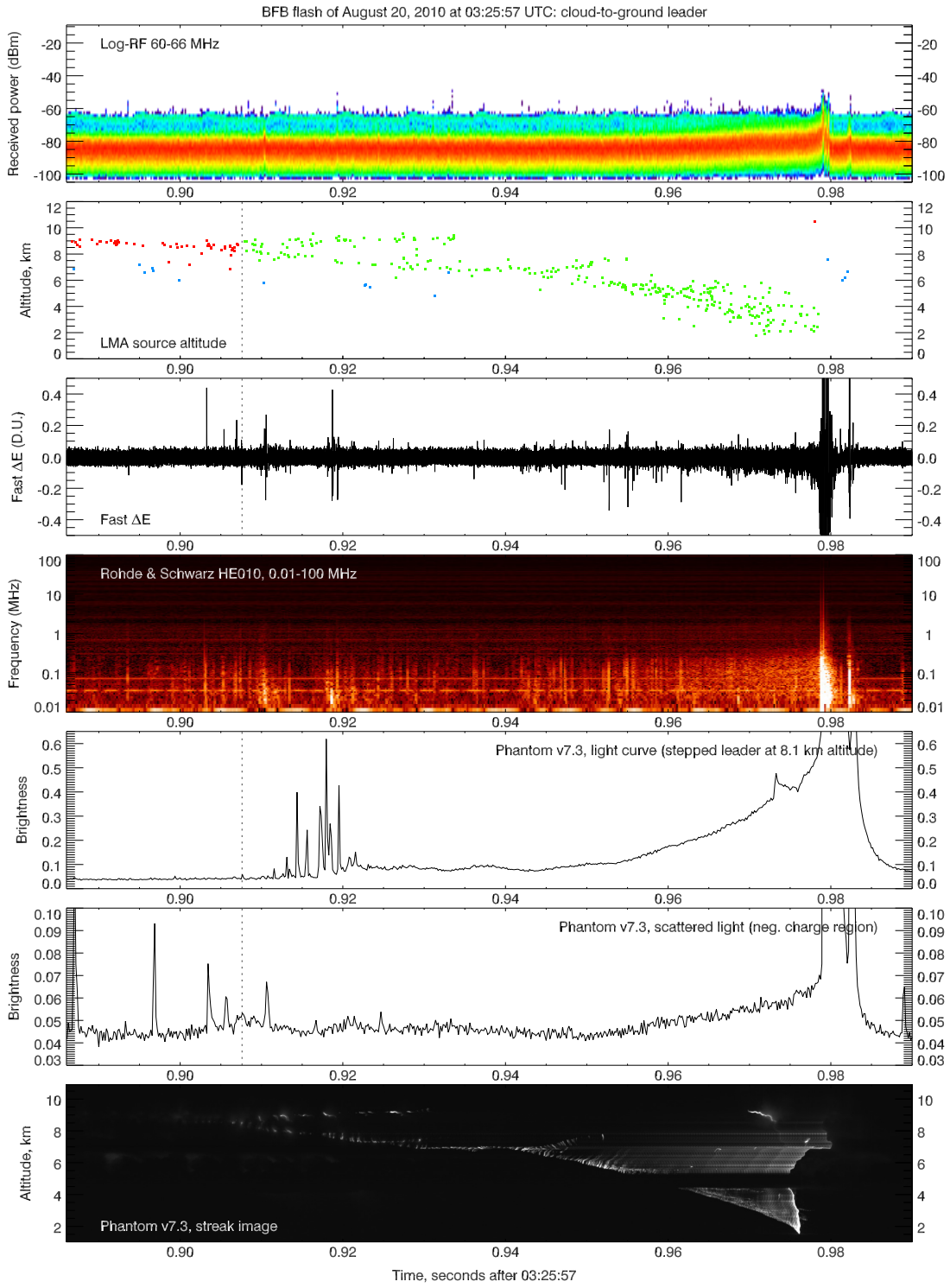

Figure 5.18: Waveforms during the cloud-to-ground leader stage. The time interval is approximately 103 ms. The dotted vertical line at 03:25:57.9076 UTC in the plots indicates the time when the leader emerged from the cloud, as determined from high-speed video imagery. The streak image uses the leader cloud exit location as time reference; the post-return-stroke frames are omitted to prevent overexposure.

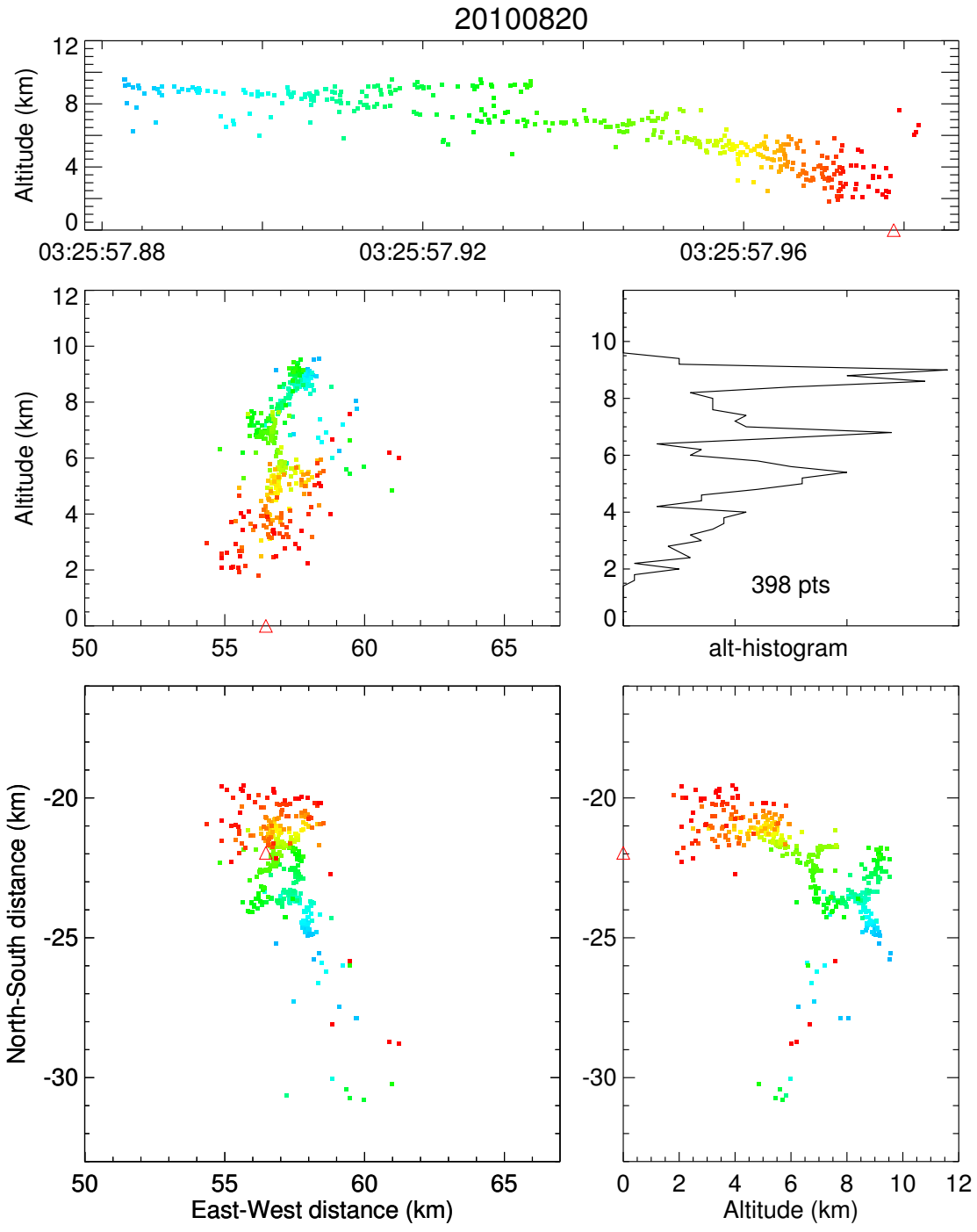

Figure 5.19: VHF sources located by the LMA during the cloud-to-ground leader stage, colored by time. Note the two major branches at high altitude.

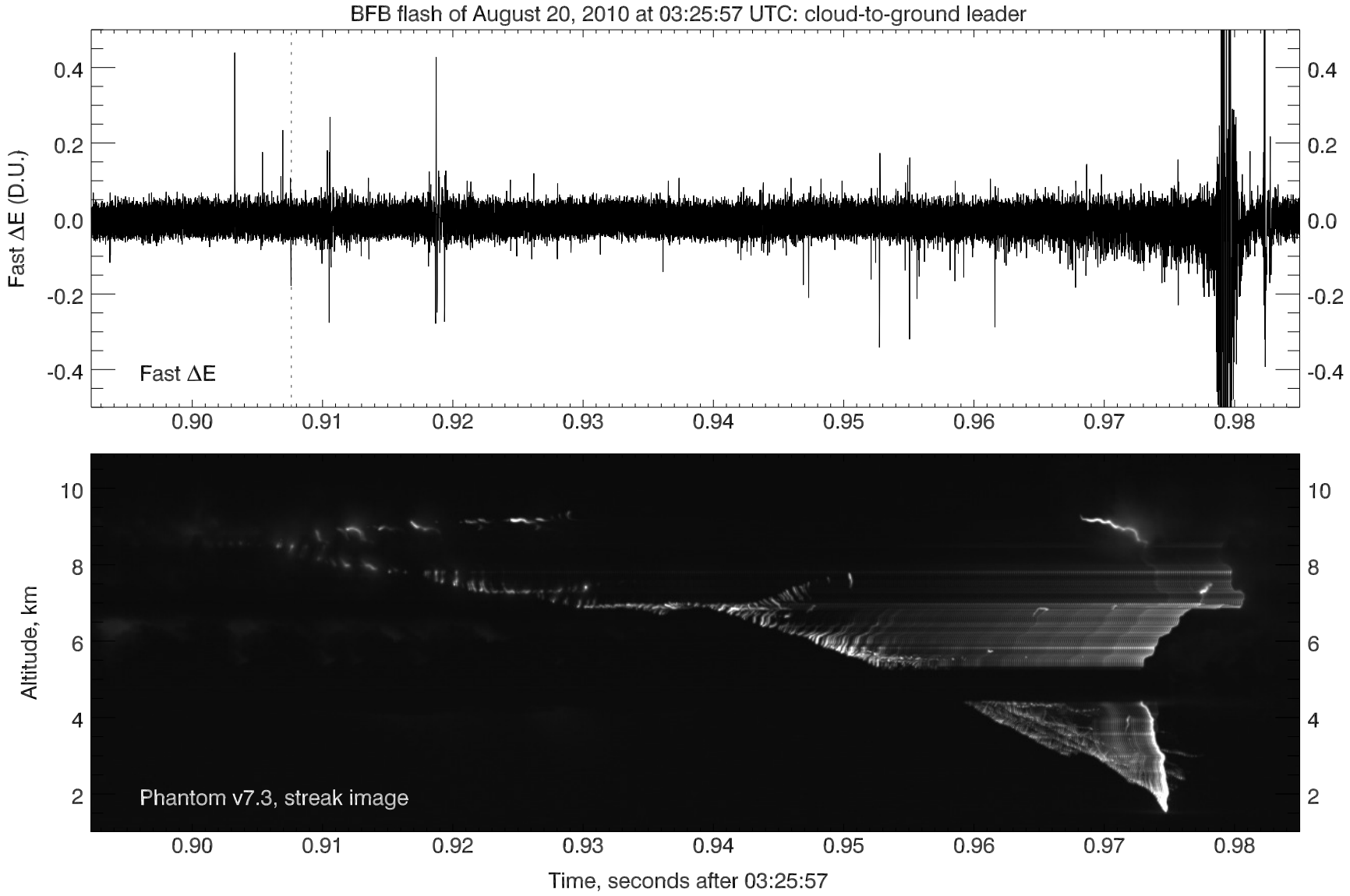

Figure 5.20: The fast ΔE waveform and streak image from Figure 5.18 reproduced at a larger scale. The time interval in this figure is 92.8 ms. The black horizontal band through the streak image near 5 km altitude is a cloud bank in the foreground.

Several interesting observations can be made from Figures 5.18 and 5.20. Perhaps the most obvious of these is the changing appearance of the stepped leader as it propagates from high altitude to low altitude, which has been discussed earlier in this work in the context of VHF emissions. The high-speed video streak image clearly shows how the leader is intermittently luminous at high altitude, transitioning to a more continuous mode of propagation at low altitude.

A second phenomenon is the general, integral brightening of the leader channel as the leader approaches ground. This was also seen in the video recordings in Chapter 4. What is interesting is that the leader luminosity also increases in steps, which occur at regular time intervals during leader propagation. From Figure 5.20 it is apparent that most or all of these changes in luminosity occurred at the time of a luminous branch at higher altitude. Since these branches are well above the cloud base they would not be observed if the leader did not exit the cloud at the side. A major branch illumination event occurred toward the end of the cloud-to-ground leader stage, when the entire upward branch at 9 km altitude was briefly luminous. These luminosity events will be discussed in Section 5.7.5.

Third, the stepped leader is seen to accelerate as it approaches ground. This could be explained by the leader changing direction (from a direction with a component toward or away from the camera to a more vertical direction), the leader increasing in speed due to the increase in ambient electric field as the leader tip approaches ground, or the increase in channel conductivity due to an increasing current.

Finally, the stepped leader (at altitudes above 5.5 km) shows retrograde illumination during several of the leader steps, as discussed in the next two sections.

5.7.3 Stepped leader at 8 km altitude

The negative stepped leader will now be discussed in detail, as it propagated between 9 and 7 km altitude.

The approximate extent of the leader during a time interval of 30 ms is indicated by the video composite frame of Figure 5.21. The leader had branched into a high-altitude branch, which propagated horizontally and up to 9 km altitude, and the main branch, which followed the cloud boundary for about 1 km downward and to the west (Figure 5.23). VHF sources were located well in both azimuth and elevation by the LMA at this time. The range of the VHF sources was poorly determined but this does not significantly affect the overlay of VHF sources on the video composite frame, since the video camera was located near the center of the LMA.

Figure 5.22 shows log-RF and fast ΔE waveforms along with a VHF spectrogram and a high-speed video streak image for a time interval of 28.8 ms, while the cloud-

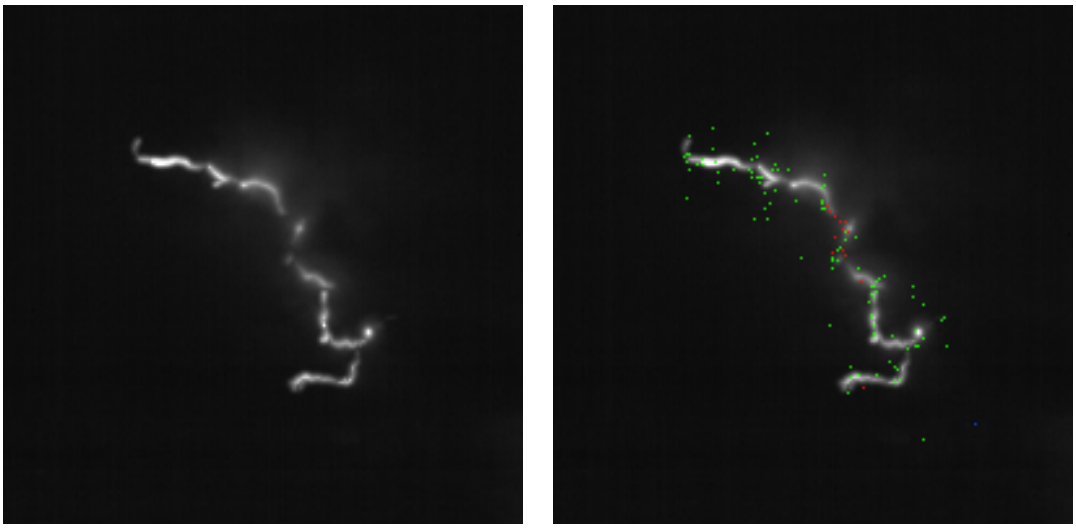

Figure 5.21: Video composite of the leader shortly after it exited the cloud, during the 03:25:57.905–935 time interval of Figure 5.22 and the black dots in Figure 5.23. The image to the right shows the same composite with located VHF sources overlaid (colored by charge). (Compare with Figures 5.7–5.9, which show the full leader channel to ground.)

to-ground leader was propagating between 9 and 7 km altitude. (Figure 5.24 shows the fast ΔE waveform and the streak image separately at a larger scale.)

The fast ΔE pulses at 0.9105 and 0.9186 seconds after 03:25:57 in Figure 5.22 indicate two K-events. They correspond to light pulses in the midlevel negative charge region that were barely detectable in the high-speed video. The second fast ΔE pulse preceded a brightening of the upward branch at 03:25:57.9193, 700 μs after the luminous event, and was coincident with a VHF pulse in the log-RF waveform. The spectrogram also shows VHF emissions during this 700 μs interval, indicating a current surge through the main channel. Also, near this point in time the main leader branched once again (forming the branch in the fourth panel of Figure 5.29). It is unclear whether or not the branching was associated with the current pulse.

The video streak image in Figure 5.24 shows the stepping of the leader well. At 8.5 km altitude, when the main leader branch emerged from the cloud and followed the cloud boundary, eight major light emissions occurred within the 03:25:57.905–915 time interval. The main leader traveled about 2 km during this time (determined from LMA data) at a velocity of 2×10^5 m s^{-1}. If each major light emission resulted from the completion of one leader step, the steps were on the order of 250 m in length at 8.2 km altitude.

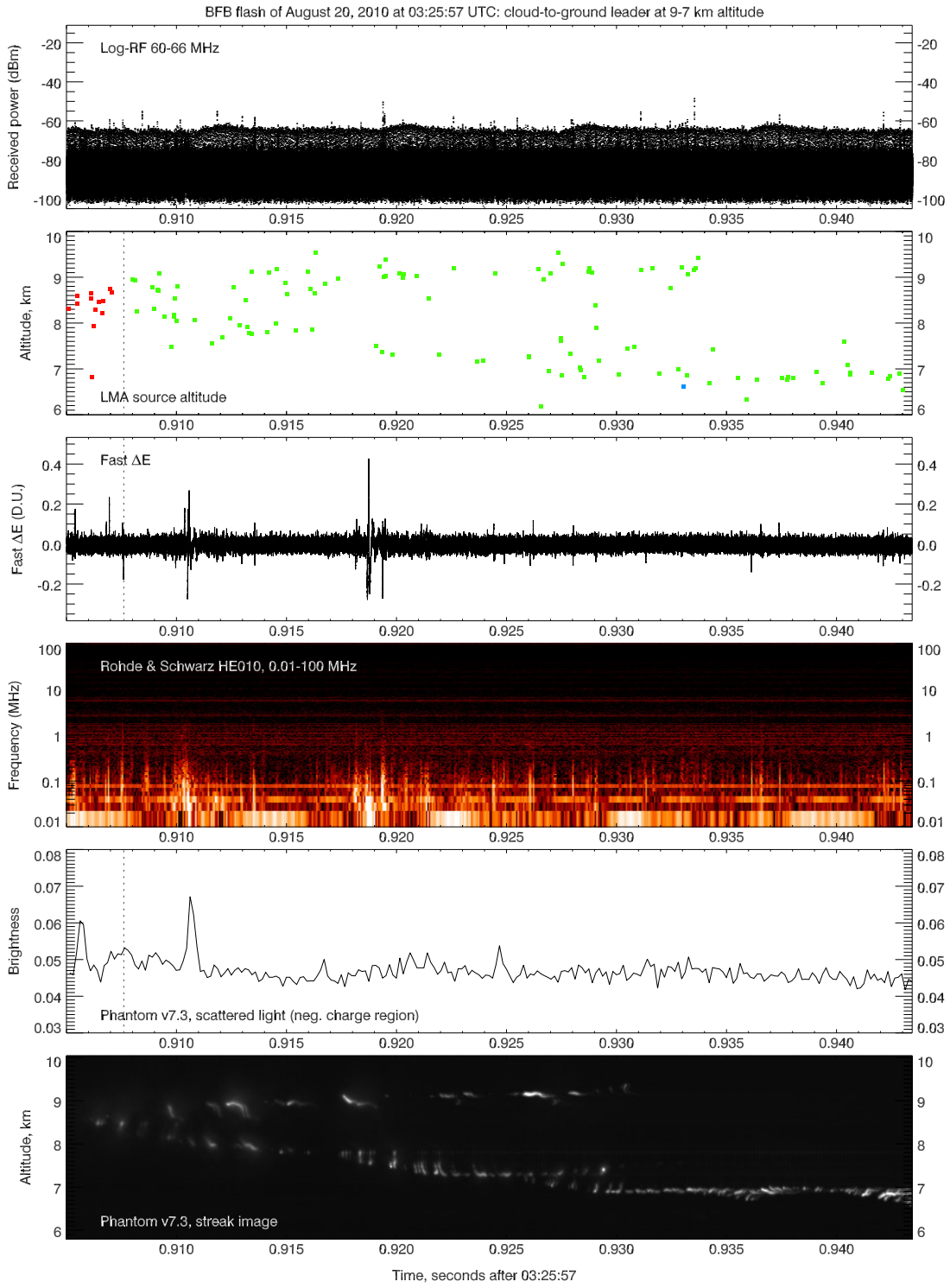

Figure 5.22: Waveforms during the time when the cloud-to-ground leader emerged from the cloud and developed the high-altitude branch. The time interval is 38.4 ms and the time when the leader exited the cloud is indicated by a dotted vertical line. (The fast ΔE waveform and streak image are reproduced at a larger scale in Figure 5.24.)

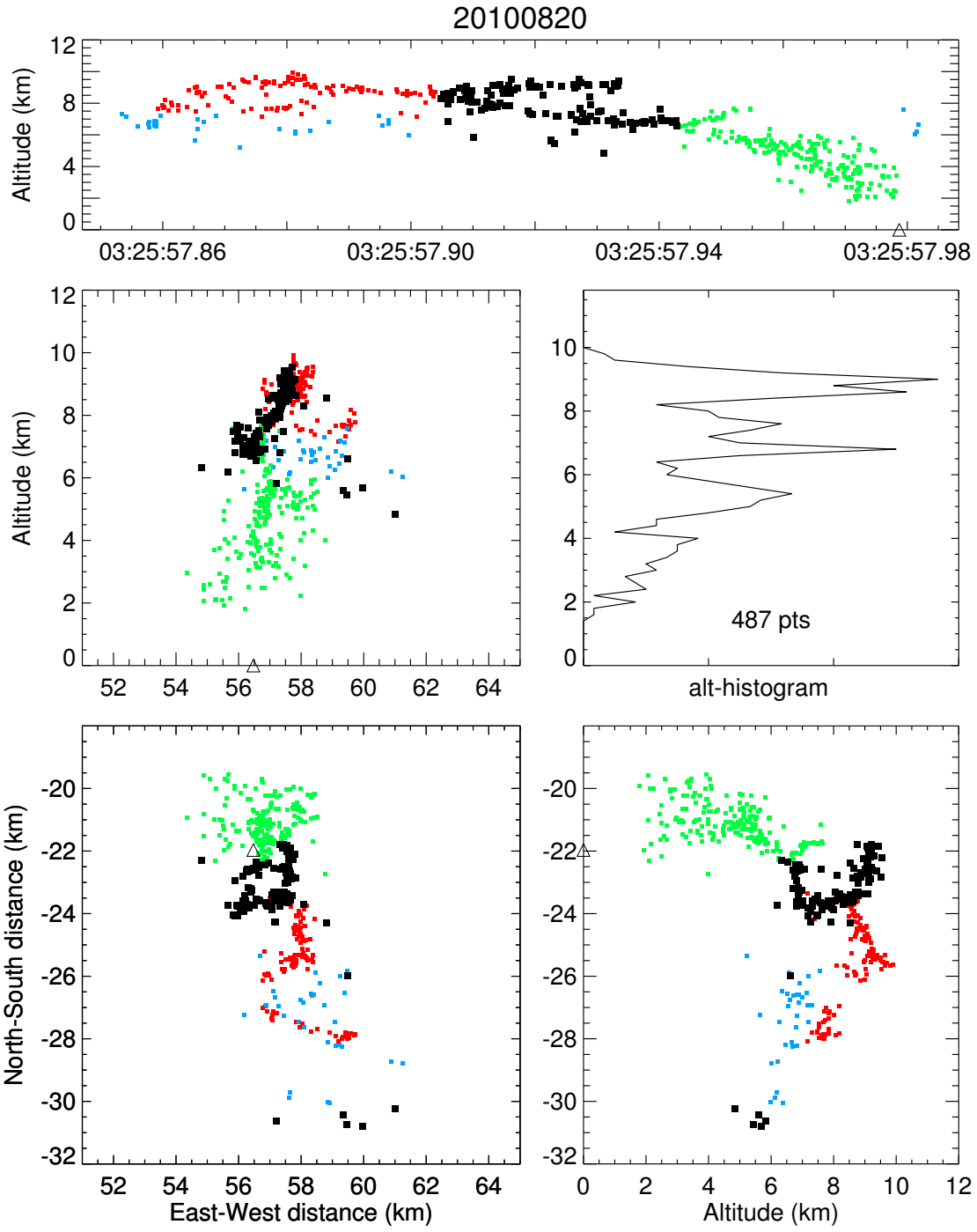

Figure 5.23: VHF sources located by the LMA (colored by charge) during the cloud-to-ground leader stage, with those sources occurring during the time interval of Figure 5.22 highlighted in black.

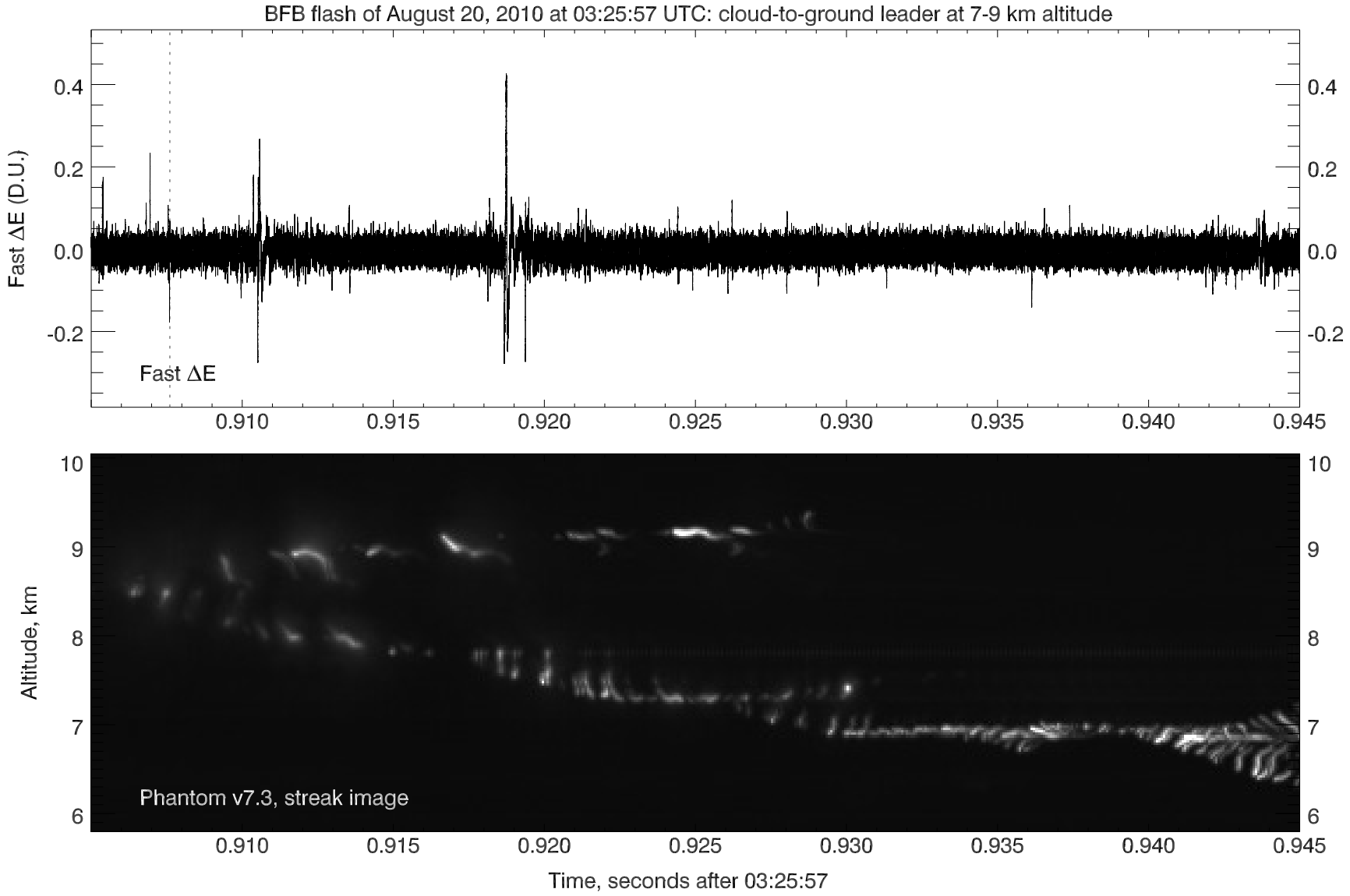

Figure 5.24: The fast ΔE waveform and high-speed video streak image from Figure 5.22 reproduced at a larger scale. The time interval is 40.0 ms.

The high-altitude branch produced (major) light emissions at an even lower rate of 11–12 emissions in 25 ms (during the 03:25:57.905–930 time interval), depending on how the emissions are counted, since they are rather variable in brightness and time in between. During this time interval the branch developed to about 2 km in length. Under the same assumptions as before, the estimated average step length would be $\sim$ 175 m at an average altitude of 9.0 km and a leader velocity of 8×10^4 m s^{-1}. Both estimates of leader step lengths have some uncertainty, because it is assumed that a major light emission is always associated with a single step, and because the length of the channel cannot be determined accurately from LMA data. However, the estimates are comparable to the step length of 200 m that was inferred from Figure 5.1 for a negative leader at 11 km altitude.

By comparing VHF sources located by the LMA with the light emissions visible on video in Figure 5.22, it is clear that the two are not directly correlated. A good comparison cannot really be made from Figure 5.22 because the leader is not propagating vertically and is therefore plotted with a nonzero pixel shift relative to the time reference most of the time. The light emissions are probably not directly related to the source of VHF radiation in negative breakdown itself, but an accompanying phenomenon. However, the VHF sources are mostly located near or at the tips of the leaders.

The light emissions near the leader tips exhibit the interesting effect of retrograde luminosity along the leader channel, starting at or near the tip and extending back along the leader channel for a length of 100 m or more. The video is best seen in animation to fully appreciate this effect, but the video streak image of Figure 5.24 does show this retrograde luminosity in some instances. One good example occurs at 03:25:57.920 when the leader tip is luminous along a length of $\sim$ 100 m, while the next frame shows a luminous segment of $\sim$ 300 m in length, backward along the channel. The next event at 03:25:57.921 also shows the retrograde luminosity, and although it is less bright than the earlier event, it occurs during three video frames of 156.25 μs in duration.

A possible explanation for the retrograde luminosity is that it is the start of a *recoil wave* of positive charge after the completion of a leader step. This phenomenon has been observed by *Winn et al.* [2011], who measured the vector electric field with a balloon-borne instrument close to a negative stepped leader at 9.1 km altitude. They found that recoil waves of positive charge (or, equivalently, a deficit of negative charge) were associated with each leader step and propagated backward along the leader channel, away from the leader tip.

The retrograde luminosity events observed here occur at rather irregular time intervals and with varying brightness on high-speed video. If the luminosity events are directly associated with leader steps, this indicates that the leader steps also occur at an irregular rate. Figure 5.1 suggests that the average step length (at 11 km

altitude) is actually fairly uniform, but that small-scale branches occur during most of the steps. The irregular rate and extent of the luminosity events may thus be explained by the formation of small branches that are generally too small to be resolved on high-speed video in this case. In general, by observation of the high-speed video, it appears that the brighter events are associated with longer path lengths and occur less frequently than the weaker-luminosity events.

The fast ΔE waveform in Figure 5.24 has several small-amplitude pulses that appear to be associated with the luminosity events, but since the instrument is far away from the flash and there are most likely at least three leaders active (two major branches of negative breakdown and at least one branch of positive breakdown), correlating these pulses—or associated VHF pulses from the spectrogram of Figure 5.22—with leader steps seen on video cannot be done with confidence.

5.7.4 Stepped leader at 6 km altitude

When the negative leader had propagated down to 6 km altitude it still exhibited retrograde luminosity events at the leader tips, but the light emissions were becoming gradually more continuous in nature.

Figures 5.26 and 5.27 show a video streak image and correlated waveform data for a time interval of 7 ms during which the cloud-to-ground stepped leader was propagating at 6 km altitude. Figure 5.25 is a composite of all video frames of the stepped leader until the end of the time interval at 03:25:57.958. During the 7 ms of time it traveled a transverse distance of about 500 m at an apparent average velocity of 7.1×10^4 m s^{-1}. The leader still produced retrograde luminosity events at its tip, but remained luminous for most of the time, unlike when it was at higher altitude. The channel luminosity (at 8.1 km altitude) is indicated by the light curve in Figure 5.26 (fourth panel). At 03:25:57.9557 a 1.2 km long segment of leader channel appears luminous, which resulted from a particularly bright luminosity event at the leader tip. The video images indicate that a branch was forming, but the leader tip(s) were about to enter a bank of cumulus cloud, thus being obscured from view.

Several fast ΔE pulses in Figure 5.26 are correlated in time with relatively bright luminosity events at the leader tips. The three fast ΔE pulses at 0.9521, 0.9525 and 0.9528 seconds past 03:25:57 were associated with luminosity events near the main leader tip, of which the third was the brightest both optically and in VHF, and produced the largest-amplitude fast ΔE pulse of the three. Three more fast ΔE pulses occurred at 0.9547, 0.9549 and 0.9551 seconds past 03:25:57 and correlate with two luminosity events of the main leader (first and third pulse) and a solitary luminosity event at the tip of Branch B2 at 7.5 km altitude (the second fast ΔE pulse of the three). The LMA located two VHF sources associated with the luminosity event on Branch B2; these appear shortly before the event on high-speed video

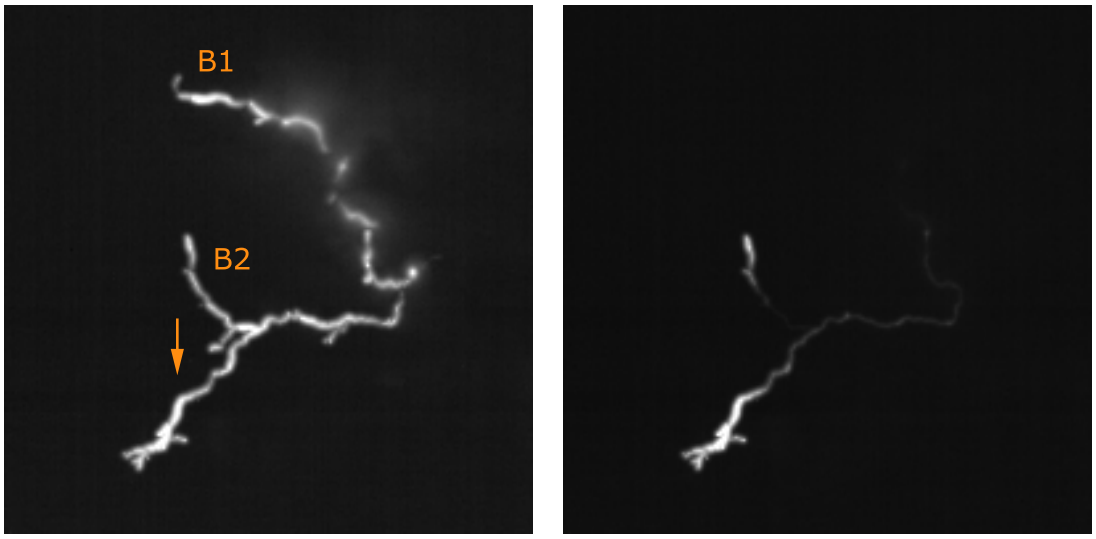

Figure 5.25: Video composite of all frames up to 03:25:57.958 (left) and of the frames during the 7 ms time interval of Figures 5.26 and 5.27 (right). The arrow indicates the pixel column that was used as time reference in the streak images. B1 indicates the first (high-altitude) branch that formed, followed by branch B2 at lower altitude.

but the tip of Branch B2 was slightly offset to the right of the time-calibration pixel column (Figure 5.25) and the video frame is only displayed at the end of the 156.25 μs exposure time interval. In general, the various VHF sources located by the LMA during the time interval of 7 ms do correlate somewhat with the brighter optical emissions from the leader tips, but not convincingly so.

Several more retrograde luminosity events follow in the last 3 ms of the time interval, some of which make the leader channel luminous over a length of 1 km or longer. These channel illumination events are also seen to retrograde upward along the channel, taking 2–3 video frames to travel a distance of $\sim$ 1 km, or at an apparent velocity of $\sim 2.5 \times 10^6$ m s^{-1}.

From the video data it appears that the leader tip is stepping at a rate of once per video frame or perhaps once every other frame and only some of the steps produce bright leader illumination events. With an average leader velocity of 1.0×10^5 m s^{-1} as a nominal value and a frame interval time of 156.25 μs, the leader steps would be on the order of 15 m in length if one step occurs during each frame, or 30 m in length if one step occurs every other frame (assuming only one leader tip is active). These estimates are significantly shorter than the estimated step lengths of 150–250 m at 9–11 km altitude.

Toward the end of the time interval of Figure 5.27 the leader is at 5.5 km altitude and the VHF sources located by the LMA suffer from increasingly larger altitude

inaccuracies, due to the sources being closer to the plane of the array and the flash being distant. Also, the leader starts producing numerous branches at this point with multiple active leaders, which are harder for the LMA to resolve.

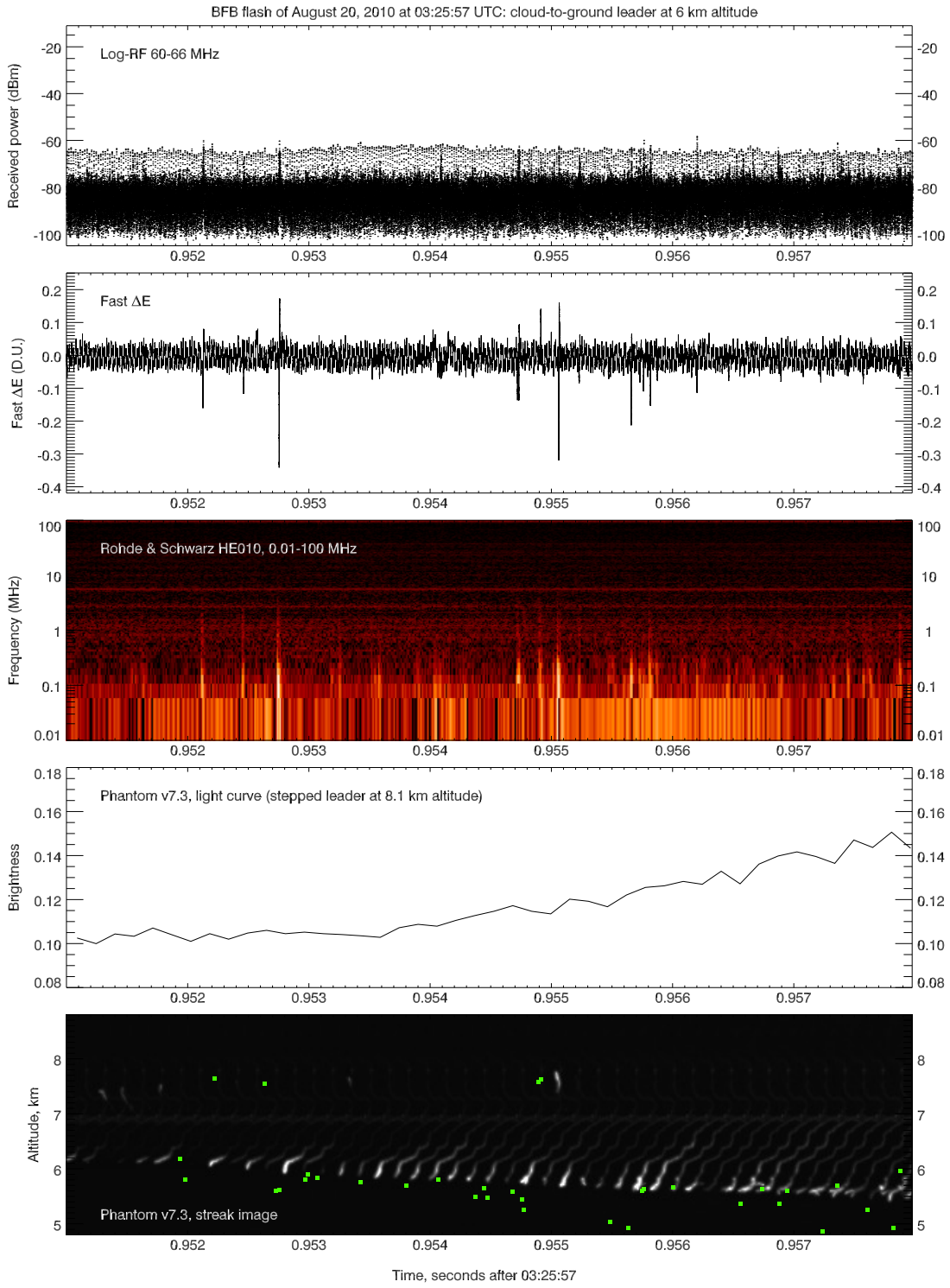

Figure 5.26: Waveforms for a time interval of 7 ms while the cloud-to-ground leader propagated at 6 km altitude. The fast ΔE pulses (second panel) correlate with VHF pulses in the spectrogram (third panel) and luminosity events near the leader tips (fifth panel). The scattered-light curve of the negative charge region is not shown since it does not show any cloud illumination events. The streak image has VHF sources overlaid (colored by charge).

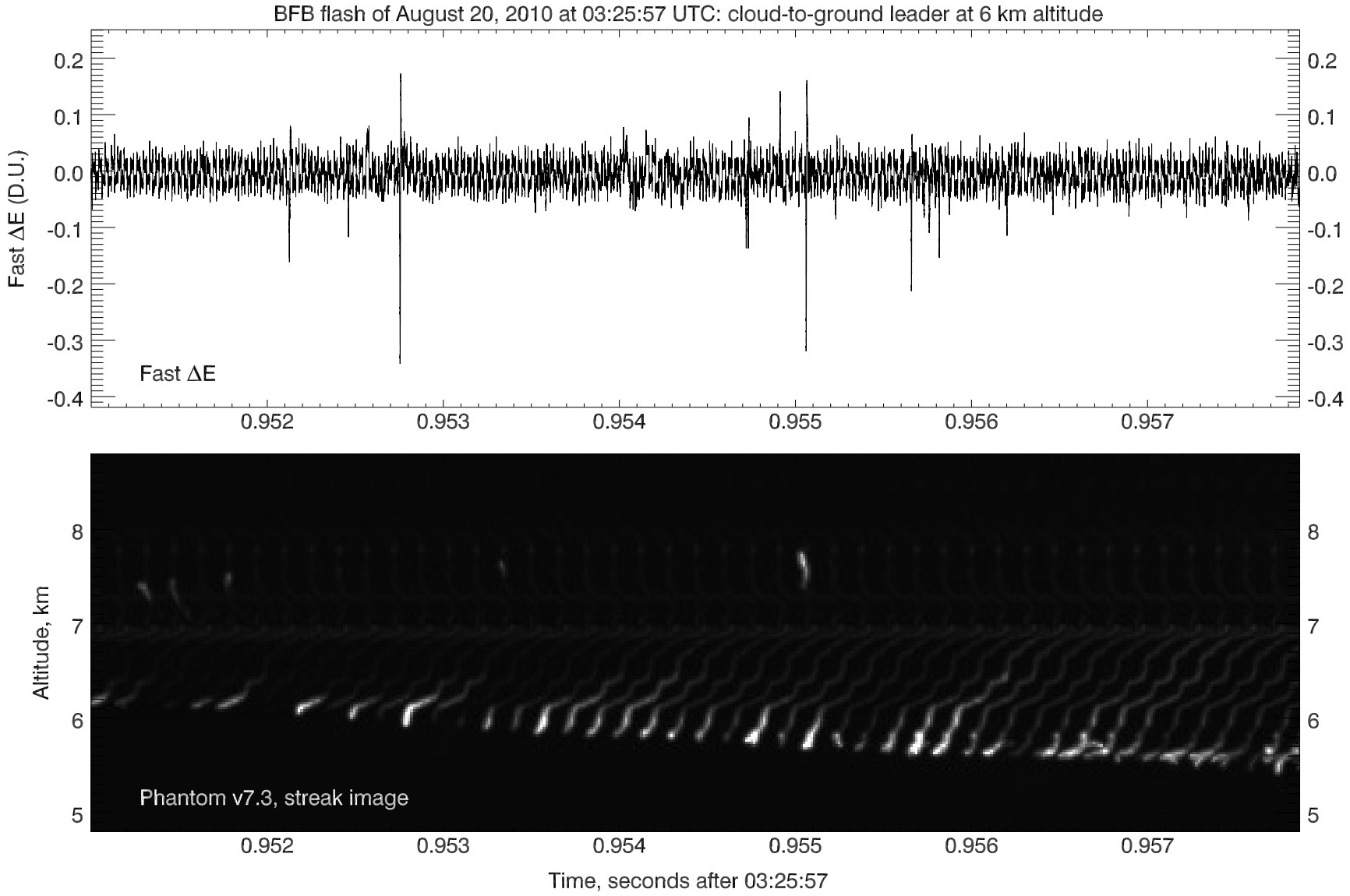

Figure 5.27: The fast ΔE waveform and high-speed video streak image of Figure 5.26 reproduced at a larger scale. The time interval is 6.9 ms.

5.7.5 Step increase in channel luminosity

As the stepped leader propagated to lower altitude, the leader channel as a whole becames more luminous. This effect is seen in most if not all high-speed video recordings; also in those of regular –CG flashes. A possible explanation is that the current in the leader channel is increasing because the number of branches—and thus the number of active leader tips—is increasing as the leader propagates to lower altitude. Additionally, the stepped leader becomes faster as it approaches ground, requiring a higher current. Interestingly, superimposed on the gradual increase in luminosity of the leader channel are several step changes in luminosity, which will be studied now.

Figure 5.28 shows a high-speed video streak image along with the fast ΔE waveform and two channel luminosity curves of the main leader channel: one for the leader at 9 km altitude (near the cloud exit location), and the other for the leader at 6 km altitude.

The smooth appearance of both luminosity curves indicates that the step changes in luminosity of the leader channel are a physical phenomenon and not caused by discretization in the A/D conversion of the pixel values. Four such step changes in luminosity occur during the final 20 ms of the leader propagation to ground. In each case the step change is accompanied by the illumination of a branch at medium to high altitude (i.e. well above the cloud base); the video frames with the luminous branches are reproduced in Figure 5.29. The times of the events and the altitude and estimated lengths of the branches are listed in Table 5.2.

Event time (UTC)	Alt. (km)	Min. length (m)	Change (%)
03:25:57.9679	6.84	480	+16
03:25:57.9706	6.95	240	+8
03:25:57.9731	8.58	2110	+23
03:25:57.9757	7.27	430	+20

Table 5.2: Current surges from four branches as determined from high-speed video imagery. The table lists the altitude of the junction point of each branch with the main channel, a lower-bound estimate of the length of the branch (i.e. not taking into account the unknown extent of the branch toward or away from the camera), and the relative increase in luminosity of the main leader.

Interestingly, only the segment of the main channel that is *below* the subject branch exhibits the step change in luminosity; the leader channel above the branches appears unchanged. This is true for at least three of the four luminosity events; it could not be determined for the third event that was associated with the high-altitude branch, because that branch originated from the leader while it was still in the cloud, or

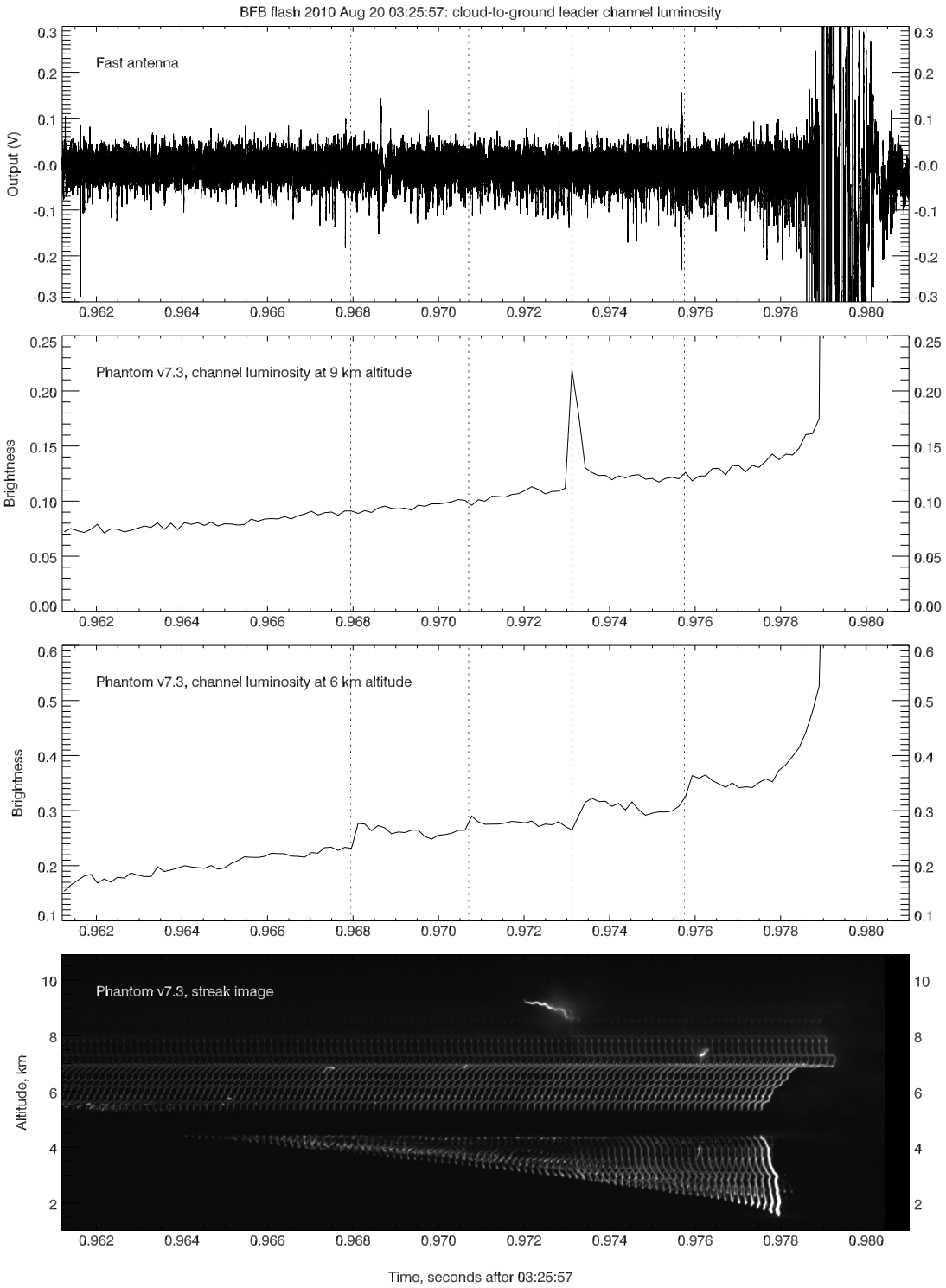

Figure 5.28: Fast ΔE waveform, light curves, and streak image during a time interval of 19 ms while the stepped leader was approaching ground. The light curves are of the leader at 9 km altitude (second panel) and the leader at 6 km altitude (third panel). The vertical dotted lines indicate the approximate times of the luminosity changes. The video streak image is calibrated in time by using the cloud exit point as time reference.

barely outside it, and no section of main leader channel above that junction point was visible. Also, the bright luminosity pulse of the main channel for the third event (Figure 5.28, second panel) was likely due to scattered light from the nearby branch.

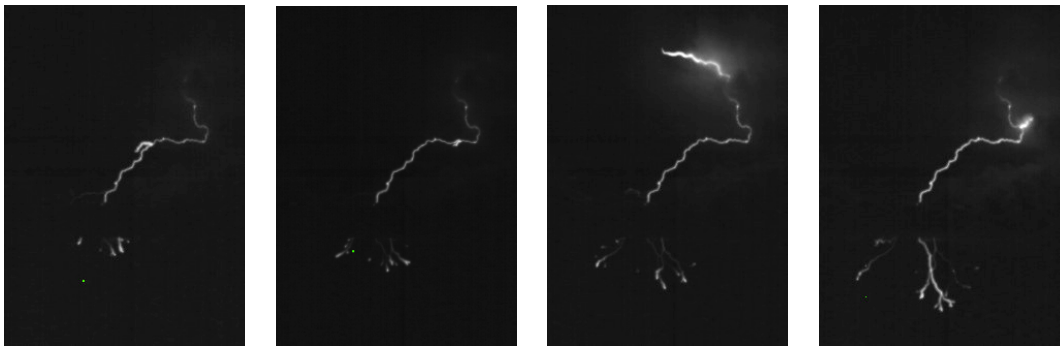

Figure 5.29: Video frames with luminous branches, in chronological order from left to right (compare Table 5.2). VHF sources that occurred during each frame exposure time are overlaid. Note the difference in channel luminosity below and above each branch junction point for the first, second and fourth events.

The step changes in luminosity and the fact that only the part of the main leader channel below the branch junction point responds with an increase in luminosity suggest that there are no in-cloud breakdown processes responsible for the enhancements, but that the channel luminosity enhancement is a direct consequence of the branch luminosity event.

The proposed explanation for this phenomenon is as follows. First, the stepped leader channel becomes more conductive by heating due to the continual transfer of negative charge toward the various leader tips. This is inferred from high-speed video by a general increase in leader luminosity as the leader propagates to lower altitude (and an increase in current as inferred from ΔE waveforms of other BFB flashes). Second, the high-altitude branches have stopped developing and are thus defunct as far as the main leader is concerned, but negative charge is still distributed along their length. As the main cloud-to-ground leader continues to propagate, the electric potential of the main leader channel at the branch junction point is at first highly negative, but decreases in magnitude as the main leader develops downward, away from the junction point. As the main leader channel becomes longer, the potential difference between the branch junction point and the active leader tips increases; in other words, the potential of the main channel at the base of the branch becomes more neutral. Negative charge along the inactive branch might then be expected to flow back into the main channel but is initially prevented from doing so, probably due to resistivity in the branch (from cooling). However, if the electric potential of the main channel drops sufficiently, the charge may surge back into the main channel

and flow down toward the active leader tips. This would temporarily increase the negative downward current in the main channel and heat it.

Some downward motion of channel luminosity can be discerned in the high-speed video, but the frame rate is too low to accurately resolve the velocity of the current surges. It takes at most two video frames of 156.25 μs duration for the luminosity wave to travel a distance of ~ 5 km along the leader channel, indicating a minimum velocity of $\sim 1.5 \times 10^7$ m s^{-1}.

There appear to be multiple branch discharge events during the cloud-to-ground leader stage, but the four major events are observed toward the later stage of the stepped leader.

For some of the events the fast ΔE waveform in Figure 5.28 does show a fast ΔE pulse indicating negative charge moving downward, but the pulses have small amplitudes and are unreliable due to the background noise in the waveform.

These luminosity surges from branch discharges before the return stroke would be less likely to occur in regular –CG flashes, because these flashes generally have channels of shorter length. The cloud-to-ground leader of a BFB flash can be very extensive since it travels via the upper positive charge region, with a correspondingly larger potential drop along the full length of the channel.

5.8 Final stage

After the return stroke positive breakdown in the midlevel negative charge region continued, as is evident from a number of VHF sources located by the LMA (Figure 5.4). This positive breakdown propagated in a general easterly direction near 6 km altitude and in at least three branches.

The first attempted dart leader occurred at 03:25:58.067 UTC, 88 ms after the onset of the return stroke and 362 ms after the initiation of the flash. The first high-speed video frame that shows a light pulse in the cloud (near the cloud base) was completed at 03:25:58.066718. This frame and the 11 frames that succeed it are reproduced in Figure 5.30. The dart leader stopped halfway down to ground somewhere within or near the bank of cumulus clouds at 5 km altitude. While the dart leader propagated it became less bright and also appeared to slow down; a single VHF source was located by the LMA near the tip of the dart leader at the time when the dart leader stopped. Three earlier VHF sources were located while the dart leader was at higher altitude (Figure 5.32). VHF emissions from the leader were bright (Figure 5.33, log-RF waveform and spectrogram).

Figure 5.30: Twelve successive high-speed video frames of the first attempted dart leader. Each frame represents 156.25 μs of time with an exposure time of 150.00 μs. Note the dart-stepped leader along the high-altitude branch.

From high-speed video the minimum velocity of the dart leader was estimated to be 6.7×10^6 m s^{-1} while it was at 8 km altitude, slowing down to 3.0×10^6 m s^{-1} at 6 km altitude, shortly before disappearing in a cloud and stopping. The full length of the channel followed by the dart leader was on the order of 18 km, measured from the extreme end of the positive breakdown back to the initiation point of the flash, up to the positive charge region, northward out the side of the cloud and finally halfway down to ground.

The first attempted dart leader (Figure 5.33) also reionized the high-altitude upward branch and continued out along it as a slow dart-stepped leader. Four frames of the high-speed video show this, starting with the eighth frame in Figure 5.30 as a luminous section of channel 1 km in length. The next three frames show a short luminous segment, $\sim$ 250 m in length, propagating out along the branch at a rather slow velocity of 1.6×10^6 m s^{-1}, while the connecting segment is weakly luminous. The slowly propagating tip of the dart leader was also located by the LMA as two VHF sources.

The first attempted dart leader must have left a substantial amount of negative charge distributed along the cloud-to-ground channel, since the second attempted dart leader (initiating at 03:25:58.0749, 8.2 ms after the first attempted dart leader) chose not to follow the same path to ground but only the high-altitude upward branch. This dart leader was fast and the high-speed video only recorded one frame with the branch in clear air luminous along its full extent. The successive locations of light flashes in the cloud leading up to this suggest a minimum velocity of 1.2×10^7 m s^{-1}. It is not surprising that this leader was faster than the first, since the first dart leader had made the channel more conductive by heating it.

Possibly one more dart leader was attempted at 03:25:58.0823, 5.6 ms after the second attempted dart leader had stopped. This is hinted at in LMA data by a single point near 8 km altitude along the upward intracloud channel, close to the initiation point of the flash. About 560 μs after this event a few more VHF sources were located by the LMA from positive breakdown in the midlevel negative charge region, after which VHF activity ceased and the flash ended.

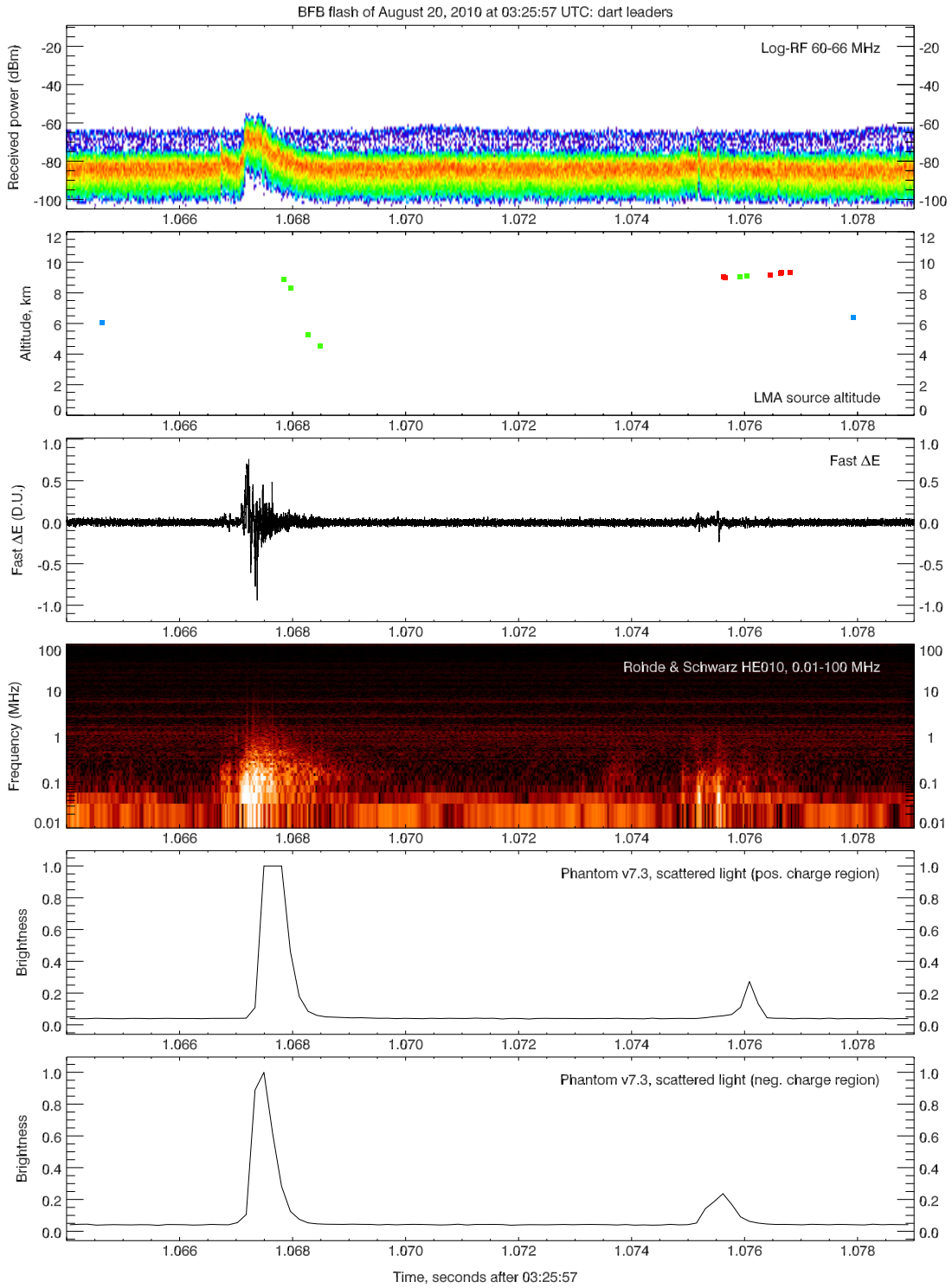

Figure 5.31: Waveform data of two attempted dart leaders. The scattered-light curve for the positive charge region was derived from a pixel coordinate close to the cloud exit location of the negative leader near 9.0 km altitude; the curve for the negative charge region represents 6.4 km altitude.

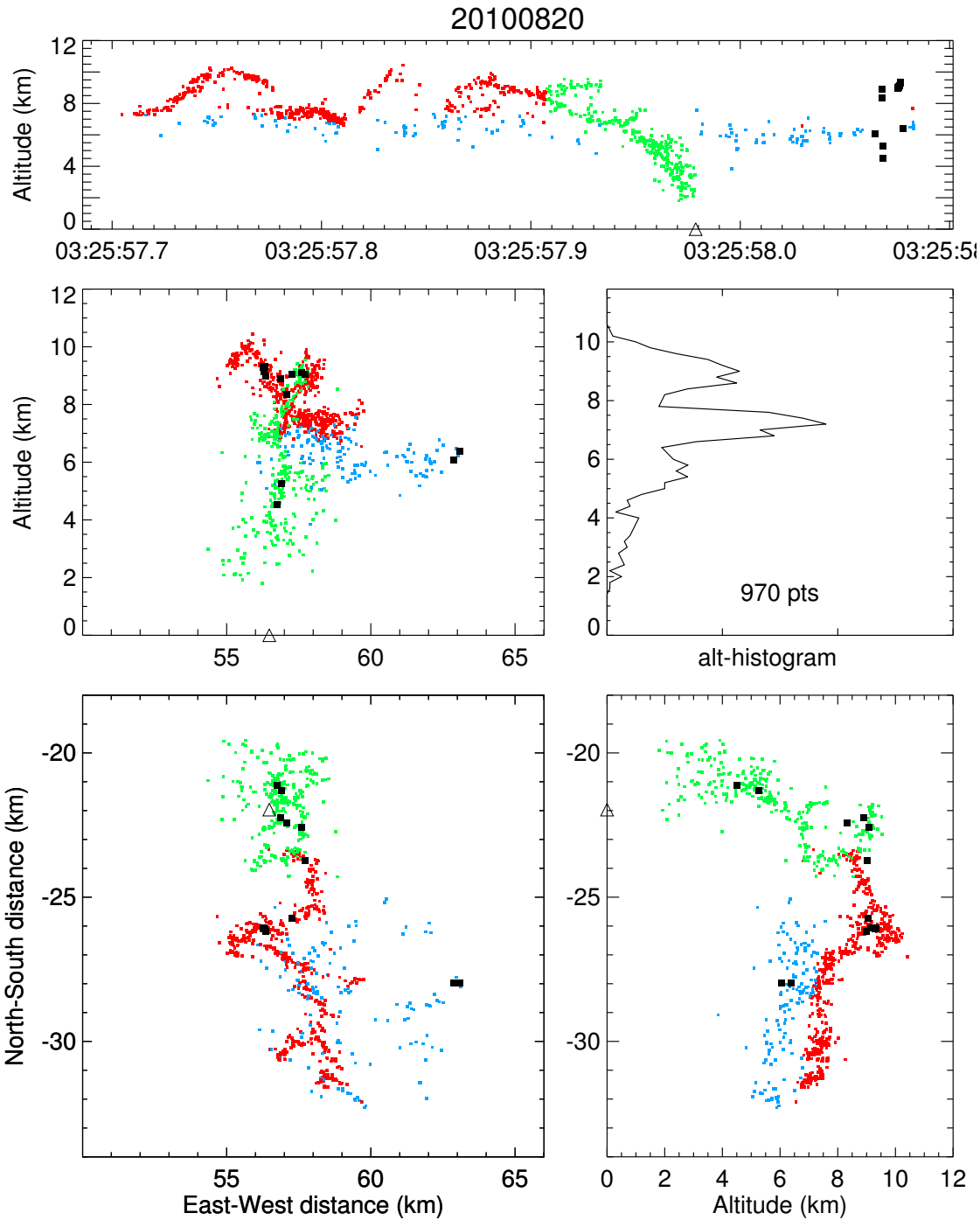

Figure 5.32: Mapped VHF sources of the full BFB flash (colored by charge) with the VHF sources associated with the two attempted dart leaders (Figure 5.31) highlighted in black.

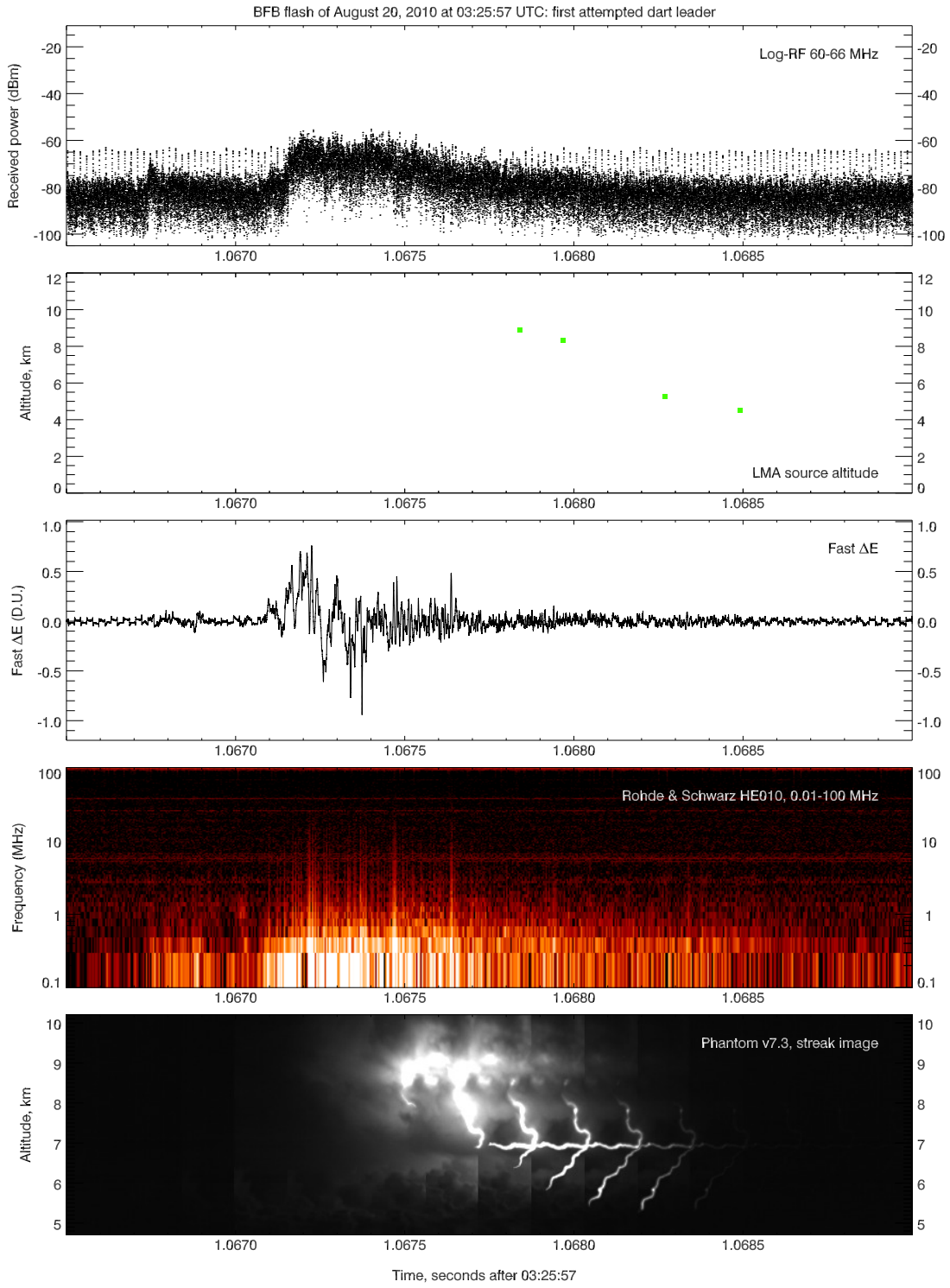

Figure 5.33: Waveform data for a time interval of 2.5 ms during the first attempted dart leader. The initial stage of the dart leader is quite active in VHF while the leader is traveling from the negative to the positive charge region; VHF emissions are much weaker during the later stage while the dart leader is outside the cloud.

5.9 Summary

In this chapter a BFB flash was studied by correlating broadband waveform, LMA and high-speed video data. Although the flash occurred at a relatively large distance from the laboratory, a number of interesting observations could be made, particularly from high-speed video.

5.9.1 Summary of BFB flash

The flash was a Type-II BFB flash of 382 ms duration that occurred in a normal-polarity storm. It initiated at 7.3 km altitude with a single upward negative leader that propagated upward to 10 km altitude. The leader initially propagated more or less horizontally for 500 m at a velocity of 8.0×10^4 m s^{-1} before heading upward. As soon as the leader changed direction from horizontal to vertical, a series of K-events occurred. These K-events may have been induced by the leader effectively shorting out an increasing potential difference between the midlevel negative and upper positive charge regions when it started propagating upward. The negative breakdown was somewhat intermittent, similar to that of the BFB flash studied in Chapter 4.

After the initial upward negative leader stopped, a number of subsequent negative breakdown events occurred along the upward channel, as well as horizontally away from the initiation region. The leader of the third negative breakdown event propagated at 2.0×10^5 m s^{-1}, faster than the initial upward negative leader. It was helped along by a series of faster K-leaders that each propagated a little further along the upward channel and produced brief negative breakdown at their point of termination.

The fourth negative breakdown event was faster than the third, at 2.5×10^6 m s^{-1}, and stopped just beyond the later branching point of the cloud-to-ground leader along the upward channel. The fifth negative breakdown event, which became the cloud-to-ground leader, may therefore have branched off the main channel because of residual negative charge from the earlier leader.

The cloud-to-ground leader exited the cloud at 9 km altitude. (Most of the eight BFB flashes observed in the storm exited the cloud near that location.) It produced two branches at medium to high altitude (7–9 km) outside the cloud.

The tip of the cloud-to-ground leader produced intermittent luminosity pulses while it was at high altitude; as it propagated to lower altitude the light emissions became more continuous. This correlates well with the transition from impulsive to apparently continuous VHF emissions discussed earlier in this work.

As the cloud-to-ground leader approached ground, the channel produced a number of branches and became more luminous.

After the return stroke two or perhaps three dart leaders were attempted, none of which succeeded in reaching ground. The first attempted dart leader followed the main channel to ground (as well as a high-altitude branch), but stopped near 5 km altitude. The second dart leader only followed the high-altitude branch, probably avoiding the cloud-to-ground channel due to the negative charge left in it by the first attempted dart leader.

5.9.2 Retrograde luminosity waves at leader tips

The leader stepping process at medium to high altitude (between 6 and 10 km) produces luminous events that appear to propagate backward along the leader channel, away from the leader tip. Most of these luminosity waves were visible over distances of 100–300 m, with a few instances of up to 1.2 km in length. The longer luminosity waves appeared to propagate away from the leader tip at a minimum speed of 2.5×10^6 m s^{-1} when the leader was at 6 km altitude. It is likely that these luminosity waves are associated with positive recoil waves away from the tip of a negative leader as reported by *Winn et al.* [2011].

5.9.3 Branch discharges

The cloud-to-ground leader developed two major branches above 6 km altitude and numerous branches at low altitude. As the leader approached ground the channel gradually became more luminous, with four step changes in luminosity superimposed on the gradual increase in luminosity. These step changes were in each case associated with a *branch discharge*: a branch of the negative leader at medium to high altitude (6–9 km) that had become inactive was suddenly discharged and the negative charge from the branch propagated down toward the leader tip, heating the channel and making it more luminous. These branch discharges are explained by a drop in the electric potential of the main channel at the branch junction point as the leader continues to propagate away from it. This eventually causes a discharge of the negative charge from the branch into the main leader channel. The velocities of the ensuing luminosity waves down along the main channel were estimated to be 1–2$\times 10^7$ m s^{-1}.

5.9.4 Streamer-to-leader transition

A photograph was obtained of a negative leader in clear air at 11 km altitude (Figure 5.1). The leader had visible streamers along the channel, appearing as clusters of up to eight or more streamers that were spaced at regular intervals along the channel. Each interval was on the order of 200 m in length; the streamers were on the order of 50–100 m in length, forming *streamer zones* of 100–200 m in diameter. Each streamer zone is associated with a single leader step.

The same photograph also shows a "space stem": an unconnected leader segment that appears to show the streamer-to-leader transition in progress. The center of the space stem is about 100 m distant from the leader and connects to it with a diffuse, narrowly collimated blue streamer that would be of positive polarity. The other end of the space stem shows negative streamers that are more defined in appearance. These space stems have been reported in laboratory spark studies of negative leaders [e.g. *Gorin et al.*, 1976] and apparently also occur during the stepping process of natural lightning.

Two high-resolution photographs of negative leaders of BFB flashes (discussed in Section C.2) at 3 km altitude also show short unconnected branches, which are believed to be the same phenomenon.

5.9.5 Leader step length

The length of negative leader steps was estimated from high-speed video as well as from a photograph of a high-altitude leader. From the photograph a step length of $\sim$ 200 m was inferred for a leader in clear air at 11 km altitude. From high-speed video in conjunction with LMA data a minimum step length of 140 m was inferred for a leader at 8.9 km altitude (ignoring channel tortuosity) while a step length on the order of 250 m was estimated for a leader at 8.2 km altitude. In summary, an estimate for the step length of a negative leader between 8–11 km altitude is about 200 m.

At an altitude of 6 km the leader step length appeared to be $\sim$ 15–30 m or shorter in length, although this could not be accurately determined and is only an estimate based on the assumption that each step produces a detectable luminous event, and that there was only one leader active at that time. At altitudes below 4 km leader step lengths could not be estimated for the BFB flash studied, due to the limited spatial resolution of the video images. However, from photographs of two BFB flashes on July 24, 2010 (Section C.2), a step length on the order of 16 m was inferred for a negative leader at 3 km altitude. Typical values for negative leader step lengths reported in the literature are on the order of 50 m or less [e.g. *Berger and Vogelsanger*, 1966; *Rakov and Uman*, 2002, pp. 7 and 131].

5.9.6 Transition from impulsive to continuous breakdown

The main, most important result from these studies is the cause of the transition from impulsive to more continuous breakdown that occurs in a BFB flash as the cloud-to-ground leader propagates from an altitude of 8–9 km down to ground. This distance is similar to one scale height of atmospheric pressure. A negative leader at high altitude does not appear to travel at a different velocity than at low altitude, but the leader steps are longer at high altitude and therefore occur at a lower rate. It is suggested that the longer, more intermittent leader stepping is mainly responsible for the intermittent VHF emissions observed in high-altitude leaders.

An additional explanation for the apparently continuous VHF emissions of low-altitude leaders is that they tend to be more branched, with multiple leader tips active concurrently, while high-altitude leaders tend to produce only few branches.

The branching itself may simply be a stochastic process: If a leader has a certain probability of producing two viable branches during every leader step, more steps per unit length mean a larger number of branches produced on average per unit length. Since the leader steps appear to be longer at high altitude than at low altitude, fewer branches per unit length would be expected to occur at high altitude.

6. Other flashes of interest

6.1 Introduction

A total of eight BFB flashes are briefly discussed in this chapter, using correlated waveform and LMA data. These flashes are shown here to illustrate some interesting characteristics and to discuss their various features using the findings from the preceding chapters.

6.2 BFB flash with multiple strokes to ground

This Type-II BFB flash occurred on July 23, 2010 at 18:45:30 UTC and is a good example of a multi-stroke BFB flash. It lasted 504 ms and produced three strokes to ground. Figure 6.1 shows waveform data for the flash. The storm was normal-polarity with upper positive charge over midlevel negative charge, with the boundary situated near 8.5 km altitude at the location where the flash initiated (Figure 6.3).

The flash initiated about 1 km to the northeast of Langmuir Laboratory (Figure 6.2). Because it was so close to the instruments, well within the reversal distance for intracloud lightning electric field waveforms, the ΔE waveform has the characteristic excursion associated with a close intracloud flash. Initially, a gradual negative change in the ΔE waveform occurs as negative charge is carried upward in the storm, away from the instrument. This is followed by a positive excursion of the electric field as the negative leader propagates to ground, approaching the instrument, after which a negative step change in the electric field occurs due to the return stroke lowering negative charge to ground.

Like the BFB flash of August 2, 2010 studied in Chapter 4, this flash produced a short continuing current during the later return strokes (the second and third) with the longer continuing current during the third stroke. These strokes occurred during extensive positive breakdown in the midlevel negative charge region, extending horizontally for about 9–10 km in a general northward direction at 6–8 km altitude.

The positive breakdown occurred almost exclusively to the north of the flash initiation region while the negative breakdown occurred to the southwest of it, perhaps indicative of wind shear that may have caused vertically displaced charge layers. The atmospheric soundings of Albuquerque on July 24 at 00 UTC show winds generally from the southwest at 5 knots up to 7 km altitude, backing to south at higher altitudes. On the other hand, the El Paso sounding from the same time indicates the opposite, and both soundings were made 5 hours after the flash; hence, not much can be said about the effect of wind shear on the charge configuration in this case.

The upward negative breakdown produced three major branches before the cloud-to-ground leader initiated, all of which went in a general upward direction but of a relatively short length of about 1 km. An animation of the LMA data indicates that the intracloud negative breakdown (colored red in Figure 6.3) occurred first, followed after a short pause by the cloud-to-ground leader. Thus, the cloud-to-ground leader was initiated by a fast K-leader, similarly to the flashes studied in Chapters 4 and 5. By general observation of Figure 6.3, the large extent of the positive breakdown compared to the smaller extent of negative breakdown is remarkable.

The Rohde & Schwarz spectrogram in Figure 6.1 clearly shows the increase in VHF emission rates associated with negative breakdown during the stepped leader to ground. In the log-RF waveform the increase in maximum received power toward the final stage of the stepped leader is on the order of 5–10 dB. This could be due to a decrease in distance between the stepped leader and the instruments. Two to three major branches were resolved by the LMA below 7 km altitude. The two dart leaders are also bright in VHF. (The Sirio spectrogram and the log-RF waveform both suffer from corona discharge in the vicinity of their antennas after the first return stroke.)

The spectrograms and the fast ΔE waveform demonstrate that the final stage of this BFB flash is not at all quiet, with numerous fast ΔE pulses and bursts of VHF emissions occurring during the extensive positive breakdown. Very few VHF sources along the existing path to ground were located by the LMA for the two dart leaders, even though the second dart leader only occurred about 200 ms after the first dart leader.

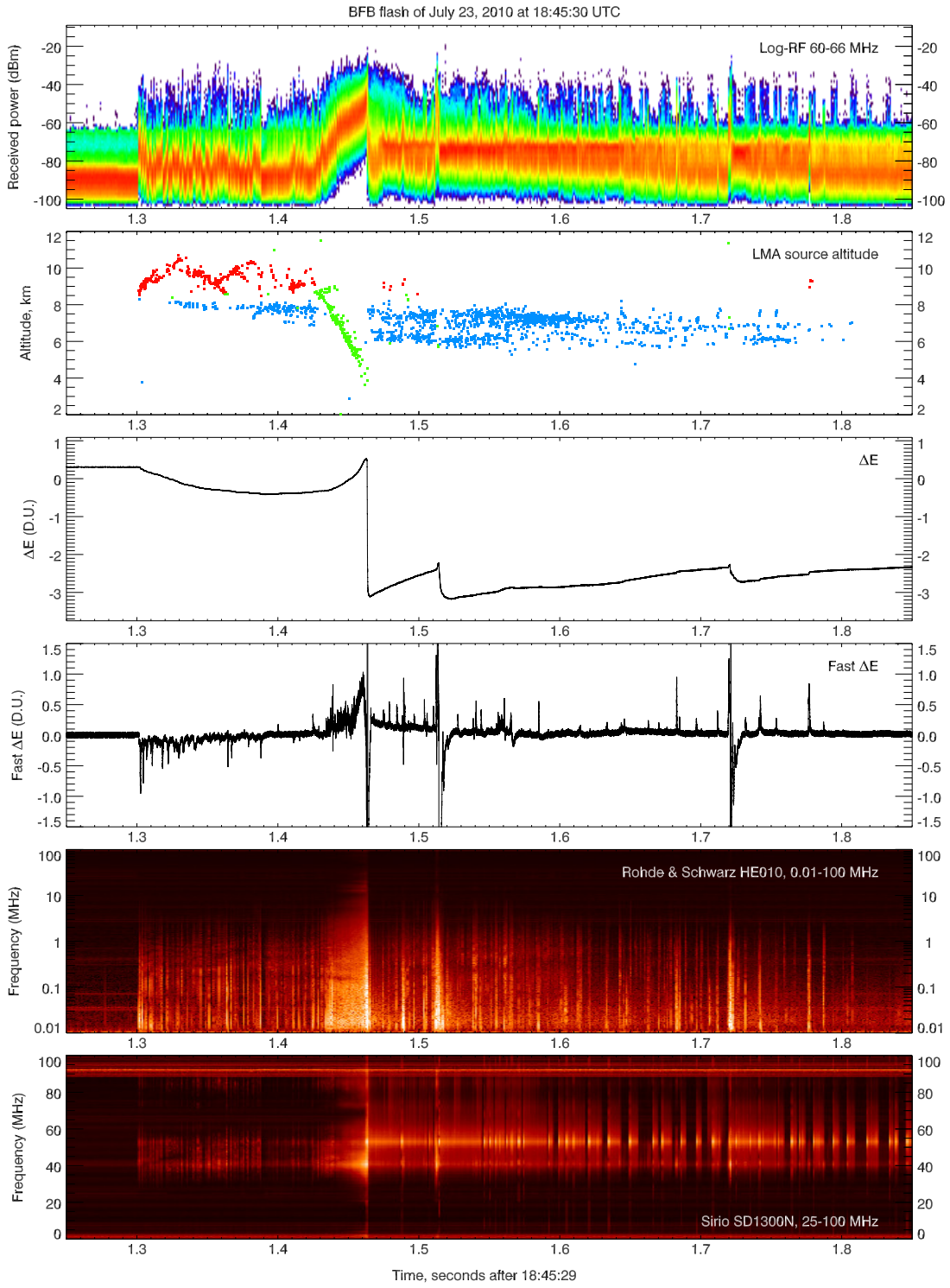

Figure 6.1: Waveforms for the BFB flash of July 23, 2010 at 18:45:30 UTC. The plotted time interval is 600 ms. The log-RF waveform (top panel) and the Sirio spectrogram (bottom panel) are both affected by corona discharge, masking most of the VHF emissions from positive breakdown between the second and third return strokes. VHF sources in the second panel are colored by charge, corresponding with Figure 6.3.

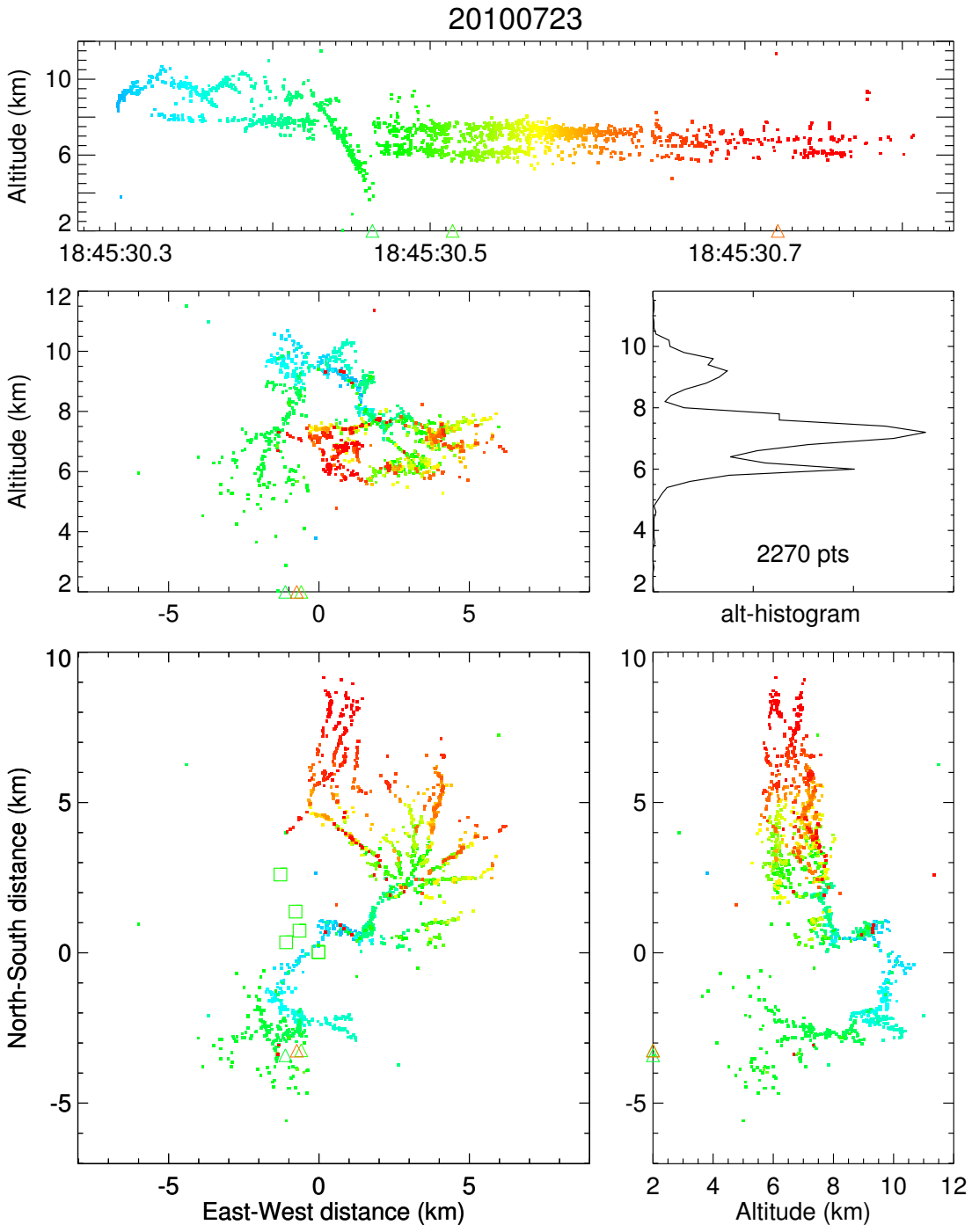

Figure 6.2: VHF sources located by the LMA for the BFB flash of July 23, 2010 at 18:45:30 UTC. The sources are colored by time from blue (indicating earlier in time) to red (later in time). Note the retracing of existing channels by K-leaders in the midlevel negative charge region during ongoing positive breakdown.

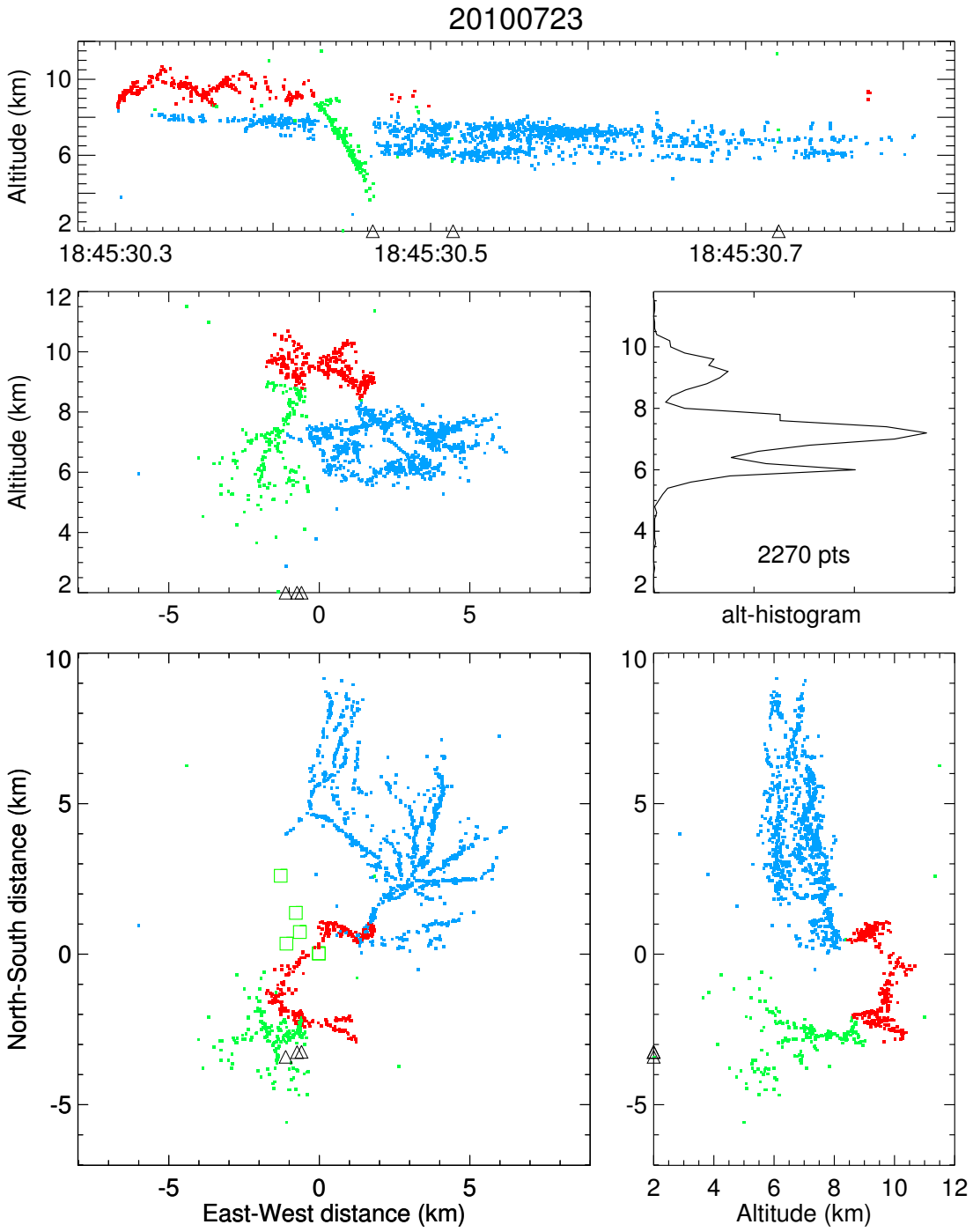

Figure 6.3: VHF sources located by the LMA for the BFB flash of July 23, 2010 at 18:45:30 UTC, colored by charge. Red indicates negative breakdown in positive charge; blue indicates positive breakdown in negative charge. Green VHF sources are associated with negative breakdown propagating through undetermined space charge, and may or may not be outside the cloud.

6.3 BFB flash with long continuing current

This three-stroke BFB flash occurred on July 30, 2010 at 21:28:04 UTC. It initiated 19 km to the north of the laboratory at an altitude of 7 km and lasted 450 ms. It was a Type-II BFB flash that exhibited a relatively long continuing current following the second return stroke (Figure 6.4, ΔE waveform). The field change induced by the continuing current was of at least the same magnitude as the change produced by the first return stroke. The continuing current lasted 200 ms. The first dart leader, which produced the continuing current, occurred about 25 ms after the first return stroke and no VHF sources from the dart leader along the cloud-to-ground channel were located by the LMA.

The storm had a normal-polarity charge configuration (Figure 6.6), with the negative breakdown in the upper positive charge region shifted several kilometers to the south of the midlevel positive breakdown, similar to the BFB flash of Section 6.2. Interestingly, the charge layers appear to be tilted, since the positive breakdown in the midlevel negative charge terminates at an altitude of 8 km at the far northern end of the flash, which is of comparable altitude to the negative breakdown in upper positive charge to the south.

The flash initiated with a large-amplitude fast ΔE pulse of positive polarity, indicating negative charge moving up in altitude (Figure 6.4, fourth panel). The fast ΔE waveform then appeared relatively quiet until the onset of the cloud-to-ground leader. This leader initiated after a short pause in upper negative breakdown, likely started by a K-event along the original channel.

During the continuing-current stage extensive positive breakdown continued along multiple branches in the midlevel negative charge region. A number of VHF sources in upper positive charge were mapped by the LMA during the continuing current stage. These were not located along the branch that connected to ground, but along a short upward branch of about 1 km in length that was situated almost directly over the initiation point of the flash (at an east–west distance of 2.5 km, and north–south distance of 18.0 km in Figure 6.5). These upward K-leaders did not produce a visible field change in the waveforms, but their VHF emission signature can be seen clearly in both spectrograms in Figure 6.4.

At 21:28:05.545 UTC another dart leader occurred. This leader went mostly undetected by the LMA, probably due to the channel to ground still being conductive from the prior continuing current. One single VHF source was located along the channel to ground. Concurrently with this dart leader, a new stepped leader propagated upward in upper positive charge and made a channel of 2 km in length (Figure 6.5). The dart leader appears as a bright burst of VHF emission in both spectrograms, followed by another bright burst about 20 ms later that was not associated with a change in electric field.

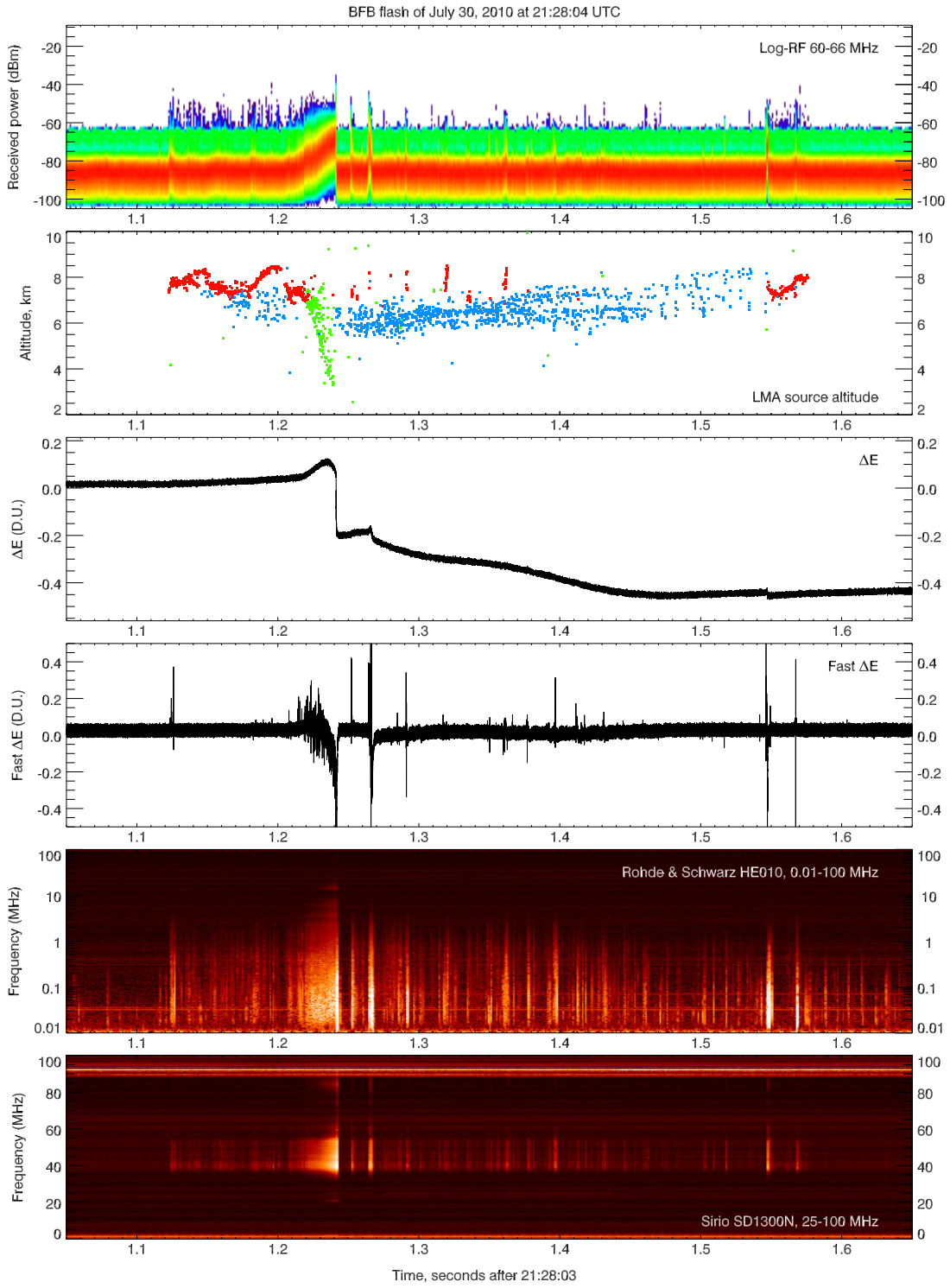

Figure 6.4: Waveforms for the BFB flash of July 30, 2010 at 21:28:04 UTC. The plotted time interval is 700 ms; the flash lasts about 450 ms. The log-RF waveform (top panel) and the Rohde & Schwarz spectrogram (fifth panel) clearly show the characteristic increase in VHF emissions during the cloud-to-ground leader stage. VHF sources in the second panel are colored by charge in correspondence to Figure 6.6.

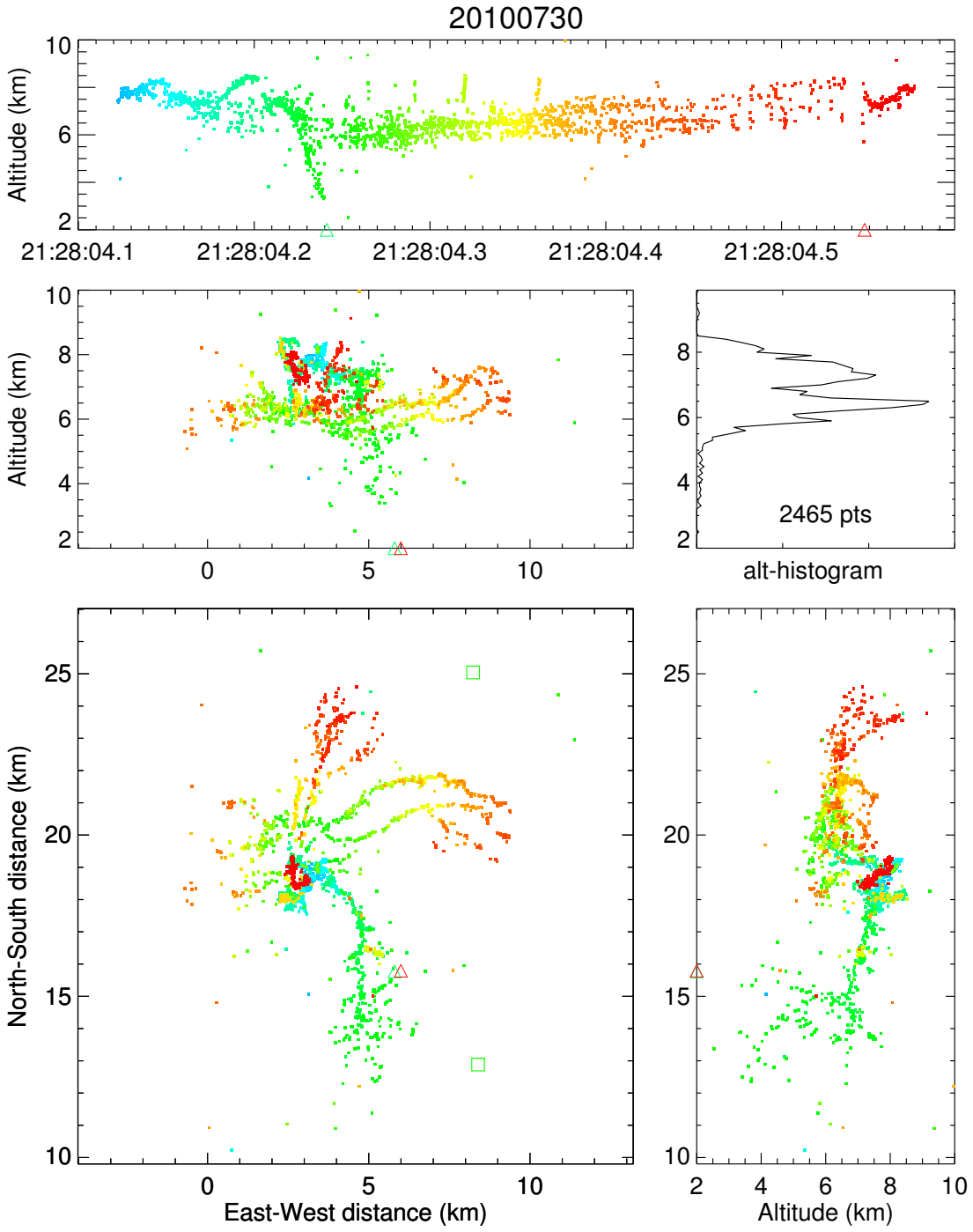

Figure 6.5: VHF sources located by the LMA for the BFB flash of July 30, 2010 at 21:28:04 UTC (colored by time). Note the retracing of existing channels (by K-leaders) in the midlevel negative charge region by positive breakdown later on.

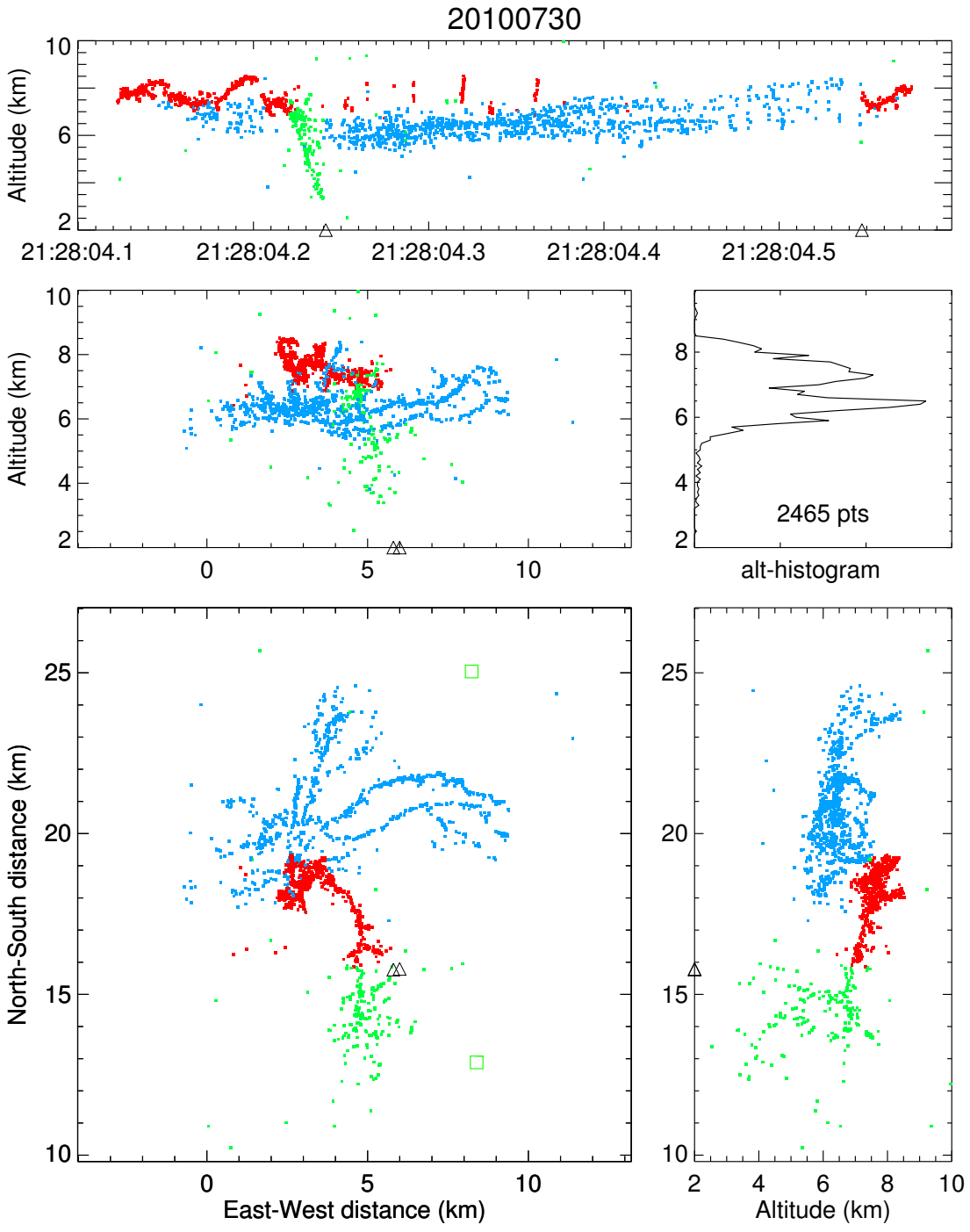

Figure 6.6: VHF sources located by the LMA for the BFB flash of July 30, 2010 at 21:28:04 UTC (colored by charge).

6.4 BFB flash with large horizontal extent

This Type-II BFB flash occurred on August 6, 2010 at 21:00:52 UTC. It initiated 32 km to the SSW of Langmuir Laboratory at an altitude of 8 km. It is discussed here for its remarkably long horizontal extent of over 25 km (Figure 6.8). The cloud-to-ground leader contacted ground well over 10 km south of the initiation region, which itself was displaced several kilometers to the south from most of the positive breakdown. It was of normal polarity with negative breakdown into upper positive charge (Figure 6.9) and lasted 872 ms, which was the longest duration of all 59 BFB flashes discussed in Chapter 3.

This flash and the two flashes discussed in Sections 6.2 and 6.3 have very similar general appearances, with negative breakdown in upper positive charge displaced to the south of positive breakdown in midlevel negative charge, and the cloud-to-ground leader developing to the south as well. Their resemblance is particularly striking considering that these three flashes occurred in different storms, which occurred a week after one another.

Like the BFB flash in Section 6.3, the flash started with a single large-amplitude fast ΔE pulse (Figure 6.7, fourth panel) that was followed by numerous smaller pulses as the negative breakdown continued to develop. The upward negative breakdown initially took a path that was different from the later cloud-to-ground branch, by first developing the main northwest branch at 8–9 km altitude (Figure 6.8). The cloud-to-ground leader later branched off and propagated toward the south.

The flash produced four strokes to ground and at least five attempted dart leaders (K-leaders) that were launched from the midlevel positive breakdown upward through the upper positive charge and toward the cloud-to-ground channel (Figure 6.7, second panel). These attempted leaders were mapped quite well by the LMA (and can also be seen clearly in the spectrograms), unlike the successful dart leaders that were hardly mapped at all, likely because they were fast and propagated along a conductive channel. Similar to the BFB flashes discussed in Chapter 4 and Section 6.2, the later return strokes exhibited increasingly longer continuing currents.

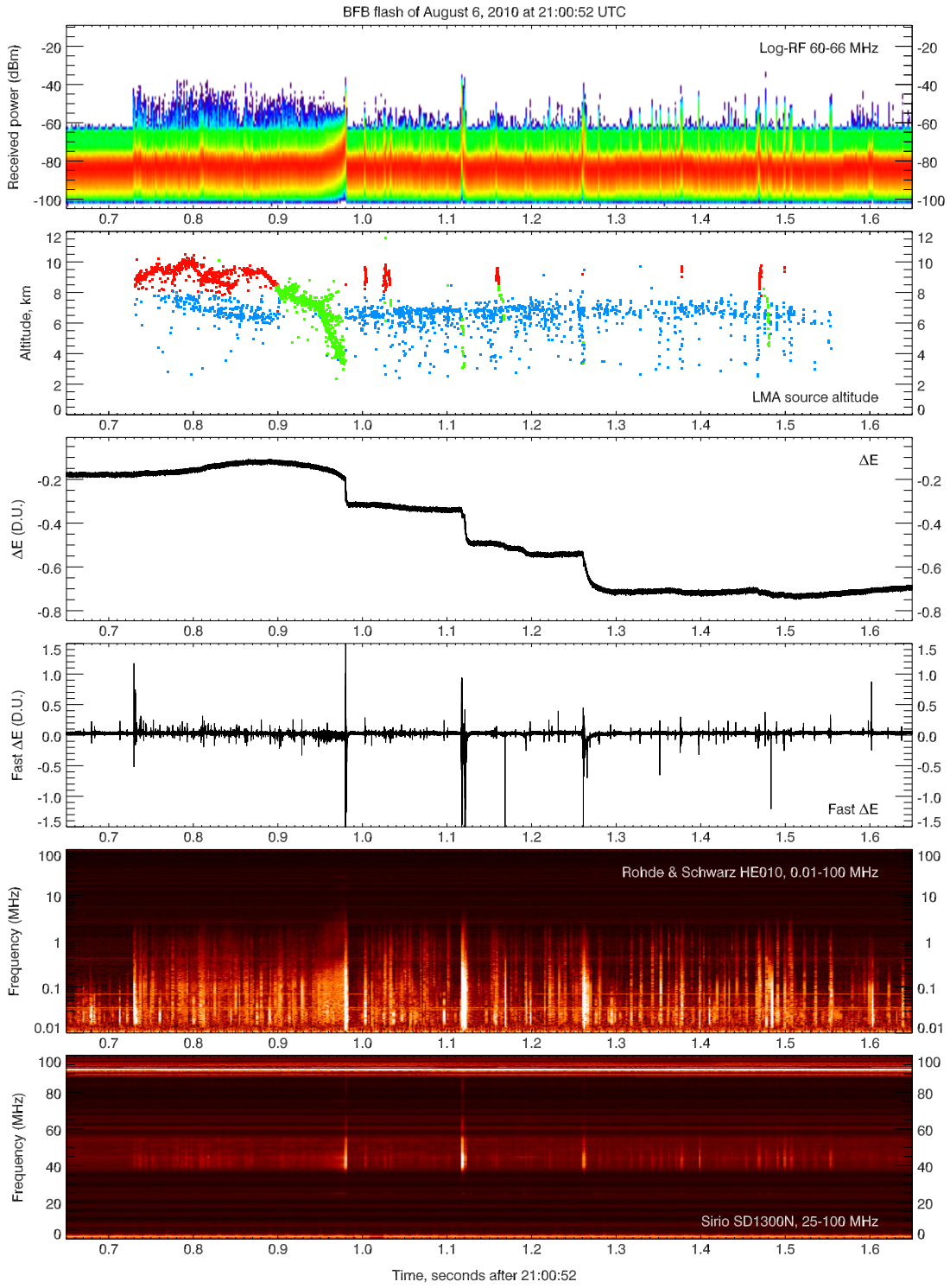

Figure 6.7: Waveform data for the BFB flash of August 6, 2010 at 21:00:52 UTC. This was a particularly active flash with four strokes to ground. VHF emissions associated with the return strokes change from narrow and bright to less intense but longer-duration pulses with each successive stroke (see spectrograms). Note the brief quiet periods in the spectrograms immediately following the first and second return strokes.

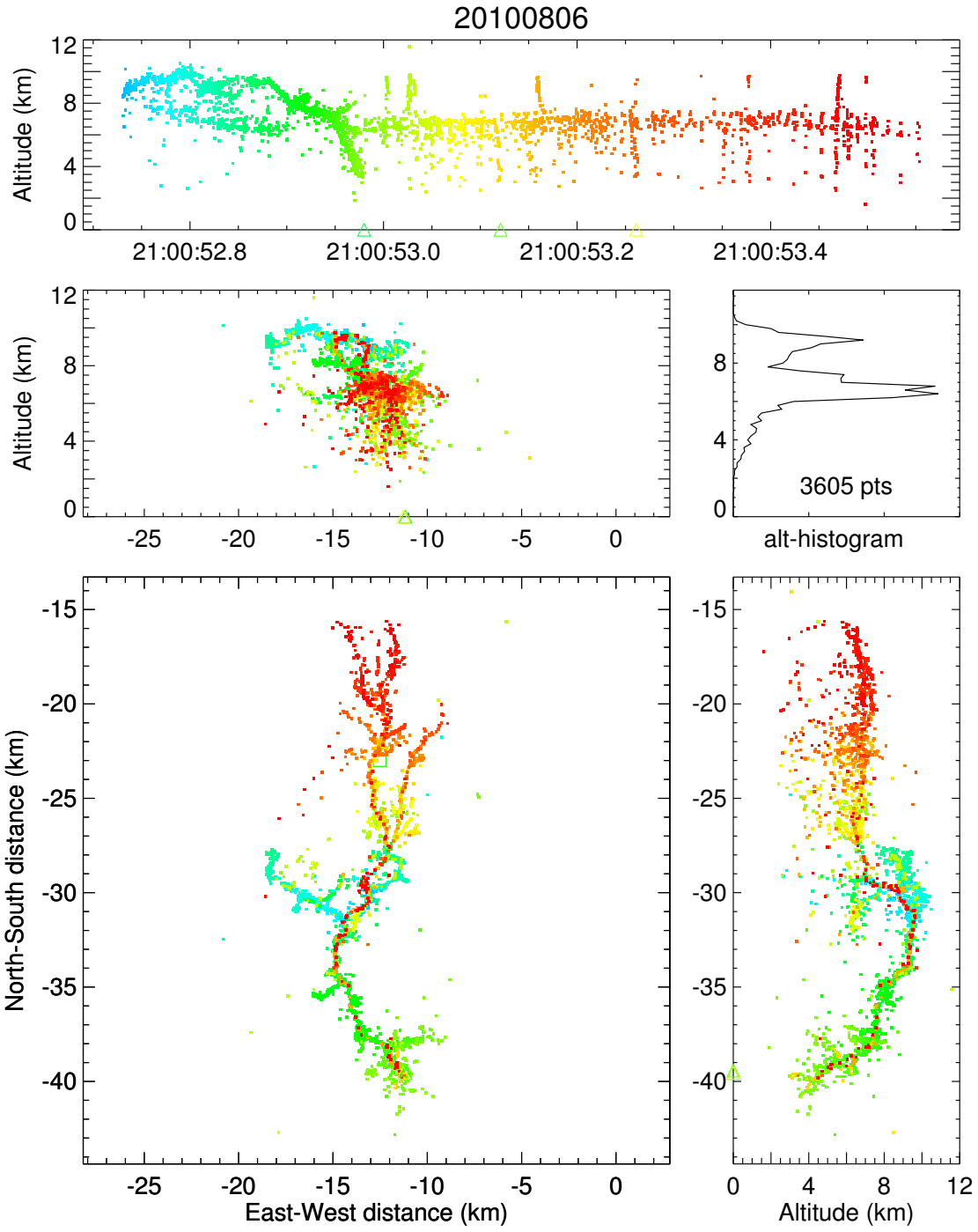

Figure 6.8: VHF sources located by the LMA for the BFB flash of August 6, 2010 at 21:00:52 UTC. Sources are colored in time. The cloud-to-ground leader is retraced by VHF sources associated with dart leaders.

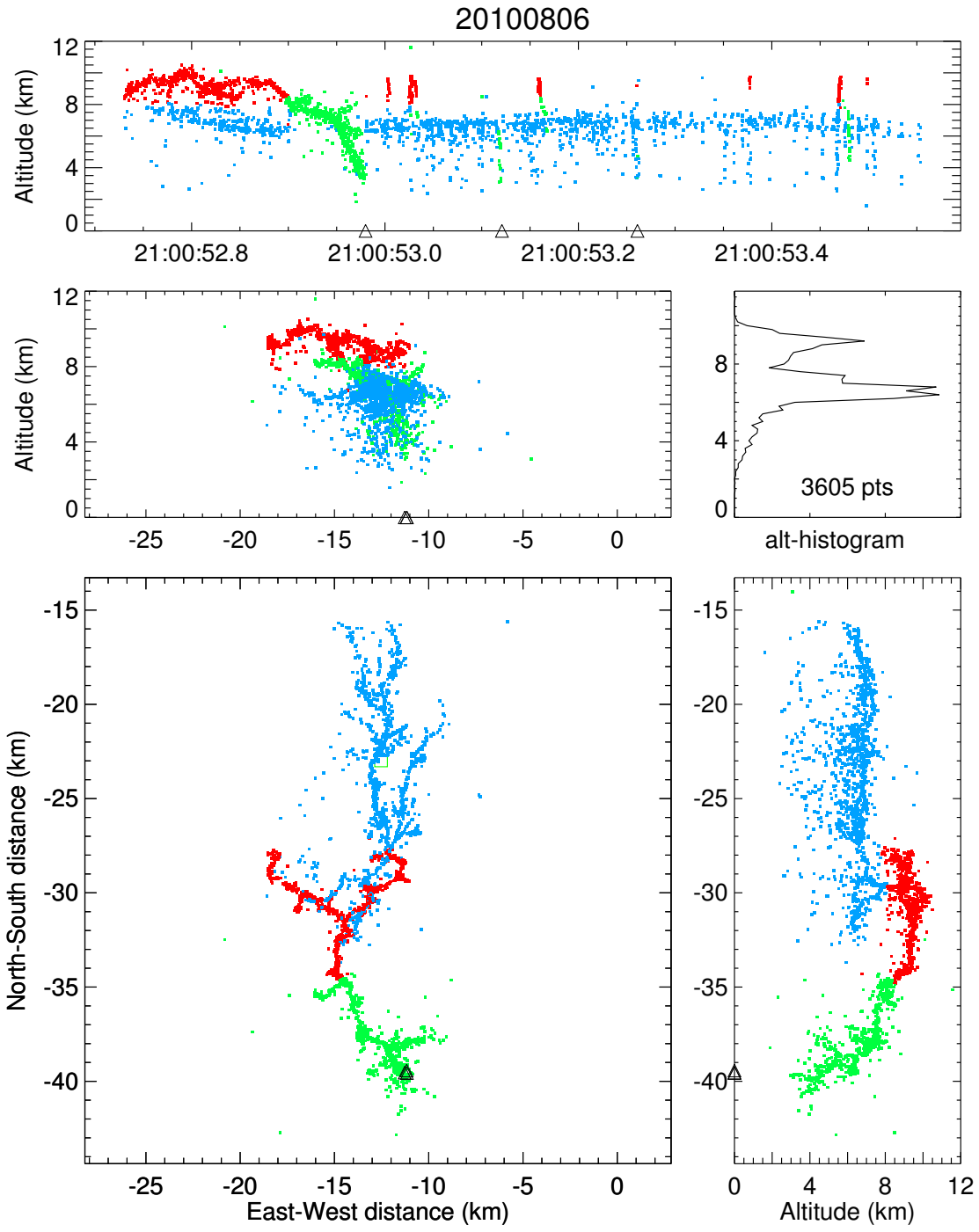

Figure 6.9: VHF sources of the BFB flash of August 6, 2010 at 21:00:52 UTC, colored by charge. The undetermined charge (green) is only indicative, as it is unknown at what point the cloud-to-ground leader emerged from the side of the cloud, if it did so at all. Note the numerous dart leaders (K-leaders) propagating through upper positive charge.

6.5 BFB flash with impulsive intracloud stage

This BFB flash occurred on August 16, 2010 at 01:20:49 UTC, 29 km to the ESE of Langmuir Laboratory. It was a Type-II BFB flash that initiated at 8.5 km altitude (Figure 6.11) and was of normal polarity (Figure 6.12). The duration of the flash was 564 ms. It is shown here for the rather impulsive, intermittent mode of propagation of the initial upward leader. This is most evident in the ΔE waveform in Figure 6.10.

Two other flashes were active about 80–100 km to the NE of the laboratory during the BFB flash. Both flashes appear to have been –CG flashes (inferred from LMA) and therefore the various waveforms in Figure 6.10 may be affected to some degree by RF and VHF radiation from those other two flashes.

The BFB flash started with an upward negative leader that reached an altitude of 12 km and then turned SW. This channel was about 6 km in length and was completed in two stages with a pause of 20 ms in between (Figure 6.10, second panel). After another pause of about 30 ms a negative leader branched off this upward channel at an altitude of 9.5 km and propagated horizontally for 5 km to the NW, where it stopped. Three K-leaders then occurred—which were mapped by the LMA—of which the first reached upward to 11 km altitude along the original upward intracloud channel. The second reached upward to the junction point of the NW branch, and the third followed the NW branch further out, resuming negative breakdown and reaching a terminal altitude of 5.5 km where it stopped. After a delay of 15 ms another K-leader initiated and completed the path to ground. This K-leader was not mapped by the LMA but is resolved well in the ΔE and fast ΔE waveforms and both spectrograms (Figure 6.10). The LMA mapped a number of low-altitude branches from the cloud-to-ground leader quite well.

A number of K-changes (step changes in electric field) are seen in the ΔE waveform during the cloud-to-ground leader stage. The polarity of these K-changes indicate surges of negative charge toward the instrument. Since the cloud-to-ground leader propagated in the general direction of the laboratory, these K-changes are most likely associated with fast K-leaders along the leader path to ground before its completion. Such K-changes during the cloud-to-ground stage are generally not observed in BFB flashes; normally the electric field changes gradually during the cloud-to-ground leader stage (e.g. Sections 6.2 and 6.3).

One post-return-stroke K-leader was initiated, which followed the original upward channel into upper positive charge to an altitude of 11 km, when it stopped. Another bright VHF pulse is seen in both spectrograms of Figure 6.10, but the LMA did not locate any VHF sources associated with this event in the BFB flash, and it was probably caused by a return stroke during one of the concurrent –CG flashes.

Considering the intermittent behavior of this flash, the K-changes during the cloud-to-ground leader stage, and the limited extent of positive breakdown in the midlevel negative charge region, it appears as if the various negative leaders were to a certain degree starved for charge and negative breakdown could not be sustained over long distances. The relatively short duration of the final stage supports this view.

Considering the impulsive, hesitant propagation of the negative cloud-to-ground leader, this flash can be thought of as an "ultimately successful" attempted BFB flash.

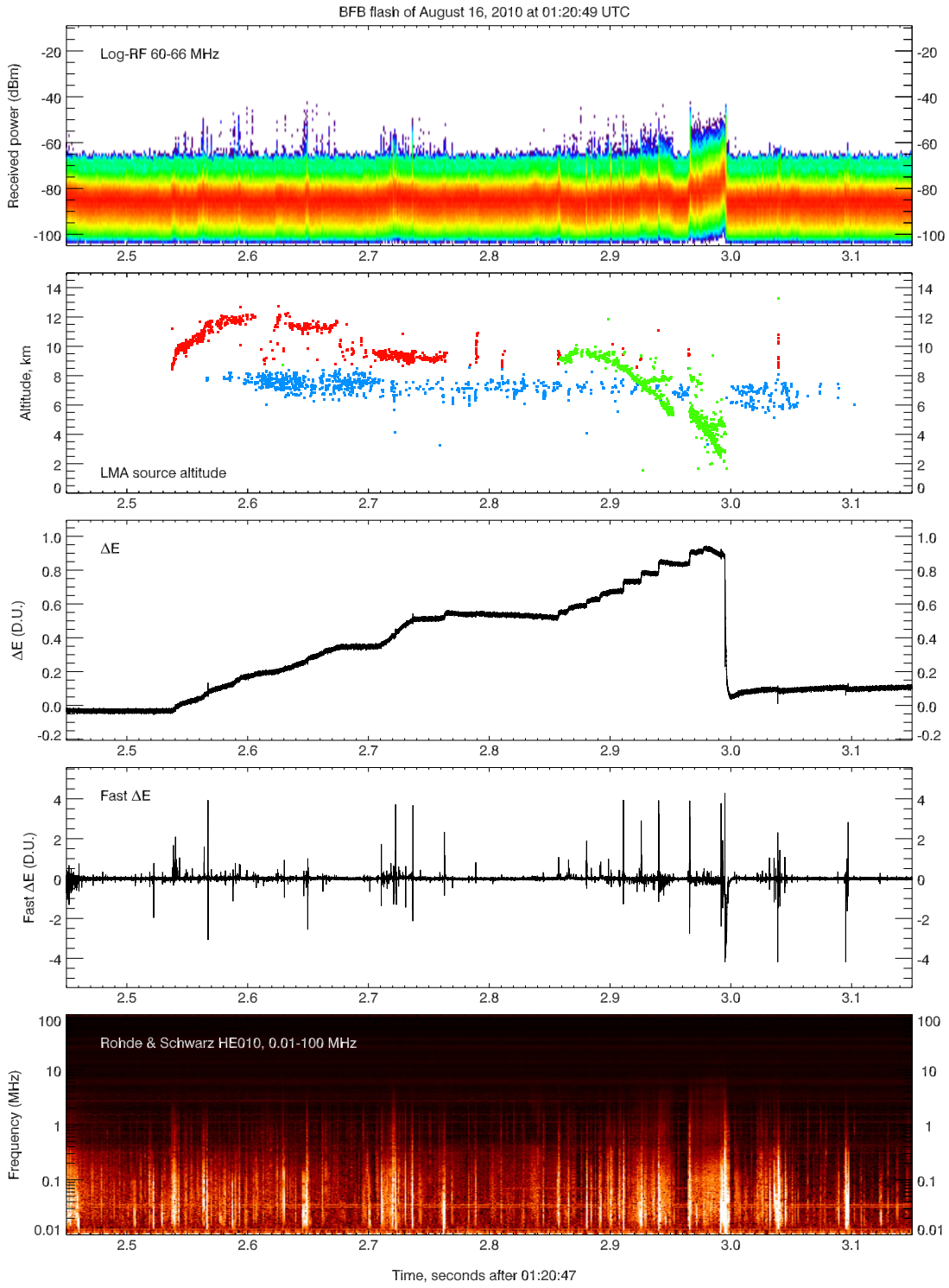

Figure 6.10: Waveform data of the BFB flash on August 16, 2010 at 01:20:49 UTC. This flash was triggered using the real-time LMA display of LiveLMA (Section A.7.3). Because of its 2-second latency and the limited recording buffer, the digitizer sampling the log-RF, ΔE and fast ΔE waveforms had to be run at 10 MS/s instead of the usual 25 MS/s, thereby slightly undersampling the log-RF waveform.

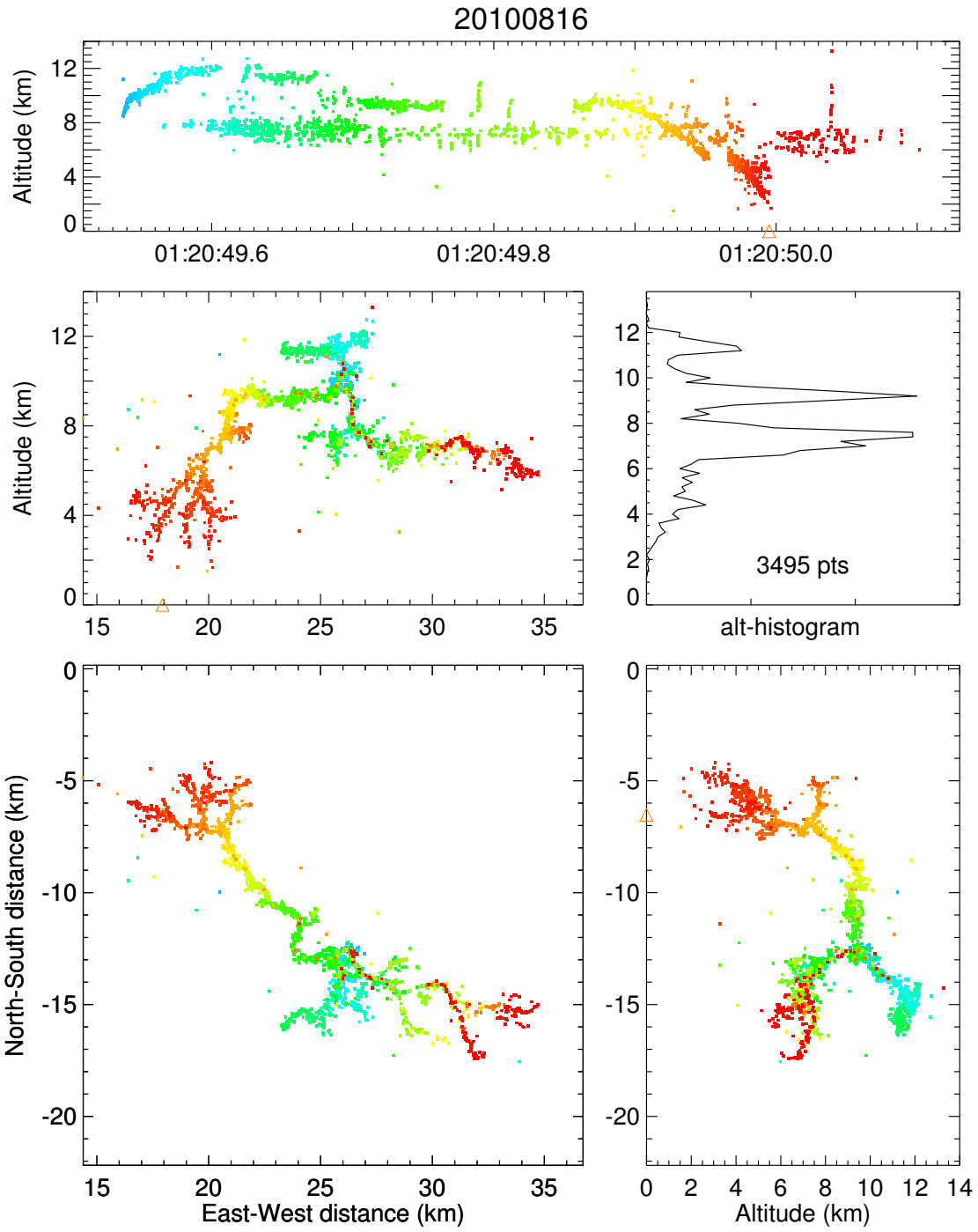

Figure 6.11: VHF sources of the BFB flash of August 16, 2010 at 01:20:49 UTC. Sources are colored in time. The lower-altitude branches of the cloud-to-ground leader were mapped quite well. Note the major branch of the cloud-to-groud channel at 8 km altitude, a feature that appears in several BFB flashes.

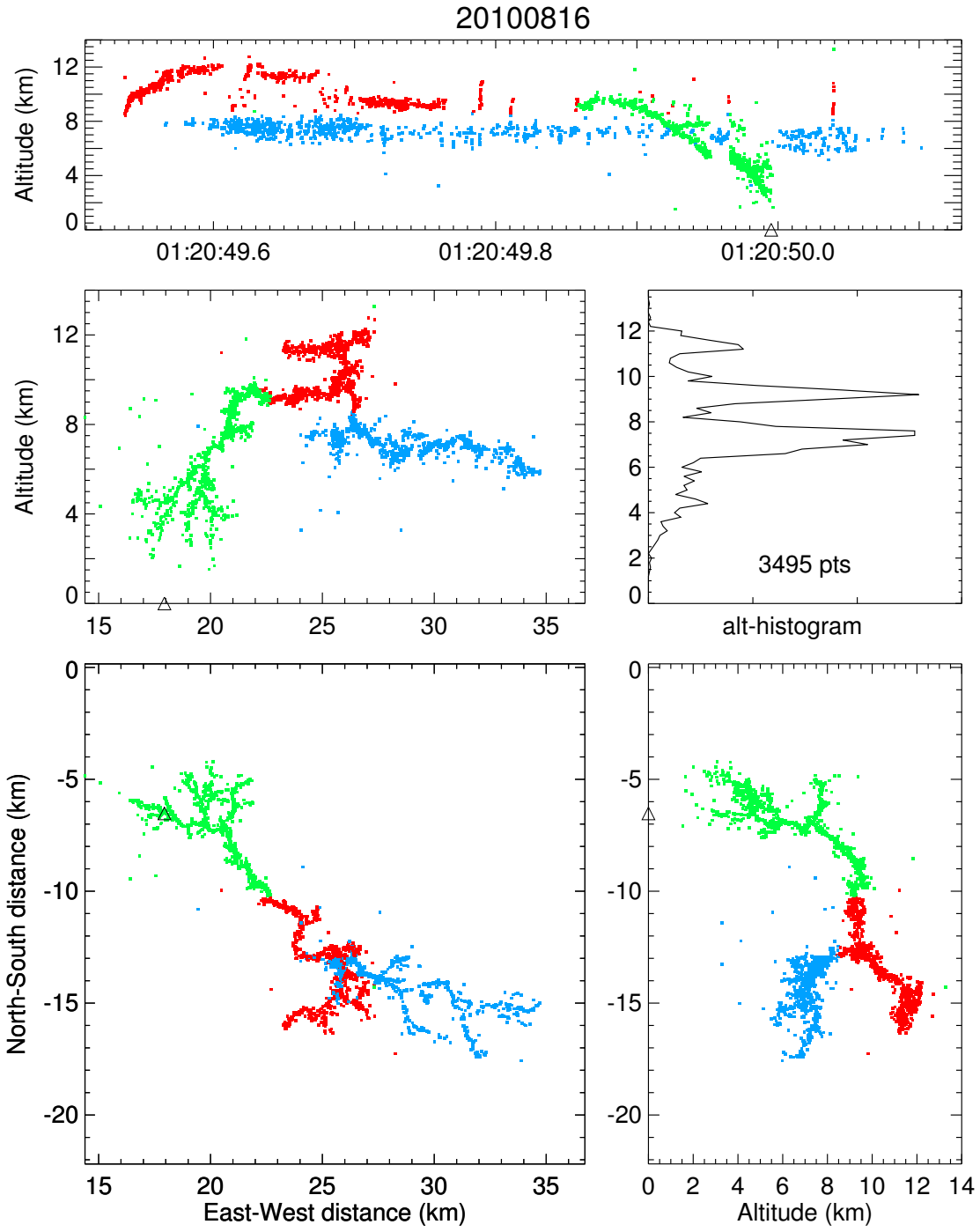

Figure 6.12: VHF sources of the BFB flash of August 16, 2010 at 01:20:49 UTC, colored by charge. Even though the flash is of small extent in upper positive and midlevel negative charge, the cloud-to-ground leader is extensive, reaching well over 10 km in length.

6.6 BFB flash with five attempted dart leaders

This BFB flash occurred on August 16, 2010 at 01:54:55 UTC, on the same day as the flash discussed in Section 6.5 but in a different storm. This storm was 20 km to the northeast of the laboratory, situated over an area between the Pound and Sandwell LMA sites (Figure 6.14). This flash stands out for its series of attempted dart leaders, which are obvious in the ΔE waveform of Figure 6.13. As many as five distinct attempted dart leaders are resolved, none of which succeeded in contacting ground. The flash was a Type-I BFB flash that lasted 545 ms and occurred in a normal-polarity storm.

The flash initiated at an altitude of 8.3 km with a negative leader propagating upward to about 10 km altitude, producing several branches in the process. One of these branches became the cloud-to-ground leader, which exited the storm to the SE.

The LMA mapped this flash wonderfully well, because it occurred in a favorable area relative to the LMA station configuration. In contrast with other BFB flashes, this flash was more symmetric in its upper negative breakdown and midlevel positive breakdown (Figure 6.15); its general appearance is a "textbook example" of a BFB flash, especially in the north–south vs. altitude plot of Figure 6.14.

The log-RF waveform and both spectrograms in Figure 6.13 clearly show the characteristic transition from impulsive to apparently continuous VHF emissions during the intracloud and cloud-to-ground stages of the flash. The log-RF waveform also shows that the peak power of early, high-altitude VHF emissions is not very different from those of the cloud-to-ground leader. This was also found in Chapter 4: the *rate* of VHF emissions increases as the leader propagates to lower altitude, but the *maximum source power* of VHF emissions does not appear to change much.

After the cloud-to-ground stroke, continued negative breakdown in the upper positive charge region established the westward branch in that charge region (Figure 6.15). That negative breakdown was of a more impulsive nature than the earlier negative breakdown in upper positive charge, judging from the relatively large-amplitude fast ΔE pulses detected by the fast antenna (Figure 6.13, fourth panel). The VHF emissions during this breakdown also show up well in the Rohde & Schwarz spectrogram, as a series of pulses that are brighter (i.e. higher power) than the emissions during the early intracloud breakdown. The higher-power events are likely associated with relatively high-current K-leaders that provide negative charge to the upper-level negative breakdown. Such K-leaders can now propagate unhampered along the vertical segment of channel between upper positive and midlevel negative charge, since that channel would still be conductive due to the earlier return-stroke current.

The various attempted dart leaders are mapped quite well by the LMA and appear to reach altitudes down to 4 km before terminating. The second attempted dart leader

(at 01:54:55.91 UTC in Figure 6.14) is seen to decelerate while it propagates down to its terminal point along the preexisting channel (which is mostly vertical at this location, so the deceleration is not an apparent but real effect). (Such a deceleration of an attempted dart leader was also observed in the BFB flash studied in Chapter 5.) The same attempted dart leader also propagated along the westward branch of the channel in upper positive charge, which was created by negative breakdown after the first return stroke.

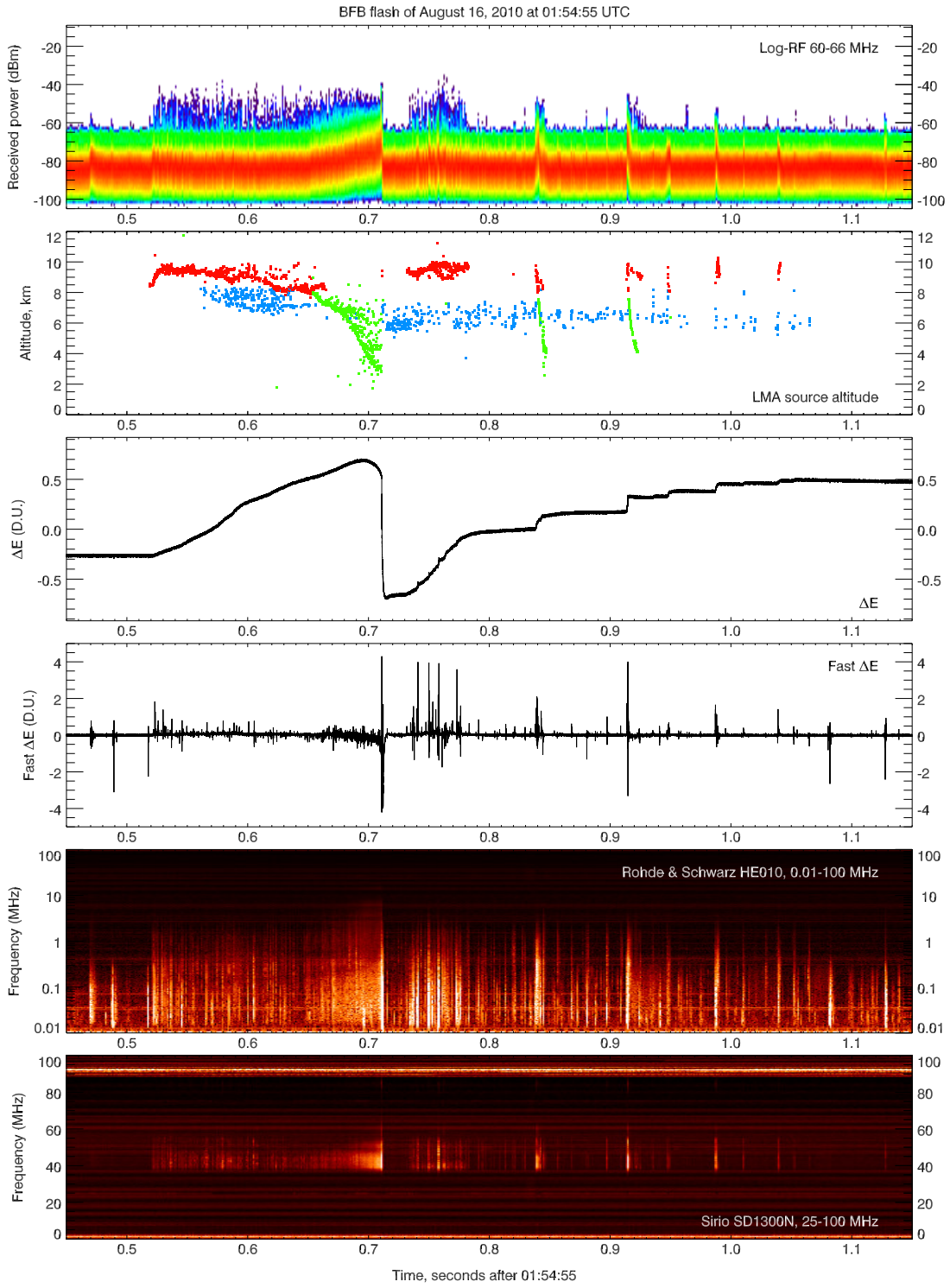

Figure 6.13: Waveform data for the BFB flash of August 16, 2010 at 01:54:55 UTC. Activity is seen in the various waveforms and spectrograms before the onset of located VHF sources. This was an active storm day and these pulses are most likely due to other, distant flashes. The VHF emissions associated with secondary upper-level breakdown (see text) and with the attempted dart leaders show up well in both spectrograms.

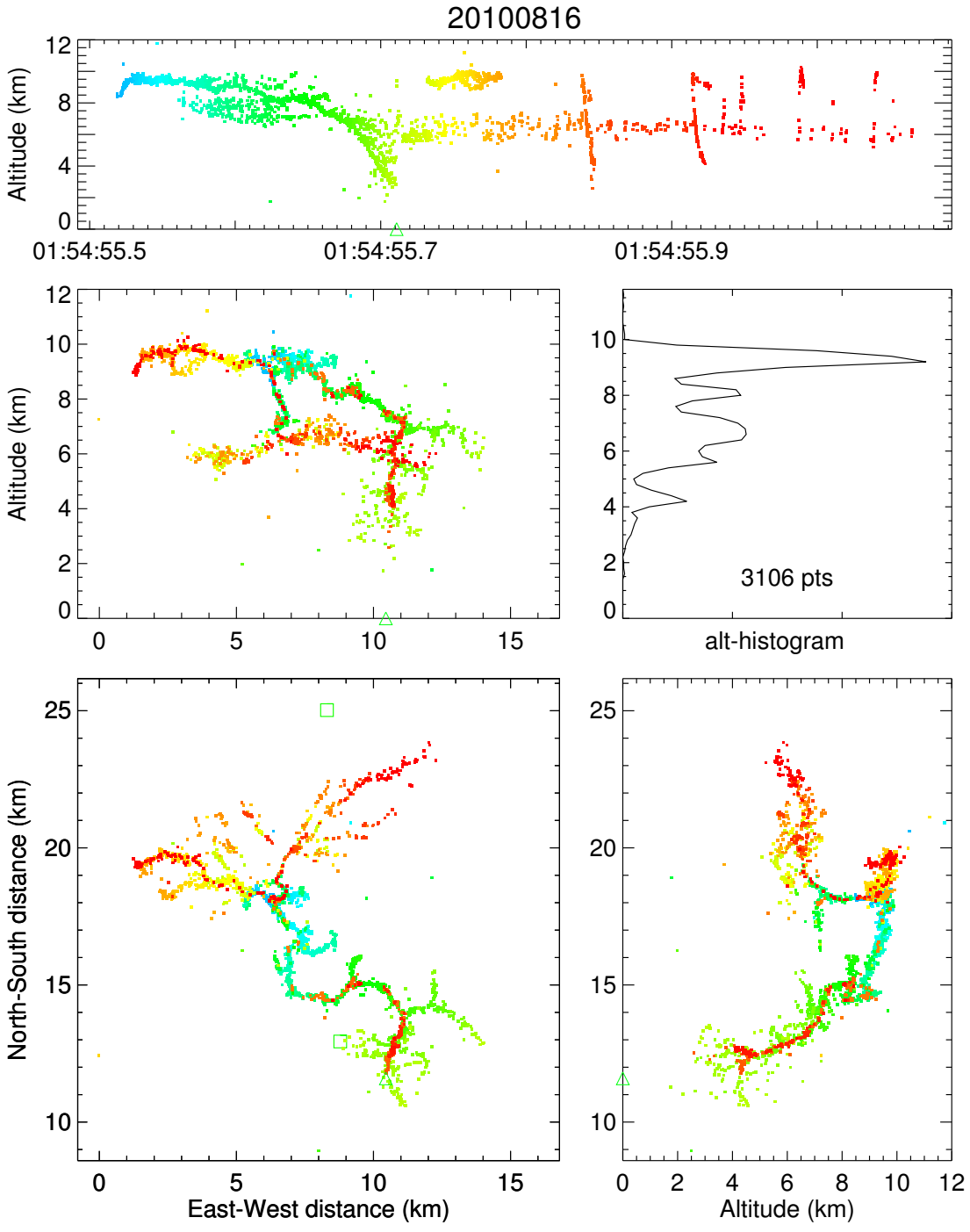

Figure 6.14: VHF sources of the BFB flash of August 16, 2010 at 01:54:55 UTC (colored by time). The attempted dart leaders are mapped well, following the cloud-to-ground channel down to 4 km or even lower altitude.

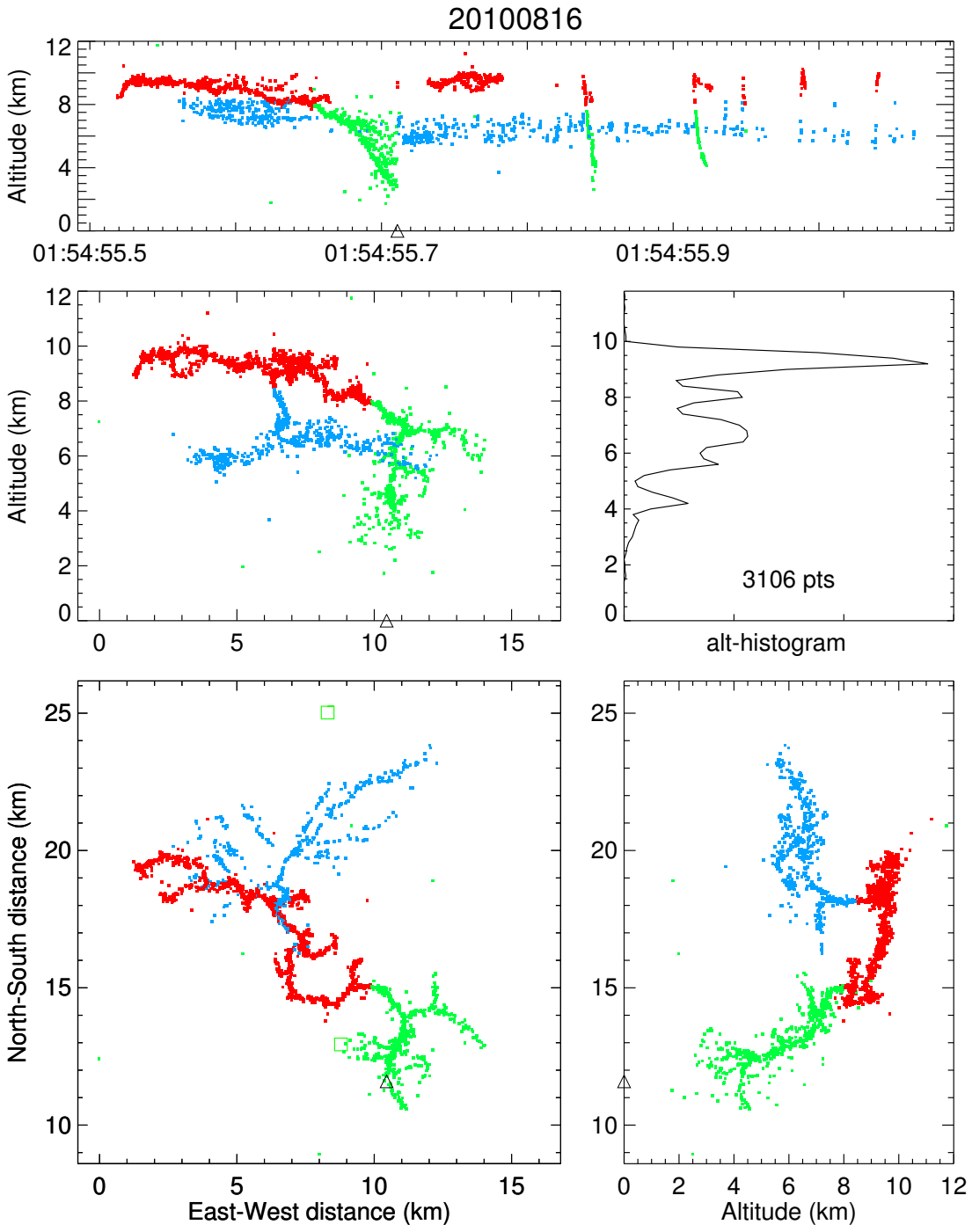

Figure 6.15: LMA data for the BFB flash of August 16, 2010 at 01:54:55 UTC (colored by charge). Note the relatively long vertical channel that was identified as downward positive breakdown; usually, most of the length of this vertical section is associated with negative breakdown. The transition from negative breakdown (red) to undetermined (green) is indicative only and does not indicate the location of the cloud or charge boundary, which is not known.

6.7 BFB flash with low-altitude horizontal branch

This flash occurred in the same storm that produced the BFB flash studied in Chapter 5, about 41 minutes later in time. It was different from the series of BFB flashes that occurred earlier on, as those exited the storm at the northwest flank while the BFB flash discussed here stayed mostly within the cloud and struck ground to the southwest of the main downdraft area.

This BFB flash is unusual in that it exhibited an extensive branch of negative breakdown at low altitude, discharging the (inferred) lower positive charge region. The storm was also producing regular –CG flashes, which indicates lower positive charge being present. The flash occurred in the evening of August 19, 2010 at 04:07:09 UTC. Since this was well after sunset, a photograph could be obtained (Photo 6.1).

Photo 6.1: Still photograph of the BFB flash of August 20, 2010 at 04:07:09 UTC. The cloud-to-ground leader remained mostly within the cloud until it emerged from the cloud base, producing a low-altitude branch that propagated along the cloud base and through precipitation. Note the visible branch to the left of the frame, which may either belong to positive breakdown in the midlevel negative charge region, or be an extension of the low-altitude negative leader.

The flash was a Type-II BFB flash that lasted 456 ms, of which the initial 240 ms were spent by the intracloud and cloud-to-ground stages (Figures 6.16 and 6.17). It

occurred at a distance of 70 km to the ESE of the laboratory. The flash initiated at 8.5 km altitude with an upward negative leader, which propagated up to 10 km altitude and created one branch toward the NW, another to the east, and ultimately a south branch which became the cloud-to-ground leader.

At 4 km altitude the cloud-to-ground leader produced a branch which propagated to the northeast through positive charge near the cloud base, giving the flash an appearance reminiscent of a left-handed corkscrew (Figures 6.17 and 6.18). Horizontal branches near the cloud base are commonly seen in photographs of regular –CG flashes that occur in the vicinity of the main downdraft; it is therefore not surprising that this BFB flash did the same, since its cloud-to-ground leader went near the main downdraft. Usually cloud-to-ground leaders from BFB flashes are somewhat distant from the main precipitation area, however, and such low-altitude horizontal development is therefore not often observed in BFB flashes.

One dart leader was attempted, about 110 ms after the return stroke, which may or may not have contacted ground.

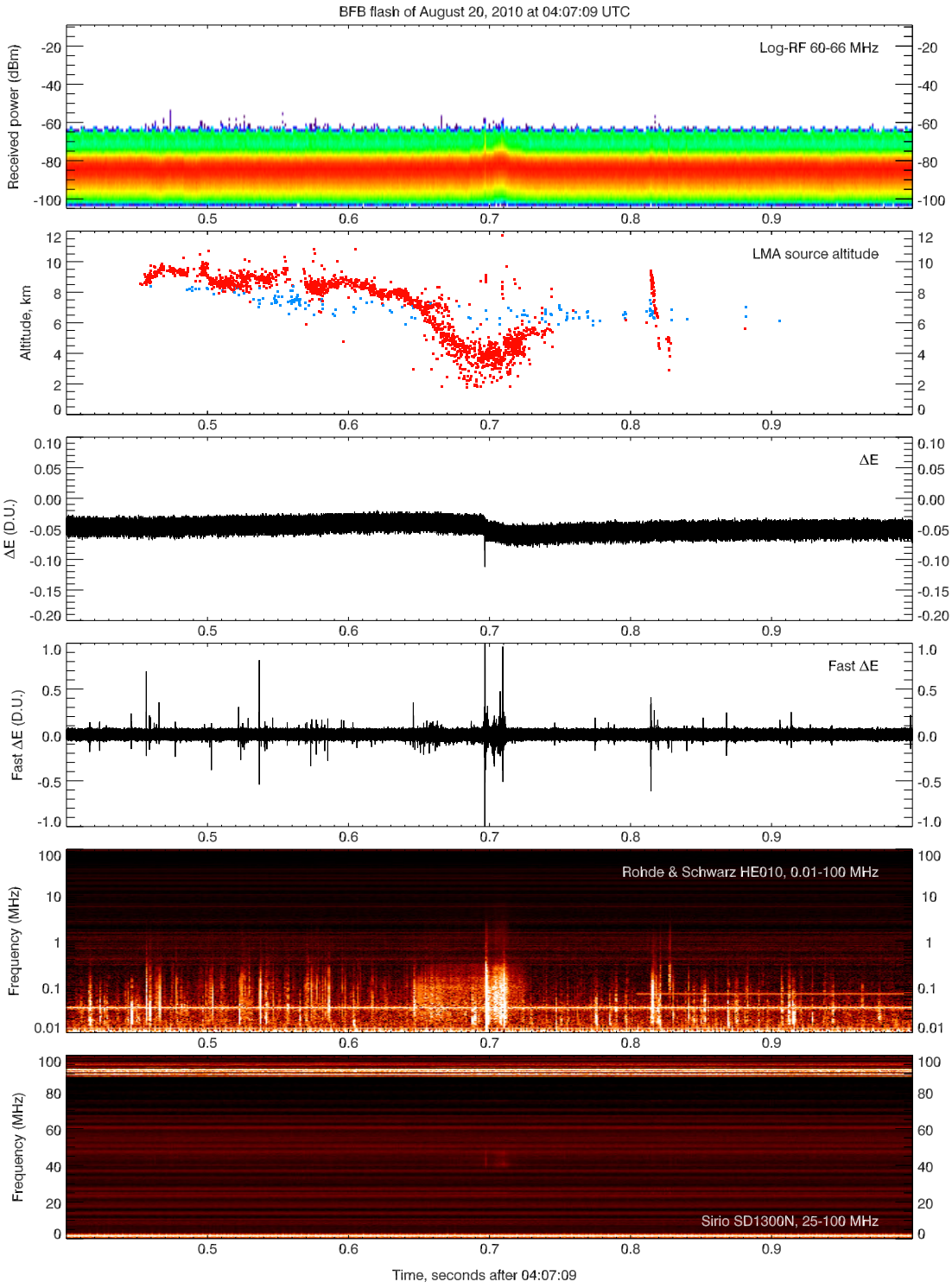

Figure 6.16: Waveform data for the BFB flash of August 20, 2010 at 04:07:09 UTC. This flash was distant from the laboratory, resulting in noisy and weak signals. Note the bright VHF emissions from the low-altitude negative breakdown in the spectrogram.

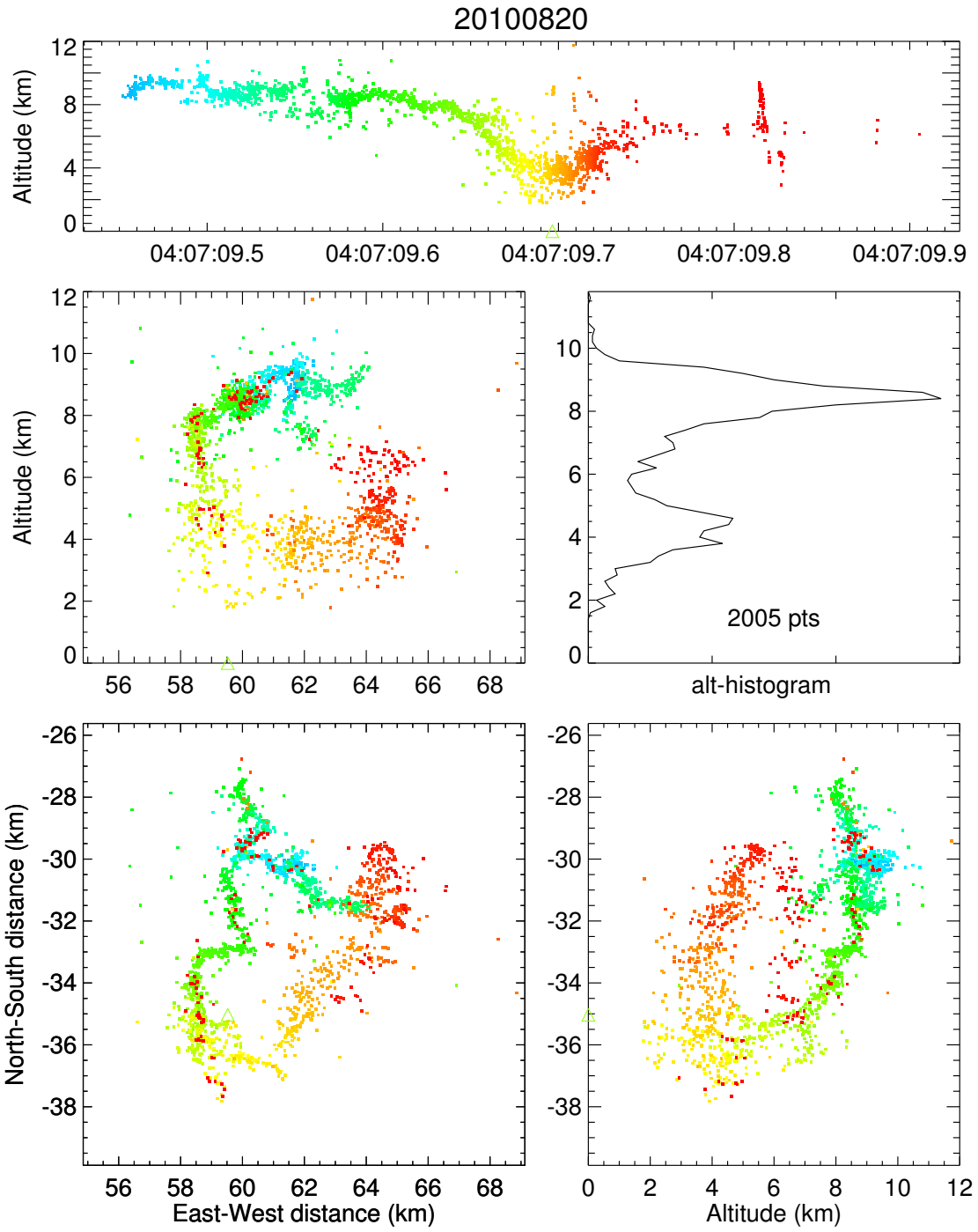

Figure 6.17: VHF sources of the BFB flash of August 20, 2010 at 04:07:09 UTC (colored by time). The low-altitude negative breakdown is more poorly located by the LMA, partly due to the low altitude of the sources and partly to the more numerous VHF emissions from the leader, making precise timing correlations difficult.

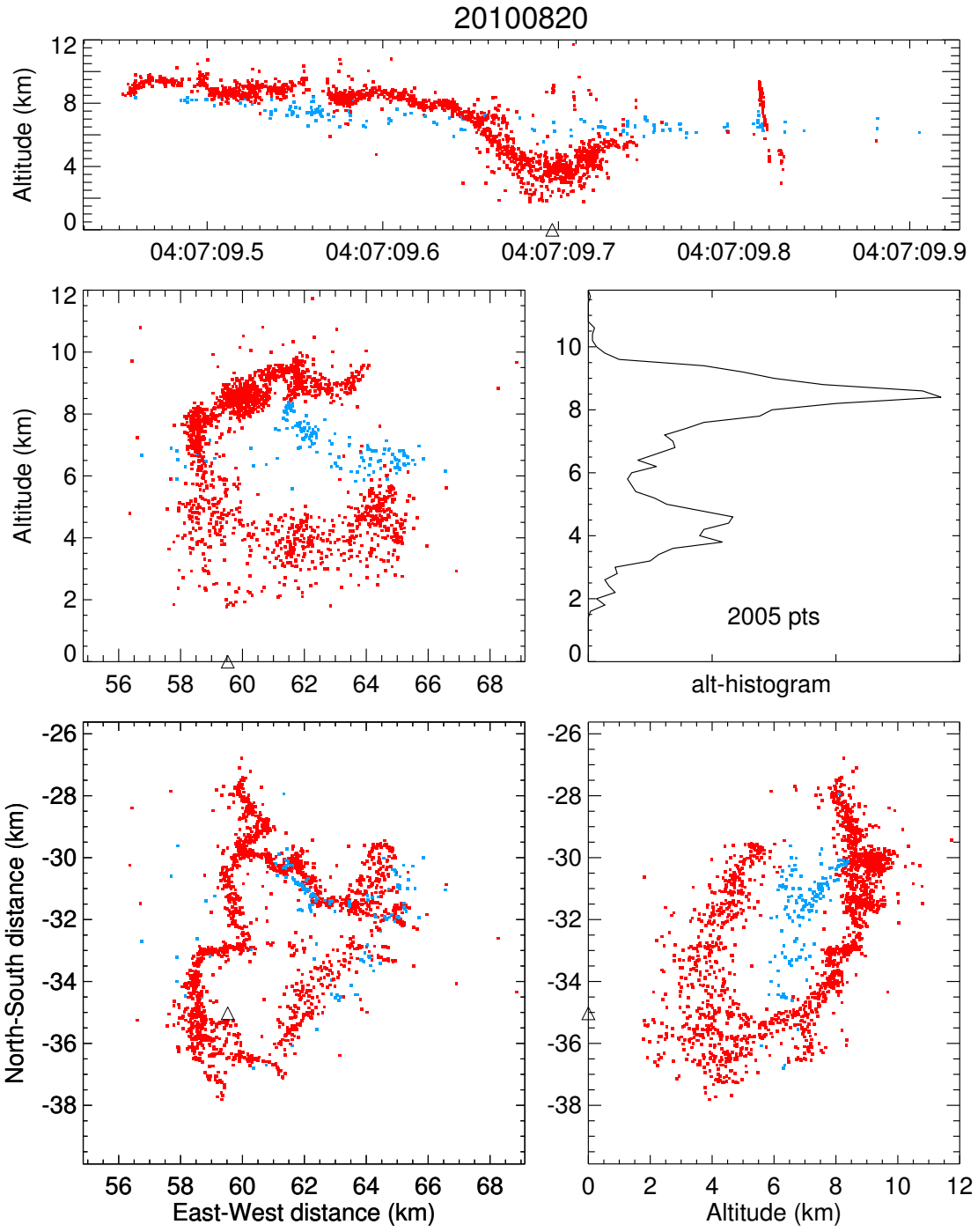

Figure 6.18: LMA data for the BFB flash of August 16, 2010 at 01:54:55 UTC (colored by charge). The low-level negative leader propagated directly under the region where the flash initiated.

6.8 Classic Type-I BFB flash

The BFB flash shown in Figure 6.20 is a classic example of a BFB flash with an intracloud leader that became the cloud-to-ground leader without interruption. As such, it serves as a good example of a Type-I BFB flash, along with the Type-I flash discussed in Section 6.6.

The flash occurred on August 22, 2010 at 21:50:47 UTC at a distance of 38 km to the NE from Langmuir Laboratory. It had a total duration of 298 ms and produced a return stroke only 74 ms after initiation. Two more return strokes occurred, the first of which produced some continuing current (Figure 6.19).

Although Figure 6.20 does not show it very well, it is clear from viewing an animation of the LMA data that the negative leader propagated continuously until it contacted ground. It initiated at 8 km altitude, propagated upward to 10 km and turned south, developing the cloud-to-ground path. Another branch of negative breakdown was initiated and completed while the leader propagated to ground; this extended to the NE by 4–5 km. The cloud-to-ground leader itself also produced a major branch, diverting from the main channel at 8 km altitude.

The log-RF waveform of Figure 6.19 nicely shows the transition from impulsive to apparently continuous VHF emissions during the intracloud and cloud-to-ground stages. The initial upward leader produced bright VHF emissions (Figure 6.19, Rohde & Schwarz spectrogram), along with several fast ΔE pulses of large amplitude, indicative of K-leaders during the initial upward negative leader.

As the negative breakdown propagated to lower altitude very few VHF sources within the midlevel negative charge region were located by the LMA. They were probably being masked by the stronger, near-continuous VHF emissions from the negative breakdown at this stage. The LMA did locate VHF sources associated with positive breakdown until about 20 ms before the return stroke, when the negative leader was near 5 km altitude. At this point a rather large fast ΔE pulse of positive polarity occurred (indicative of negative charge moving up in altitude), which also shows up well in the Rohde & Schwarz spectrogram. Since no other concurrent flashes were detected by the LMA, this pulse was likely produced by this flash and was probably caused by a fast current surge along the cloud-to-ground channel under development.

After the return stroke two dart leaders propagated to ground, the first occurring 50 ms after the first return stroke (producing some continuing current) and the second occurring 200 ms after the first return stroke (Figure 6.19, second and third panels). Interestingly, very few VHF sources were located by the LMA during the brief continuing current stage of ~ 10 ms after the second return stroke; the spectrograms in Figure 6.19 appear quiet in VHF as well during this interval.

Overall, the BFB flash was fairly localized with both the negative breakdown in the

upper positive charge region and the positive breakdown in the midlevel negative charge region being only 4–5 km in horizontal extent (Figure 6.21). Like other BFB flashes studied in this chapter, the midlevel negative charge region appears to be shifted laterally relative to the upper positive charge region in a generally opposite direction to the negative cloud-to-ground leader. In other words, the negative leader to ground tends to occur on the cloud flank away from midlevel negative charge. It is unclear what is cause and effect here: the leader choosing a preferred cloud flank to exit, away from the negative charge region; or the negative charge region simply being displaced for the same reason(s) that causes the BFB flash to occur in the first place (perhaps wind shear, along with the depletion of upper positive charge).

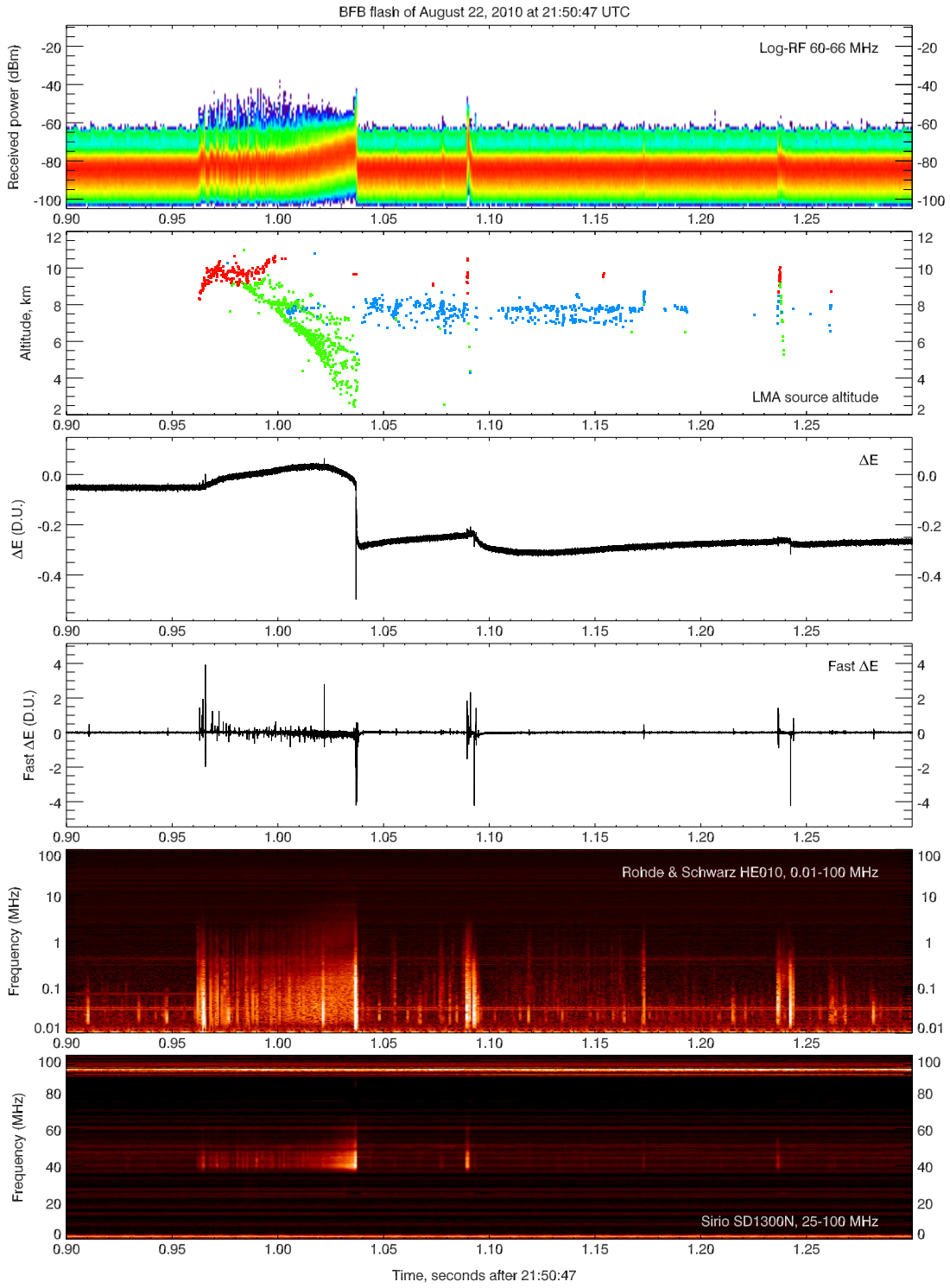

Figure 6.19: Waveform data for the BFB flash of August 22 at 21:50:47 UTC. This is the fastest stroke-producing BFB flash studied, with only 74 ms between the initiation of the flash and the return stroke. Note the fast ΔE (and VHF) pulse during the cloud-to-ground leader stage.

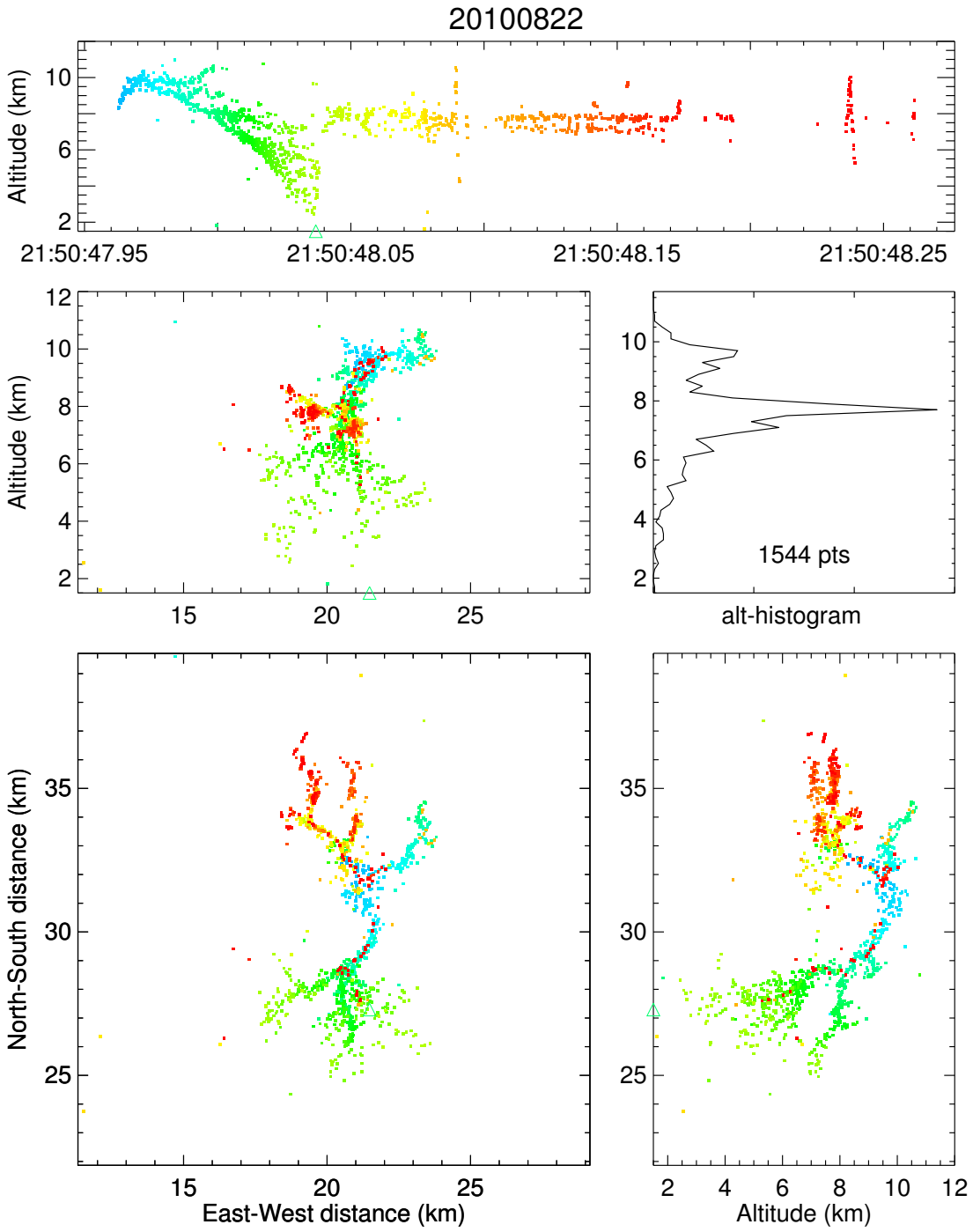

Figure 6.20: VHF sources located by the LMA for the BFB flash of August 22 at 21:50:47 UTC, colored by time. Note the characteristic "inverted-V" appearance of the final dart leader in the altitude–time panel, a common feature of slow-moving dart leaders in BFB flashes.

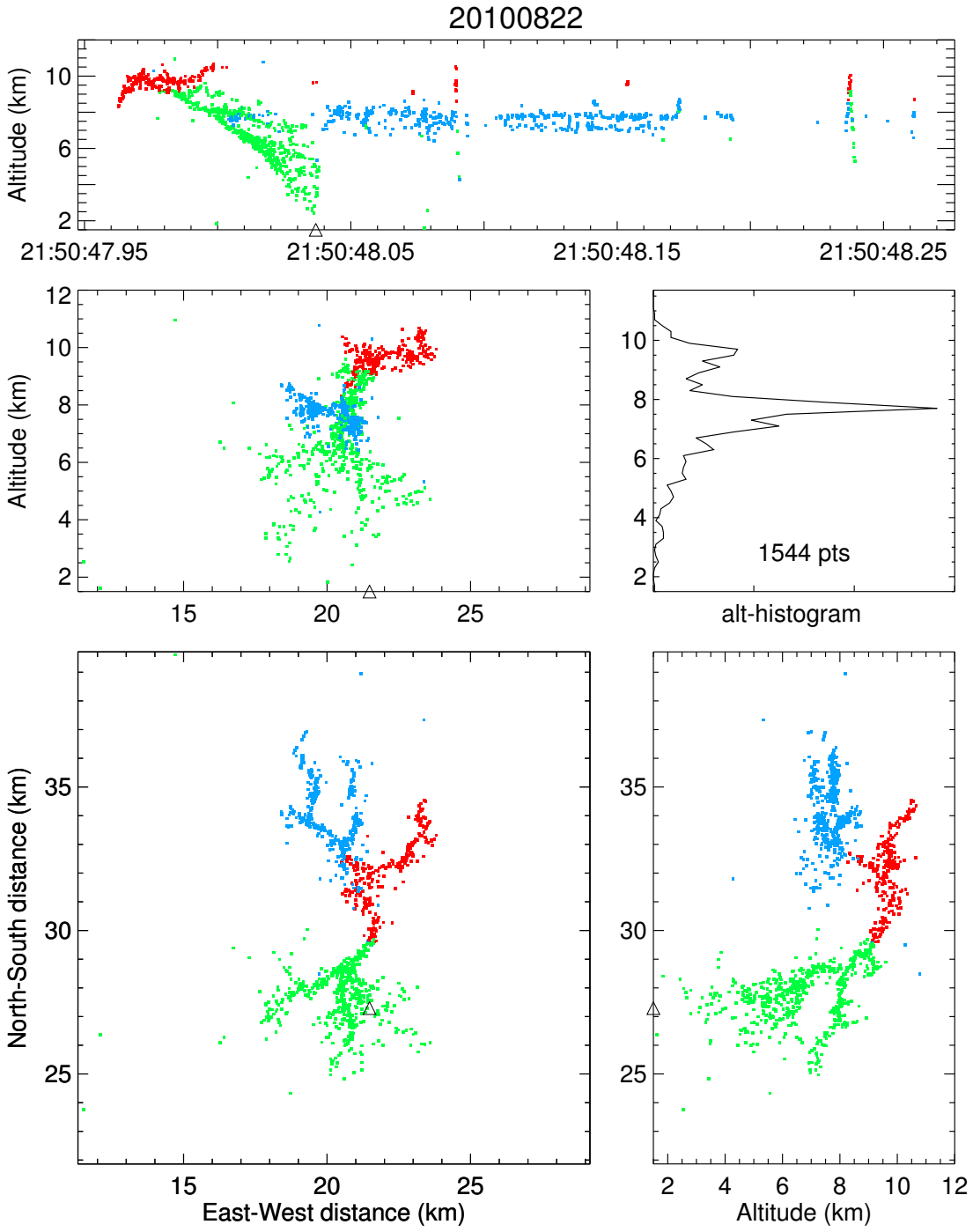

Figure 6.21: VHF sources located by the LMA for the BFB flash of August 22 at 21:50:47 UTC, colored by charge. The flash was fairly localized, with only about 5 km horizontal distance between the point of initiation and the ground contact point.

6.9 BFB flash with high-altitude upward leader

This quite interesting flash occurred on August 22, 2010 at 22:37:07 UTC, about 47 minutes after the BFB flash discussed in Section 6.8. It occurred in another storm that was part of a loosely defined cluster of storms to the NE of the laboratory. It is an example of a BFB flash with an upward leader (Figure 6.23). At the time of the flash several storms were ongoing with frequent intracloud lightning, which reached up to 15.5 km in some storms. The BFB flash discussed here occurred in a storm to the west of the Pound LMA site, about 12 km to the NNE of Langmuir Laboratory.

According to the atmospheric sounding of Albuquerque at 00 UTC on August 23, the winds were from the SW at 10–15 knots up to 8 km altitude, veering to the NW but diminishing to 0–5 knots up to $\sim$ 13 km altitude, and becoming SE at 20–25 knots above 13 km altitude. These winds would have caused anvils between 8 and 13 km altitude to shear in a generally SSW direction. This appears to be the case in Figure 6.24, which shows extensive intracloud development of the negative leader in upper positive charge to the SSW of the flash initiation point.

The BFB flash was a Type-II flash that initiated as a normal-polarity intracloud flash at 8.5 km altitude (Figures 6.23 and 6.24). It was preceded by a precursor event 700 ms earlier in time, which the LMA mapped as a pair of VHF sources within a few hundred meters of where the flash initiated. The negative leader went upward (at a slant angle to the north) to 11 km altitude, where it paused. Positive breakdown in the midlevel negative charge region continued. The negative leader then continued upward, now at a slant angle to the west, terminating at 13.5 km altitude. Upon terminating it produced several branches of short length, giving the tip of the leader a plume-like appearance.

The upward leader propagated relatively fast just before terminating, traveling about 1.5 km in 3 ms (determined from LMA data using 23 VHF sources), at a velocity of 5×10^5 m s^{-1}.

Positive breakdown still continued in the midlevel negative charge, eventually initiating new negative breakdown in upper positive charge that formed the extensive south branch. This branch continued to propagate without interruption, producing an attempted-BFB branch and then the successful cloud-to-ground branch without halting. The leader went to ground in a southeasterly direction (Figure 6.23). Interestingly, the negative leader near 8 km altitude continued to propagate during and after the return stroke.

Positive breakdown continued at a slow but steady pace, producing at least one attempted dart leader at 22:37:08.24 UTC that almost made it to ground (Figure 6.22, second and third panels). After this attempted dart leader numerous successive dart leaders were attempted, some of which may have produced return strokes. The

slow antenna detected negative field changes during these dart leader events, but these could also have been produced by attempted dart leaders, since the cloud-to-ground channel made a turn to the east, away from the instrument.

Since both negative and positive breakdown propagated relatively near to the instruments, making this a complex flash to study, not much can be concluded from the nature of VHF emissions during the intracloud and cloud-to-ground stages (Figure 6.22, log-RF waveform and spectrograms). VHF emissions appear as high-power and near-continuous during most of the lifetime of the extensive negative intracloud breakdown. The attempted dart leader at 22:37:08.24 UTC is quite bright at VHF. Bursts of VHF emissions from K-events in positive breakdown can be seen clearly in both spectrograms.

The return stroke had some continuing current, possibly due to the extensive negative and positive breakdown. When the continuing current ceased (at 22:37:08.2 UTC) a pause of 50 ms in activity occurred, followed by an attempted dart leader. Another flash was active just to the northeast of this flash, producing the VHF emissions seen in the log-RF waveform and spectrograms during the pause. After the attempted dart leader, numerous K-leaders occurred before the flash ended.

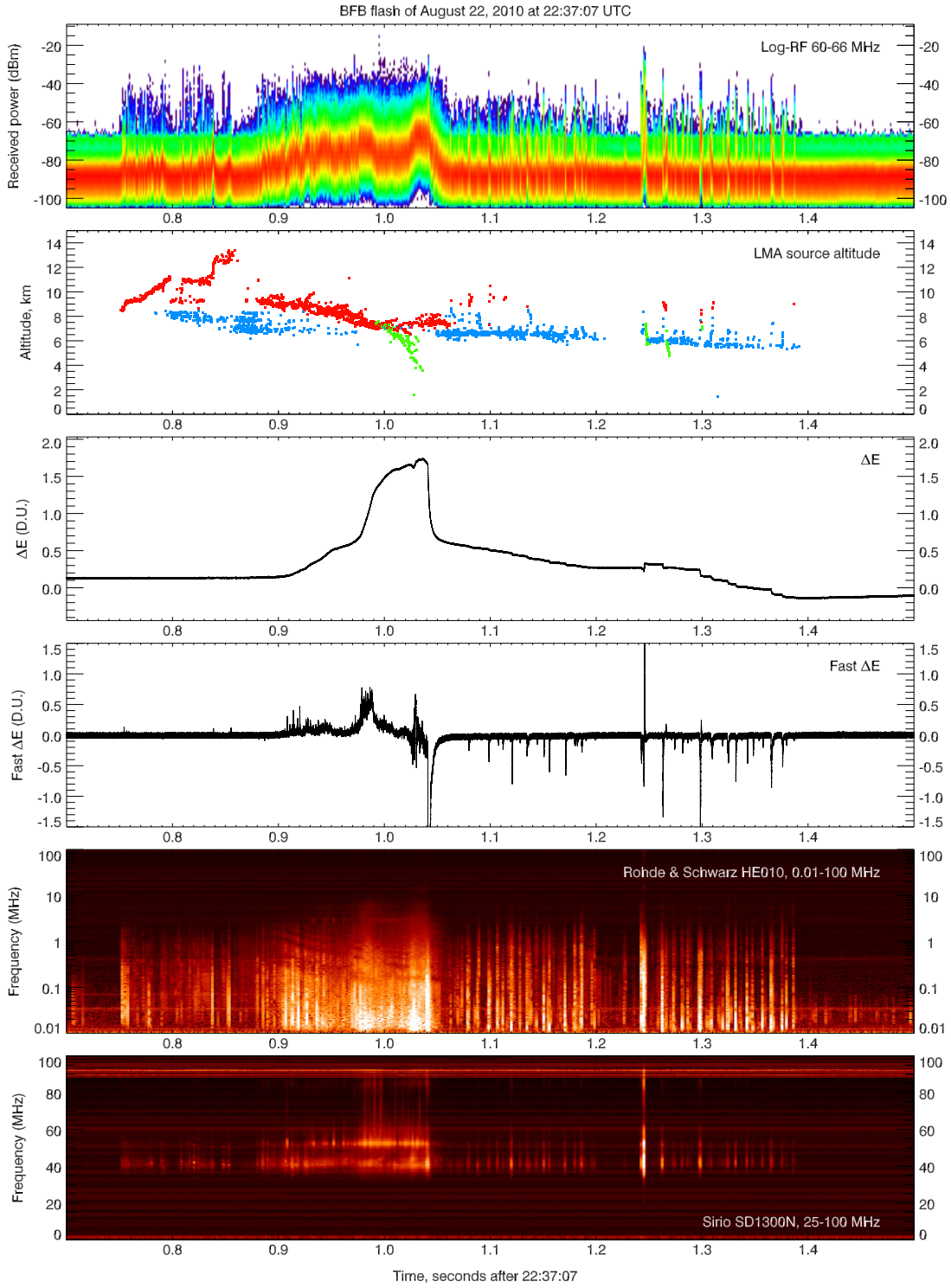

Figure 6.22: Waveform data of the BFB flash of August 22, 2010 at 22:37:07 UTC. Note the numerous attempted dart leaders (K-leaders) toward the final stage of the flash.

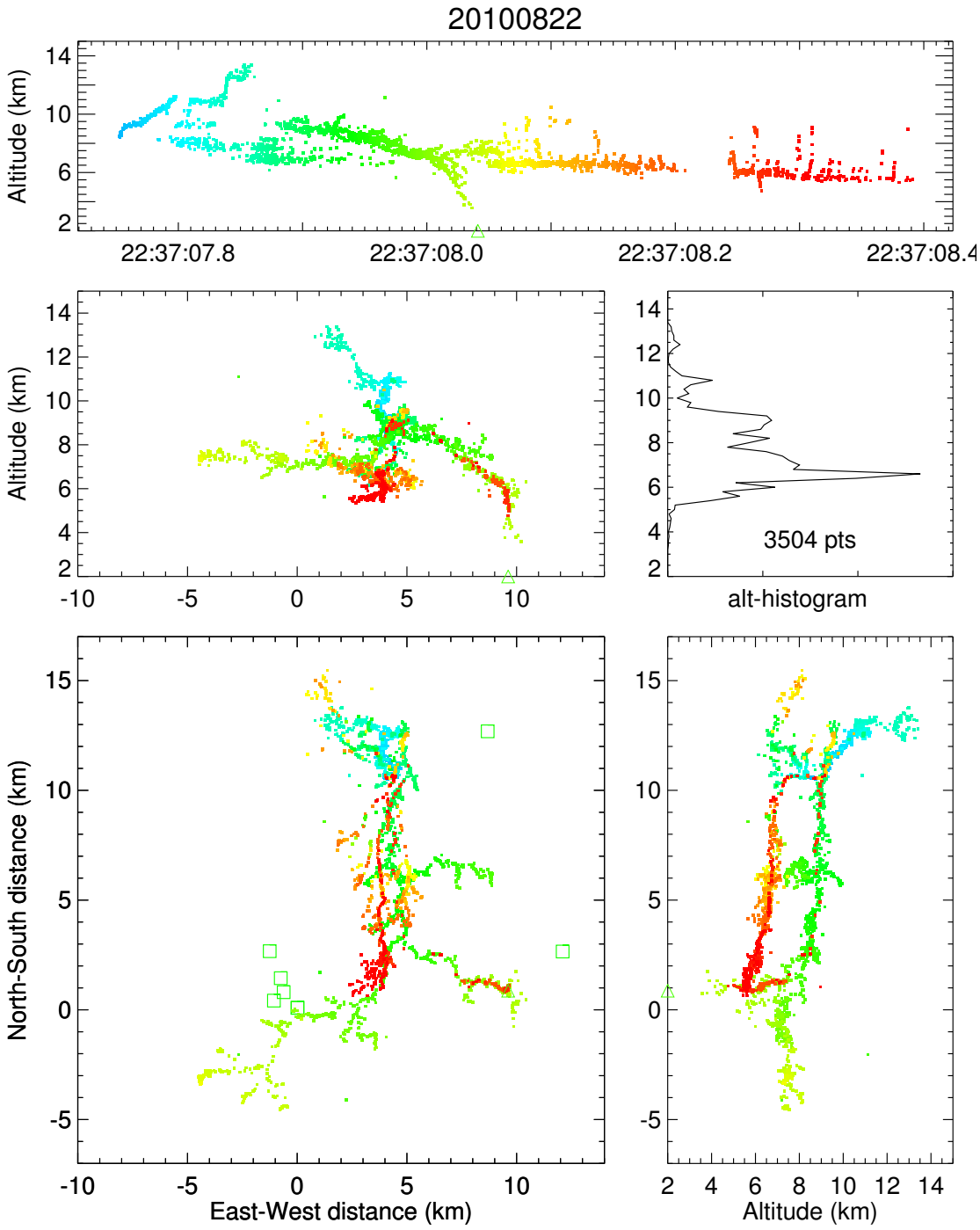

Figure 6.23: VHF sources located by the LMA for the BFB flash of August 22, 2010 at 22:37:07 UTC, colored by time. The station to the northeast is Pound LMA; Sixmile LMA is to the east. The negative breakdown in upper positive charge propagated over the LMA stations on Magdalena Ridge.

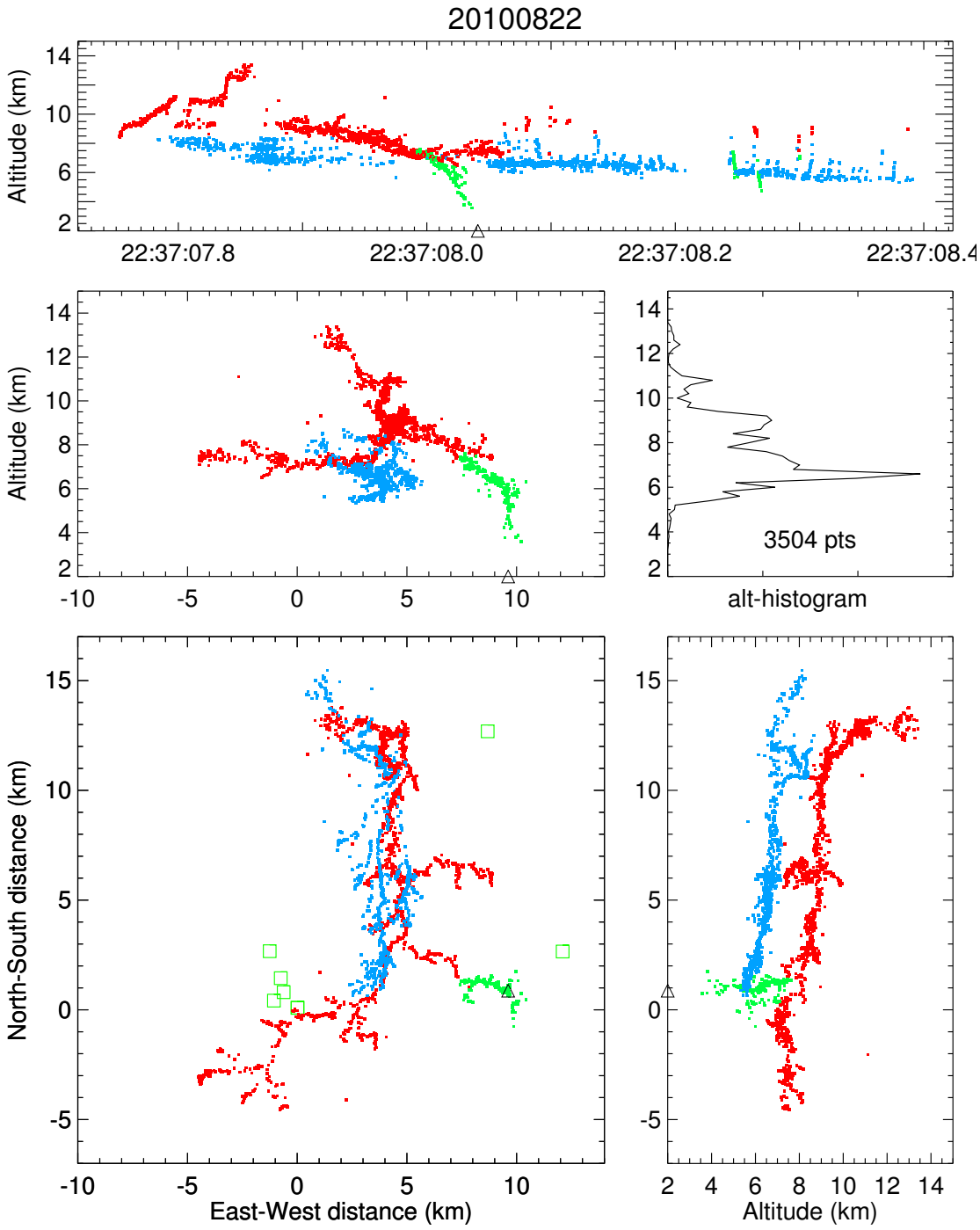

Figure 6.24: VHF sources located by the LMA for the BFB flash of August 22, 2010 at 22:37:07 UTC, colored by charge. The east branch of negative breakdown, situated to the north of the cloud-to-ground branch, may be an attempted BFB; it is unclear if it actually exited the cloud. Note the general subsidence of both the upper positive and midlevel negative charge regions toward the south, downwind of the convective region to the north.

6.10 Summary

Eight BFB flashes were discussed in this chapter for their unusual or otherwise interesting characteristics. Two BFB flashes were Type-I and the other six were Type-II BFB flashes. Some observations are briefly summarized here.

6.10.1 Number of strokes to ground

Five of the studied BFB flashes produced multiple strokes to ground, and most flashes produced at least attempted dart leaders. Several multi-stroke flashes had some continuing current during the return strokes, which tended to be of longer duration in the later strokes.

6.10.2 Unequal extent of positive and negative breakdown

Several BFB flashes were asymmetric in the extent of leader activity within the midlevel negative charge region relative to the upper positive charge region; negative breakdown in the upper-level negative breakdown tended to be less extensive than the midlevel positive breakdown. The BFB flashes discussed in Sections 6.2, 6.3 and 6.4 are good examples of this, indicating that the upper positive charge region was depleted relative to the midlevel negative charge region.

6.10.3 Lateral displacement of charge regions

In most of the BFB flashes studied here, VHF sources associated with negative breakdown in the upper positive charge region were (as a group) laterally displaced relative to those associated with positive breakdown in the midlevel negative charge region. The cloud-to-ground leader generally occurred away from the direction in which the positive breakdown was displaced.

6.10.4 Final stage: K-leaders and dart leaders

The final stages of all BFB flashes studied in this work always had some activity, which mostly occurred in the midlevel negative charge region. There are no cases where a final stage did not occur, with the flash ending after the first return stroke. Attempted dart leaders along the cloud-to-ground channel as well as K-leaders elsewhere are frequently observed during the final stage. BFB flashes are therefore a

confirmation that the final ("junction") stage of classic IC flashes and the late stages of regular –CG flashes share the same kind of activity of positive breakdown, and K-leaders and dart-leaders are thus the same phenomenon [*Shao and Krehbiel*, 1996]. The only distinction between K-leaders and dart leaders made in this work has been of a historical nature, by reference to their respective targets: K-leaders propagate from the midlevel negative to the upper positive charge region, while dart leaders propagate from the midlevel negative charge region to ground. However, the fact that a BFB flash goes through the upper positive charge region graphically illustrates and confirms the point made by *Shao et al.* [1995] that there is no physical difference between K-leaders and dart leaders.

6.10.5 K-leaders during leader development

In several cases, such as the BFB flashes studied in Chapter 4 and in Section 6.5, K-leaders are seen to occur *during* propagation of an upward negative leader, as well as of the cloud-to-ground leader. Some BFB flashes develop rather intermittently, helped along by (fast) K-leaders. Such K-leaders were also inferred by *Ogawa and Brook* [1964] in a streak photograph of a cloud-to-air leader.

6.10.6 Transition in VHF emissions of cloud-to-ground leader

All eight BFB flashes studied in this chapter show the characteristic increase in the rate of VHF emissions during the intracloud and cloud-to-ground stages, which is due to negative breakdown being more impulsive at high altitude than at low altitude. Also, according to the log-RF waveforms, the maximum power of VHF emissions associated with high-altitude negative breakdown is not very different from that produced by low-altitude negative breakdown—and certainly not much lower in power. This is true for the BFB flash studied in Chapter 4 as well as for five of the BFB flashes studied in this chapter, but could not be concluded from the other three: The flash in Section 6.2 was too close to ignore the variable distance to the sources; the flash in Section 6.7 was too distant; and the flash in Section 6.9 had an active negative intracloud leader during the cloud-to-ground leader stage, which generated additional VHF emissions. In conclusion, the rate of VHF emissions increases as a negative leader propagates down in altitude, but the maximum source power of the emissions does not appear to change significantly. What does increase is the *time-averaged* power of VHF emissions by the leader, since the rate of emissions increases. This gives rise to the characteristic log-RF waveform of BFB flashes.

7. Conclusions

7.1 Summary

Summaries and conclusions appear at the end of the four preceding Chapters 3–6 and all of these will not be repeated here, but a short overview will be given below.

A *bolt from the blue* is a negative cloud-to-ground flash that initiates as a classic bilevel intracloud flash between the midlevel negative and upper positive charge regions in a storm. Its occurrence indicates depleted upper positive charge with respect to midlevel negative charge.

In Chapter 3, two types of BFB flashes were defined, based on the mode of initiation of the cloud-to-ground leader. Also, three stages for a BFB flash were defined: the intracloud stage, cloud-to-ground stage, and the final stage.

An overview of 59 BFB flashes was given to summarize basic characteristics of BFB flashes, such as the number of strokes to ground, flash initiation altitude, flash duration, time to first stroke to ground, and "strike distance". All of these BFB flashes were of negative polarity (lowering negative charge from the cloud to ground) and about half of the 59 flashes produced more than one stroke to ground. Also, a weak correlation between wind shear and the cloud exit location of BFB flashes was found, where BFB flashes show a preference for the upwind side of a storm.

The VHF emissions from the negative cloud-to-ground leader of a BFB flash transition from impulsive (characteristic of negative leaders in classic intracloud flashes at 8 km and higher altitude) to apparently continuous in nature (characteristic of –CG and low-altitude IC flashes, which occur at altitudes typically below 5 km). The log-RF waveform, which is the received power of VHF emissions in time, shows this transition well, and it is also seen in fast ΔE waveforms.

Chapter 4 discusses one BFB flash in detail using correlated LMA, waveform and high-speed video data. This flash was a Type-II BFB flash that produced four strokes to ground, and exhibited a short continuing current during the later return strokes. Dart leaders, attempted dart leaders and K-leaders were observed. In particular,

fast K-leaders were observed *during* the cloud-to-ground leader stage. The K-leaders caused a brief enhancement in luminosity of the leader channel, as well as an enhancement in the rate of VHF emissions by the leader immediately after each event. The K-leaders, which originate from K-events in the positive breakdown region, assist the negative leader with propagation by supplying negative charge to the channel and heating it, thereby making it more conductive.

Chapter 5 studied another BFB flash using correlated LMA, waveform and high-speed video data. This flash was distant from the laboratory but the leader was visible at high altitude (above 8 km). It was a Type-II BFB flash producing one stroke to ground and two attempted dart leaders.

During the cloud-to-ground leader stage the interesting phenomenon of *branch discharges* was observed. These are transient, bright discharges of a leader branch that has become inactive. The negative charge distributed along a branch can eventually overcome the resistive properties of the inactive branch channel and surge back into the main leader channel. The supplied quantity of negative charge then flows down along the active leader channel toward the leader tips, enhancing the channel luminosity and conductivity.

Another phenomenon during the propagation of the negative leader to ground are waves of retrograde luminosity that are seen to propagate backward, away from the tip of the leader. These events were observed when the leader was between 9 and 6 km altitude and are thought to be surges of positive current away from the leader tip that occur upon the completion of a leader step. Some of these luminosity events were visible over a distance of 1.2 km along the leader channel.

A photograph was obtained of a negative cloud-to-air leader at 11 km altitude, which shows streamers at discrete locations along the leader channel, as well as a "space stem"—an unconnected segment of leader channel that is in the process of becoming a new leader step. Similar unconnected leader segments were also observed at the negative leaders at 3 km altitude in two photographs of other BFB flashes.

From high-speed video, LMA and photographic observations, the step length of a negative leader is found to be on the order of 200 m at 11 km altitude, 15–30 m at 6 km altitude and 16 m at 3 km altitude.

Chapter 6 discussed eight other BFB flashes. It was found that the intracloud negative and positive breakdown in BFB flashes is often asymmetric in extent, suggesting a lateral displacement of the two major charge regions. This displacement is possibly an effect of wind shear.

7.2 Main conclusion

The main motivation for this work has been to find a possible cause of the transition from impulsive to apparently continuous VHF emissions of negative breakdown. BFB flashes provide an excellent means to study this, because these flashes produce negative leaders that propagate from high altitude down to ground, often outside the cloud.

It is found that this transition manifests itself as an increase in the *rate* of VHF emissions (not power) and is most likely caused by two effects.

First, leader steps appear to be shorter in length at lower altitudes than at higher altitudes. The step length of a negative leader at 3 km altitude was found to be about one order of magnitude shorter than the step length of a leader at 8–11 km altitude. Since the velocity of a negative leader does not appear to change significantly as it propagates to lower altitude, the *rate* of the stepping process must increase.

Second, the negative cloud-to-ground leader of a BFB flash is observed to produce numerous branches at low altitude, while the leader at high altitude exhibits little or no branching. This would further increase the rate of VHF emissions by the leader at lower altitudes, since there are multiple active leader tips. The more numerous branches at low altitude might be explained by shorter leader step lengths: All else being the same, if a leader has a certain probability of producing a viable branch at each leader step, shorter step lengths translate to more branches produced per unit length on average.

In summary, the transition from impulsive to apparently continuous VHF emissions by a negative leader, as it propagates from high altitude to low altitude, appears to be a consequence of shorter leader step lengths and an increasing number of active leader tips.

A. Instrumentation

A.1 Lightning mapping array

A.1.1 Principle of operation

A typical lightning mapping array (LMA) is composed of 10–12 stations (16 in the case of the Langmuir LMA in 2009–2010) which operate autonomously and independently of each other. Each station utilizes a 25 MHz oscillator which is accurately synchronized to GPS time using an onboard GPS receiver.

An LMA station typically receives VHF emissions from lightning in the 60-66 MHz band and uses a logarithmic detector to accurately time-tag peak-power events within successive time windows of a specific length. This window length is always set to 10 μs for the Langmuir LMA, while the standard window length for operational LMAs is 80 μs. At an oscillator frequency of 25 MHz the timing accuracy is 40 ns. The peak-power events together with their arrival times are stored locally on the station as (P, t) pairs, informally called *triggers*.

For processing, triggers from all stations are analyzed and suitable combinations are selected for data inversion, yielding three-dimensional lightning VHF source locations and time. The location accuracy is typically 6–12 m RMS horizontally within the network and 20–30 m in altitude [*Thomas et al.*, 2004]. Outside of the network the location accuracy decreases by a factor of $1/r^2$ in range and altitude, and by a factor of $1/r$ in azimuth.

The data processing algorithm is computer-intensive, with a run time that depends very strongly on the window length (smaller windows taking much longer to process) and the number of stations active in the array (more stations producing more triggers to do combination searches on).

The LMA is highly sensitive to VHF emissions from electrical breakdown, and routinely locates sources of 100 mW or lower source power over the network. It locates negative breakdown quite well, but positive breakdown (due to the much weaker VHF

emission of positive leaders) less so. Positive breakdown is often masked by negative breakdown when they occur concurrently, which is the case in natural lightning (Section C.1). The higher sensitivity to negative breakdown does have the advantage that the polarity of lightning can usually be determined from the processed data and charge layers in storms can be identified.

A.1.2 History of the Langmuir Laboratory LMA

The LMA of Langmuir Laboratory has been continually expanded and improved over the past years. Initially, starting in 2001–2002, eight stations were deployed on Magdalena Ridge in a compact configuration network having a diameter of ~ 3 km. Four additional stations were set up on the plains around the mountain, making the entire array about 50 km in diameter. All station receivers at the time were configured for channel 3 (60–66 MHz). However, interference from distant channel 3 television transmitters compromised data quality due to the relatively high rate of false triggers at the exposed stations on Magdalena Ridge. An attempt was made to shield most stations from a transmitter in Portales, New Mexico by placing their antennas such that the low horizon to the east was blocked by terrain.

In 2008 the decision was made to run the stations in a compact configuration on the ridge at receiver channel 9 (180–186 MHz passband). Although lightning radiates less at higher frequencies, the lower noise floor could have compensated for the loss in sensitivity, yielding a network that would be less susceptible to television transmitter interference or RF noise from nearby electric equipment. However, another television transmitter at channel 9 near El Paso now interfered with the ridge stations. (This was verified by connecting a television set to an LMA antenna and tuning to channel 9, after which a directional antenna was used to determine the signal azimuth.) The semi-coherent interference in the ridge stations now yielded numerous false solutions in the processing, and in fact preempted the location of valid sources, so much so that a fairly restrictive solution-finding algorithm had to be used to obtain usable lightning data.

In 2009 all of the LMA stations were reconfigured to channel 3, and in June of that year television transmitters in the U.S. changed to all-digital broadcasts at higher frequencies, leaving the 60–66 MHz band mostly unused and quiet. From then on, the Langmuir LMA has yielded unprecedented sensitivity and clean VHF source locations.

Also, starting in 2009, more stations were added to the array. In 2009, several stations were moved off-ridge to the lower plains. This was done in an attempt to reduce the number of false solutions (chance correlations) due to local corona on the ridge at high electric field, as well as to improve location accuracy and effective coverage further out from the ridge. Three LMA stations of the portable design were

not used elsewhere and these were then temporarily installed on the ridge locations left by the stations that were moved.

In 2010 all permanent LMA stations were converted to solar power, further reducing their noise background. A total of 17 stations were operational in 2010, of which two were co-located at Langmuir Laboratory. A map of the LMA station configuration in 2010 is shown in Figure A.1.

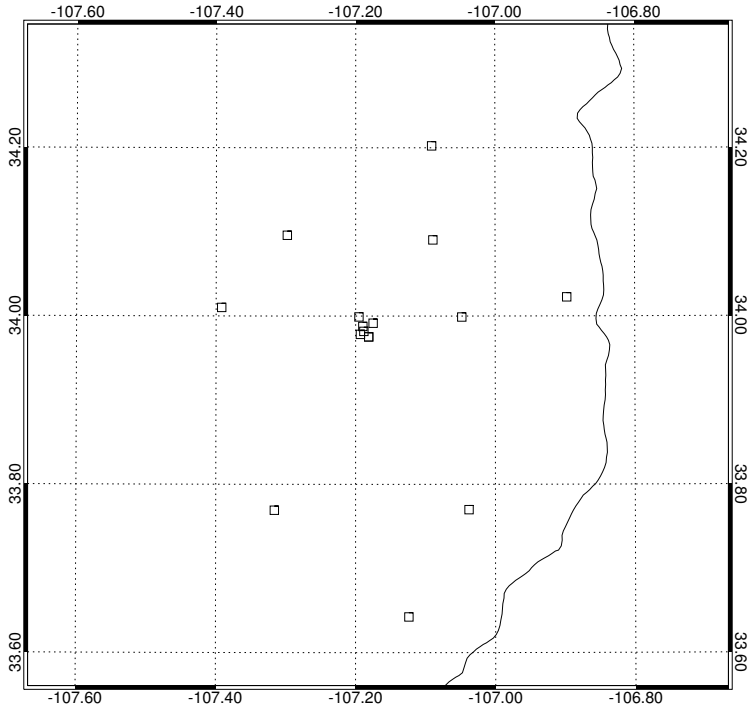

Figure A.1: A latitude–longitude plan view of the configuration of the Langmuir Laboratory LMA stations (small black squares) in 2010.

A.1.3 Operation

All LMA stations are run in 10 μs mode (detecting peak-power impulsive VHF radiation in successive windows of 10 μs in length) and listen in the 60–66 MHz band (channel 3). Their threshold is automatically adjusted once per minute (if necessary) to yield an average of approximately 1,000 triggers per second, or 1% of the maximum trigger rate. Stations have typical noise background levels on the order of -85 to -90 dBm.

Starting in 2010, all stations broadcast a reduced dataset over the wireless commu-

nications network that is processed in real-time by a central processing computer. That processed data is then broadcast over the network and used by real-time display software. The latency of 2 seconds is short enough to monitor lightning in real-time and proved to be very helpful in identifying flash types during waveform data acquisition.

The two co-located stations at the Annex of Langmuir Laboratory were always run as a co-located receiver pair, one at channel 3 (60–66 MHz) and the other at another frequency. That other frequency was, every summer, successively changed from channel 2 to channel 10 (including channel 3), and lightning from a suitable thunderstorm was recorded with both stations at each frequency pair, in a direction that would not cause one of the two stations' antennas to be blocked by the nearby main building. Data from this receiver pair is invaluable in continuing to better understand and improve upon LMA data processing and the LMA itself.

A.2 Log-RF

The logarithmically-detected waveform of a 60–66 MHz LMA receiver was digitized continuously. This waveform was obtained at the output of the LMA logarithmic amplifier and the input of the A/D converter. Since this signal is identical to that which is peak-detected by the LMA, and is sensitive to low-power events, it is an important part of the set of waveforms recorded during these studies.

The LMA station that provided the log-RF waveform also sampled it by peak-detection, which facilitates the time and power calibration of the waveform.

A.3 Slow and fast antennas

An inverted salad-bowl-type slow/fast antenna system was installed on the observation deck of the Langmuir Laboratory Annex to record slow and fast electric field-change (ΔE and fast ΔE) waveforms. These waveforms were digitized along with the other broadband and log-RF waveforms and thus share the same time base.

The slow antenna has a relaxation time constant of 10 seconds and has six different gain settings which vary approximately by a factor of 3, yielding an analog dynamic range of 10^3. The fast antenna has a relaxation time constant of 0.1 ms and a higher gain than the slow antenna ($\times 100$). The bandwidth of both the ΔE and fast ΔE waveforms is on the order of 1 MHz.

Part of the difficulty in operating the slow and fast antenna is in determining the correct gain setting based on lightning range, type, background electric field strength

(giving a bias in output voltage), and frequency of flashes. Since the noise level of both waveforms is several tens of mV even at the least sensitive gain setting, choosing an optimal gain setting was important.

A.4 Rohde & Schwarz HE010 broadband antenna

The Rohde & Schwarz (RS) HE010 broadband antenna is a vertical active rod antenna of the monopole design, 1000 mm in length. It can be used for electric field measurements at frequencies between 10 kHz and 80 MHz. It has a highly linear impedance converter to convert the high-impedance input voltage of the antenna to an output voltage that is mostly frequency-independent and that can be calibrated to measure the (vertically polarized) electric field strength.

The antenna factor k as specified by the manufacturer is about 17 dB on average over the usable bandwidth. This antenna factor is defined as

$$k = 20 \log \left(\frac{E_z}{V_{\text{out}}} \right) \tag{A.1}$$

where E_z is the vertical component of the electric field $\mathbf{E}$ in V m^{-1} and V_{out} is the antenna output voltage (at 50 Ω impedance). E_z is related to the effective antenna length L and input voltage V_{in} by

$$E_z = \frac{V_{\text{in}}}{L} \tag{A.2}$$

L is related to the physical antenna length h by $L = H + h/2$, where H is the antenna mast height. For the lightning studies in this work $H = 0$, as the broadband antenna was mounted on an aluminum ground plane of about 80×80 cm in size. This ground plane was supported by wooden blocks about 10 cm above the observation deck of the Annex building, as far from surrounding metal structures as possible. This configuration was far from optimal and reflections and shielding from nearby metal structures and buildings are likely, but the antenna was better shielded against high-voltage transients from nearby lightning.

Given k as specified by the manufacturer, the vertical component of the electric field E_z can be calculated from V_{out}, which is sampled by the A/D converter.

When used for lightning studies, the output waveform of the Rohde & Schwarz antenna tends to be dominated by large-amplitude field changes associated with return strokes and K-changes. In order not to clip the waveform, the input range of the A/D converter had to be adjusted accordingly, leaving less dynamic range for the smaller-amplitude high-frequency components. Without high-pass filtering the antenna is most useful for lightning electric field recordings in the lower frequency range from

0.01 to approximately 10–20 MHz, and the associated spectrograms calculated from the time-domain waveforms are plotted logarithmically in frequency.

To minimize undersampling the RS antenna output at the usual sampling rate of 200 MS/s, its output was filtered by a custom-made low-pass filter with a passband of 0.3–100 MHz and stopband at 120 MHz (with an attenuation $\geq$ 40 dB at 120 MHz). This filter was inserted between the antenna output and the input to the A/D converter.

A.5 Sirio SD1300N broadband antenna

The second broadband antenna used in these studies was manufactured by Sirio, model SD1300N. It is of the "discone" design, which is a single cone with its apex pointing upward and a disc mounted on top. Both the cone and disc are constructed of steel rods. The antenna has a usable bandwidth of 25–1300 MHz and has a geometric gain pattern similar to that of a dipole. A vertical element was mounted on the disc that improves reception at the lower frequencies (mostly around 50 MHz). According to the manufacturer, this vertical element negatively affects performance at the higher frequencies, but since the antenna was low-pass filtered at 100 MHz this did not matter. The vertical element did, however, create a complex frequency response.

The antenna was configured in a manner similar to an LMA receiver. A low-pass filter (identical to the filter used for the Rohde & Schwarz antenna) was mounted on the antenna mast between the antenna and a Channel Master 7777 preamplifier, identical to the type used in LMA stations. A second, identical low-pass filter was installed between the power injector for the preamplifier and the A/D converter.

The Sirio antenna was used to augment the Rohde & Schwarz broadband antenna, since the higher frequency components from lightning tend to be poorly resolved by the latter (due to the limited dynamic range of the A/D converter and high-amplitude low-frequency components of lightning RF emissions). The output of the Sirio antenna lacked these components, allowing a higher input gain to be set for the A/D converter.

The Sirio antenna was mounted on a metal mast 5 feet in height at the northwest corner of the Annex observation platform. It was directly under an overhead ground wire (for personnel lightning protection) to reduce the chance of lightning damage, particularly to the expensive digitizers. However, the waveforms were highly susceptible to effects of corona, most likely emitted from sharp protrusions on the overhead ground wire. This limited its usefulness for overhead storms; its optimal range of operation was for storms that were 5–20 km distant.

A.6 Computation of spectrograms

In these studies the broadband waveform data was always plotted in the frequency domain as a set of spectrograms, since these convey much more information than the time-domain waveforms. The calculation of these spectrograms is outlined here.

The spectrograms are calculated in IDL using its built-in Fast Fourier Transform (FFT) function. The time interval being plotted was subdivided into 602 windows (which happens to be the pixel-width of the various plot panels in the IDL software). Each of these windows contains the same number of samples in both time-domain broadband waveforms. In order not to skip samples, the next-higher power of 2 was chosen as the number of samples represented in each window; an integer power of 2 for the number of samples greatly improves computational speed of the FFT function. There is therefore almost always some overlap of samples between successive windows, but never more than twice the number of samples in a window.

The FFT function returns an array with the complex amplitudes of all frequency components. Only the positive frequencies are selected and the absolute value is taken. These frequency amplitudes are then stored at the proper time in a two-dimensional image array. The time associated with the FFT is taken to be at the middle of each window.

Next, the spectrogram is converted to logarithmic amplitudes (intensities) to accentuate small-amplitude features. Then it is normalized to values between 0.0 and 1.0, and a simple image transformation is carried out by applying contrast and brightness adjustments. The contrast a is a number that multiplies all log-intensity values and the brightness b is an offset. When these adjustments are made, the image is mapped to a color table of 256 colors. The image transform is therefore:

$$\begin{aligned} G(f,t) &= \log_{10}|F(f,t)| \\ H(f,t) &= \frac{G(f,t) - G_{\min}}{G_{\max} - G_{\min}} \\ I(f,t) &= aH(f,t) + b \end{aligned} \tag{A.3}$$

where $F(f,t)$ is (the positive part of) the original Fourier transform. For $G_{\min}$ the minimum value of $G(f,t)$ or -12 is taken, whichever is larger. (The minimum and maximum values of $G(f,t)$ are calculated from the entire spectrogram, and -12 is substituted for all values of f and t for which $G(f,t) < -12$.) $I(f,t)$ is the normalized intensity of the spectrogram that is mapped to a color table.

When plot time intervals are relatively long, the windows used in calculating the FFT function contain relatively many samples. Hence $F(f,t)$ has a large number of frequency components for each time value and it is necessary to downsample the spectrogram along the frequency dimension. This is done by taking the mean value of a number of successive frequency components for each time value.

The spectrograms are only used qualitatively in these studies and use different contrast and brightness adjustments in each case.

A.7 Data acquisition system

A.7.1 Digitizers

Six waveforms in total were typically recorded for each lightning flash: log-RF of 60–66 MHz, log-RF of the second LMA station at a variable center frequency, slow ΔE, fast ΔE, and the two broadband waveforms from the Rohde & Schwarz and Sirio antennas. A set of two digitizers were used to sample these waveforms: a Gage CompuScope 8244 (CS8244) and a Gage CompuScope 12400 (CS12400).

Gage CompuScope 8244

This digitizer has four single-ended analog inputs and can sample at a maximum of 50 MS/s at 12-bit resolution. It has 256 MB of onboard memory, which stores up to 1.34 seconds of recording time when used with all four analog input channels at 25 MS/s, which was generally done for these studies. It has a PCI-bus form factor.

The CS8244 digitizer has an external trigger input and trigger output. The trigger output can be used to trigger the other digitizer. The trigger input was connected both to the other digitizer's trigger output and to a hand-operated trigger switch.

Gage CompuScope 12400

This digitizer is very similar to the CS8244 model except for its higher sampling frequency of 400 MS/s (single-channel) or 200 MS/s (dual-channel). It has 1 GB of onboard memory, also allowing 1.34 seconds of recording time at 200 MS/s for two channels. It has two analog input channels (at 50 Ω or 1 MΩ input impedance, which is user-selectable in software) that are sampled at 12-bit resolution, which were used to sample the broadband antenna waveforms. It also has an external trigger input and trigger output with the same arrangement as the CS8244 board.

Host computer

The two Gage digitizers were installed in a desktop computer and data acquisition software was written in Visual C++ to control the boards in a graphical user inter-

face. It was necessary that the recorded waveforms could be previewed on the screen to monitor correct gain settings and signal amplitudes and to save only the more interesting and high-quality lightning data. The digitizing computer therefore had the functionality of a six-channel oscilloscope (without real-time waveform display).

When the two digitizers are triggered and their full memory is used, it takes approximately 30–40 seconds to read out all data. After triggering, the system can either be rearmed (thereby discarding the waveforms) or the waveforms can be previewed; in the latter case the data are read out from some of the channels and displayed on the screen. The full data can be downloaded and saved to disk, or the system can be rearmed without saving the data.

In 2009 and 2010 a faster RAID-array of hard disks was used to save the data to, improving the download speed, but the PCI bus with its $\sim$ 100 MB/s throughput still limits the transfer. In practice the system is down for at least 30 seconds after a trigger if the waveform data is stored to disk.

The same computer also controlled the high-speed video camera.

A.7.2 Triggering

Triggering of the digitizers can be done using any of the six waveforms at either a rising or falling edge, or by hand. The choice depends on the characteristics of lightning on the particular day, flash frequency, and whether or not the video camera is also being operated.

The two digitizers were each connected with their trigger output to the trigger input of the other board so both boards were triggered irrespective of which board the trigger occurred on. In addition to this, a hand-controlled trigger switch was also connected to the trigger input on both boards, allowing for manual triggering of the digitizer system.

Triggering on a waveform

For distant lightning ($\gtrsim$ 50 km) typically the log-RF waveform is used for triggering since it has the highest success rate of producing good triggers. For waveform-triggering of not too distant lightning ($\lesssim$ 50 km) the Rohde & Schwarz broadband antenna waveform is suitable, especially so because of the typically bipolar waveforms. The log-RF waveform is generally not suitable for triggering lightning in overhead thunderstorms since it tends to yield false triggers from the effects of nearby corona.

When triggering on a waveform the pre-trigger time was usually set to 25% (335 ms) of the total record length of 1.34 s. This yielded the most consistent complete recordings of flashes.

Manual triggering

When using the high-speed video camera in conjunction with waveform recordings, when lightning was frequent, or when only waveforms of specific types of lightning (e.g. BFB flashes) were desired, the digitizer system was manually triggered. When triggering manually the pre-trigger time was always set to the full record length.

A.7.3 Trigger discrimination

Since one needs to be selective in what the digitizer system triggers on, particularly when several thunderstorms are in the vicinity, the digitizer system requires full attention and additional sources of information are most helpful to increase chances of capturing high-quality waveforms. If this is not done properly, the system tends to trigger too often on either distant or uninteresting flashes and this precludes flashes of interest from being triggered on. This is why it is unprofitable to operate the digitizer system autonomously, although it can do so.

For the 2006–2010 lightning studies at Langmuir Laboratory a number of indicators were used to try to tell triggers from flashes of interest from false or uninteresting triggers, thereby maximizing the duty cycle and success rate of the digitizer system.

Thunder and/or scattered light

For very close lightning (within 300 m) the thunder and scattered light would obviously indicate a valid trigger. Such close lightning generally produces clipped waveforms and numerous corona pulses in the data. However, triggering on such close flashes was always attempted.

Direct observation

Waveform-triggering in conjunction with a visible lightning flash (either –CG or BFB, or sometimes a low-level IC) often indicates a good trigger. The direct observation method was always used when the digitizers were operated in conjunction with the high-speed video camera, but in that case both the camera and digitizers were manually triggered.

Audible corona discharge

For relatively close lightning (within a range of $\sim$ 10 km) the rapid onset of (or reduction in) audible corona discharge can be a clear indicator that a flash occurred. This is particularly helpful during the daytime when the flashes (in particular IC flashes) are undetected visually.

Electric field mill

For several years, the output of an electric field mill was used to decide what type of lightning might be triggered on; with a thunderstorm overhead or in the direct vicinity, the electric field excursion together with thunder signatures would usually give a rough indication of what type of lightning occurred. The field mill was also used when triggering manually, but with varying success due to its slow sampling rate of 1 sample per second.

Optical transient detector

A transient detector with a photovoltaic cell and flash counter was installed in the Annex Tower room. This detector produces an audible tone when the ambient brightness changes rapidly, such as during a lightning flash. This detector does not detect distant IC flashes very well and may trigger on raindrops, rendering the detector mostly useless for detecting small-amplitude light changes. However, it is a fairly reliable method of trigger discrimination, particularly since its sensitivity can be adjusted.

LiveLMA

LiveLMA, the program used to monitor lightning in real-time (with a latency of $\sim$ 2 seconds) can also be used in conjunction with both waveform and manual triggering.

When triggering is done on any of the waveforms, the digitizer system waits for a user response after triggering to either download the data or rearm the system. It takes two seconds for a flash to be plotted on the LiveLMA display, which then immediately provides feedback on what type of flash, if any, was triggered on. This method works well if lightning is not too frequent.

When triggering manually in conjunction with LiveLMA, the recording length of the digitizers is increased to 2.68 seconds. This requires slightly under-sampling the log-RF waveforms at 10 MS/s instead of the required 12 MS/s, and only sampling the

Rohde & Schwarz antenna waveform with the two-channel digitizer in single-channel mode. The LiveLMA display is watched and the digitizer system is triggered by hand as soon as a flash of interest is displayed.

Monitoring LiveLMA (either with waveform-triggering or triggering by hand) has proven to be by far the best discriminatory information to use in conjunction with digitizer triggering. In 2010 it even allowed triggering on precursor-intracloud events and was quite helpful in capturing BFB flash waveforms. Also, the real-time LMA display indicated at which flank of a storm BFB flashes were occurring and in what direction to aim the high-speed video camera. As an added benefit, it immediately indicated if there was a problem with one or more of the LMA stations.

A.8 High-speed video

The high-speed video camera is a Vision Research Phantom v7.3 with monochrome sensor, which is digitized at 14 bits per pixel. Its maximum resolution is 800 × 600 pixels and it can acquire up to 6600 frames per second (FPS) at that maximum resolution; the frame rate is limited to 6400 FPS when the camera is synchronized to GPS. At this resolution and frame rate, the onboard 16 GB of memory allows up to 2.8 seconds of recording time before the buffer fills up and must be read out or deleted. The memory can be partitioned into segments to allow more than a single recording; for these studies it was partitioned into three buffers of equal length of about 0.9 seconds. The camera could therefore be triggered three times (even in rapid succession) before video data had to be read out. The transfer of data takes relatively long; over the 1 Gbit ethernet link of the camera it takes about 8 minutes for the entire 16 GB of memory to be transmitted to the host computer.

A.8.1 Time reference

The high-speed video frame acquisition can be synchronized to GPS using the IRIG-B standard. In this mode, the exposure of the n^{th} frame in a second starts at

$$t_n = t_0 + (n-1)t_{\text{f}} \tag{A.4}$$

where t_0 marks the beginning of the GPS second and the frame time interval t_{f} is related to the frame rate r as

$$t_{\text{f}} = \frac{1}{r} \tag{A.5}$$

The exposure time t_{e} can be selected such that $t_{\text{e}} < t_{\text{f}}$. It cannot be equal to t_{f} due to the time required to read out and digitize the sensor data.

The IRIG-B time reference is encoded for each frame at the end of the exposure *plus* the read-out (or inter-frame) time. For example, for the fourth frame in a second, when synchronizing the camera using IRIG-B, at a frame rate of 6400 FPS and an exposure time $t_\mathrm{e} = 10\ \mu$s, the frame interval time t_f, inter-exposure time t_d, exposure start time $t_\mathrm{e,start}$, exposure end time $t_\mathrm{e,end}$ and the IRIG timestamp t_IRIG are:

$$\begin{array}{lll} t_0 & & = 0.000000000\ \mathrm{s} \\ t_\mathrm{f} & = \frac{1}{6400}\ \mathrm{s} & = 0.000156250\ \mathrm{s} \\ t_\mathrm{d} & = t_\mathrm{f} - t_\mathrm{e} & = 0.000146250\ \mathrm{s} \\ t_\mathrm{e,start} & = t_0 + 3 \cdot 156.25\ \mu\mathrm{s} & = 0.000468750\ \mathrm{s} \\ t_\mathrm{e,end} & = t_\mathrm{e,start} + 10.0\ \mu\mathrm{s} & = 0.000478750\ \mathrm{s} \\ t_\mathrm{IRIG} & = t_\mathrm{e,start} + 156.25\ \mu\mathrm{s} & = 0.000625000\ \mathrm{s} \end{array} \tag{A.6}$$

The time t_IRIG is the time that the frames are tagged with in the .cine file format of Vision Research. An accuracy of 1 μs in the IRIG-B timing is quoted by the manufacturer.

A.8.2 Sensor dimensions

In the file header of each recorded .cine file the two resolution values named bitmapInfo.biXpelsPerMeter and bitmapInfo.biYpelsPerMeter are specified to be 45454 (in units of pixels m^{-1}), which represent the sensor resolution in x (width) and y (height). To verify this it was decided to measure the sensor resolution by an indirect method. Although the sensor itself could be measured, this would be risky since it can be scratched or otherwise damaged.

The video camera was mounted on a tripod and fitted with a lens of 85 mm focal length. An image of a test card, mounted on a board at a specific distance from the front element of the lens and perpendicular to the optical axis, was then acquired. After this, another image of the test card was then acquired with a Nikon D700 still camera, fitted with the same lens and set at exactly the same distance. The pixel dimensions of the test card in both images were then measured. The sensor of the D700 has known spatial and pixel dimensions and from these the sensor dimensions of the Phantom v7.3 were calculated to be 17.71 mm wide by 13.26 mm high. This gave a resolution of 45168 pixels m^{-1} in the horizontal dimension and 45249 pixels m^{-1} in the vertical dimension, with an estimated error of $\sim 0.5\%$ (due mostly to the inaccurate measurement of the test card dimensions on the 800×600-pixel image).

The sensor resolution as indicated in the file headers is within the range of the measured resolution, both in the horizontal and vertical dimensions. It is therefore assumed that the resolution $h = 45454$ pixels m^{-1} is correct and should be used for all distance measurements on the high-speed video imagery. Assuming this, the physical dimensions of the imaging area of the sensor are (for a full frame) $800/h = 17.60$ mm and $600/h = 13.20$ mm.

A.8.3 Optimal exposure settings

In a basic optical camera system the amount of light reaching the sensor or film can be controlled by setting the lens aperture (controlling light flux), the exposure time (controlling the duration of exposure) and the sensitivity of the recording medium. With the Phantom v7.3 the sensitivity of the sensor cannot be adjusted, so a correct exposure can only be controlled by either the lens aperture or the exposure time.

For lightning, it is better in most cases to maximize the exposure time and adjust the aperture accordingly, rather than choosing a short exposure time in combination with a large aperture (i.e. a small f-ratio). Although lightning leaders are imaged at better *stop-action* at short exposure times, small current pulses and other transient features can be entirely missed due to the relatively long time between exposures (effectively a *dead-time*). At longer exposures lightning leaders appear to be lengthened due to their motion during the exposure, but brief channel luminosity events are not missed. During the lightning studies at Langmuir Laboratory in 2009 and 2010 the exposure time was therefore always maximized. Since (in most cases) it was desirable to maximize the frame size to 800 $\times$ 600 pixels and the IRIG-B time reference was a necessity, the frame rate was limited to 6400 FPS, yielding an exposure time interval of 156.25 μs and an exposure time of 150 μs, which was the maximum that could be selected by the software. The inter-frame time of 6.25 μs is, apparently, needed for sensor read-out.

A.8.4 Overlaying LMA data on video frames

When correlating high-speed video imagery with LMA data it is helpful to be able to overlay VHF sources located by the LMA on video frames. The mathematical formulation describing how this is done is outlined below.

To overlay sources on a video frame a point-projection must be made of a VHF source s with known coordinates (x_s, y_s, z_s, ct_s) in a certain reference frame onto an image plane with spatial dimensions d_x and d_y.

When the coordinate conversion is performed it is important to account for the camera frame time, which is later than the VHF source time t_s, when overplotting LMA data on a video frame.

ECEF coordinate transform (WGS-84)

The most obvious choice for the coordinate frame of the VHF source is the same frame as used by the LMA processing code and display software, which is the frame

tangent to the Earth's surface at some local coordinate origin. This frame is derived from the Earth-Centered, Earth-Fixed frame (ECEF) as defined in the 1984 World Geodetic System (WGS84). This assumes an oblate-spheroid Earth with semi-major axis $a = 6378.137$ km and semi-minor axis $b = 6356.752314245$ km, usually rounded to 6356.752 km. The origin of the ECEF coordinate frame lies at the Earth's center of gravity, with the x-axis bisecting the 0° meridian and the y-axis bisecting the +90° meridian at the equator; the z-axis points upward through the North Pole.

The eccentricity e and normal $N(\phi)$ are given by

$$e = \frac{a}{b} \tag{A.7}$$

$$N = \frac{a}{\sqrt{1 - e^2 \sin^2 \phi}} \tag{A.8}$$

and a coordinate of geodetic latitude ϕ, longitude λ and height h has ECEF coordinates

$$\begin{aligned} x &= (N + h) \cos\phi \cos\lambda \\ y &= (N + h) \cos\phi \sin\lambda \\ z &= (N(1 - e^2) + h) \sin\phi \end{aligned} \tag{A.9}$$

To express an ECEF (x, y, z) coordinate of a VHF source in a local coordinate frame, tangent to the surface at some coordinate (ϕ_0, λ_0), a coordinate transformation is used that consists of a translation followed by a rotation. The translation translates the ECEF coordinate origin to a new, chosen origin at (ϕ_0, λ_0, h_0) with ECEF coordinates $\mathbf{r}_0 = (x_0, y_0, z_0)$. The rotation consists of a left-hand rotation along the z-axis over an angle ξ followed by a left-hand rotation along the (new) x-axis over an angle ψ, where

$$\begin{aligned} \xi &= \frac{\pi}{2} + \lambda_0 \\ \psi &= \frac{\pi}{2} - \phi_0 \end{aligned} \tag{A.10}$$

Thus, the transformation takes the form

$$\mathbf{r}' = R_1(\mathbf{r} - \mathbf{r}_0) \tag{A.11}$$

where

$$R_1 = R_\psi R_\xi \tag{A.12}$$

with

$$R_\psi = \begin{pmatrix} \cos\psi & \sin\psi & 0 \\ -\sin\psi & \cos\psi & 0 \\ 0 & 0 & 1 \end{pmatrix}, R_\xi = \begin{pmatrix} 1 & 0 & 0 \\ 0 & \cos\xi & \sin\xi \\ 0 & -\sin\xi & \cos\xi \end{pmatrix} \tag{A.13}$$

which yields a resultant rotation matrix, expressed in latitude ϕ_0 and longitude λ_0:

$$R_1 = \begin{pmatrix} -\sin\lambda_0 & \cos\lambda_0 & 0 \\ -\sin\phi_0\cos\lambda_0 & -\sin\phi_0\sin\lambda_0 & \cos\phi_0 \\ \cos\phi_0\cos\lambda_0 & \cos\phi_0\sin\lambda_0 & \sin\phi_0 \end{pmatrix} \tag{A.14}$$

The resulting coordinate frame has the x-axis pointing east, the y-axis pointing north and the z-axis pointing to the zenith, with its origin at (ϕ_0, λ_0, h_0).

Image plane coordinate transform

To indicate a position on the image sensor of the camera, its reference frame is chosen such that the x-axis indicates the horizontal pixel coordinate, the y-axis the vertical pixel coordinate and the z-axis lies collinear to the optical axis, pointing into the camera (Figure A.2). To express a VHF source coordinate in the camera reference frame another coordinate transformation must be carried out.

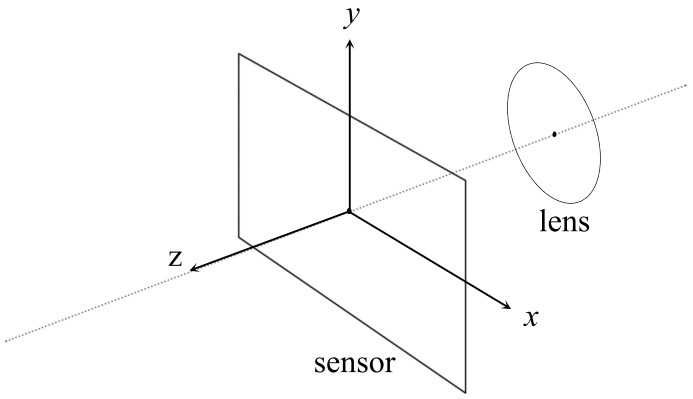

Figure A.2: The camera coordinate frame. The coordinate origin lies at the center of the imaging sensor, with the y-axis pointing up and the z-axis pointing into the camera, collinear with the optical axis.

The camera is assumed to have azimuth angle α, where $0° \leq \alpha < 360°$ (with respect to north), elevation angle η, where $-90° \leq \eta \leq +90°$, and tilt angle τ, where $-180° < \tau \leq 180°$ and $\tau > 0$ indicates that the camera is tilted in a counterclockwise direction as seen from behind the camera, looking along the optical axis. These three parameters along with its latitude, longitude and altitude uniquely determine the orientation and position of the camera.

To transform the coordinates (x_s, y_s, z_s) of a VHF source s located by the LMA from the local tangent coordinate frame to that of the image frame, three rotations need to be done. An easy way to think of this is to point the camera to the nadir in the source coordinate frame (with north oriented along the positive y-axis) and taking the inverse of that transformation. That transformation is:

1. Rotation along the z-axis over an angle $-\alpha$
2. Rotation along the x'-axis over an angle $\theta = \frac{\pi}{2} + \eta$
3. Rotation along the z''-axis over an angle τ

This results in the new coordinate frame oriented in such a way that the camera points toward the nadir in the source coordinate frame. The resultant rotation R_2^{-1} for this transformation is

$$R_2^{-1} = R_\tau R_\theta R_{-\alpha} \tag{A.15}$$

Since all matrices are orthonormal, the inverse transformation R_2 that is needed therefore becomes

$$R_2 = R_\alpha R_{-\theta} R_{-\tau} \tag{A.16}$$

where

$$R_\alpha = \begin{pmatrix} \cos\alpha & \sin\alpha & 0 \\ -\sin\alpha & \cos\alpha & 0 \\ 0 & 0 & 1 \end{pmatrix} \tag{A.17}$$

$$R_{-\theta} = \begin{pmatrix} 1 & 0 & 0 \\ 0 & \cos\theta & -\sin\theta \\ 0 & \sin\theta & \cos\theta \end{pmatrix} \tag{A.18}$$

$$R_{-\tau} = \begin{pmatrix} \cos\tau & -\sin\tau & 0 \\ \sin\tau & \cos\tau & 0 \\ 0 & 0 & 1 \end{pmatrix} \tag{A.19}$$

and R_2 in terms of camera azimuth α, elevation angle η and tilt angle τ has the form

$$R_2 = \begin{pmatrix} R_{xx} & R_{xy} & R_{xz} \\ R_{yx} & R_{yy} & R_{yz} \\ R_{zx} & R_{zy} & R_{zz} \end{pmatrix} \tag{A.20}$$

where

$$
\begin{aligned}
R_{xx} &= \cos\alpha\cos\tau - \sin\alpha\sin\eta\sin\tau \\
R_{xy} &= \cos\alpha\sin\tau + \sin\alpha\sin\eta\cos\tau \\
R_{xz} &= -\sin\alpha\cos\eta \\
R_{yx} &= \sin\alpha\cos\tau + \cos\alpha\sin\eta\sin\tau \\
R_{yy} &= \sin\alpha\sin\tau - \cos\alpha\sin\eta\cos\tau \\
R_{yz} &= \cos\alpha\cos\eta \\
R_{zx} &= \cos\eta\sin\tau \\
R_{zy} &= -\cos\eta\cos\tau \\
R_{zz} &= -\sin\eta
\end{aligned}
\tag{A.21}
$$

To improve the efficiency of numerical computations the two coordinate transforms (from ECEF-translated to local tangent frame and then to camera frame) are combined in one matrix $R = R_2 R_1$. Thus the full transform can be written as

$$\mathbf{r}'' = R(\mathbf{r} - \mathbf{r}_0) \tag{A.22}$$

where $\mathbf{r}'' = (x''_s, y''_s, z''_s)$ is the vector pointing to the VHF source s in the camera coordinate frame.

Imaging of VHF source

When the VHF source coordinates are expressed in the coordinate frame of the camera image plane, what needs to be done next is to calculate where on the sensor this source would be "imaged". The origin of the coordinate frame is at the center of the image plane, where the optical axis intersects it.

It is important to include the effects of *geometric distortion* in this calculation. Geometric distortion manifests itself as an exaggeration of transverse distances away from the center of the image and becomes more pronounced with wider-angle lenses.

Through a "perfect" camera lens (without *optical distortion*) the image of a point-object appears at an equal angle to the optical axis as the object itself, as indicated in Figure A.3. In the case of the high-speed video camera, and still cameras in general, the image is made on a planar surface, where equal angles translate to larger distances on the image plane away from the optical axis (center of the image). To correctly "image" a VHF source (e.g. to plot a point where the VHF source would have occurred) the following calculations need to be done:

1. Determine the angle β between the line from camera to source and the optical axis;

2. Calculate the image distance away from the center of the image plane corresponding to this angle;

3. Calculate the polar angle γ of the source in the image plane;

4. Calculate the coordinates x_i and y_i of the source in the image plane;

5. Convert x_i and y_i to units of pixels;

6. Convert VHF source time to camera frame time.

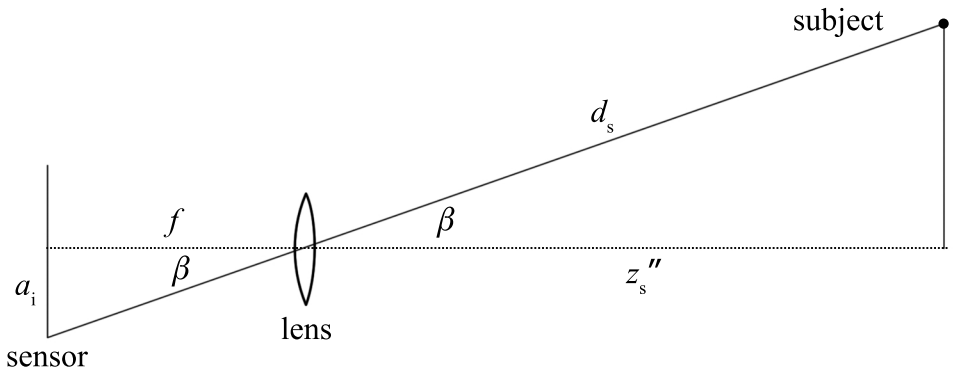

Figure A.3: Imaging of a subject on a camera sensor with a lens of focal length f. The subject is at a distance d_s from the camera lens and its light path is at an angle β with the optical axis.

Figure A.4 indicates the various quantities to be determined in the image plane. The angle β between the light path and the optical axis is

$$\beta = -\cos^{-1}\left(\frac{z_s''}{d_s}\right) \tag{A.23}$$

where $d_s = \sqrt{(x_s'')^2 + (y_s'')^2 + (z_s'')^2}$ is the distance from the VHF source to the camera, and the minus sign is due to the fact that $z_s'' < 0$ for a source in front of the camera. The polar angle γ is

$$\gamma = \tan^{-1}\left(\frac{y_s''}{x_s''}\right) \tag{A.24}$$

When implementing the tangent function (periodic by π) in computer software care must be taken to choose the correct quadrant for γ.

It is assumed (and certainly hoped!) that the VHF lightning source is close to infinity with respect to the lens focal length f. In that case the coordinates x_i and y_i are

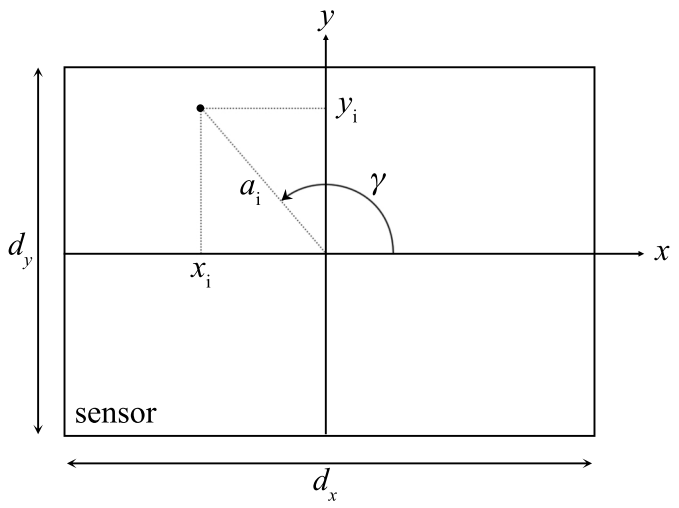

Figure A.4: A subject is imaged on a sensor at coordinates (x_i, y_i). The sensor dimensions are $d_x \times d_y$. The view is toward the front of the camera.

found from

$$\begin{aligned} a_i &= f \tan \beta \\ x_i &= a_i \cos \gamma \\ y_i &= a_i \sin \gamma \end{aligned} \tag{A.25}$$

and the pixel coordinates (u, v) relative to the lower left corner of the image are then determined from

$$\begin{aligned} u &= h \left(x_i + \frac{d_x}{2} \right) \\ v &= h \left(y_i + \frac{d_y}{2} \right) \end{aligned} \tag{A.26}$$

In the case of the Phantom v7.3, the sensor resolution $h = 45454$ pixels m^{-1} (equal in both horizontal and vertical dimensions, i.e. the sensor has square pixels) and the sensor's physical dimensions are (for a full frame) $d_x = 800/h = 17.60$ mm and $d_y = 600/h = 13.20$ mm.

When using a higher frame rate the usable size of the sensor is reduced to compensate for the shorter available time for sensor read-out. This changes d_x and d_y accordingly, but h is fixed for the sensor in question. Therefore, to retain the same image field of view, a wider-angle lens must be used at higher frame rates.

The effects of optical lens distortion (e.g. *barrel*- or *pincushion*-distortion) are neglected here. For the high-speed video camera high-quality fixed focal-length Nikon

lenses were used that show very little, if any, distortion. Also, the sensor of the video camera is smaller (by a factor of 2) than the full 35 mm frame for which the lenses were designed, further reducing the effect of any optical distortion.

Correction for retarded VHF source time

To account for camera frame time, an LMA source with source time t_s is only plotted if it satisfies

$$t_{i,\text{start}} \leq t_s + \frac{d_s}{c} \leq t_{i,\text{end}} \tag{A.27}$$

for the i^{th} frame with exposure start time $t_{i,\text{start}}$ and exposure end time $t_{i,\text{end}}$. The speed of light c is taken to be the value at 600 mbar of 299,792,458.0 / 1.0002 m s^{-1}. The exposure time interval limits are both inclusive since the camera timing accuracy of ~ 1 μs is much larger than the LMA timing accuracy (typically on the order of 40 ns), and close to the exposure start and end times it is unclear if a VHF source time occurs before or after the shutter state change. The camera timing accuracy could be included explicitly in the exposure time limits of equation A.27 if one wants to make sure that all pertinent LMA data is plotted on the frame.

B. Calibration

B.1 Waveform timing calibration

The two digitizers that sample the broadband antennas, slow and fast antennas and log-RF waveforms were free-running during the 2010 studies and no time base was recorded along with the various waveforms. To find the actual trigger time, the log-RF waveform is used as a reference. Since this same waveform is used by the LMA station's digitizer for its peak-detection algorithm, the peak-power values recorded by the LMA station and the digitized waveform can be overlaid and a time shift applied to the waveform data until the various peaks in the waveform overlap with the peak-power events from the LMA (Figure B.1). This is a reliable method of finding the correct trigger time to within the same timing accuracy as the LMA station (40 ns), provided that the LMA station is running and taking data during waveform digitization.

The precise sampling rate of the digitizer at the time of digitization can be found by doing a time calibration on one part of the log-RF waveform and by measuring the time shift between correlated peaks in another part of the waveform. Because the recorded waveforms are generally not longer than 1.34 seconds, a constant sampling rate during this time can be assumed and only two calibrations need to be done.

The time calibration only calibrates the digitizer (CompuScope 8244) that records the log-RF waveforms and the slow and fast ΔE waveforms. The other digitizer (CompuScope 12400) recording the broadband waveforms is also free-running and runs independently from the first. It has a delay in triggering that causes waveform data to be shifted in time. This time is erratic and the best way to time-calibrate the broadband waveforms is to align them with the fast ΔE waveform recorded by the other digitizer. The Rohde & Schwarz broadband antenna records many of the low-frequency (< 1 MHz) sferics that also appear in the fast ΔE waveform, and the same is true for the log-RF waveform and the Sirio broadband antenna, which both record VHF radiation at 63 MHz. All waveforms can as such be calibrated to well within 1 μs accuracy, which was deemed sufficient for these studies.

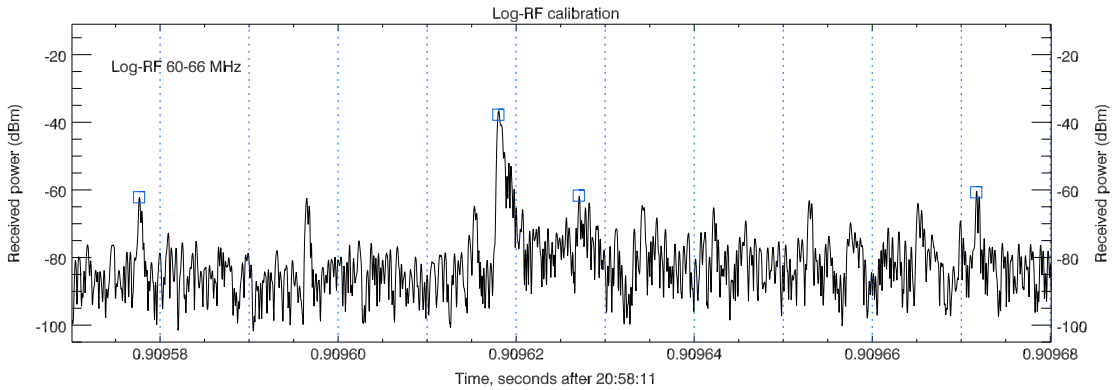

Figure B.1: Calibration of a log-RF waveform in time and amplitude. The blue squares indicate peak-power events recorded by the LMA station. Peak-power events within 10 μs windows (blue dotted lines) are only recorded if the waveform is above a software-adjustable threshold.

B.2 Slow antenna

The slow and fast antennas can be calibrated for electric field strength when the effective surface area of the antenna plate is known along with the value for C, the feedback capacitor in the charge-integrating amplifier. For field changes much shorter than $\tau = RC$ (10 s in the case of the slow antenna) the charge induced on the sensor plate of effective area A_{eff} of the slow antenna by an atmospheric electric field change ΔE is given by [*Krehbiel et al.*, 1979]:

$$\Delta Q = \epsilon_0 A_{\text{eff}} \Delta E \tag{B.1}$$

which produces a change in output voltage ΔV of the charge amplifier

$$\Delta V = \frac{\Delta Q}{C_f} \tag{B.2}$$

Therefore ΔV is proportional to ΔE (if the time scale of the change is short with respect to the characteristic relaxation time of the slow antenna).

A_{eff} can be much larger than the actual area A of the sensor plate, partly due to it being inverted and the electric field lines wrapping around the stand. In practice the instrument needs to be calibrated by experimental methods; a good way is to calibrate it on level ground using another slow antenna as a reference, which is a flat plate that is flush with the ground. Electric field changes detected by that calibration antenna can be calculated more reliably and can be used to find the calibration factor of the inverted-plate slow antenna.

In these studies the slow antenna was suspended over the railing around the roof of the Langmuir Laboratory Annex in a highly complex geometry for electric field cal-

ibrations, and calibration was not required because the ΔE and fast ΔE waveforms from the instrument are only used in a qualitative way in this work.

B.3 Fast antenna

The fast ΔE waveform is derived from the slow ΔE waveform by differentiation using an RC filter with a time constant of 0.1 ms. It is then amplified by a factor of 100. The fast ΔE waveform can therefore be calibrated if the calibration for the slow antenna were known. In these studies, the fast ΔE waveform is only used in a qualitative way, and calibration was therefore not needed.

The units of amplitude in both the slow and the fast ΔE waveforms throughout this work are referred to as "D.U.", or Digitizer Units. The digitizer units in this case are simply the output voltages of the slow and fast antenna instrument as recorded by the high-speed digitizer.

B.4 Broadband antennas

The Rohde & Schwarz broadband antenna can be calibrated to units of electric field strength by using the conversion formulae given in Section A.4, which are provided by the manufacturer. However, for these studies calibration was neither necessary nor desirable, because the spectrograms are discussed in a qualitative manner and a calibration would attenuate the higher frequencies in the spectrograms even more.

The Sirio broadband antenna has a complex gain figure. The vertical element on top of the "discone" design is meant to improve reception at the lower frequencies, but (as can be seen in the various spectrograms) its response in the 25–100 MHz range is far from flat. Like the Rohde & Schwarz spectrograms, the Sirio spectrograms are only used qualitatively.

B.5 LMA

The log-RF waveform used by the LMA stations for peak detection has a known calibration factor to convert from A/D converter counts to received power P_r in units of dBm. With n being the A/D converter count for a sample P_r is equal to

$$P_r \text{ (dBm)} = 0.488n - 110.0 \text{ dB} \tag{B.3}$$

The transmitted source power P_t is related to the received power P_r at a receiver a distance d from the source by

$$P_\mathrm{r} = \frac{P_\mathrm{t} G_\mathrm{t} G_\mathrm{r}}{\left(4\pi \frac{d}{\lambda}\right)^2} \tag{B.4}$$

where G_t is the gain of the transmitter (source) in the direction of the receiver and G_r is that of the receiver. In LMA operations it is assumed that both G_t and G_r equal unity, i.e. the source radiates isotropically and the gain pattern of the LMA receiving antenna (although it is a dipole) is also assumed to be isotropic by approximation.

The factor $(4\pi/\lambda)^{-2}$ depends on the passband frequency of the receiver of an LMA station and equals -8.43 dB for channel 3 (60–66 MHz).

Because VHF sources most likely do not radiate isotropically and the gain pattern of the receiving antennas is not taken into account, the source power estimate by all LMA stations has a large variance and typically the median value from all participating stations is chosen as a best estimate.

B.6 Log-RF

The amplitude of the log-RF waveform recorded by the high-speed digitizer can also be calibrated to units of received power using the same approach as that in Section B.5. However, due to an unknown source of signal attenuation the log-RF waveform data are still offset from the calibrated peak-power events recorded by a LMA station even after calibration, and it was easiest to calibrate the log-RF waveform using the LMA data directly.

To do this calibration an IDL algorithm was written to pick samples from the waveform closest in time to a set of recorded peak-power values from the LMA and calculate the average power offset between each pair of sample and peak power, after which this offset was subtracted from the waveform samples. Figure B.1 shows an example of a log-RF waveform with LMA peak-power events overlaid, which are calibrated both in time and in power.

C. Other observations

C.1 LMA airplane track masking

Figure C.1 shows 5 minutes of LMA data (in 80 μs mode) starting at 21:44:20 UTC on July 23, 2010. An aircraft to the west of the array was creating a track by flying through space charge (a charged ice-crystal cloud) and generating corona discharges. Such discharges likely occur at the "electrostatic wicks" that are mounted near the tips of the wings, horizontal stabilizers and tail fins of aircraft. (A similar example of a VHF-mapped airplane track can be found in *Thomas et al.* [2004].)

The aircraft flew at an altitude of 11.9 km (Flight Level 390) to a bearing of 167 degrees at 925 km/h and was most likely a commercial airliner. At 12 km altitude, it was probably flying through positive charge since the storms on this day were of normal polarity, with upper positive charge over midlevel negative charge, and the charge was probably left there in storm-anvil clouds. The track was mapped by the LMA over a distance of 56 km along the aircraft's flight path.

Interestingly, the track was briefly "interrupted" during lightning flashes. The BFB flash at 21:45:53 UTC was such a flash interrupting the airplane track, and LMA data for this flash is shown in Figure C.2 (at the full 10 μs rate). The plan view of the figure has been zoomed out to also include the position of the airplane, which was about 27 km to the west and 10 km to the north of Langmuir Laboratory at that time.

The interruption of the airplane track is due to the negative breakdown from the lightning flash *masking* lower-power VHF emissions from the corona discharges off the airplane. The log-RF (peak-power) of VHF emissions is time-tagged by each LMA station in successive time windows of 10 μs length, and if a stronger pulse from lightning-associated breakdown occurs in the same time window as a pulse from a weaker corona discharge, that corona pulse is not recorded by the LMA station. The example in this section shows this effect very well. Both the aircraft and the flash are at about equal distances from the main laboratory (and from the center of the LMA); for a number of LMA stations the flash is closer than the aircraft, but for about an

equal number of stations it is farther away, so source distance is not believed to have a significant effect in this case.

A zoomed-in view of the airplane track during the 2.8-second time interval of Figure C.2 is shown in Figure C.3. During this time interval 183 sources were located for the airplane, which was therefore producing corona discharges at a rate of ~ 65 per second.

The source power of the airplane corona discharges (not shown) during the time interval of Figure C.2 is sharply peaked at 100 mW. The source power distribution of the VHF events from the BFB flash is shown in Figure C.4. This figure shows that most of the VHF sources had a source power ranging from -20 to $+25$ dBW, and the negative leader (propagating to the SSE) tends to produce higher-power VHF sources than the positive breakdown in the midlevel negative charge region, with the difference being at least 10–15 dB. The highest-power sources are associated with the return stroke and various K-leaders or dart leaders.

The VHF sources from the aircraft are at the lower end of the VHF source power distribution for the BFB flash, and this is the reason that it appeared to be interrupted (i.e. undetected) during the flash. This effect becomes stronger when the LMA is operated with longer time windows, such as 80 μs or 400 μs, because that increases the probability of concurrent airplane corona and lightning pulses in the same time window. As the windows become shorter, the probability increases that two sources are time-tagged in different windows. It is remarkable that even in such a short time-window mode as 10 μs, the effect is still significant.

This is an indication that the same masking effect may also occur in lightning flashes, with the higher-power VHF emissions associated with negative breakdown masking the lower-power emissions associated with concurrent positive breakdown in LMA time windows. The effect is noticeable in some of the BFB flashes studied in this work: The cloud-to-ground leader transitions from impulsive to apparently continuous breakdown, which masks the VHF emissions from positive breakdown.

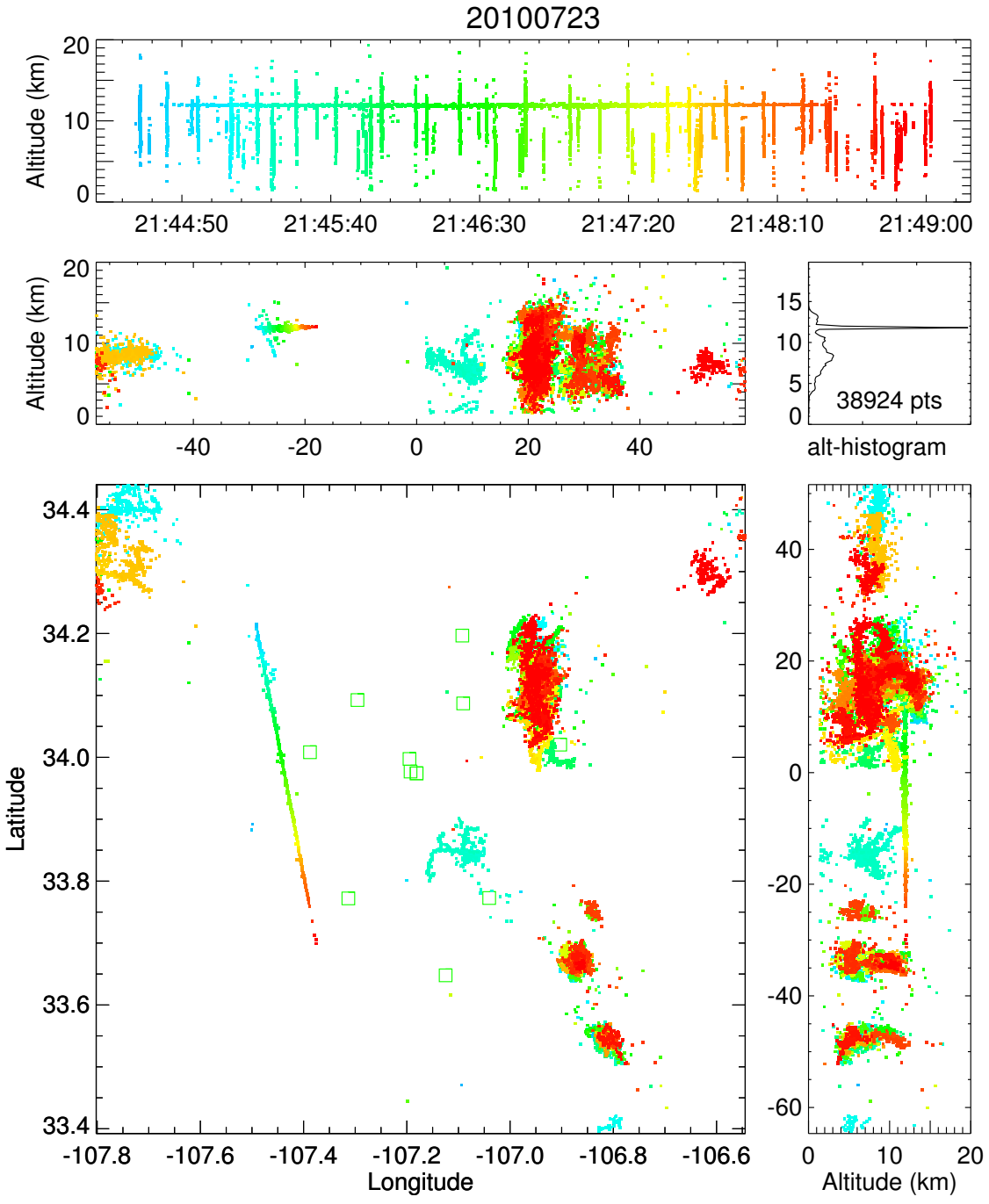

Figure C.1: LMA data (at 80 μs rate) showing several active storms and an airplane track to the west of the LMA during a 5-minute time interval on July 23, 2010.

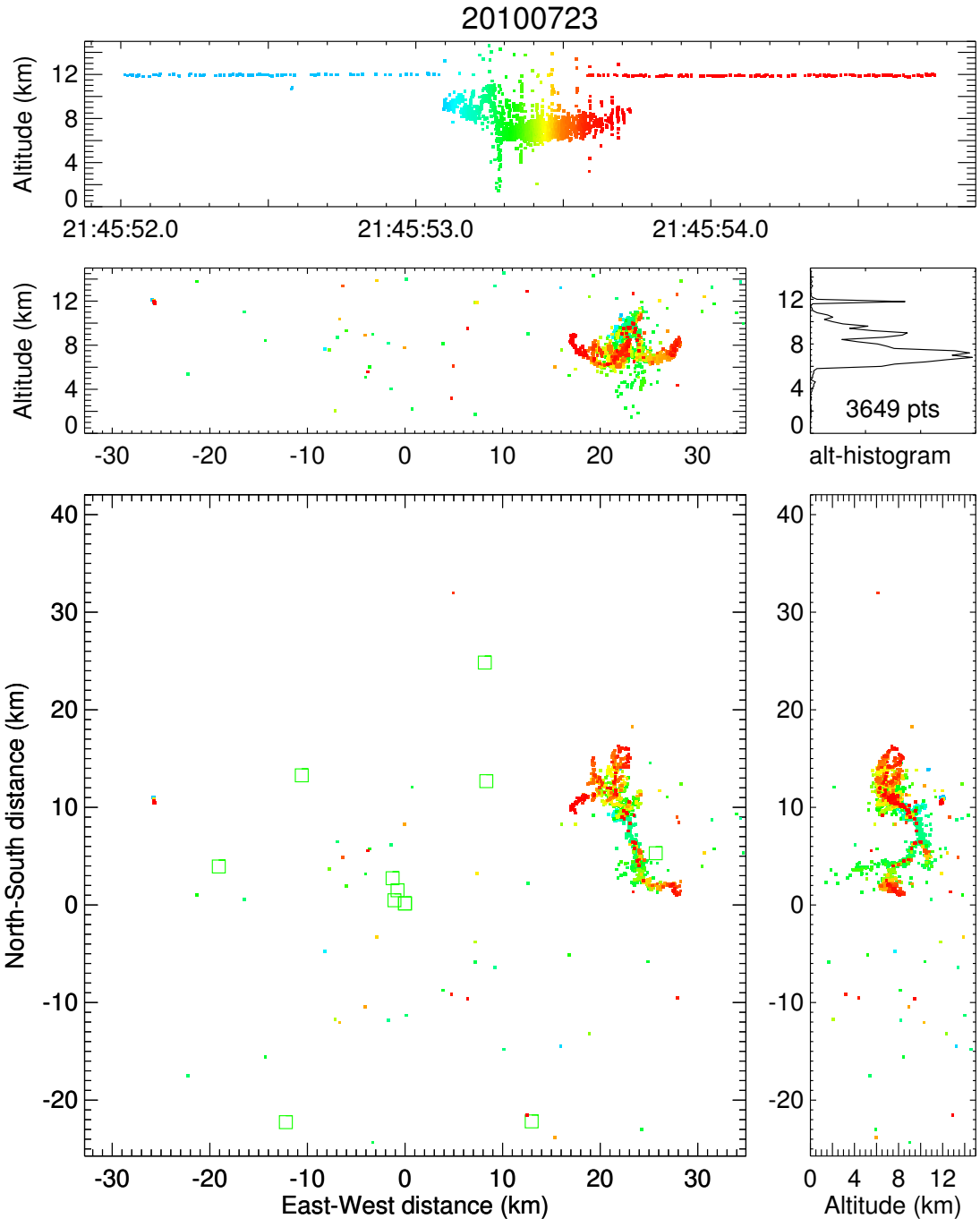

Figure C.2: Three seconds of 10 μs LMA data showing a BFB flash to the east of Langmuir Laboratory and an aircraft producing corona discharges to the WNW. The aircraft is about 26 km to the west and 10 km to the north of the laboratory at $(0, 0)$ in the plan view.

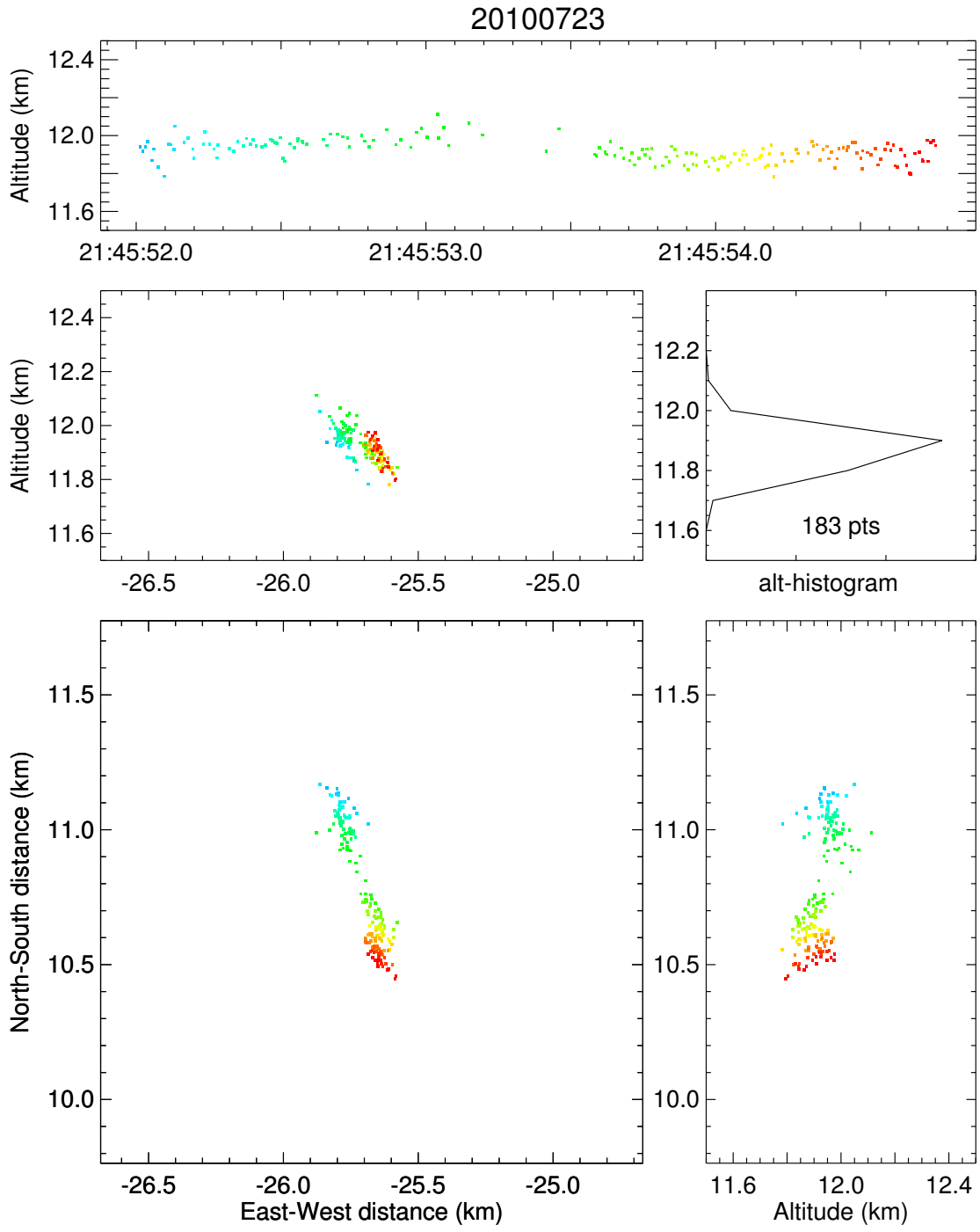

Figure C.3: A detailed view of the corona sources created by the aircraft during a time interval of 3 seconds.

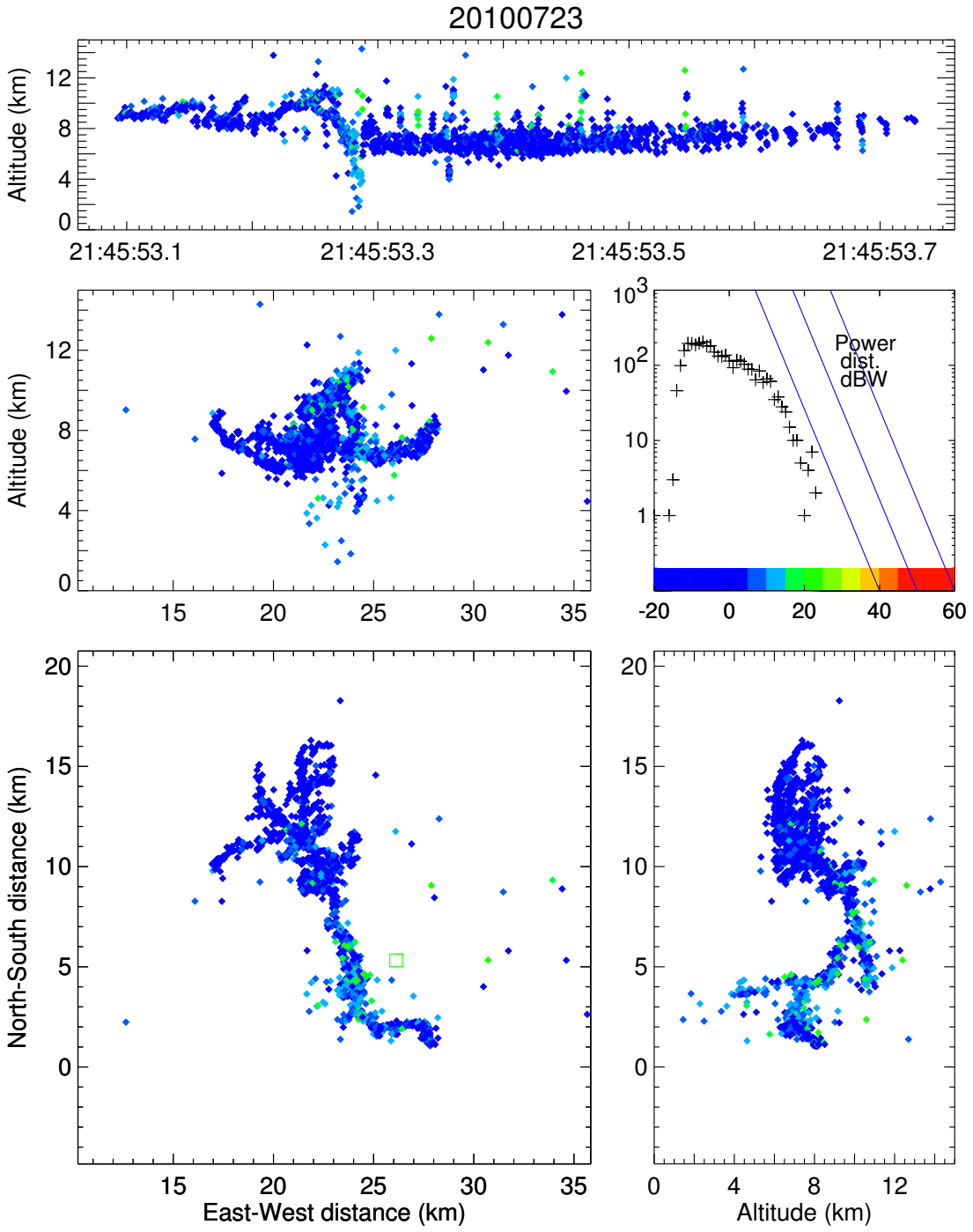

Figure C.4: VHF source power for the BFB flash of July 23, 2010 at 21:45:53 UTC. The VHF sources associated with negative breakdown are at least 10–15 dB stronger than those associated with positive breakdown.

C.2 Unconnected branches

In the evening of July 23, 2010 a storm was positioned between Langmuir Laboratory and the Pound LMA site, with the storm about 10 km from the laboratory. The cloud base was quite low, at about the same elevation as the laboratory (3.2 km above MSL) or a few hundred meters higher, and the lab was quickly clouded in by cold, moist outflow of this storm. Before this happened, two BFB flashes could be photographed with a digital still camera at a range of approximately 4 km.

The camera, a Nikon D700 digital SLR camera, was fitted with a telephoto zoomlens set at 135 mm focal length and was aimed in a NNE direction toward Blue Cut. The lens aperture was set at $f/7.1$ during the first exposure and at $f/9.0$ during the second exposure. The sensitivity of the camera was set at the base setting of ISO 200 and both exposures were 30 seconds in duration.

Photos C.1 and C.2 show the two BFB flashes. The first flash occurred at 04:16:01 UTC and the second at 04:20:50 UTC. Both struck the mountain area north of the Blue Cut LMA station. Although the leaders were only visible along a short length due to intervening clouds, both show an interesting phenomenon of *unconnected branches*. On each photo three such cases can be identified, which are shown in Figures C.5–C.10. These are probably the same phenomenon as the "space stem" that was photographed at a cloud-to-air leader at high-altitude during the August 20, 2010 storm (Section 5.3.2) and show the streamer-to-leader transition during (unsuccessful) leader steps.

Both flashes are identified as BFB flashes from LMA data, which is shown in Figures C.11 and C.12. The leader of the first flash was approximately 4.5 km distant from the camera, while that of the second flash was at a distance of 3.5 km. The D700 camera has a pixel size of 8.45 μm, which at a focal length of 135 mm translates to an actual imaging resolution of 0.282 m/pixel for a leader at 4.5 km distance from the camera, and a resolution of 0.216 m/pixel for a leader at 3.5 km distance.

An estimate of the leader step length can be made by measuring the length of each unconnected branch, or space stem, and adding the length of the gap between the space stem and main leader channel (at a location in line with the space stem). By studying the laboratory spark-gap streak images and diagram from *Bazelyan and Raizer* [2000], adding the lengths of the space stem and the gap is a good approximation for the leader step length. In the photographs from July 24 the various lengths can, of course, only be determined in two dimensions and therefore only give a lower-bound estimate. Also, the estimate depends on the assumption that these space stems do indeed represent unsuccessful leader steps.

The space-stem lengths and gaps as well as the estimates for step lengths are listed in Table C.1. The inferred minimum step lengths are on the order of 10–20 m (an

average of 16 m) for the negative leaders at an altitude of ~ 3 km, which is an order of magnitude smaller than the step length of 200 m for a negative leader at 11 km altitude inferred from Figure 5.1.

Time, UTC	Figure	Stem (m)	Spacing (m)	Step (m)
04:16:01	C.5	19.8	7.5	27.3
04:16:01	C.6	7.6	3.9	11.5
04:16:01	C.7	7.4	4.2	11.6
04:20:50	C.8	3.9	10.7	14.6
04:20:50	C.9	6.2	5.9	12.1
04:20:50	C.10	5.4	13.9	19.3

Table C.1: Six estimates of leader step lengths of the two BFB flashes of July 24, 2010. The length of each space stem and the distance from the near tip of the stem to the main leader channel are also listed.

No streamers or corona are resolved in the two photos due to the very low luminosity of such phenomena; the two photographs shown here were taken with about 8 stops less sensitivity (i.e. a factor of about 4×10^{-3}) than the photograph of Figure 5.1.

Photo C.1: The cloud-to-ground leader of the BFB flash of July 24, 2010 at 04:16:01 UTC. The small triangular object under the arrow is the Blue Cut LMA station. The numbers 1–3 indicate locations of unconnected branches and correspond to the cropped images in Figures C.5–C.7. The leader is estimated to be at a distance of 4.5 km from the camera and the resolution of the photo is 0.28 m/pixel at the location of the leader. The photograph reproduced here represents a transverse area (width$\times$height) of approximately 966×799 m.

Photo C.2: The cloud-to-ground leader of the BFB flash of July 24, 2010 at 04:20:50 UTC. The small triangular object under the arrow is the Blue Cut LMA station. The numbers 1–3 indicate locations of unconnected branches and correspond to the cropped images in Figures C.8–C.10. The leader is estimated to be at a distance of 3.5 km from the camera and the resolution of the photo is 0.22 m/pixel at the location of the leader. The photograph reproduced here represents a transverse area (width×height) of approximately 621×542 m. Note the similarities in both branches at center right (above the number 3).

Figure C.5: Frame 1 of Photo C.1 (79 × 79 m). The segment is at least 19.8 m in length.

Figure C.6: Frame 2 of Photo C.1 (79 × 79 m). The segment is at least 7.6 m in length.

Figure C.7: Frame 3 of Photo C.1 (79 × 79 m). The segment is at least 7.4 m in length.

Figure C.8: Frame 1 of Photo C.2 (61 × 61 m). The segment (faint, at center) is at least 3.9 m in length.

Figure C.9: Frame 2 of Photo C.2 (61 × 61 m). The segment is at least 6.2 m in length.

Figure C.10: Frame 3 of Photo C.2 (61 × 61 m). The brightest of the three segments is at least 5.4 m in length.

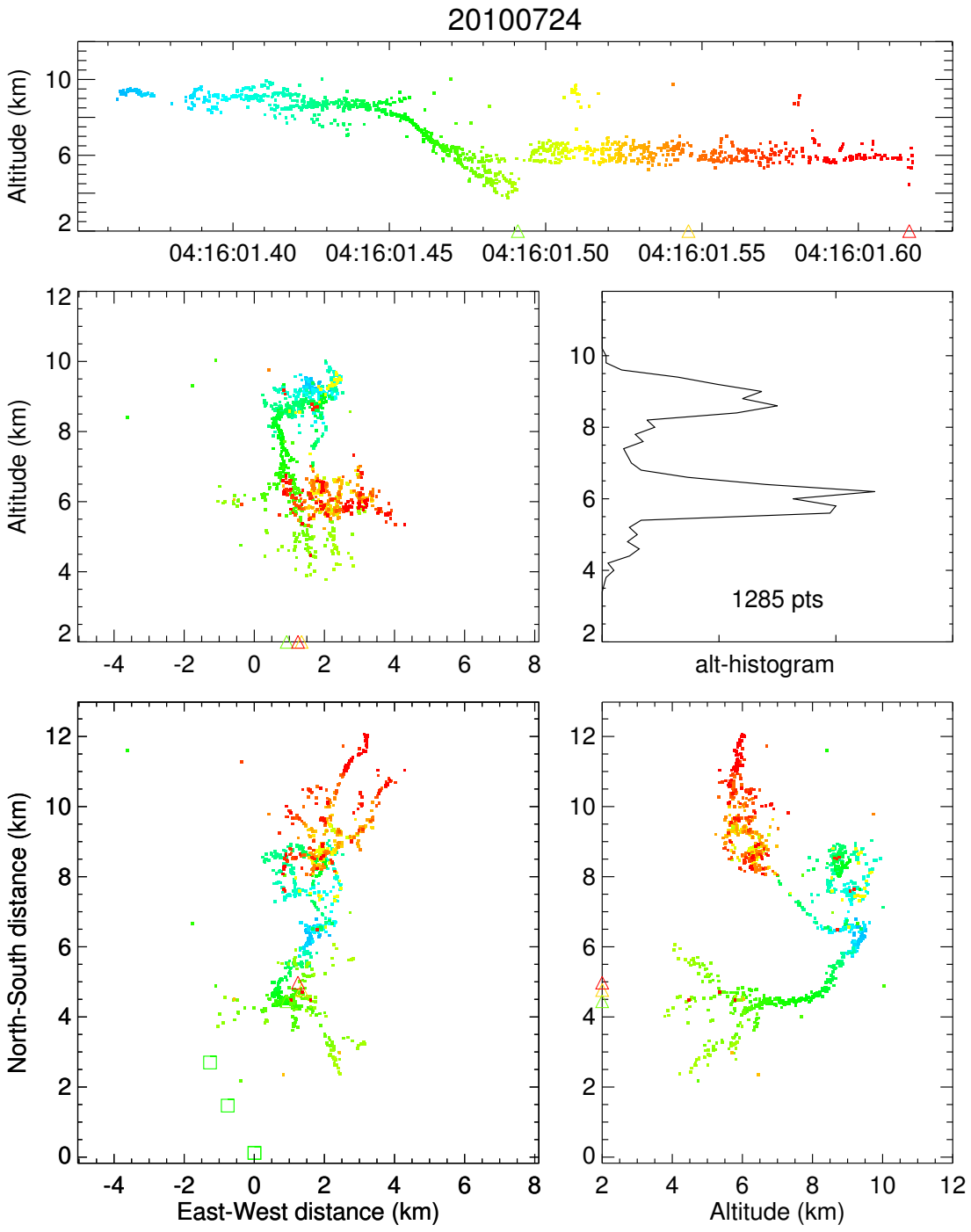

Figure C.11: VHF sources located by the LMA of the BFB flash of July 24, 2010 at 04:16:01 UTC. Sources are colored by time. The Langmuir Laboratory Annex is at the plot origin.

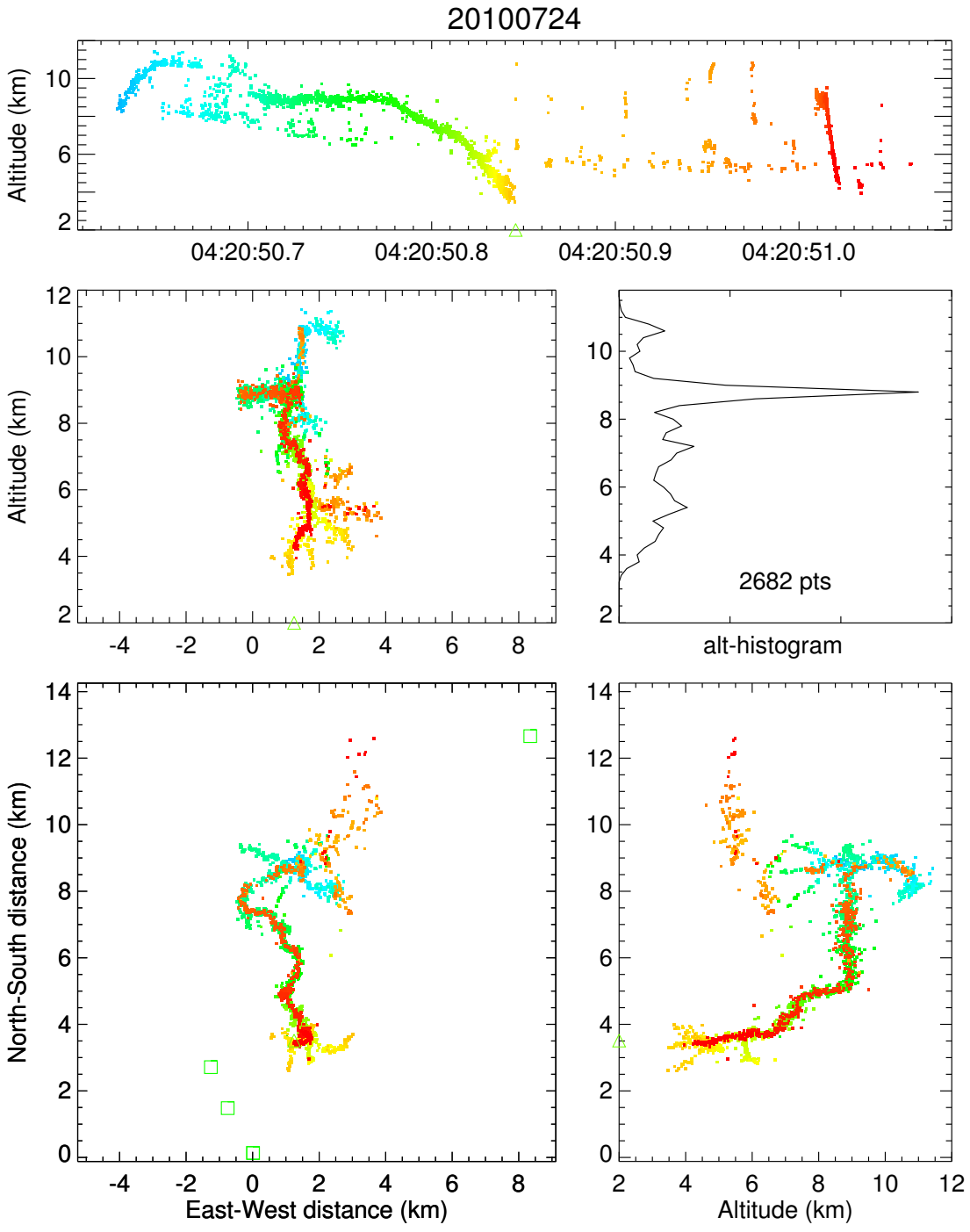

Figure C.12: VHF sources located by the LMA of the BFB flash of July 24, 2010 at 04:20:50 UTC. Sources are colored by time. The Langmuir Laboratory Annex is at the plot origin. Note the dart leader along the main cloud-to-ground channel toward the end of the flash.

D. Photographs

D.1 Introduction

Photographs of 35 BFB flashes are presented here, in support of Chapter 2 and other chapters. The photographs are arranged in six categories:

Typical BFB flashes (12 photographs)

BFB flashes following cloud boundaries (8 photographs)

Forked (multi-channel) BFB flashes (2 photographs)

Cloud-enshrouded BFB flashes (3 photographs)

Attempted BFB flashes (6 photographs)

BFB flashes with upward leader (4 photographs)

The date and time of each photograph are noted in the captions, if known. Since the time in a digital camera tends to be off by several seconds to more than a minute, all times that are listed as hh:mm are approximate. Times listed as hh:mm:ss are accurate to one second.

All photographs were taken by the author, and were obtained at Langmuir Laboratory unless indicated otherwise.

D.2 Typical BFB flashes

Photo D.1: BFB flash in the evening of August 15, 2002 in a storm across the shore of Lake Pontchartrain, New Orleans.

Photo D.2: BFB flash (and IC flashes) in a supercell storm over the Texas Panhandle on May 31, 2007.

Photo D.3: BFB flash (leaving the frame) at the upwind side of an evening storm on August 8, 2007 to the NNW of Langmuir Laboratory.

Photo D.4: BFB flash (after the flash in Photo D.3, in same storm of August 8, 2007). Note profuse low-altitude branching of the leader.

Photo D.5: BFB flash in a distant storm over central New Mexico on September 29, 2007 at 04:37 UTC. A line of storms moved north, producing numerous BFB flashes.

Photo D.6: Extensive BFB flash around 06:27 UTC (this is the same storm as in Photo D.5). The two ground flashes to the left did not occur simultaneously with the BFB flash.

Photo D.7: BFB flash with extensive leader path to ground at 07:05 UTC on September 29, 2007. Note increase in channel tortuosity as the leader propagated downward.

Photo D.8: BFB flash in a small, sheared storm over the San Mateo mountains in the evening of August 28, 2008. The leader exited the storm along the cloud shelf.

Photo D.9: BFB flash on September 9, 2009 at 04:43 UTC. The leader propagated along the lateral cloud boundary. The view is to the south.

Photo D.10: BFB flash to the WNW of Langmuir Laboratory in a storm that was "shearing apart" and dissipated after this flash. August 25, 2009 at 02:38 UTC.

Photo D.11: BFB flash at the upwind (southern) flank of a cluster of storms that produced a blue starter about 12 minutes later. August 3, 2010 at 04:02 UTC.

Photo D.12: BFB flash on August 7, 2010 at 03:35 UTC.

D.3 BFB flashes following cloud boundaries

Photo D.13: BFB flash with leader following cloud boundary (date and time unknown).

Photo D.14: BFB flash with leader following cloud boundary, September 9, 2008 at 04:16 UTC, looking south from Langmuir Laboratory (same storm as Photo D.9).

Photo D.15: BFB flash with leader following cloud boundary on the upwind side of a storm. July 23, 2009 at 05:34 UTC, over the San Mateo mountain range.

Photo D.16: BFB flash with leader following cloud boundary (visible above cloud shelf), just north of the city of Socorro. July 10, 2010 at 03:22 UTC.

Photo D.17: BFB flash with leader following cloud boundary, August 3, 2010 at 03:42 UTC (in blue-starter producing storm).

Photo D.18: BFB flash with leader following cloud boundary on August 13, 2010 at 02:52 UTC.

Photo D.19: BFB flash with leader following cloud boundary on August 20, 2010 at 03:06:15 UTC (see Section 5.4).

Photo D.20: BFB flash with leader following cloud boundary on August 20, 2010 at 03:57:19 UTC (see Section 5.4).

D.4 Forked (multi-channel) BFB flashes

Photo D.21: Forked BFB flash (with two channels to ground) on September 29, 2007 at 04:41 UTC.

Photo D.22: Forked BFB flash (with two channels to ground) on September 29, 2007. Exact time is not known, but shortly after 04:41 UTC when Photo D.21 was taken.

D.5 Cloud-enshrouded BFB flashes

Photo D.23: BFB flash mostly within the cloud. July 20, 2007 around 04:24 UTC.

Photo D.24: BFB flash mostly within or at the boundary of the cloud. July 20, 2007 around 04:24 UTC.

Photo D.25: BFB flash mostly within the cloud. August 13, 2010 at 03:38 UTC, looking west.

D.6 Attempted BFB flashes

Photo D.26: Attempted BFB flash with the cloud-to-air leader reaching almost halfway down to ground. September 9, 2008 at 04:39 UTC.

Photo D.27: Cloud-to-air discharge in a storm in high wind shear. July 23, 2009 at 04:58 UTC, over San Mateo mountain range. The leader has visible streamers at the tips.

Photo D.28: Cloud-to-air discharge at 05:03 UTC, about 5 minutes after the flash in Photo D.27 in the same storm and in the same area.

Photo D.29: Cloud-to-air discharge at 05:08 UTC, about 5 minutes after the flash in Photo D.28 and in the same area.

Photo D.30: Attempted BFB flash in an evening storm to the WSW of Langmuir Laboratory. August 3, 2010 at 03:10 UTC.

Photo D.31: Attempted BFB flash with leader changing direction upward. August 5, 2010 at 03:26 UTC.

D.7 BFB flashes with upward leader

Photo D.32: BFB flash with upward branch (faint in photograph). July 20, 2007, around 04:28 UTC.

Photo D.33: BFB flash with upward branch on July 20, 2007 at 04:30:12 UTC. The flash is mostly confined to the cloud.

Photo D.34: BFB flash with two upward branches on September 9, 2008 at 03:52 UTC.

Photo D.35: BFB flash with upward branch on August 31, 2010 at 05:24:25 UTC, over the Organ Mountains near Las Cruces. The main leader follows the cloud boundary.

References

Bazelyan, E. M., and Y. P. Raizer (2000), *Lightning Physics and lightning protection*, IOP Publishing Ltd.

Behnke, S. A., R. J. Thomas, P. R. Krehbiel, and W. Rison (2005), Initial leader velocities during intracloud lightning: Possible evidence for a runaway breakdown effect, *J. Geophys. Res.*, *110*(D10207), doi:10.1029/2004JD005312.

Berger, K., and E. Vogelsanger (1966), Photographische Blitzuntersuchungen der Jahre 1955-1965 auf dem Monte San Salvatore, *Bull. Schweiz. Elektrotech.*, *57*, 599–620.

Berger, K., and E. Vogelsanger (1969), New results of lightning observations, *Planetary electrodynamics*, *1*, 489–510.

Edens, H. E. (2011), Photographic and lightning mapping observations of a blue starter over a New Mexico thunderstorm, *Geophys. Res. Lett.*, submitted for publication.

Gorin, B. N., V. I. Levitov, and A. V. Shkilev (1976), *Some principles of leader discharge of air gaps with a strong non-uniform field*, Gas discharges, IEEE Conf. Publ. 143.

Kasemir, H. W. (1960), A contribution to the electrostatic theory of a lightning discharge, *J. Geophys. Res.*, *65*(7), 1873–1878.

Kitagawa, N. (1957), On the mechanism of cloud flash and junction or final process in flash to ground, *Pap. Meteor. Geophys.*, *7*(4), 415–424.

Kitagawa, N., and M. Brook (1960), A comparison of intracloud and cloud-to-ground lightning discharges, *J. Geophys. Res.*, *65*(4), 1189–1201.

Krehbiel, P. R., M. Brook, and R. A. McCrory (1979), An analysis of the charge structure of lightning discharges to ground, *J. Geophys. Res.*, *84*(C5), 2432–2456.

Krehbiel, P. R., J. A. Riousset, V. P. Pasko, R. J. Thomas, W. Rison, M. A. Stanley, and H. E. Edens (2008), Upward electrical discharges from thunderstorms, *Nat. Geosci.*, *1*, 233–237.

Liu, X. S., and P. R. Krehbiel (1985), The initial streamer of intracloud lightning flashes, *J. Geophys. Res.*, *90*(D4), 6211–6218.

Marshall, T. C., and M. Stolzenburg (1998), Estimates of cloud charge densities in thunderstorms, *J. Geophys. Res.*, *103*(D16), 19,769–19,775.

Marshall, T. C., and W. P. Winn (1982), Measurements of charged precipitation in a New Mexico thunderstorm: Lower positive charge centers, *J. Geophys. Res.*, *87*(C9), 7141–7157.

Mazur, V. (1989), Triggered lightning strikes to aircraft and natural intracloud discharges, *J. Geophys. Res.*, *94*(D3), 3311–3325.

Ogawa, T., and M. Brook (1964), The mechanism of the intracloud lightning discharge, *J. Geophys. Res.*, *69*(24), 5141–5150.

Pasko, V. P. (2010), Recent advances in theory of transient luminous events, *J. Geophys. Res.*, *115*(A00E35), doi:10.1029/2009JA014860.

Pasko, V. P., M. A. Stanley, J. D. Mathews, U. S. Inan, and T. G. Wood (2002), Electrical discharge from a thundercloud top to the lower ionosphere, *Nature*, *416*, 152–154.

Proctor, D. E. (1981), VHF radio pictures of cloud flashes, *J. Geophys. Res.*, *86*(C5), 4041–4071.

Rakov, V. A., and M. A. Uman (2002), *Lightning Physics and Effects*, Cambridge University Press.

Rhodes, C. T., X. M. Shao, P. R. Krehbiel, R. J. Thomas, and C. O. Hayenga (1994), Observations of lightning phenomena using radio interferometry, *J. Geophys. Res.*, *99*(D6), 13,059–13,082.

Rison, W., R. J. Thomas, P. R. Krehbiel, T. Hamlin, and J. Harlin (1999), A GPS-based three-dimensional lightning mapping system: initial observations in central New Mexico, *Geophys. Res. Lett.*, *26*(23), 3573–3576.

Schonland, B. F. J. (1956), *The lightning discharge*, *Handbuch der Physik*, vol. 22, pp. 576–628, Springer-Verlag, Berlin.

Shao, X. M., and P. R. Krehbiel (1996), The spatial and temporal development of intracloud lightning, *J. Geophys. Res.*, *101*(D21), 26,641–26,668.

Shao, X. M., P. R. Krehbiel, R. J. Thomas, and W. Rison (1995), Radio interferometric observations of cloud-to-ground lightning phenomena in Florida, *J. Geophys. Res.*, *100*(D2), 2749–2783.

Shao, X. M., C. T. Rhodes, and D. N. Holden (1999), RF radiation observations of positive cloud-to-ground flashes, *J. Geophys. Res.*, *104*(D8), 9601–9608.

Su, H. T., R. R. Hsu, A. B. Chen, Y. C. Wang, W. S. Hsiao, W. C. Lai, L. C. Lee, M. Sato, and H. Fukunishi (2003), Gigantic jets between a thundercloud and the ionosphere, *Nature*, *423*, 974–976.

Thomas, R. J., P. R. Krehbiel, W. Rison, T. Hamlin, J. Harlin, and D. Shown (2001), Observations of VHF source powers radiated by lightning, *Geophys. Res. Lett.*, *28*(1), 143–146.

Thomas, R. J., P. R. Krehbiel, W. Rison, S. J. Hunyady, W. P. Winn, T. Hamlin, and J. Harlin (2004), Accuracy of the Lightning Mapping Array, *J. Geophys. Res.*, *109*(D14207), doi:10.1029/2004JD004549.

Uman, M. A. (1984), *Lightning*, Dover Publications, Ltd.

Villanueva, Y., V. A. Rakov, M. A. Uman, and M. Brook (1994), Microsecond-scale electric field pulses in cloud lightning discharges, *J. Geophys. Res.*, *99*(D7), 14,353–14,360.

Wescott, E. M., D. Sentman, D. Osborne, D. Hampton, and M. Heavner (1995), Preliminary results from the Sprites94 aircraft campaign: 2. Blue jets, *Geophys. Res. Lett.*, *22*(10), 1209–1212.

Wescott, E. M., D. D. Sentman, M. J. Heavner, D. L. Hampton, D. L. Osborne, and O. H. Vaughan Jr. (1996), Blue starters: Brief upward discharges from an intense Arkansas thunderstorm, *Geophys. Res. Lett.*, *23*(16), 2153–2156.

Williams, E. R. (1989), The tripole structure of thunderstorms, *J. Geophys. Res.*, *94*(D11), 13,151–13,167.

Winn, W. P., G. Aulich, S. J. Hunyady, R. G. Sonnenfeld, K. B. Eack, H. E. Edens, P. R. Krehbiel, W. Rison, and R. J. Thomas (2011), Vector electric field near a negative lightning leader, *J. Geophys. Res.*, submitted for publication.